2008

Strategies to test nuclear localization of non-viral gene delivery vectors in vitro and in vivo

Garrett Richard Rettig
University of Iowa

STRATEGIES TO TEST NUCLEAR LOCALIZATION OF NON-VIRAL GENE DELIVERY VECTORS IN VITRO AND IN VIVO

by

Garrett Richard Rettig

An Abstract
of a thesis submitted in partial fulfillment
of the requirements for the Doctor of
Philosophy degree in Pharmacy (Medicinal and Natural Products Chemistry)
in the Graduate College of
The University of Iowa

December 2008

Thesis Supervisor: Professor Kevin G. Rice

ABSTRACT

Non-viral gene delivery is plagued by low transfection levels compared to viral delivery. The nuclear envelope presents a significant obstacle for non-viral vectors. A peptide-based nuclear localizing sequence has been incorporated into non-viral vectors to traverse the nuclear envelope. Here, we selected a photo-chemical method for covalently labeling the peptide onto plasmid DNA. The hypothesis of this work was to incorporate a nuclear localizing sequence into a non-viral delivery vector, demonstrate increased nuclear uptake and show a subsequent increase in transgene expression both in vitro and in vivo.

We focused on pursuing in vitro and in vivo methods by which to test non-viral vectors for increases in gene expression based on the nuclear localizing sequence. Hydrodynamic dosing and intramuscular dosing (followed by electroporation) are two efficient delivery routes for dosing DNA in vivo. Through preliminary experiments, we became confident that whole animal bioluminescent imaging was a reliable and quantitative method by which to detect luciferase expression by either delivery route. Moving forward, both hydrodynamic and intramuscular dosing would be used to test formulations for nuclear localizing ability in vivo.

Nuclear localizing peptides containing a photo-activatable functionality were synthesized and characterized. We quantitatively explored the photo-labeling capabilities on plasmid DNA via a radioactive peptide. In vitro, tissue culture-based experiments were carried out to show increased nuclear uptake by confocal microscopy as well as increased transgene expression. Throughout the literature, achieving an increase in expression by incorporating a nuclear localizing sequence into a non-viral vector has been elusive. The complexity of achieving this goal is increased when considering an in vivo system for improving gene transfer efficiency. Several strategies have been explored

to demonstrate an increase in reporter gene expression from this type of non-viral vector, and the methods developed herein can be applied to other nuclear localizing vectors.

Abstract Approval: _____
Kevin G. Rice, Thesis Supervisor

_____
Title and Department

_____
Date

STRATEGIES TO TEST NUCLEAR LOCALIZATION OF NON-VIRAL GENE DELIVERY VECTORS IN VITRO AND IN VIVO

by

Garrett Richard Rettig

A thesis submitted in partial fulfillment
of the requirements for the Doctor of
Philosophy degree in Pharmacy (Medicinal and Natural Products Chemistry)
in the Graduate College of
The University of Iowa

December 2008

Thesis Supervisor: Professor Kevin G. Rice

Graduate College
The University of Iowa
Iowa City, Iowa

CERTIFICATE OF APPROVAL

_____

PH.D. THESIS

_____

This is to certify that the Ph.D. thesis of

Garrett Richard Rettig

has been approved by the Examining Committee
for the thesis requirement for the Doctor of Philosophy
degree in Pharmacy (Medicinal and Natural Products Chemistry) at the
December 2008 graduation.

Thesis Committee: _____
Kevin G. Rice, Thesis Supervisor

_____
Jonathan A. Doorn

_____
Michael W. Duffel

_____
Robert J. Kerns

_____
Michael D. Henry

ABSTRACT

Non-viral gene delivery is plagued by low transfection levels compared to viral delivery. The nuclear envelope presents a significant obstacle for non-viral vectors. A peptide-based nuclear localizing sequence has been incorporated into non-viral vectors to traverse the nuclear envelope. Here, we selected a photo-chemical method for covalently labeling the peptide onto plasmid DNA. The hypothesis of this work was to incorporate a nuclear localizing sequence into a non-viral delivery vector, demonstrate increased nuclear uptake and show a subsequent increase in transgene expression both in vitro and in vivo.

We focused on pursuing in vitro and in vivo methods by which to test non-viral vectors for increases in gene expression based on the nuclear localizing sequence. Hydrodynamic dosing and intramuscular dosing (followed by electroporation) are two efficient delivery routes for dosing DNA in vivo. Through preliminary experiments, we became confident that whole animal bioluminescent imaging was a reliable and quantitative method by which to detect luciferase expression by either delivery route. Moving forward, both hydrodynamic and intramuscular dosing would be used to test formulations for nuclear localizing ability in vivo.

Nuclear localizing peptides containing a photo-activatable functionality were synthesized and characterized. We quantitatively explored the photo-labeling capabilities on plasmid DNA via a radioactive peptide. In vitro, tissue culture-based experiments were carried out to show increased nuclear uptake by confocal microscopy as well as increased transgene expression. Throughout the literature, achieving an increase in expression by incorporating a nuclear localizing sequence into a non-viral vector has been elusive. The complexity of achieving this goal is increased when considering an in vivo system for improving gene transfer efficiency. Several strategies have been explored

to demonstrate an increase in reporter gene expression from this type of non-viral vector, and the methods developed herein can be applied to other nuclear localizing vectors.

TABLE OF CONTENTS

LIST OF TABLES

LIST OF FIGURES

LIST OF SCHEMES

LIST OF ABBREVIATIONS

ANOVA…..analysis of variance

ATP…..adenosine 5’-triphosphate

BCA..bicinchoninic acid

BLI.....bioluminescence imaging

bp.....base pairs

CCD. ..... charge-coupled device

CHO. .....Chinese hamster ovary

DAPI.. .....4',6-diamidino-2-phenylindole

DCM.....dichloromethane

DIC.....diisopropylcarbodiimide

DIPEA.. .....diisopropylethylamine

DMEM.....Dulbecco’s modified Eagle’s medium

DMF.. .....*N*,*N*-dimethylformamide

DNA.....deoxyribonucleic acid

dsRNA.. ..... double-stranded RNA

EDTA.....ethylenediaminetetraacetic acid

EP…... ..... electroporation/electropermeabilizatoin

ESI.....electro-spray ionization

EtOH.. .....ethanol

FBS.....fetal bovine serum

HD..... hydrodynamic

Fmoc.. .....9-fluorenylmethoxycarbonyl

HepG2.. .....human hepatocellular liver carcinoma cells

HOBt.. ..... 1-hydroxybenzotriazole

IM…... .....intramuscular

IP…... intraperitoneal

MEM. ..... modified Eagle's medium

mRNA ..... messanger RNA

miRNA ..... micro RNA

NIH/3T3.…..... murine embryo fibrobalst cells

NMP.. ..... *N*-methylpyrrolidone

NLS..... nuclear localization sequence

NPC..... nuclear pore complex

pDNA..... plasmid DNA

PBS..... phosphate-buffered saline

PEI... ..... polyethyleneimine

pGL3 (+/+) ..... pGL3 Control plasmid (SV40 promoter and enhancer)

pGL3 (+/-)..... pGL3 Promoter plasmid (SV40 promoter)

pGL3 (-/-)..... pGL3 Basic plasmid (neither SV40 promotor nor enhancer)

PL.…... ..... photo-label (4-azido-2,3,5,6-tetrafluorobenzoate)

RISC... ..... RNA interference silencing complex

RLU... ..... relative light units

RNA... ..... ribonucleic acid

RNAi... ..... RNA interference

RP-HPLC... ..... reverse-phase high-pressure liquid chromatography

SEAP... ..... secreted alkaline phosphotase

shRNA... ..... short-hairpin RNA

siRNA... ..... small-interfering RNA

SPPS..... solid-phase peptide synthesis

SV40... ..... simian virus 40

TFA... ..... trifluoroacetic acid

CHAPTER 1
LITERATURE REVIEW

Abstract

Despite nearly two decades of research, the successful application of systemically delivered non-viral gene therapies to treat human disease is still limited by poor transfection efficiency. The major barriers in the circulation and in the cell that limit transfection efficiency have been identified, and the field is in a phase of design and testing of more sophisticated carrier systems that attempt to circumvent these barriers. These studies are increasingly conducted in vivo using rapid quantitative measures of gene transfer efficiency as a guide. Although there has been steady progress in developing DNA nanoparticles that navigate the circulation, enter the target cell, and escape lysosomal targeting, the final goal of efficiently traversing the nuclear membrane remains the most significant challenge. The goal remains to develop elegant delivery systems that work in concert to deliver DNA from the needle to the nucleus.

Introduction

The development of a safe and efficient non-viral gene delivery system remains as a significant hurdle toward the application of gene therapy to treat human disease. Although viral delivery systems are much more efficient in the delivery of genetic material, there are concerns regarding toxicity, high costs of producing therapeutic doses, immunogenicity and possible integration of viral genetic material into the human genome[1]. Chemically defined non-viral vectors can potentially avoid these drawbacks of viral delivery and can be developed and manufactured more similarly to traditional pharmaceuticals. The recent discovery of RNA interference (RNAi) has expanded the scope of gene therapy to include applications for knocking down or otherwise modulating gene expression[2]. Protein regulation by RNAs and antigen expression by DNA vaccines

are two additional applications of gene therapy that hold great promise if the *delivery* of oligonucleotides to nucleus can be solved (Figure 1-1).

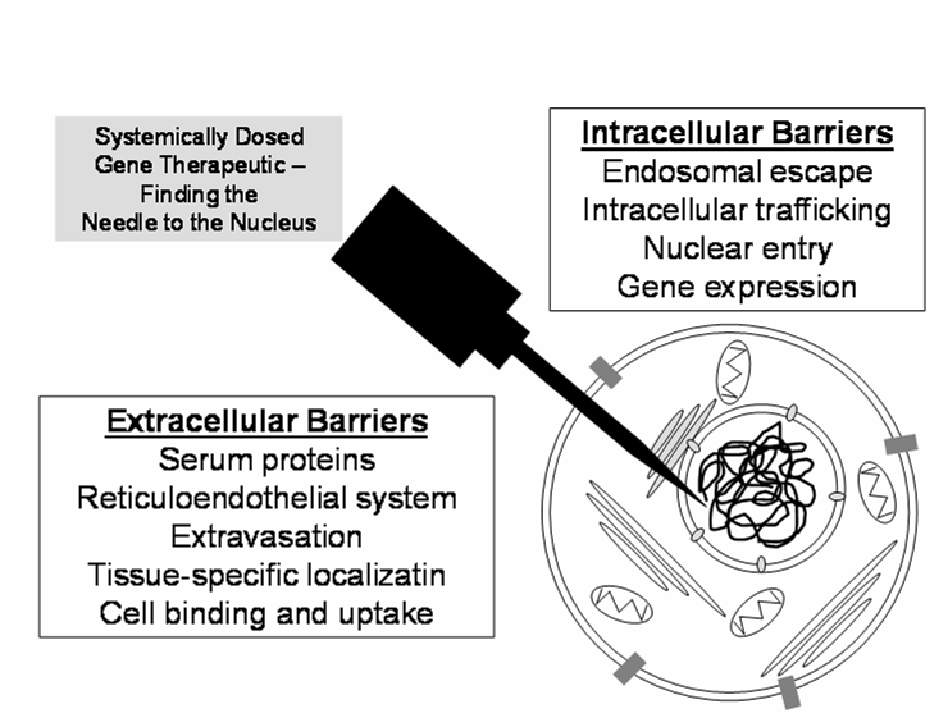

Figure 1-1. *Barriers to systemic gene delivery*. There are many physical and molecular barriers that a gene therapeutic must overcome to achieve the goal of gene expression following a systemic dose. Barriers arise both extracellularly and intracellularly. The objective of the gene therapy community is to design a therapeutic that can take the least inhibited path from the needle to the nucleus.

There are several barriers to be overcome for the efficient systemic delivery of DNA. In the circulation these include blood cells, proteins and enzymes that bind to DNA or its carrier system. Binding to serum proteins leads to decreased stability, an increase in particle size or charge and premature metabolism[3]. DNA nanoparticles in circulation encounter endothelial cells lining blood vessels, macrophages, tight capillary beds and the reticulo-endothelial system (RES). All of these barriers act collectively to prevent

non-viral vectors from reaching the target site[4]. Upon exiting the vasculature through fenestrae in the liver, lung and tumors, the DNA nanoparticles must bind and gain entry into target cells. A targeting ligand may allow the vector to be internalized by receptor-mediated endocytosis. These extracellular barriers present a challenge; however, research from many groups has shown significant advances in systemic stability and tissue-targeting specificity[5,6]. Navigating intracellular barriers is a more delicate process because the payload has to arrive at the nucleus as a *functional* biomolecule.

The seemingly short distance from the cell surface to the nucleus is littered with safe-guards designed to protect the cell from foreign invasion. Assuming that the nanoparticle can be engineered to escape the lysosome, it still must uncoat, and release its DNA cargo, prior to nuclear entry[7]. Once in the cytosol, naked DNA will encounter a different group of binding proteins and enzymes that attempt to block its diffusion and cause its degradation. At the nuclear membrane, the DNA encounters its most significant barrier which is to cross the nuclear envelope via small and selective nuclear pores. Without the aid of facilitated transport across the nuclear membrane, a dwindling fraction of the DNA arrives at the target. The following review of the literature will first discuss challenges in research that inhibit effective non-viral gene delivery and will subsequently focus specifically on nuclear targeting of non-viral systems.

Overcoming Barriers to Non-viral Gene Delivery In Vivo

Primary Targeting

Primary targeting is defined as the events that occur from the moment of injection of DNA nanoparticles into a venous blood supply to the point that they gain access to the target cell (Figure 1-2). Systemic delivery of a non-viral vector requires that the DNA nanoparticles are stable in the blood and can access and target specific cells.

Most DNA nanoparticles are constructed by ionic interaction of a polycationic carrier molecule and DNA[8]. This interaction is susceptible to dissociation at high ionic

strength, the concentration of which ranges from approximately 0.1-1 M depending on the length of the polymer and the number of cationic amines[9]. Cationic DNA nanoparticles are colloidal and are known to aggregate in the presence of sodium ions. They also immediately bind electronegative proteins in the blood such as serum albumin[10].

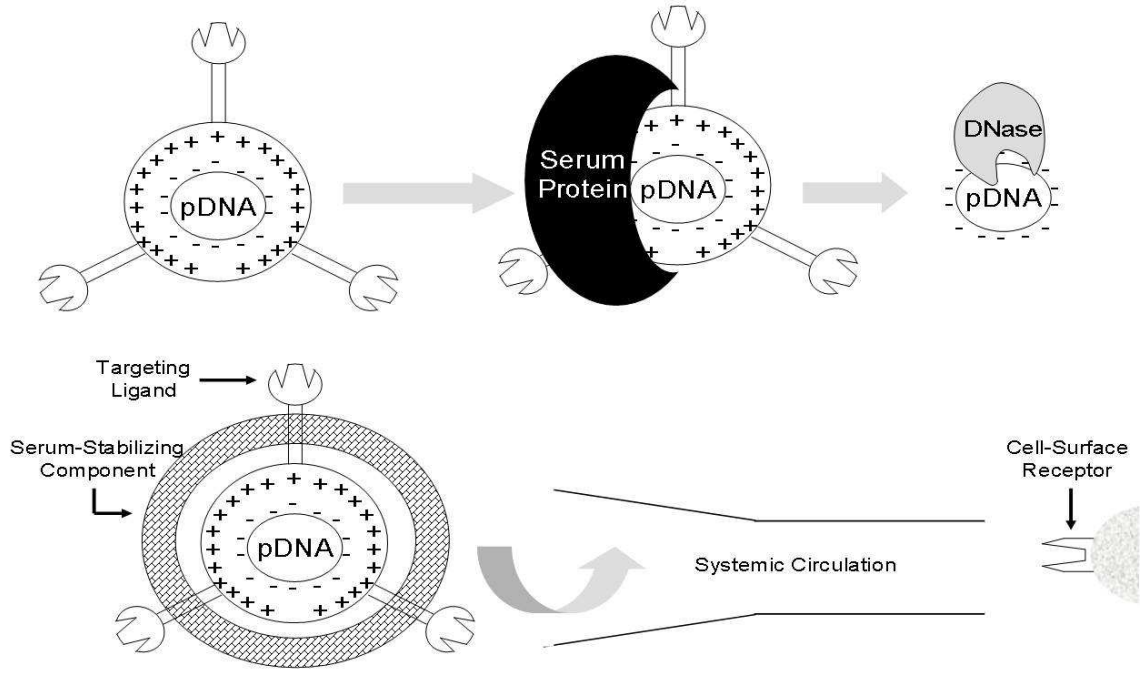

Figure 1-2. *Primary targeting*. Targeting ligands are recognized by cell-surface receptors to mediate selective uptake of DNA nanoparticles. PEGylation is used to block the binding and aggregation of DNA nanoparticles with serum proteins that otherwise results in a rapid increase in particle size in serum. DNA nanoparticles can dissociate in normal saline, leading to the metabolism of naked DNA in serum. PEGylation and cross-linking have been used to overcome these barriers resulting in the normal biodistribution of DNA nanoparticles in the systemic circulation.

Almost all in vivo applications of non-viral delivery of DNA nanoparticles attempt to minimize the particle size to less than 250 nm in diameter to allow for

biodistribution and extravasation from the circulatory system[11]. Small DNA nanoparticles can more readily undergo extravasation from the capillaries and gain access to the extracellular matrix and the target cells in the liver, lungs or tumors[12].

To achieve stabilized DNA nanoparticles that resist dissociation in physiological concentrations of salt (0.15 M), high molecular weight cationic polymers such as PEI (25 kDa) or polylysine (25 kDa) have been used[13]. Likewise, low molecular weight cationic peptides can also be stabilized by incorporating a cross-linking strategy such as glutaraldehyde or disulfide bond formation (Figure 1-2)[14,15]. The disulfide bond polymerization of small cationic peptides is particularly attractive in that it offers a built-in mechanism for DNA to escape the polyplex after it has entered the reducing environment of the cell.

Premature dissociation of DNA nanoparticles in the blood leads to rapid metabolism of naked DNA in the serum and targeted uptake of anionic DNA to Kupffer cells of the liver via the scavenger receptor[16]. Liver endothelial cells have also been shown to efficiently take up and digest naked DNA[17]. Nanoparticles that remain in tact may suffer from poor biocompatibility. Stabilized cationic DNA nanoparticles attract and bind serum albumin, resulting in a rapid increase in particle size and entrapment in the capillary beds of the lung[18].

The most common approach to overcoming this barrier during primary targeting is to introduce polyethylene glycol (PEG) onto the surface of DNA nanoparticles, which acts to "stealth" the surface charge (Figure 1-2)[19]. The size and loading density of PEG on DNA nanoparticles influences the degree to which albumin binding will be blocked and unobstructed biodistribution restored. However, the introduction of PEG onto the surface of DNA nanoparticles simultaneously introduces other complications. There is a potential occurrence of an immune reaction to PEGylated DNA nanoparticles[20]. Also, PEG with an average molecular weight of 5 kDa can mask the recognition of small receptor ligands attached to the cationic DNA carrier or to DNA itself. Several strategies have been used

to overcome this issue, but most often the use of small ligands such as monosaccharides or folate necessitate the use of bi-functional PEG that allows incorporation of a ligand at one end of the PEG polymer and acts to anchor the ligand to the non-viral vector via the other end of PEG (Figure 1-2)[21].

DNA nanoparticles can be targeted to a specific cell type by exploiting ligand interactions with receptors that are selectively expressed on the cell surfaces. There are several examples of ligand-receptor combinations that have been incorporated into targeted gene delivery systems[22,23]. One of the earliest and best-studied examples involves targeting the asialoglycoprotein receptor (ASGP-R) on hepatocytes using galactose-containing ligands[24,25]. Formulations have been endowed with targeting specificity for the ASGP-R by conjugation of a triantennary N-glycan ligand to a PEG-peptide[26,27]. A similar effect can be gained by galactose-containing PEGylated nanoparticles[28]. Advancements in primary targeting have been shown to improve vector uptake in parenchymal cells of the liver. Receptor targeting has been further verified by galactose-inhibited gene expression mediated by these targeting vectors[28].

The over-expression of the transferrin receptor on the surface of many cancer cells has led to its frequent use to direct non-viral vectors to tumors. Aside from exploiting this ligand-receptor interaction, tumor targeting is facilitated by increased tumor vascularization and permeability of the fenestrae which allow extravasation and retention of DNA nanoparticles in tumors[29].

The target organ is the primary factor in determining the difficulty of systemic delivery. Liver targeting is inherently easy since the liver is the largest internal organ and is extensively vascularized. In the absence of any targeting ligand, PEGylated DNA nanoparticles will target to liver and spleen. Cells of the RES in both liver and spleen actively survey the blood for foreign particles. ASGP-R is abundantly expressed on the surface of hepatocytes, and high affinity targeting ligands on a non-viral vector can re-direct a large percentage of the dose (already in the liver) to bind rapidly and enter

hepatocytes[30]. In contrast, an attempt to target DNA nanoparticles to a solid tumor that is poorly perfused[31] and has only a modest over-expression of target receptor, results in a competition between the natural biodistribution to the liver and spleen RES and the less efficient process of receptor binding and internalization in the tumor. For this reason, it remains challenging to demonstrate that an appreciable percentage (>10%) of the DNA nanoparticle dose can be targeted to organs other than the liver from the systemic circulation. The exceptions to inherent liver specificity are hypervascularized tumors that promote uptake of nanoparticles for gene therapy and lung targeting[32], which is often the result of non-specific entrapment of large DNA particles in the vasculature[33].

Secondary Targeting

Following entry into the cell via receptor mediated endocytosis, DNA nanoparticles must escape targeting to the lysosome and its mechanism of digestion (Figure 1-3). There are two hypotheses by which a non-viral vector escapes the endosome, and currently, both are being explored experimentally. The pH buffering hypothesis is supported by ample in vitro evidence involving PEI or poly-histidine peptides that improve transfection efficiency in a variety of cell lines (Figure 1-3)[34]. However, it is unlikely that PEI will have the same ability to mediate endosomal escape in vivo following systemic delivery. It is difficult to achieve the same buffering capacity in the target cell in vivo as suggested in the expression results of IP dosed PEI-DNA condensates[35].

The other major approach to achieve endosomal escape involves the use of fusogenic peptides such as HA2[36], GALA[37], and melittin[38]. Peptides like melittin are well-known to mediate membrane lysis (Figure 1-3)[39]. Structurally, the peptides promote lysis via an amphipathic α-helix that inserts into the membrane of the endosome. Most in vivo strategies of gene delivery with this type of peptide incorporate an anionic fusogen that achieves an endosomal lytic conformation at pH 4-5.

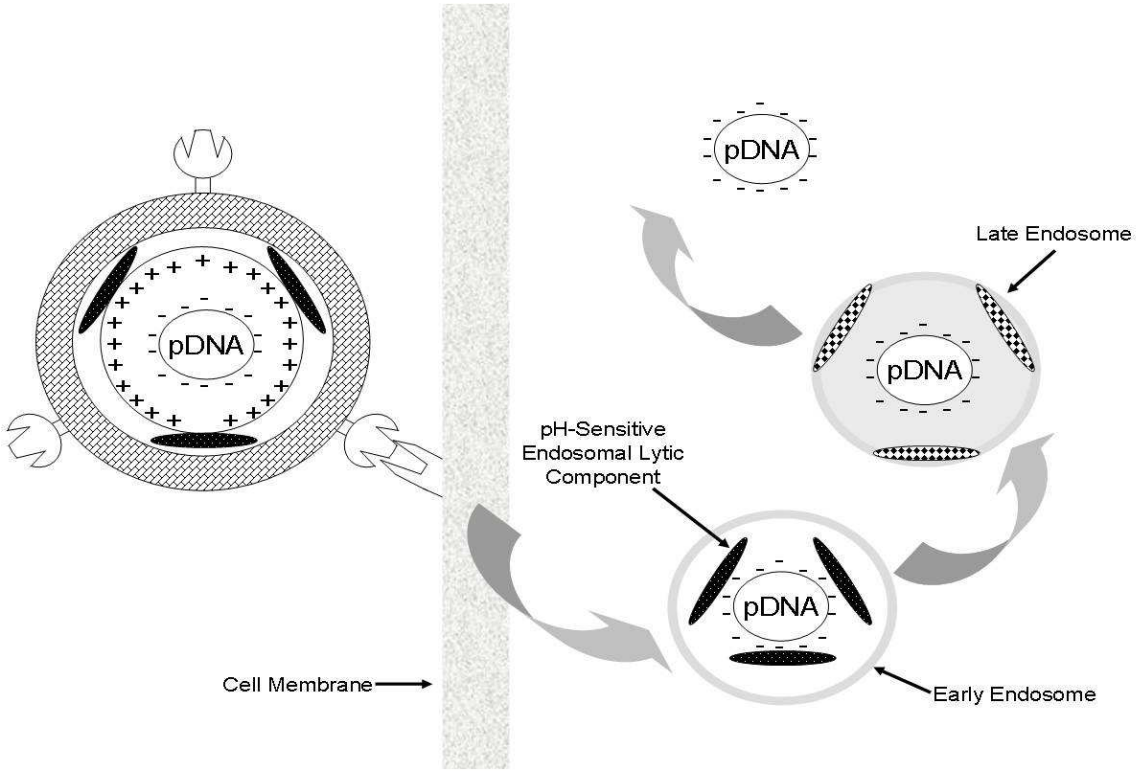

Figure 1-3. *Secondary targeting*. The use of endosomal buffering agents or using endosomal lytic peptides are two approaches to mediate secondary targeting of DNA into the cytosol. Upon receptor-mediated endocytosis, endosomal osmotic disruption or lysis leads to DNA nanoparticle delivery to the cytosol. The uncoating of DNA nanoparticles to release naked plasmid DNA is prerequisite prior to tertiary targeting.

Like endosomal buffering agents, the activity of all fusogenic peptides are also concentration dependent. Since most viruses mediate their own endosomal escape via fusogenic activity, there is reason to believe that incorporation of a potent fusogen into a non-viral gene delivery system could also achieve endosomal escape in vivo. However, because most of the fusogenic peptides in this class undergo a pH-dependent conformational change in the endosome, their method of incorporation into the DNA nanoparticle can dramatically influence their function. Fusogenic peptides are often difficult to synthesize and purify, which further complicates their routine use. The

activity of these peptides may also need to be tailored since the endosomal pH is known to be cell-type dependent.

The final phase of secondary targeting involves uncoating of the DNA nanoparticle to release naked DNA (Figure 1-3). There is still much debate about where this occurs, but not much argument regarding the necessity of the completion of this step prior to DNA being rendered functional in the nucleus. The continued interaction between cationic carrier and DNA or a newly formed interaction between nucleosomes and DNA are identified as evidence for the importance of the uncoating step[40,41]. Recent studies have focused on developing chemical mechanisms to allow PEGylated DNA nanoparticles to shed their PEG[42]. Other strategies include the design of polymers with multiple disulfide bonds that reduce intracellularly resulting in smaller polycations that more readily dissociate from DNA[43]. It remains a significant challenge to design non-viral DNA particles that package and release DNA during secondary targeting as efficiently as their viral counterparts.

Tertiary Targeting

Tertiary targeting involves the transport of DNA from the cytosol to the nucleus and is currently the most difficult part of systemic non-viral gene delivery. DNA that escapes the endosome has been shown to reach the nucleus without any targeting mechanism if cells are actively dividing. Since cells are generally quiescent during in vivo gene transfer, much effort has been focused on developing a way to mediate nuclear targeting to boost gene transfer efficiency (Figure 1-4). It has also been shown that the viscosity of the cytosol inhibits free diffusion of DNA. Thereby, the migration of DNA in the cytosol is believed to be supported by dynein-mediated transport along the microtubule network of the cell[44].

A key consideration in nuclear targeting is choosing a nuclear localizing sequence (NLS)[45]. The sequence is most often peptide-based; however, DNA sequences that bind

transcription factors have been shown to impart a similar nuclear-localizing effect[46]. The NLS is incorporated to selectively traffic the non-viral vector to the nucleus via the nuclear pore complex (NPC). The NPC is a multimeric protein spanning the nuclear envelope. Molecular trafficking through the NPC is dependent on molecular weight and shape. A variety of studies have borrowed NLS peptide sequences from endogenous nuclear targeting proteins and incorporated these into DNA nanoparticles. NLS peptides are typically lysine and arginine-rich. Several strategies in bioconjugate chemistry have been applied to incorporation of an NLS and will be discussed in more detail below.

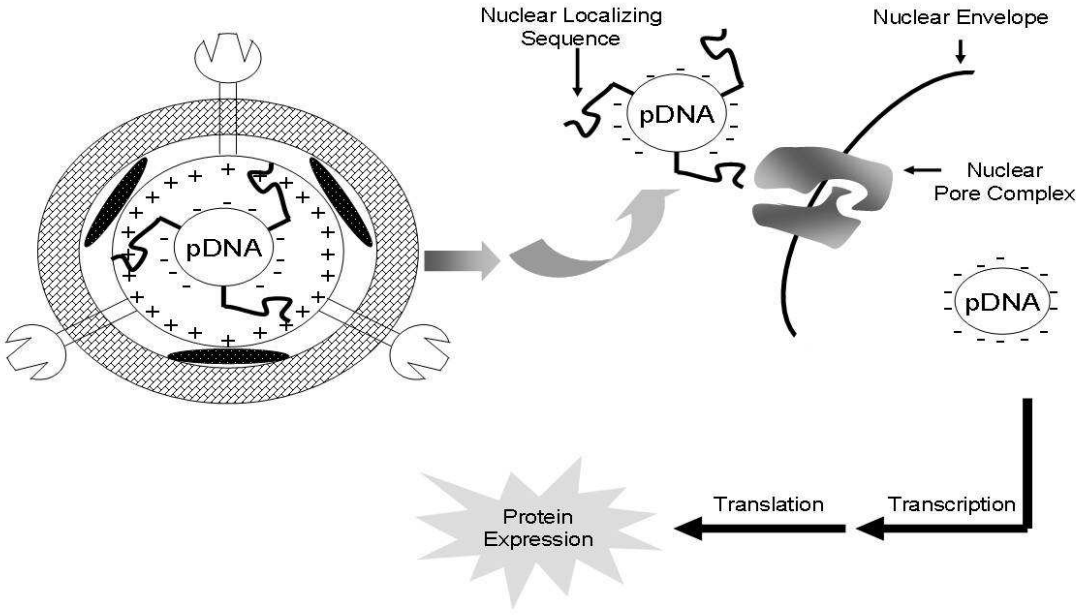

Figure 1-4. *Tertiary targeting*. Tertiary targeting of a non-viral vector results from a nuclear targeting strategy. Once in the cytosol, plasmid DNA is actively transported across the nuclear pore complex. In the nucleus, plasmid DNA is transcribed and translated with the endogenous cellular machinery to express the encoded protein.

In Vivo Assays for Measuring Gene Transfer Efficiency

As with in vitro gene transfer, the direct quantitation of gene transfer efficiency in vivo requires a sensitive assay to measure the generation of a gene product. The gene therapy field has gained considerable experience in evaluating in vivo gene transfer data from a variety of secreted and non-secreted reporter genes as well as therapeutic gene products. A therapeutic effect has been observed in a mouse model of prostate cancer. Tumor vascularization and overall tumor growth were shown to decrease following the dose of pDNA encoding siRNA for vascular endothelial growth factor[47]. Cationic lipids carrying therapeutic genes have been analyzed in clinical trials for cystic fibrosis and ovarian cancer[48,49]. Regarding reporter genes, the consensus view is that luciferase expression is still the most reliable and broadly applicable indicator of gene transfer.

Bioluminescence Imaging

Bioluminescence imaging (BLI) has emerged as a powerful method to quantify luciferase expression in vivo[50]. BLI uses a cooled charge-coupled device (CCD) camera to detect photon emission from living animals that express luciferase, or otherwise fluorescent species. Luciferase from the firefly (*Photinus pyralis*) is a chemiluminescent enzyme widely used as a reporter gene. The substrate D-luciferin is oxidized in the presence of ATP, Mg^{2+} and O_2 to produce oxyluciferin. The energetically favorable reaction also produces a chemiluminescent response in the form of photon emission with a broad peak at 560 nm. The observable maximum wavelength emission is closer to 610 nm from living animals because photons of lower wavelengths are preferentially absorbed in the tissue – particularly by hemoglobin and melanin[51].

Luciferase is widely used in mammalian cells for gene transfer experiments since it is nearly impossible to produce false-positive results. The sensitivity of detection for this imaging modality is a great advantage and contributes to its popularity. As few as 300 cells expressing luciferase will produce a bioluminescent signal that is detectable by

a CCD camrera[52]. In vitro, this number drops to 30 cells to define the limit of detection. Detection and analysis methods allow for the selection of a region of interest (ROI) in which luciferase expression is observed. Luciferase expression is quantifiable in terms of photons normalized on the basis of ROI area and the time of image acquisition. Compared to other methods of detecting in vivo transgene expression, BLI eliminates the need for tissue harvesting. As a result, the same animals can be serially sampled over a time course. The total number of animals used is greatly reduced and the precision of the data is improved by BLI.

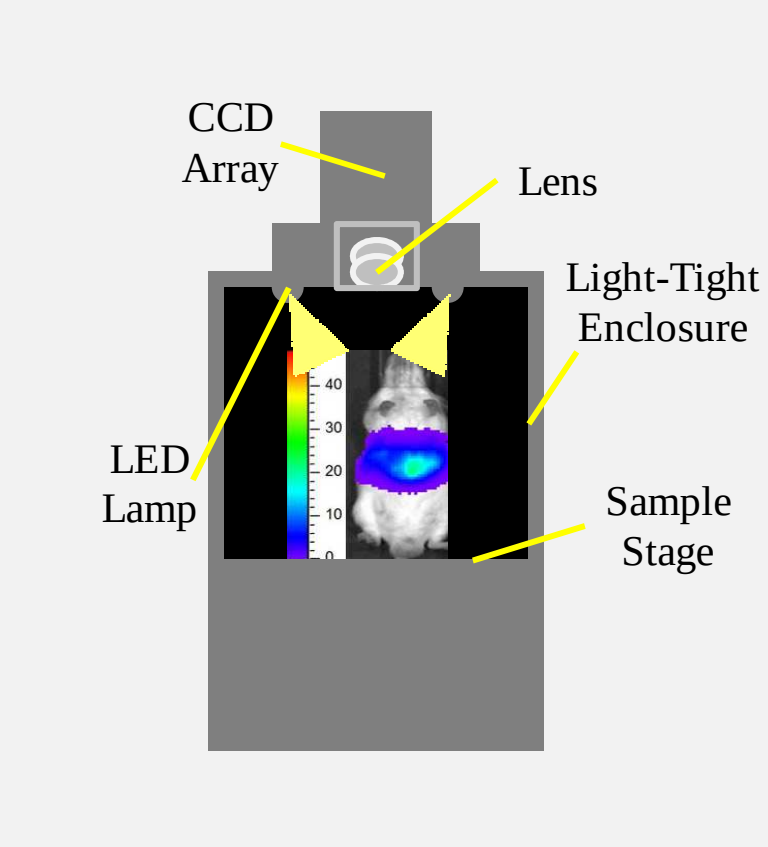

Figure 1-5. *Bioluminescent imaging.* The Xenogen® system is engineered to facilitate the detection of luciferase expression in living animals. The above diagram depicts some of the relevant components of the instrument.

BLI can be used to monitor in vivo luciferase expression from any source: virus[53], tumor[54], or gene delivery vector[55]. For purposes of our investigations, this powerful optical imaging modality was adapted to detect luciferase expression from two commonly targeted tissues for in vivo non-viral gene transfer. Liver-specific expression was achieved by hydrodynamic (HD) dosing. Liver-targeting via non-viral vectors is common due to the organ's aforementioned central role in metabolism[56]. Skeletal muscle is also a frequent target for muscle-related therapies[57], DNA vaccines[58], and secretable therapeutic proteins.

Hydrodynamic Dosing

Hydrodynamic dosing is now a well-established technique by which DNA is delivered rapidly to mice via the tail vein in a high volume[59,60]. The result is the selective expression of the transgene product in hepatocytes. The procedure involves a 5-sec tail vein dose of DNA in a volume equal to 10% of the mouse weight – a high-pressure and high-volume dose. This overwhelming dose triggers transient heart failure, a decreased heart rate and an increase in the internal pressure of the vena cava. The excess fluid begins a retrograde flow that triggers observable liver swelling[61], enlargement of liver

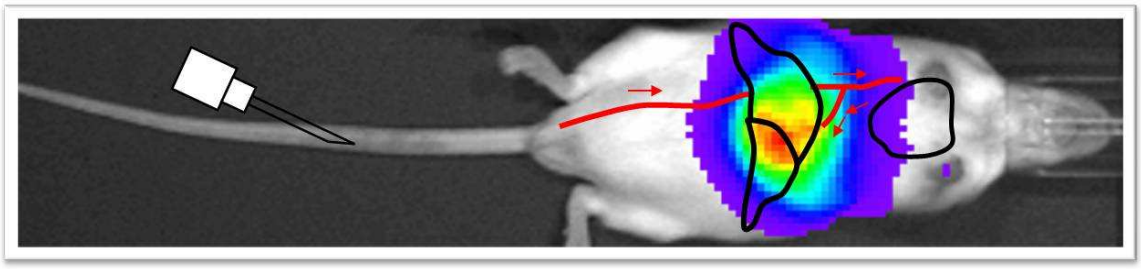

Figure 1-6. *Hydrodynamic dosing*. The high-volume, rapid dose of plasmid DNA is delivered via the tail vein and is capable of mediating high levels of transgene expression in the liver. Above, we see a color-map overlay indicating luciferase expression in the liver as detected by bioluminescence imaging.

fenestrae and generation of transient pores in liver hepatocytes[62] by which DNA can extravasate from the hepatic circulation. Less is known about the intracellular mechanism on DNA trafficking following HD dosing though one notable response is the formation of massive endocytic vesicles[63]. This type of dose is surprisingly well-tolerated as the irregularity of heart function, sharp increase in venous pressure, enlargement of liver fenestrae, and enhancement of membrane permeability of the hepatocytes are all transient events[62]. There are many applications for this method as a research tool and potentially as a therapeutic form of non-viral gene delivery[64,65].

When coupled with HD dosing of luciferase-expression pDNA (pGL3), HD-BLI provides a quantitative assay to be used as a benchmark to compare against other methods of non-viral gene transfer[66]. The detection of luciferase in the liver following HD dosing of pGL3 is linear over 5 orders of magnitude in a dose-dependent fashion. Both Wolff and Liu and co-workers[59,60] have independently determined that a 5 μg dose of pGL3 delivered hydrodynamically produced a "therapeutic" level of transgene product at 24 hrs in the liver . Similarly, following hydrodynamic dosing of a 5 μg DNA dose, therapeutic levels of secreted factor VIII or IX were produced in hemophilic mice[67]. The expression achieved following hydrodynamic dosing of a 5 μg dose is also a reasonable efficiency benchmark toward achieving efficacy from a calculated scaled-up dose of 1-2 mg of DNA delivered to humans via a more conventional and pharmaceutically elegant delivery method. Based on these considerations, BLI detection 24 hours following a HD dose of 5 μg of DNA encoding luciferase may serve as a benchmark standard to which many systemically delivered non-viral systems could be compared. Similar in vivo benchmarks based on luciferase expression and BLI may also be developed to calibrate the expression in other tissues such as muscle, lung or tumors.

Intramuscular Dosing and Electroporation

Electroporation (EP) or elctropermeabilization (as may be a more accurately descriptive term since "pores" have never actually been visualized[68]) is an effective means to transfer DNA and other hydrophilic macromolecules across the plasma membrane. Like HD dosing, this is a safe and efficient physical method for delivering pDNA. EP is typically used following intramuscular (IM) dosing to increase expression, but the delivery technique is also used in liver[69], lung[70] and tumor tissues[71]. The most notable use of EP is in clinical trials where there has been much success in treating malignant melanomas with plasmids encoding Interleukin-12[72].

The physical principle behind the mechanism of electroporation is that an electric field of sufficient intensity is applied to a tissue which induces position-dependent change in the resting membrane potential[68]. This leads to membrane destabilization and transient permeabilization. The electric field also induces movement of charged molecules like DNA. This phenomenon drives extracellular DNA into cells that lie within the electric field. Parameters have been optimized for delivery of DNA by EP following an IM dose[73].

siRNA-Mediated Knockdown In Vivo

RNA interference (RNAi) is an endogenous defense mechanism conserved through most eukaryotic organisms including mammals[74]. The phenomenon involves 21-23 nucleotide double-stranded RNA that combines with RNAi-associated enzymes to target and degrade mRNA in a sequence-specific manner. The discovery of siRNA[2] and other RNA-based mechanisms that modulate protein expression has significantly altered the understanding of the central dogma to biology. No longer can the linear progression of transcription→translation→protein expression be described in such a simple form. It is now well-understood that RNAs play an important role in regulation at the post-transcriptional level. Micro RNA (miRNA) operates via an endogenous process that

affords regulation of mRNAs via site-specific binding in the 3'-untranslated region. It is thought that miRNAs prevent assembly of translational proteins, but the mechanism of action is not yet completely known. Conversely, the mechanism of siRNA is more completely understood (Figure 1-7). A 21-nucleotide sequence is site-specifically bound to mRNA through the RNA-induced silencing complex (RISC). In complex with RISC, siRNA has a permanent effect on mRNA by triggering strand cleavage by nuclease activity of RISC.[75]

Short-hairpin RNA (shRNA) is named based on the structure of this single strand of ~80 nucleotide bases that exhibits intramolecular base-pairing. shRNA is a predecessor to the 21-nucleotide siRNA and this type of RNA is unique in that it can be expressed in a plasmid-based system. Further intracellular processing is required to produce the functional molecule form shRNA as Dicer (Figure 1-7) cleaves hairpin to yield siRNA.

Clinical applications for RNAi-based therapies abound. Virtually any disease state that is dependent on activity from 1 to a few genes is a candidate for this type of therapy. As in non-viral gene therapy and the delivery of pDNA, the major battle for clinical success of RNAi-based therapeutics is achieving successful delivery. Advances have recently been made in this regard[76,77]; however, attaining in vivo efficacy in the absence of a fully formulated dose for systemic delivery can allow for key proof-of-principle experiments to be conducted. HD dosing of RNAi vectors targeting luciferase has been shown to enable the observation of in vivo knockdown by BLI[78].

Nuclear Targeting

Background

As the previous discussion has detailed, non-viral gene therapy is generally focused on overcoming barriers that inhibit cellular trafficking of polyplexed pDNA (i.e., pDNA that is condensed or electrostatically bound by cationic molecules to form sub-

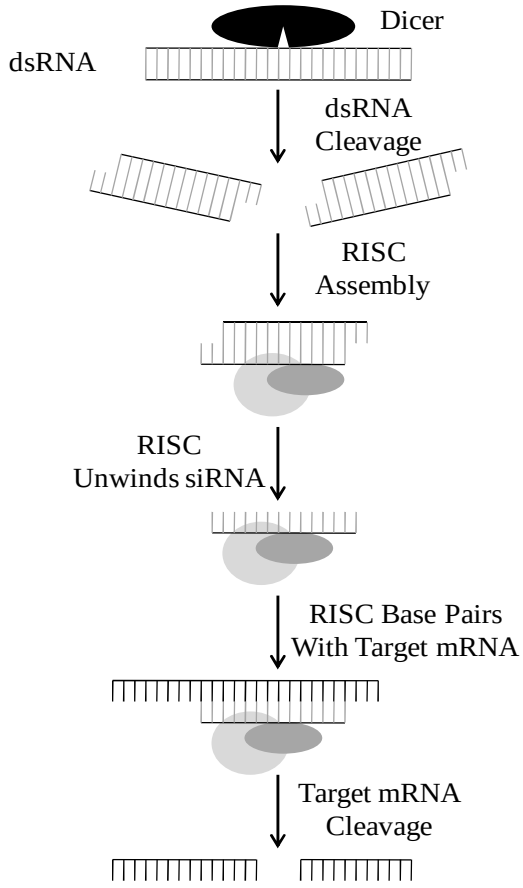

Figure 1-7. *Molecular mechanism of siRNA*. Knockdown of protein expression can be triggered by introducing double-stranded RNA (21-23 nucleotides in length). Above is a general diagram of Dicer-mediated cleavage of dsRNA to yield siRNA, RISC assembly and mRNA cleavage.

micron particles). Non-viral vectors are recognized as foreign to the cell, so endogenous defenses are in direct opposition to the goals of non-viral gene delivery. In contrast to a non-viral vector, a virus has a tremendous ability circumvent these barriers and target DNA to the nucleus[79,80]. This phenomenon is well-documented, and despite significant drawbacks as therapeutics, much research has focused on viral vectors because of their efficiency. The following sections will address background and considerations regarding potential non-viral nuclear targeting agents. The discussion is directed from the point at

which cytoplasmic delivery is achieved, so as to narrow the focus of this section to the considerations involved in targeting non-viral vectors to the nucleus. (Figure 1-4)

Nuclear targeting remains a formidable barrier in the race to optimize the efficiency of non-viral vectors. The magnitude of this barrier is has been quantified through micro-injection studies. It was discovered that less than 1% of gold-labeled pDNA microinjected into the cytosol actually reaches the nucleus[81]. This result suggests the potential for a great increase in transgene expression (> 100-fold) if a non-viral vector can maximize nuclear deliver of polyplexed pDNA. Unfortunately, current synthetic methods applied toward nuclear targeting of a non-viral vector have been largely unsuccessful.

Two scientists in the field of non-viral nuclear targeting have verbalized their thoughts on the challenges associated with this task. John Wolff, Professor of Pediatrics and Medical Genetics at the University of Wisconsin-Madison, gave an apt description to this issue when he referred to nuclear targeting as the "grand problem" facing the non-viral gene therapy community[82]. The challenge is "grand" in its inherent difficulty, the scale of effort directed in this area and the potential therapeutic advantages. "Grand" also describes the steps toward therapeutic relevance if a significant advancement is made in the area of nuclear targeting.

David Jans, Director of the Nuclear Signaling Laboratory, Monash University, Australia, cites a lack of nuclear targeting capability as "the major limitation of non-viral gene transfer"[83]. Jans and others are conducting basic research that is focused on defining the endogenous mechanism of nuclear signaling. The aim of this research is to develop an understanding of the nuclear transport pathway used by nuclear-targeted proteins and subsequently apply this information to improving non-viral vectors. Nuclear signaling, from a molecular biology perspective, provides a foundation upon which advances in non-viral nuclear targeting can be built.

Molecular Mechanism

Success of targeting a non-viral vector to the nucleus depends directly on the ability of the vector to take advantage of cellular processes. The aim is to hijack the endogenous mechanism that traffics proteins to the nucleus. This involves introducing a non-viral vector that is directly shuttled across the nuclear-envelope (NE) via the NPC, to the nuceoplasmic space.

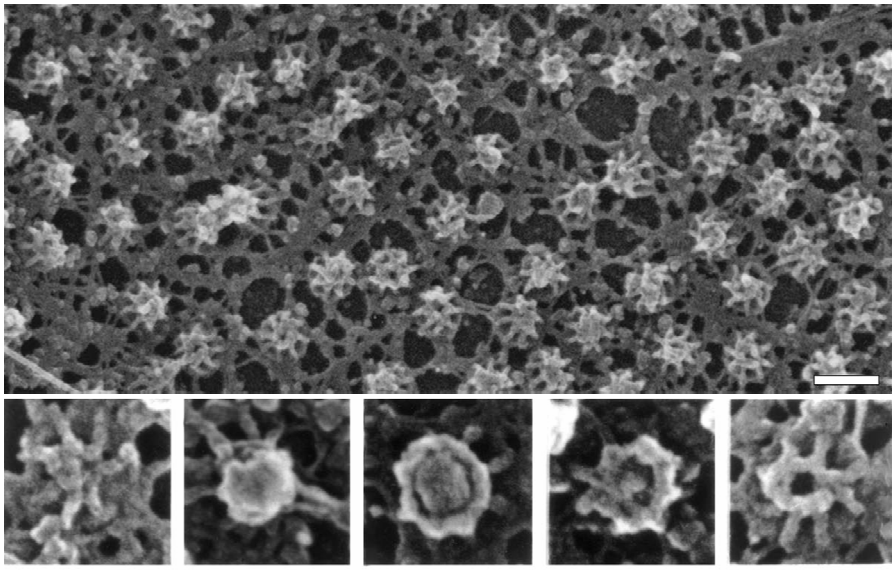

Figure 1-8. *The nuclear face of the nuclear envelope*. Electron microscopy of the nuclear side of the nuclear membrane displays the uniform appearance of NPCs on the nuclear envelope. Figures below are of individual NPCs in varying configurations. (Scale bar, 100 nm) (Re-printed with permissions from Elsevier)

The nucleus is physically defined by the NE which separates the nucleoplasm and genetic material from the cytoplasm in eukaryotic cells. The outer membrane is continuous with the rough endoplasmic reticulum which plays a role in protein biosynthesis. The NE is approximately 150 nm thick and the two membranes are fused by the envelope-spanning NPCs. Each NPC is comprised of about thirty proteins, or

nucleoporins, that collectively allow for passive diffusion of ions and molecules less than 40 nm in diameter and active transport of macromolecules that contain an NLS. NPCs are prevalent on the nuclei of mammalian cells, and give a dimpled appearance when observed under a transmission electron microscope (Figure 1-8).

Structurally, EM images of the NPC demonstrate that it contains 8 membrane-spanning spokes that have both cytoplasmic and nuclear filaments. Each NPC exhibits symmetry in the plane of the NE, and despite differences in size, the overall NPC structure is largely conserved from yeast to vertebrates. The NE and NPC jointly function to regulate cyto-nuclear translocation and protect the genetic material contained within the nucleus.

NPCs allow passive diffusion of ions and small molecules. A recent publication supports the widely held belief that a NPC can accommodate cargo as large as 40 nm in diameter[84]. Likewise, this study highlights the notion that NPCs are plastic, and their conformation is dependent on movable nucleoporins – a result of the demands of the nuclear import cargo[85]. Larger macromolecules that contain a nuclear localizing sequence (NLS) of amino acids can pass through the NPC by chaperone proteins in an energy-dependent manner. Lusk and co-workers have defined a set of rules for nuclear import. Among them is the suggestion that proteins >25 kDa and contain an NLS that has a strong affinity for NPC-related proteins, may traverse the NE[86]. Additionally, Jans recognizes that macromolecules >40nm in diameter require an NLS in order to undergo cyto-nuclear transport, and 150 nm is the upper-limit for cytonuclear translocation[87]. Each NPC can mediate as many as 1,000 translocations per second. Key components to this efficient trafficking are NLS-recognition proteins (Importin-α and Importin-β) that create a functional interaction between NLS-containing cargo and the pore-lining nucleoporins of the NPC.

In the classic pathway, NLS-containing proteins are recognized and chaperoned to the nucleus via cytosolic proteins. In the presence of the classic NLS sequence, a series of

negatively-charged residues on Importin-α interact with Lys and Arg residues. As a result of this interaction with NLS, a conformational change of Importin-α exposes the Importin-β binding (IBB) domain. As the name implies, the IBB domain is recognized by Importin-β, which subsequently binds to form the ternary complex (NLS/Importin-α/Importin-β) for nuclear transport. Importin-β is the component that is responsible for directing translocation through the NPC.

The pore is lined with several nucleoporins that contain Phe-Gly repeats with side chains projecting toward the lumen of the pore. Importin-β has transient affinity for these FG regions which is hypothesized to be sufficient to direct the ternary complex through the NPC. The specific mechanism of transport across the NPC remains to be elucidated, but there are a number of models that have been put forth. In the "sequential binding" and "gated-complex" models, cargo is first bound to cytoplasmic filaments and then to Phe-Gly repeats that line the pore[88,89]. This draws Importin-β in the nuclear direction. The "molecular sieve" model predicts that the hydrophobic residues in the channel are an interconnected network that forms a size-exclusion "gel" and restricts the passage of molecules that are greater than 40 nm[90]. The hypotheses put forth in these models do not appear to be mutually exclusive, or necessarily in conflict, so the actual mechanism likely combines the positive aspects identified in these proposed systems.

The nuclear import machinery (Importin-α and Importin-β) is recycled after the complex has traversed the nuclear envelope. RanGTP binds Imp-β and triggers dissociation of the complex. There is some overlap between the IBB domain and the RanGTP binding site, so the Importin-α/β interaction is disrupted. RanGTP is a nuclear localized form of Ran, and the RanGTP-triggered dissociation effectively removes the ternary import complex from the nucleus, so nuclear-directed flow of other ternary complexes follows Le Chatelier's Principle of dynamic equilibrium. Nucleoporin-50, a nuclear filament of NPC has been implicated in dissociating Importin-α from the cargo. RanGTP and CAS (cellular apoptosis susceptibility protein) subsequently bind Importin-

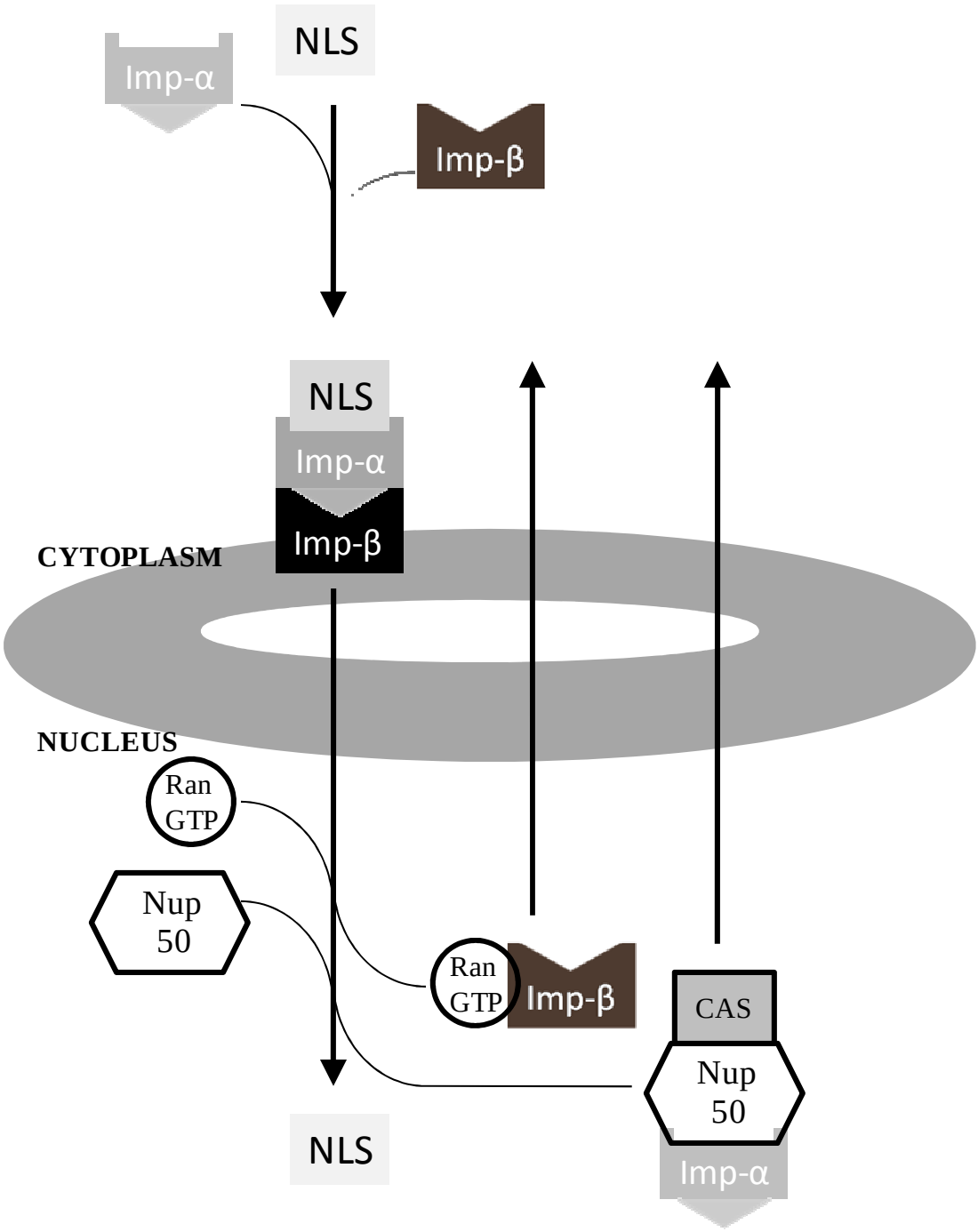

Figure 1-9. *Molecular mechanism of nuclear import*. The NPC enables cytonuclear translocation. This is accomplished by shuttling of accessory proteins that maintain the directionality of the flow of NLS-containing cargo.

α and shuttle it to the cytoplasm. The various phosphorylation states of Ran obviously play an important role in the directionality of this process. RanGTP is maintained in high nuclear concentration by RanGEF (GDP-GTP exchange factor); whereas, RanGDP is the cytosolic form and RanGAP (GTPase activating protein) dephosphorylates RanGTP to trigger cytoplasmic dissociation from Importin-β (Figure 1-9). The constant cycling of importins maintains the players in the process at the appropriate concentrations in their functional locations.

Dozens of gene therapy groups have taken-on nuclear targeting strategies by attempting to incorporate a peptide-based NLS into an otherwise polyplexed DNA. Based on the discussion of the molecular mechanism, it is apparent that this is an efficient and relatively unsaturable process with an achievable rate of 1,000 translocations per second per NPC and thousands of NPCs per nuclei[91]. In vitro experiments have displayed varying degrees of success, but there have not been any significant examples of NLS-mediated increases in gene transfer efficiency in vivo. Throughout the following paragraphs, we will review and comment on the existing work in the literature that specifically addresses increasing nuclear uptake of DNA.

Nuclear Localizing Sequences applied to Non-Viral Vectors

.In the early 1980's there was a significant report that identified a particular amino acid sequence of the simian virus 40 (SV40) large-T antigen as necessary and sufficient to increase nuclear targeting of the antigen[92]. This polycationic sequence (^{126}P-K-K-K-R-K-V^{132}) is known as the classic NLS that is most widely used in non-viral systems. The native sequence of targets the protein to the nucleus, but a point mutation, discovered by mixed oligonucleotide mutagenesis, resulted in ^{128}Lys→Thr mutation and cytoplasmic localization of the protein. In addition, deletion of any amino acids in the (^{127}K-K-K-R-K^{131}) sequence results in a cytoplasmic antigen[92].

Variations and extensions of the classic sequence are prevalent in endogenous nuclear localizing proteins. The SV40 NLS has been used in many forms, and still other unrelated NLS sequences have been applied to non-viral delivery vectors. There is great variability to the way in which these NLS peptides are incorporated into non-viral systems – all with the goal of enabling nuclear uptake and increasing transgene expression.

Proteins, Histones and DNA Sequences in Nuclear Targeting

In typical cell processing, whole proteins are the functional units that undergo cytonuclear transport if they contain an NLS. There are several examples of different classes of nuclear localizing proteins that have been incorporated into non-viral gene delivery vectors. Viral proteins such as the major core protein VII from adenovirus and viral protein R of HIV-1 both contain cationic regions that bind DNA; however, both have only shown utility in increasing the amount of DNA associated with the nuclear fraction rather than data supporting nuclear internalization. Histones have an inherent ability to bind and condense DNA, protect it from nuclease digestion and target the nucleus, so they are attractive components to a delivery system. Most work has concentrated on incorporating the H1 linker histone. Finally, transcription factors also have a DNA binding region and translocate to the nucleus. Much work has been done with the yeast protein GAL4 including appending the SV40 NLS peptide via a poly-lysine linker to achieve nuclear targeting.

Transcription factor binding is the basis for a similar strategy in which the "NLS" is introduced at the level of the DNA sequence. The DNA sequence of the SV40 enhancer (not to be confused with the above-described SV40 amino acid sequence) has been shown to contain a 72-bp element that mediates increase in nuclear targeting and gene expression[93]. Transcription factors ubiquitously bind this 72-bp element and

mediate nuclear transport via the classic Importin-α/β pathway. This strategy has been shown to be effective in vivo by both increasing nuclear uptake and mediating a 40-fold increase in gene expression over plasmids that lacked the critical SV40 enhancer sequence[46].

NLS Peptides: Non-Covalent Interactions

Due to the polycationic nature of the classic NLS, these peptides inherently interact with the polyanionic backbone of DNA via electrostatics. However, the short run of cationic residues needs to be extended or otherwise modified to enable sufficient charge-based interaction that will condense the peptide-DNA polyplex to a reasonable particle size. DNA-binding peptides like the viral peptide mu (MRRAHHRRRRASHRR-MRGG)[94], s-protamine (R_6WGR_6), l-protamine ($R_4SR_6FGR_6VWR_4$)[95], and poly-l-lysine[96] have been used in various strategies to bind the classic NLS from the SV40 Large T-Antigen to DNA by ionic interactions. Additionally, Rosenecker and co-workers synthesized "NLSV404" (PKKKRKVGPKKKRKVGPKKKRKVGPKKKRKVGC) in which 4 consecutive NLS peptides were linked to provide for condensation of pDNA[97]. Bremner et al, used a similar approach with varying NLS sequences to form peptide-pDNA polyplexes[45]. In addition to an extended form of the SV40 T-antigen (SSDDEATADSQHSTPPKKKRKVEDPYC), the group also incorporated a nuclear targeting peptide derived from the human T-cell leukemia virus (MPKTRRRPRRSQRK-RPPTPWAHFPGFGQSLC), and a non-classical sequence from heterogeneous ribonuclearprotein A1 (GNQSSNFGPMKGGNFGGRSSGPYGGGGQYFAKPRNQ-GGYC), known as M9.

Results from these experiments mostly showed modest increases in gene expression and affinity for importin-α. The most significant finding was from NLSV404 polyplexes. This peptide demonstrated a 100-fold increase in transaction efficiency as compared to "controlNLSV404" when tested in vitro. In general, the route of electrostatic

interaction and the formation of peptide-pDNA polyplexes can be applied to any plasmid, but it raises a question regarding ligand presentation as related to DNA affinity. That is, the NLS may not be readily available for importin-α to bind because it can not recognize NLS when electrostatically bound to the polyplex.

Peptide nucleic acids (PNAs) simulate oligonucleotides, but contain a backbone of amide linkages which affords PNA/DNA base pairing that has a higher T_m than DNA/DNA[98]. The PNA backbone has does not introduce charge repulsion as it lacks a polyanionic phosphate backbone. Thus, PNAs can be directed to bind a specific sequence in single-stranded or dsDNA with high affinity to form triple-stranded complexes[99]. This site-specific "clamp" has been used to selectively attach an NLS to pDNA. One drawback of the PNA clamp is that the pDNA cargo is required to be engineered to contain a specific target sequence. The method cannot be universally applied without some preliminary efforts in molecular genetics. On the other hand, the number of PNA-NLS attachments on a given plasmid can be precisely controlled, and there is not an issue of the clamp binding in the coding region of the transgene to adversely affect transcription. In his survey comparing the electrostatic binding of NLS versus PNA-clamp attachment, Seymour incorporated the same sequences (extended SV40, HTLC, and M9) as are discussed above[45]. Smith and co-workers identified a similar strategy of attaching the classic SV40 NLS to a PNA clamp[100], but they synthesized the PNA-linker-NLS linearly on solid support using standard Fmoc chemistry. Seymour used maleamide coupling via the Cys-terminated peptides. In each case, nuclear uptake and transgene expression increased only up to 8-fold.

Two other methods that rely on sequence-specific, non-covalent binding of an NLS to plasmid DNA have been applied. In the first case, John Wolff and co-workers introduced a nucleotide base, modified with biotin, to linear dsDNA[101]. They subsequently coupled extended SV40 to strepavidin to enable the high-affinity interaction. Roulon et al, coupled NLS to pDNA in an impressive display of bioconjugate

chemistry[102]. A short hairpin of DNA is designed of site-specific interaction with double-stranded pDNA to form a triple-helix "padlock". The short oligomer is contains a "sticky-end" overhang to which another short hairpin can base-pair and be ligated in the presence DNA ligase. The second DNA oligomer was previously functionalized with an NLS, so the ligation process introduces the peptide of interest to the triple-helix complex. Both approaches are intriguing at the level of their bioconjugate chemistry; however, the SA-biotin-NLS approach did not put forward any quantitative measures of improved nuclear uptake or expression, and the triple-helix padlock showed no advantage over relevant controls.

Intercalating agents bind to double-stranded DNA based on the planar orientation of these polyaromatic molecules. Acridine is a small molecule intercalating agent that has been coupled to NLS in order to randomly "decorate" pDNA with the peptides of interest. At the forefront of this approach, Nielson and co-workers have synthesized bis- and tris-acridine analogs of NLS which they show to have sub-nanomolar affinity for plasmid DNA[103]. Along the same lines, Boulanger et al, use a strategy of coupling acridine to NLS via a hydrocarbon spacer/maleamide linkage[104]. In both cases, Acr-NLS-pDNA is subsequently polyplexed with PEI or lipofectamine, respectively for in vitro studies. Nielson was able to demonstrate a >20-fold increase in gene expression with the tris-acridine compared to PEI-pDNA delivery. Alternatively, work from the Vierling group was not successful in demonstrating either increased uptake or increased gene expression.

Finally, NLS has been conjugated to PEI (a well-known DNA-condensing dendrimer). This strategy has been broadly applied in gene therapy in the sense that many gene-therapy related ligands (i.e., cell type-specific ligand, endosomal-lytic agent, or NLS) have been incorporated in this way. Often, this strategy is much more effective in vitro than in vivo because the relative concentration of PEI can be controlled and dendrimer toxicity is less problematic. In this example of NLS-PEI, Seymour and co-

workers modified PEI to contain free thiol functionalities[105]. They then directed the formation of disulfide linkages between PEI-SH and thiol-containing viral hexon, which is known to have nuclear targeting capability. The hexon-modified PEI gave a 10-fold increase in gene expression compared to PEI alone and to albumin-modified PEI.

NLS Peptides: Covalent Interactions

Covalent labeling of DNA with an NLS peptide ensures that the peptide-DNA complex will move as one unit throughout the cellular trafficking process. This may be quite an advantage to keep the ligand and cargo in tact as it traverses the cytoplasmic milieu. However, the effect that one or several covalent modifications will have once the DNA reaches the nucleus is a legitimate question. Wils and Sherman have provided the greatest focus in this area, and they believe that the covalent interaction is quite important to ensure nuclear delivery of the ligand *and* its cargo. Their research has yielded two methods to label pDNA via photo-activatable chemistry. The first is sequence-specific labeling in which they introduce a psoralen-oligonucleotide-NLS conjugate to capitalize on the triple-helix formation, and lock the ligand into place with DNA adducted by the photoactivated psoralen. Their second approach is a random labeling method in which NLS, coupled to p-azidotetrafluorobenzoate via a rhodamine liner is photoactivated reacts with nucleophilic functional groups on DNA[106]. Using the random labeling method, they were able to couple both the classic SV40 sequence as well as the 62-amino acid importin-β binding domain to plasmid DNA. The Tamagaki group incorporated PEG (3400 MW) as a “stealthing” ligand and coupled the PEG-NLS to pDNA via diazocoupling, in another iteration of random modifications[107].

One of the most-noted manuscripts in nuclear targeting of non-viral vectors appeared in PNAS in 1999 and came from work in the laboratory of J.P. Behr[108]. Behr is otherwise notable for first using PEI as a condensing agent for pDNA transfections because it served the dual function of condensing DNA and buffering the endosome with

its protonatable 2^{o} amines. In the NLS arena, Behr reported an enhancement in gene transfer (via optimized nuclear targeting) of up to 10,000-fold! Their approach was unique in that they linearized the cDNA of luciferase, end-capped with hairpin oligomers, and introduced a single NLS (classic SV40 sequence) via a modified nucleotide base on one of the end-capping fragments. Their conclusions and discussion argue that more than one NLS attached to DNA will induce a "tug-of-war" between adjacent NPCs that recognize multiple NLSs on the same DNA and initiate nuclear transport in competing directions. Work done by van der Aa et al, in 2005 was an attempt to recapitulate the work done by Behr, but they did not successfully reproduce any of the grand observations of improved transgene expression via the linear DNA/end-capping NLS method[109]. The Harashima lab also repeated the study and specifically addressed the issue of one versus two NLS peptides incorporated into the endcaps of linear DNA[110]. Likewise, their results were similar to that of the Crommelin group. They observed no difference in expression based on the number of NLSs used, but did conclude that NLS attachment of any kind only served to inhibit nuclear uptake.

While pursuing the delivery of linear, double-stranded DNA discussed above, Crommelin and co-workers also reported on the nuclear localization of the cDNA containing a nuclear localization sequence introduced by way of modified PCR primers[109]. The 3' primer was conjugated to a classic NLS peptide. Extension of the luciferase cDNA from the 3'-primer resulted in the biosynthesize of both the sense and anitsense strand of linearized DNA. These products were subsequently annealed so as to deliver the linear, double-stranded DNA. This strategy did not improve the transfection efficiency of DNA when delivered by cationic polymers.

Statement of the Problem

It is evident that viral gene transfer far outpaces that of non-viral gene delivery vectors. A significant portion of this gap could be covered if a non-viral vector could be

engineered to efficiently deliver a functional payload to the nucleus. The above literature review identifies several approaches to NLS-mediated nuclear targeting. Unfortunately, there is no clear direction for a vector or experimental design that consistently leads to a significant increase in transgene expression. There are examples of research groups independently designing similar vectors, only to observe quite different results. In addition, independent reproductions of successful approaches have not been consistent with the original findings. However, the worthiness of this goal has been elevated by the availability of many new gene therapeutic targets provided by the human genome project and most recently by the discovery of siRNA

In light of the perceived challenge of research in this area, we define the reasons for choosing a photo-labeling approach to covalently attach an NLS peptide to pDNA. First, as a covalent adduct to pDNA, the NLS will be labeled onto the plasmid throughout intracellular trafficking. Much concern surrounding non-covalent methods is that the NLS is sloughed-off in this process. Free NLS in the cytosol would be of no advantage in improving nuclear uptake of the plasmid. Second, this is a universal method to coupling a peptide to DNA. Regarding the peptide, the photo-label can be coupled to the N-terminus of any peptide to allow for covalent labeling. Since the labeling method is random, there is not a specific sequence of DNA that has to be cloned into a plasmid. Any nucleotide sequence can be covalently labeled by this method. Third, coupling 4-azido-2,3,5,6-tetrafluorobenzoate to the N-terminus of the peptide is very amenable to SPPS. The photo-label is used just as any amino acid monomer and coupled by DIC/HOBt methods.

The over-arching goal for developing a nuclear localizing ligand for non-viral gene delivery is that this will come together in a systemically dosable therapeutic with primary and secondary targeting characteristics built-in, as well. Rather than test the nuclear localizing properties systemically and introduce more complexity to the system, we explored hydrodynamic delivery to the liver and intramuscular dose followed by electroporation. Both physical methods of delivery allow us to skirt some key barriers

associated with the systemic delivery. We felt that these assays provided us the opportunity to design and execute meaningful proof-of-principle experiments. We used in vitro experiments to guide our focus and define key parameters and used in vivo dosing methods coupled with bioluminescence imaging in an attempt to identify NLS-mediated increases in non-viral gene expression– a milestone in the field that has yet to be achieved.

CHAPTER 2

HYDRODYNAMIC DOSING AND BIOLUMINESCENT IMAGING: QUANTITATIVE IN VIVO LUCIFERASE EXPRESSION

Abstract

Bioluminescent imaging (BLI) is a widely used in vivo method to determine the location and relative intensity of luciferase expression in mice. Luciferase expression is observed following an IP. dose of D-luciferin, resulting in bioluminescence that is detected in anesthetized mice by a charge-coupled device (CCD) camera. To establish if BLI could be used as a quantitative measurement of luciferase expression, precise quantities of plasmid DNA (pDNA) encoding the luciferase gene were hydrodynamically (HD) dosed in mice. The results established a linear correlation between the DNA dose and bioluminescent response measured in liver which spanned 5-orders of magnitude. The level of luciferase expression was found to be a direct function of D-luciferin dose. The time course of luciferase expression, as well as the influence of multi-dosing of substrate, were measured by BLI. The recovery of luciferase from the liver of HD dosed mice allowed calibration of the BLI measurements. Repeat dosing on successive days demonstrated detectable luciferase expression through 8 days following the HD dose. The results establish BLI's limit-of-detection of 20 pg of luciferase per liver following a HD dose of 100 pg of pDNA. The primary advantages of using quantitative BLI in mouse liver and muscle are the sensitivity of the assay, the speed and ease of making measurements, the precision and linearity of the dose-response curves and the ability to conduct serial sampling of gene expression over many days or months while eliminating the need to euthanize animals. These results demonstrate that BLI is both sensitive in detection of bioluminescence and linear in its responses. This imaging modality coupled with HD dosing should allow for the direct comparison of the efficiency of gene transfer vectors that target the liver

Introduction

In vivo bioluminescent imaging is a method to non-invasively measure luciferase expression in animals. The method involves the expression of luciferase in mice followed by an IP dose of D-luciferin and subsequent imaging of the bioluminescence in anesthetized animals by a cooled CCD camera. This imaging modality has been used broadly in the examination of molecular processes due to its technical simplicity in quantifying photons emitted by the enzyme-catalyzed, chemiluminescent reaction. Specifically, BLI has been used to study tumor metastasis [111113], monitor potential anti-cancer therapies [114], evaluate novel antibiotics [115,116], measure tissue regeneration [117,118] and detect protein-protein interactions [119]. Although BLI has been broadly applied, its use as a quantitative method has not been validated.

Unlike in vitro gene transfer in which PEI-mediated gene delivery of pGL3 (a plasmid encoding luciferase) is a reliable benchmark for expression, in vivo gene transfer has no common standard of potent expression to act as a reliable benchmark. An understanding of the relative transfection efficiency is especially important when using luciferase as a reporter gene because of its exquisite sensitivity of detection and the lack of assay calibration by many labs. This often leads to the interpretation of small, almost negligible number of relative light units (RLUs) detected and cited as significant levels of expression.

BLI is also widely used in gene therapy and accepted as the most definitive method to detect transgene expression in vivo. This is primarily because BLI is fast, sensitive, and free of false positives [120]. Gene transfer studies of both viral and non-viral vectors have used BLI to measure relative transfection efficiencies *in vivo* [121124]. Although BLI has been used to compare different gene delivery methods, the linearity in response, the calibration with respect to luciferase expression, and the limit of detection have not been determined. Numerous factors can contribute to a non-linear BLI response

such as the tissue expressing luciferase, light scattering effects, and the biodistribution of D-luciferin in mice.

In the present study, we have validated BLI for linear response, limit of detection and quantity of luciferase expression for liver-targeted non-viral gene delivery. This study utilized the well-established technique of hydrodynamic dosing of pDNA [125,126] to selectively mediate luciferase expression in the liver of mice. The results presented establish that BLI produces a linear response over 5-orders of magnitude. The limit of detection is on the order of 20 pg of luciferase, which is equivalent to the limit of detection using much more laborious methods to measure luciferase in liver homogenates. Not surprisingly, the D-luciferin dose and the time of acquisition following substrate dosing both influence the magnitude of the bioluminescent response. The results of the study establish BLI as a quantitative, robust method for measuring luciferase expression following hydrodynamic dosing. The study also revealed a surprising result in which as little as 100 pg of plasmid DNA produced measurable luciferase expression.

Materials and Methods

Plasmid (pGL3 Control) encoding a luciferase reporter gene and driven by an SV40 promoter and enhancer was purchased from Promega (Madison, WI). The plasmid was grown in *E. coli* and purified by a Qiagen prep kit (Valencia, CA). Male ICR mice (15 - 20 g) were purchased from Harlan (Indianapolis, IN). D-Luciferin, was purchased from Gold Biotechnology (St. Louis, MO) and ATP and luciferase were purchased from Roche Applied Science (Indianapolis, IN).

Hydrodynamic Dosing pGL3.

Plasmid DNA (100 pg – 5 μg) was prepared in normal saline corresponding to 9 wt/vol % of the mouse's body weight (1.35 – 2.25 ml). The DNA dose was administered by tail vein to triplicate mice in 5 sec according to a published procedure [125,126]. At 24 hrs, mice were dosed intraperitoneally with 80 μl of D-luciferin (30 μg/μl in phosphate-

buffered saline), anesthetized by 3% isofluorane, and then imaged for bioluminescence by the IVIS Imaging 100 Series (Xenogen). BLI was performed in a light-tight chamber on a temperature-controlled, adjustable stage while 2% isofluorane was administered by a gas manifold. Images were acquired at a 'medium' binning level and a 20 cm field of view. Acquisition times were varied (1 sec - 1 min) depending on the intensity of the luminescence. The Xenogen system reported bioluminescence as photons/sec/cm^2/steradian in a 2.86 cm diameter region of interest covering the liver.

Time Course of Bioluminescence: Single Dose of D-Luciferin

Mice were hydrodynamically dosed in triplicate with 0.001, 0.01, 0.1 or 1 μg pGL3. After 24 hrs, an IP injection of 2.4 mg of D-luciferin was administered, and mice were imaged for bioluminescence after 4 min. To establish the time course of bioluminescence, measurements were continued at 7 min intervals for 60 min. To examine the effect of repeated D-luciferin dosing, mice were hydrodynamically dosed with 0.1 μg pGL3. After 24 hrs, mice were repeat-dosed with 2.4 mg of D-luciferin at time 0, 20, and 40 min, and bioluminescent images were continually acquired in 7 min intervals over 60 min.

Duration (in Days) of Detectable Luciferase Expression in the Liver

Mice were monitored over a period of days to determine the time course of luciferase expression that resulted in an observable bioluminescent response. Mice (n=3) were HD dosed with 1 μg of pGL3. After 24 hours, they were dosed IP with 2.4 mg (80 ul) of D-luciferin, anesthetized and imaged 4 min following substrate dose. The imaging procedure was repeated on successive days until photon flux values within the regions of interest were reduced to background levels. Image acquisition times ranged from 5 sec to 2 min, depending on the intensity of the bioluminescent response.

Dose-Response of pGL3 and D-Luciferin

The bioluminescent response was measured following hydrodynamic dosing with 100 pg - 5 μg of pGL3. At 24 hrs, D-luciferin (2.4 mg in 80 μl of PBS) was injected IP and images were acquired after 4 min. Acquisition times ranged from 1 sec for the 5 μg dose (to avoid pixel saturation) to 1 min for the 100 pg dose (to allow sufficient collection of photons to generate a color-map overlay).

Mice were hydrodynamically dosed with 0.1 μg of pGL3 and after 24 hrs were IP injected with either 0.0024, 0.024, 0.24, or 2.4 mg of D-luciferin in 80 μl of PBS. Bioluminescent images were acquired for 10 - 60 sec at 4 min post D-luciferin injection.

Measurement of Luciferase in Mouse Liver Homogenates

Mice were hydrodynamically dosed in triplicate with 100 pg – 5 μg pGL3 and imaged at 24 hrs as described above. Animals were then euthanized by cervical dislocation following an IP dose of 0.2 ml of ketamine/xylazine (20 mg/ml and 2 mg/ml, respectively). The liver was collected, immediately frozen in liquid nitrogen, and stored at -70°C. Livers were processed into a powder by adding dry ice and grinding the tissue using a mortar and pestle. Liver powders were combined with 500 μl of lysis buffer (Tris·HCl 25 mM, $MgCl_2$ 8 mM, EDTA 1 mM, 1 w/v% Triton-X 100, pH 7.8) per gram of liver, vortexed for 5 min, freeze-thawed three times and centrifuged for 3 min at 10,000 x *g*. The supernatant was recovered, tissue was re-suspended in 500 μl of lysis buffer per gram of pellet, and centrifuged as described above. The supernatants were combined and stored frozen at -70°C until assayed for luciferase.

The supernatant (100 μl) was combined with 300 μl of lysis buffer, 4.3 μl of ATP (165 mM), and 100 μl of D-luciferin (14 μg) injected automatically at the moment of analysis. The relative light units were measured over 10 sec on a Lumat LB 9501 from Berthold (Oak Ridge, TN). A standard curve was constructed by adding known quantities

of luciferase to mouse liver homogenate from untreated mice, followed by processing as described above.

Results

In vivo bioluminescence measurements are widely used to measure the location and the relative degree of luciferase expression. The intensity of bioluminescence should be proportional to the amount of luciferase assuming that D-luciferin and ATP are available at consistent levels from mouse to mouse. To validate this method for quantitative analysis of luciferase, we determined the bioluminescent readout in relation to the amount of luciferase present in mouse liver, the dose of D-luciferin, and the time of bioluminescent acquisition.

Mice were hydrodynamically dosed with 0.1 μg of pGL3 and subsequently treated with a varying dose of D-luciferin. This resulted in a linear dose-response relationship that spans three orders of magnitude (Figure 2-1) with the highest dose of D-luciferin yielding a mean photon flux of ~10^8 photons/sec/cm^2/steradian. A linear relationship was determined for D-luciferin dose and bioluminescent response down to a minimal substrate dose of 2.4 mg. Even at this small dose of D-luciferin, the photon flux was > 10^5 photons/sec/cm^2/steradian. The limit of detection (1.16 x 10^5 photons/sec/cm^2/steradian) was determined by calculating the photon flux in liver of naïve mice following D-luciferin administration (not shown).

To establish whether the bioluminescent intensity following a single dose of D-luciferin is also a function of time, photon flux was detected at 7 min intervals. The results indicate a linear decrease by 1 log unit over 60 min (Figure 2-2). This decline in response over time was observed at a pGL3 dose of 1 μg down to 1 ng and could be due to either substrate elimination from the liver or degradation of luciferase.

To distinguish between these possibilities, 2.4 mg of D-luciferin was dosed at 20 min intervals following a single hydrodynamic dose of 0.1 μg of pGL3 (Figure 2-3). The

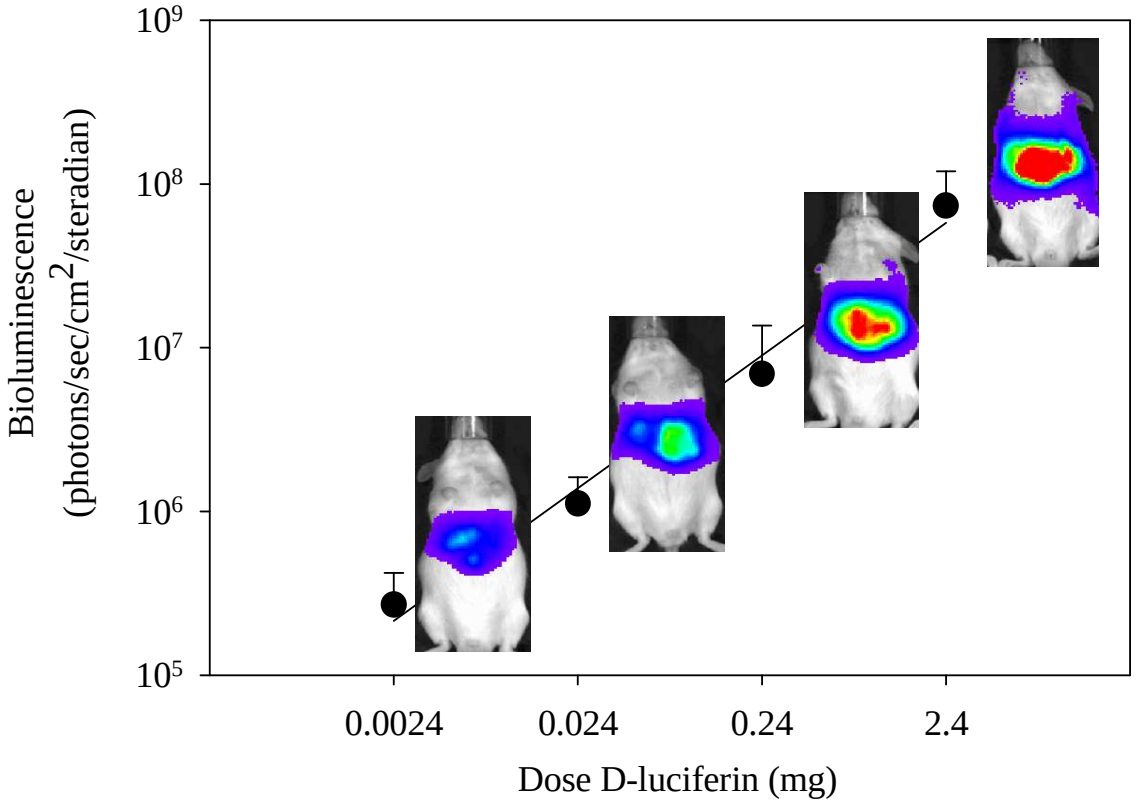

Figure 2-1. *Influence of luciferin dose on bioluminescence following hydrodynamic dosing of pGL3.* Mice were hydrodynamically dosed with 0.1 μg of pGL3. After 24 hours, triplicate mice were dosed with 0.0024 - 2.4 mg D-luciferin in 80 μl PBS. Quantitative bioluminescence measurements were collected after 4 min. The data represents the mean and standard deviation.

results established that bioluminescence could be recovered to within 2-fold of the initial value following each dose of substrate. These results are interpreted to mean that luciferase expression and activity were nearly constant over the 60 min, but the D-luciferin clearance was primarily responsible for the decreased bioluminescence over time. These experiments also suggest that ATP was not limiting in concentration in the liver.

Luciferase expression was monitored over a period of days to determine the duration of detectable bioluminescence. Maximal expression was observed on day 1

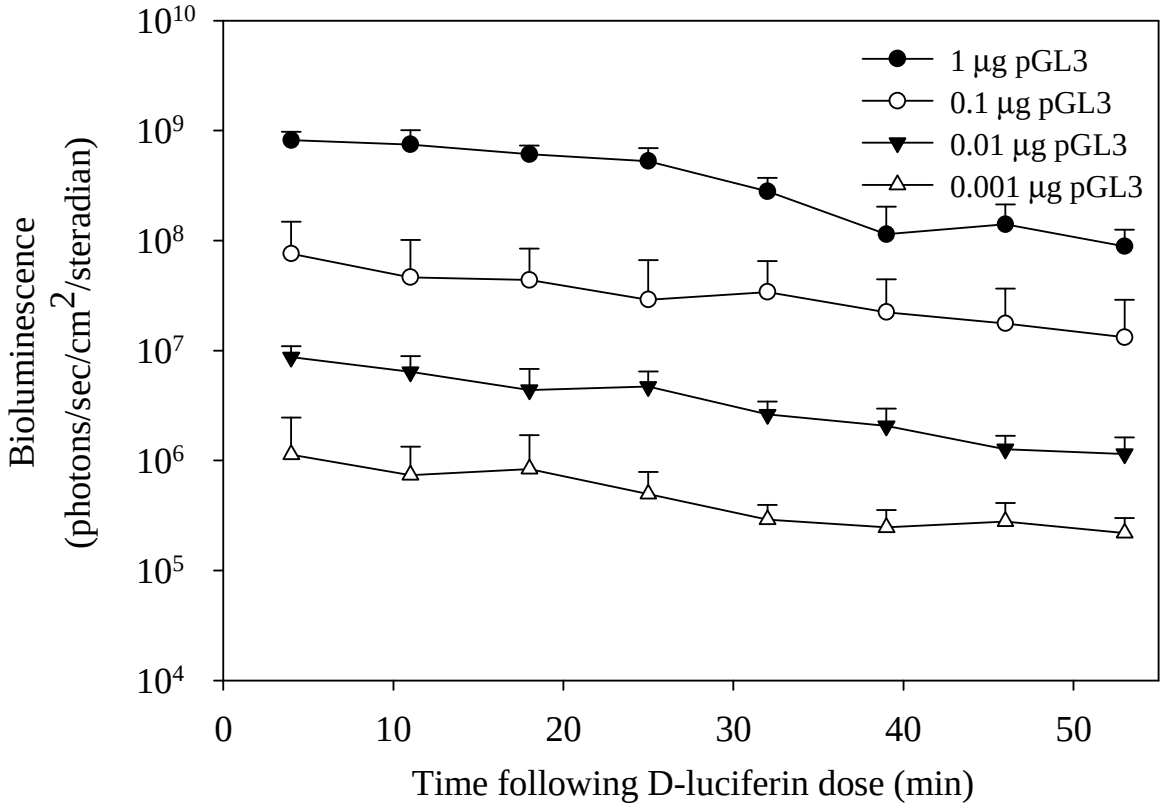

Figure 2-2. *Bioluminescence time course following a single dose of D-luciferin.* Triplicate mice were hydrodynamically dosed with 0.001, 0.01, 0.1 or 1.0 µg of pGL3. After 24 hrs, a single IP dose of D-luciferin (2.4 mg in 80 µl of PBS) was administered and bioluminescence was measured over the course of 53 min. Data points represent the mean and error bars indicate the standard deviation

(~10^9 photons/sec/cm^2/steradian). Expression levels steadily decreased out to day 5, averaging a decrease of approximately 1 order of magnitude per 24 hour period. Bioluminescence remained at a detectable level through day 8. Imaging on day 9 produced background photon flux (Figure 2-4).

Luciferase expression was measured both by whole animal imaging of bioluminescence *in vivo* and by direct luciferase assay of liver homogenates. The

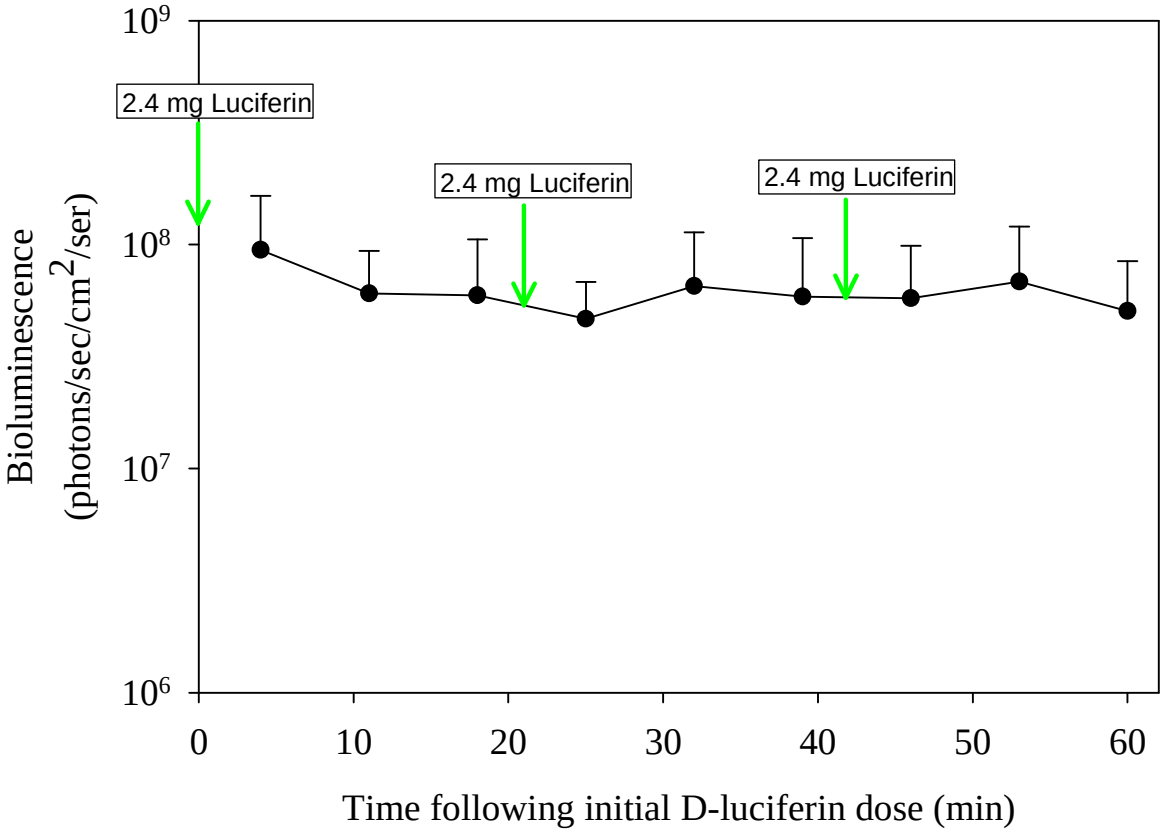

Figure 2-3. *Bioluminescence time course following repeat doses of D-luciferin*. Mice were hydrodynamically dosed in triplicate with 0.1 μg pGL3 24 hrs before imaging. D-Luciferin (2.4 mg in 80 μl PBS) was dosed at 0, 21, and 42 minutes while images were acquired every 7 minutes over the course of 60 min. Second and third doses of D-luciferin are indicated by the arrows. The data represent the mean and standard deviation..

bioluminescence determined by imaging and that recovered from liver homogenates was plotted against the dose of pGL3 (Figure 2-5). A linear relationship was observed between the hydrodynamic dose of pGL3 and luciferase expression measured by the two methods. The dose-response for pGL3 also established detection limits of 10^5 photons/sec/cm^2/steradian for BLI and 100 pg of luciferase for the direct measurement of luciferase in liver homogenates (Figure 2-6).

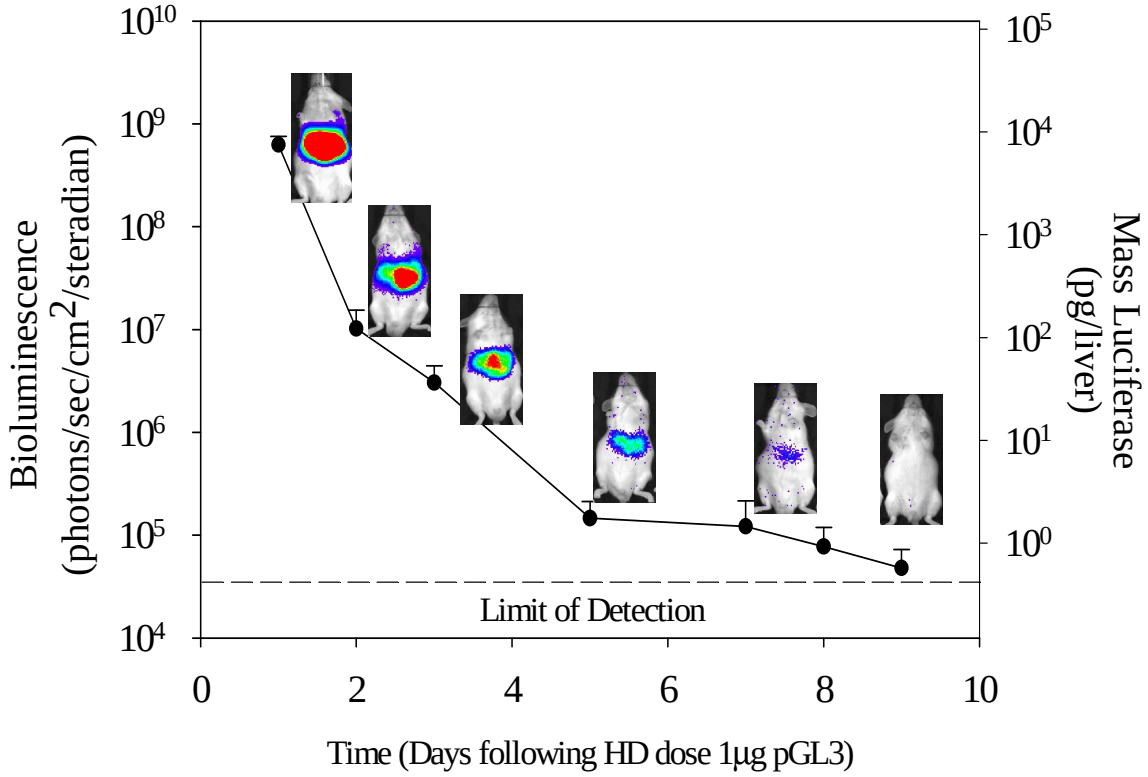

Figure 2-4. *Time-course of gene expression by HD-BLI*. pGL3 (1 µg) was dosed hydrodynamically to mice in triplicate. Luciferase expression was monitored by BLI over an extended time course following 2.4 mg delivery of substrate. The results establish the duration of observable expression for this route of pGL3 delivery

Discussion

BLI is rapidly becoming the most widely used method to measure transgene expression *in vivo*. In the present study, we have used hydrodynamic dosing of pGL3 to reliably and reproducibly express luciferase in the liver of mice. The reproducibility of the hydrodynamic dosing procedure is evident from the very low relative standard deviation in triplicate mice. In fact, the relative standard deviation of the BLI measurement for repeated analysis of the same mouse was only slightly lower that the inter-mouse variability. This route of gene delivery can function as a tool to correlate

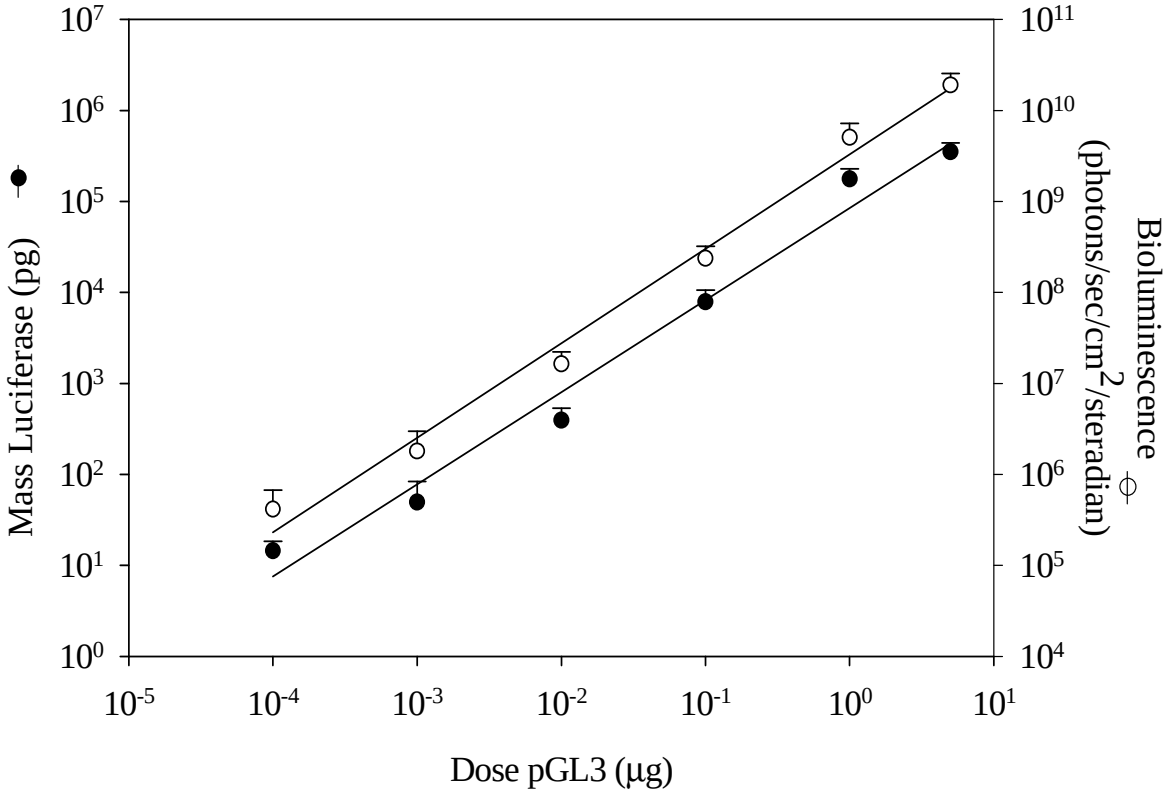

Figure 2-5. *Influence of hydrodynamic dose of pGL3 on bioluminescence*. Triplicate mice were hydrodynamically dosed with 0.0001, 0.001, 0.01, 0.1, 1.0 or 5.0 μg pGL3. After 24 hours and an IP dose of D-luciferin (2.4 mg in 80 μl PBS), bioluminescence was quantified, reported in photons/sec/cm^2/ser. This data is represented by open circles. Mice from each treatment group were subsequently euthanized and livers were harvested. The mass of luciferase, expressed in pg/liver, was determined by an *in vitro* assay, and these data are represented by the closed circles. Error bars for both data sets represent the standard deviation.

photon flux, as detected by in vivo BLI, to the actual amount of luciferase present in liver homogenates.

BLI most commonly involves 2.4 mg of D-luciferin dosed IP according to publications from the instrument manufacturer[127]. The result of Figure 2-1 establishes a linear relationship between D-luciferin dose and bioluminescent readout. These data indicate that the substrate is limiting the levels of bioluminescence that can be detected. A further increase in bioluminescence may result by increasing the D-luciferin dose

above 2.4 mg; however, the solubility of D-luciferin, which is 30 μg/μl (100 mM) in PBS is limiting. In addition, increasing the dose of D-luciferin becomes cost-prohibitive.

A second factor that influences the intensity of response is the timing of acquisition following D-luciferin dose. The rapid distribution of D-luciferin to the liver corresponds with the findings of Lee, et al [128], and indicates that photon flux will be greatest immediately following substrate injection. Thereby, the rate of decrease in photon flux over the course of 60 min is independent of the initial amount of enzyme present. The observed decrease in signal is most likely the result of clearance of D-luciferin and further supports the substrate's role as the limiting reagent in response. The data also suggests that the expression of luciferase is not diminished 24 hrs after hydrodynamic dose. The enzyme appears to remain active after the initial turnover of D-luciferin to oxyluciferin because repeat doses of substrate results in sustained levels of bioluminescence over the course of 60 min (Figure 2-3).

Hydrodynamic dosing of varying amounts of pGL3 was used in combination with BLI to establish linearity in response ($R^2 = 0.9867$) over 5 orders of magnitude. The slope of the calibrated plot established a relationship of total photon flux = $(8.88 \times 10^4) \times$ pg luciferase, and a limit of detection of 4.1×10^5 photons/sec/cm^2/steradian (S:N = 3:1) when expressing 20 pg of luciferase/liver and dosing with 2.4 mg of D-luciferin. The luciferase expression determined by BLI following hydrodynamic dosing of 1 μg of pGL3 was 1.77×10^5 pg of luciferase/liver. This value is comparable to levels of expression reported previously of 4×10^5 pg of luciferase/liver [126] and 9×10^6 pg of luciferase/liver [129].

It is interesting to note that the mouse liver contains approximately 10^8 hepatocytes. A 100 pg dose of pGL3 is 10^7 molecules, and only a fraction of the dose (40%) is taken up in hepatocytes [126,130]. Thus, it appears that BLI is able to detect

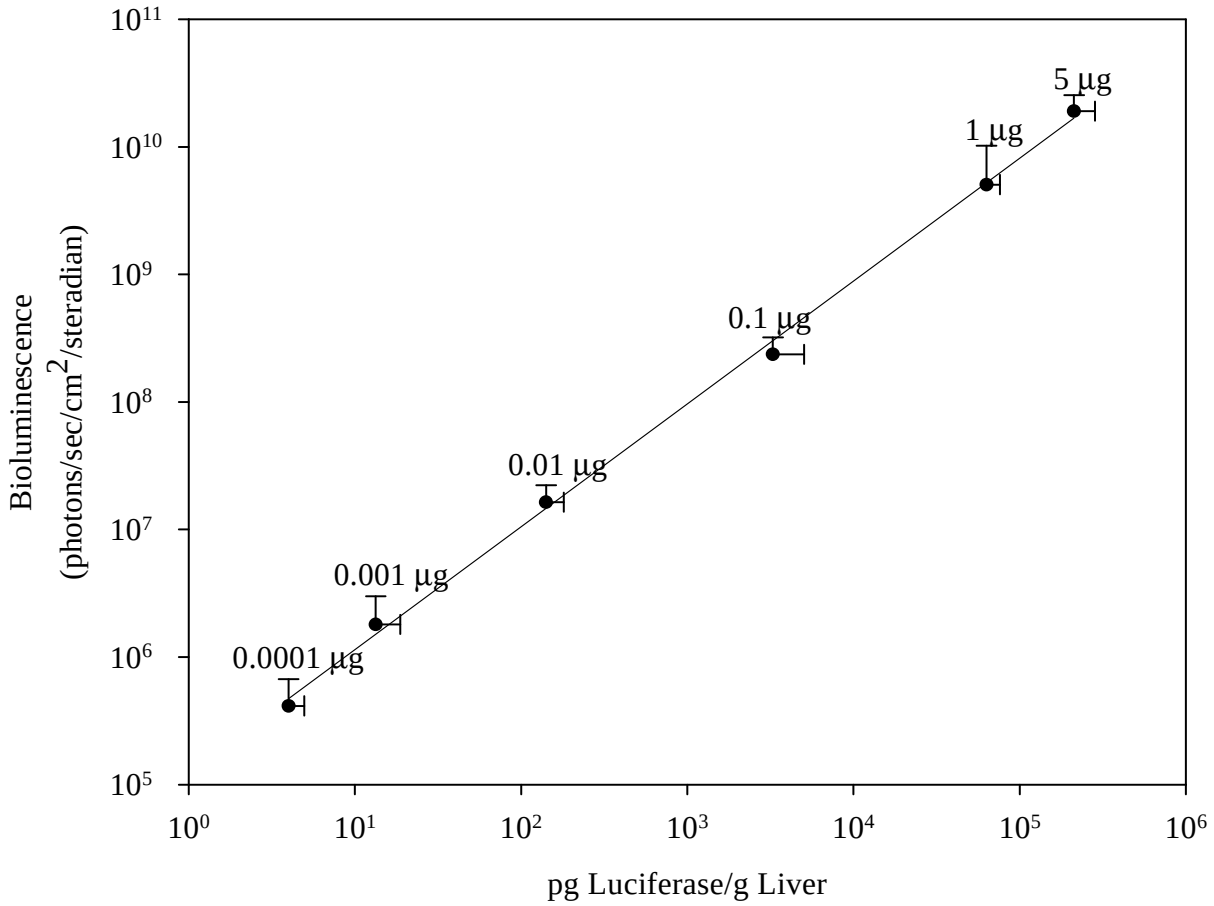

Figure 2-6. *Correlation of bioluminescence to luciferase mass.* Triplicate mice were dosed with pGL3 in the amounts indicated by the data labels. The solid line represents the regression for the presented data and has an R^2 value of 0.9867. Within the range of data shown here ($5x10^5$ - $1x10^{10}$ photons; 10^1 - $5x10^5$ pg luciferase), the correlation value is $8.88x10^4$ photons/pg luciferase.

luciferase expression mediated by a very low dose of pGL3, even when it is distributed across less than 10% of the cells in the liver.

These results highlight the advantages of BLI carried out with a CCD camera, which include its simplicity, ease of detection and reproducibility, compared to the more laborious process of homogenizing resected livers and measuring luciferase in a bioluminometer. The quantitative analysis of *in vivo* gene expression mediated by increasingly more potent gene delivery vectors is fundamental to the advancement of this

science. BLI is increasingly being established as a powerful tool to aid researchers to obtain quick and definitive gene transfer efficiency measurements *in vivo*.

CHAPTER 3

INTRAMUSCULAR DOSING AND ELECTROPORATION OF LUCIFERASE-EXPRESSING PLASMID: IN VIVO EXPRESSION DETECTED BY BIOLUMINESCENCE IMAGING

Abstract

Intramuscular (IM) dosing is a common route for dosing DNA in vivo. The method of delivery is simple, and the duration of expression is longer than achieved by HD dosing. We incorporated BLI as an efficient means to detect luciferase expression in skeletal muscle. Initial experiments exploring IM dosing and the possibility of incorporating electroporation (EP) showed that EP following an IM dose could boost transgene expression by at least 1,000-fold. Substrate delivery was found to be optimized when delivered by an IM dose, and the expression profile was monitored for 30 min following a single substrate dose. The time course of luciferase expression in skeletal muscle was persistent past 36 days, and a dose-response curve was generated by delivering varying amounts of pGL3. Bioluminescence plateaued at doses greater than 10 μg of pGL3. Tissue was harvested from mice, and the luciferase levels were measured in the tissue homogenate. These values were converted to an absolute amount of luciferase via a standard curve generated with a known amount of luciferase. Using this correlation in the dynamic range tested, a bioluminescent readout of expression from the hamstring muscle can be converted to pg of luciferase expressed in the tissue.

Introduction

IM dosing has been a popular delivery route for in vivo gene expression. It has been shown to be effective to deliver naked DNA in a bolus dose to skeletal muscle. Skeletal muscle is an attractive target because it is large tissue, has the capacity to biosynthesize large amounts of protein and is accessible to IM dosing. In addition, with an eye toward developing expertise with an in vivo assay for NLS-mediated increase in gene expression, skeletal muscle cells are post-mitotic and multinucleate. These factors are expected to enable an increase in gene expression resultant from increased uptake into nuclei relative to the proper controls. Skeletal muscle is an attractive target for expression of therapeutic proteins as well as introducing DNA-based vaccines in which the pDNA encodes an antigenic epitope.

EP is a process by which cell membranes are transiently permeabilized by electrical pulses. The membrane potential and the application of an electric field of significant strength trigger cells to adopt a polarity. In addition, morphological changes associated with field alignment trigger membrane destabilization. Under these conditions, it is theorized that pores are formed and electrophoretic movement carries charged molecules across the cell membrane and into the cytosol. This is a well-known physical method of delivery used in concert with IM dosing (as well as other routes) to achieve increased levels of transgene expression.

Luciferase may be quantitatively measured in skeletal muscle by BLI in the same way it was following HD dosing in the liver. In this approach, we have optimised luciferase expression and detection in skeletal muscle by the optimal route and dose of D-luciferin, the timing of image acquisition following pGL3 and D-luciferin dose, the profile of the dose-response curve, the limit of detection, and the amount of luciferase expressed in muscle relative to a calibration curve.

In the previous chapter, a major finding is the correlation between the BLI response and the absolute amount of luciferase which is expressed in the target tissue. An

optimal delivery route for skeletal muscle, like IM-EP, can be used to set the same sort of benchmark for optimal expression from a non-viral vector. The general approach used should be adaptable to any tissue that is capable of generating appreciable levels of luciferase expression.

Materials and Methods

pGL3 Control plasmid was obtained as described in the previous chapter. ICR male mice (25-30 g) were purchased from Harlan Labs. Ketamine (500 mg/ml, Bionichepharma, Lake Forest, IL) and xylazine (100 mg/ml, Phoenix Pharmaceutical, St Joseph, MO) were combined with normal saline (0.9% NaCl, Abbot Laboratories, North Chicago, IL) to give a dilution of ketamine (20 mg/ml) and xylazine (2 mg/ml) for delivery as an anesthetic. 1 ml monoject insulin syringes containing a 28 G x ½ inch needle were utilized. Electrical stimuli were delivered via a 2-needle array electrode (BTX Products, Harvard Apparatus, Holliston, MA) with a width of 5 mm. An ECM 830, Square Wave Electroporation System (BTX Products) was used to generate the electrical pulses.

Intramuscular Dosing and Electroporation

Male ICR mice were prepared for IM dosing and EP by anesthetization with an IP dose of 200 µl of a ketamine/xylazine (20 mg/ml and 2 mg/ml, respectively). All mice were confirmed to be anesthetized by monitoring the pedal response. The ventral aspect of the hind limbs was sheared and swabbed with 70% ethanol. A 50 µl dose of normal saline containing pGL3 was delivered to the hamstring muscle via an insulin syringe. The depth of injection was controlled by silicone tubing which sheathed the syringe up to approximately 2 mm from its point. The dose was delivered over 10 sec, and the syringe was held in place for an additional 10 sec before removing it from the tissue.

The IM dose of pGL3 was followed by EP. Successive electronic stimulation was carried out with the EMC BTX 830, Square-wave Pulse Generator as the power source.

The points of the BTX 2-Needle Array Electrode were carefully pressed into the skin with the electrodes straddling the pGL3 dosing site. One minute following the dose of pGL3, the pulse generator was initiated to deliver six successive pulses of 100 V each. The 100 V pulses were 20 msec in duration followed by a 100 msec latent period. The size of the electrical field was equivalent to the width of the needles in the electrode array – 5 mm.

Mice were allowed to recover from the anesthetic in bedding-free cages in a warmed environment. They were returned to the vivarium following recovery, and mice were handled according to approved protocol from the University of Iowa, Offices of Animal Resources.

Bioluminescence Imaging of Luciferase Expression in Skeletal Muscle

Luciferase expression was quantified by BLI from 24 hrs and for an extended duration following the IM dose of pGL3. Imaging was carried out in the IVIS Imaging System 200 Series (Xenogen). Prior to imaging, mice were anesthetized by isofluorane (2% flow with oxygen). Subsequently, mice were placed in the imaging chamber, and maintained under anesthesia via a gas-flow manifold. In the chamber, mice were dosed IM (at the site of pGL3 dosing) with 40 μl (30 mg/ml) of D-luciferin. Acquisition of bioluminescent images began 10 min following substrate administration. Images were acquired from 5 sec up to 3 min (depending on the intensity of the bioluminescent signal) with a 24.6 cm field of view and medium binning.

The resultant grayscale images with a colormap overlay were analyzed using the IgorPro 4.09 software (LivingImage). Luciferase expression was quantified in terms of the resultant photons/sec/cm^2/steradian within a uniformly defined region of interest.

Intramuscular Dose of pGL3 Compared to an Intramuscular Dose Followed by Electroporation

Mice were dosed in groups of 3 (n=6) for this experiment. pGL3 was diluted in normal saline up to 0.4 mg/ml. All mice were dosed in both legs with 50 µl of the pGL3 dilution (20 µg pGL3). For 3 mice, the IM dose was followed by EP after 1 min, as described above. Luciferase expression was compared between the groups by BLI after 24 hrs. D-luciferin (40 µl of a 30 mg/ml dilution in PBS) was delivered IM at the site of pGL3 dosing.

Dose-Response of pGL3 by IM-EP

Two mice were used in each dosing group (n=4). pGL3 was diluted in normal saline so that each 50 µl dose contained 0.1, 1, 5, 10, 15 or 20 µg of pGL3 (0.002, 0.02, 0.1, 0.2, 0.3 and 0.4 µg/µl, respectively). The 50 µl doses were delivered by IM injection followed by EP, as described above. Mice were imaged by BLI after 24 hrs. Additional BLI images were acquired 23 days following IM-EP dosing, and the magnitude of expression was compared.

Following the second image acquisition, the luciferase-expressing skeletal muscle was harvested. Mice were IP dosed with 300 µl ketamine/xylazine. In the absence of a pedal response, both legs were sheared and the dermal layer was removed to expose the muscle of interest. Mice were then euthanized by cervical dislocation, and the muscle was quickly excised from each leg. Following muscle isolation, the tissue was weighed, rapidly frozen in liquid nitrogen, transferred to a 2 ml screw-top microfuge vial and maintained at -70^{o}C.

Frozen tissue sections were ground with a mortar and pestle in the presence of dry ice and the resultant powder was maintained at -70^{o}C. Samples were then allowed to thaw at which time 500 µl of lysis buffer was added to the tissue homogenate. Samples were inverted/mixed and cells were lysed in a series of 3 freeze-thaw cycles (from in dry

ice to a 37^{o} water bath) to disrupt cell membranes via ice crystal formation. Lysate was then centrifuged for 3 min at 10,000 x *g*. Supernatant was removed and 500 µl of lysis buffer was added back to the samples that were again centrifuged.100 µl aliquots of the combined supernatants were assayed for luciferase expression in the standard luminometer assay as described in the previous chapter:

Skeletal muscle tissue that was not dosed with luciferase-encoding plasmid was also processed as described above. Supernatant from the lysate of this tissue was used in a standard serial dilution of a known amount of luciferase to generate a standard curve to correlate the bioluminometer readout (RLUs) with an absolute amount of gene product.

Duration of Luciferase Expression in Skeletal Muscle

Mice that were IM-EP dosed with 1 µg of pGL3 were incorporated into a study to examine the duration of luciferase expression (n=4). Luciferase expression was monitored by BLI beginning 24 hrs after IM-EP dosing. On each day of imaging, 40 µl of D-luciferin (30 mg/ml) was delivered IM at the site of pGL3 dosing. Mice were dosed while under isofluorane anesthetic and images were acquired 10 min later. Expression was followed by BLI up to 36 days after delivery of the IM-EP dose.

Bioluminescent Response based on D-Luciferin Dose

The route of substrate dosing was compared prior to EP being incorporated into IM dosing experiments. Briefly, 4 mice (n=8) were dosed with 20 µg of pGL3 in 20 µl of normal saline. After 24 hrs, 2 mice were IP dosed with 80 µl of D-luciferin (30 mg/ml), anesthetized and imaged for luciferase expression. Successive 2 min images were acquired up to 9 min following IP dosing. The remaining 2 mice were anesthetized and the substrate was dosed IM, at the site of pGL3 injection. Images were acquired (30 sec) until 9 min following the dose of D-luciferin.

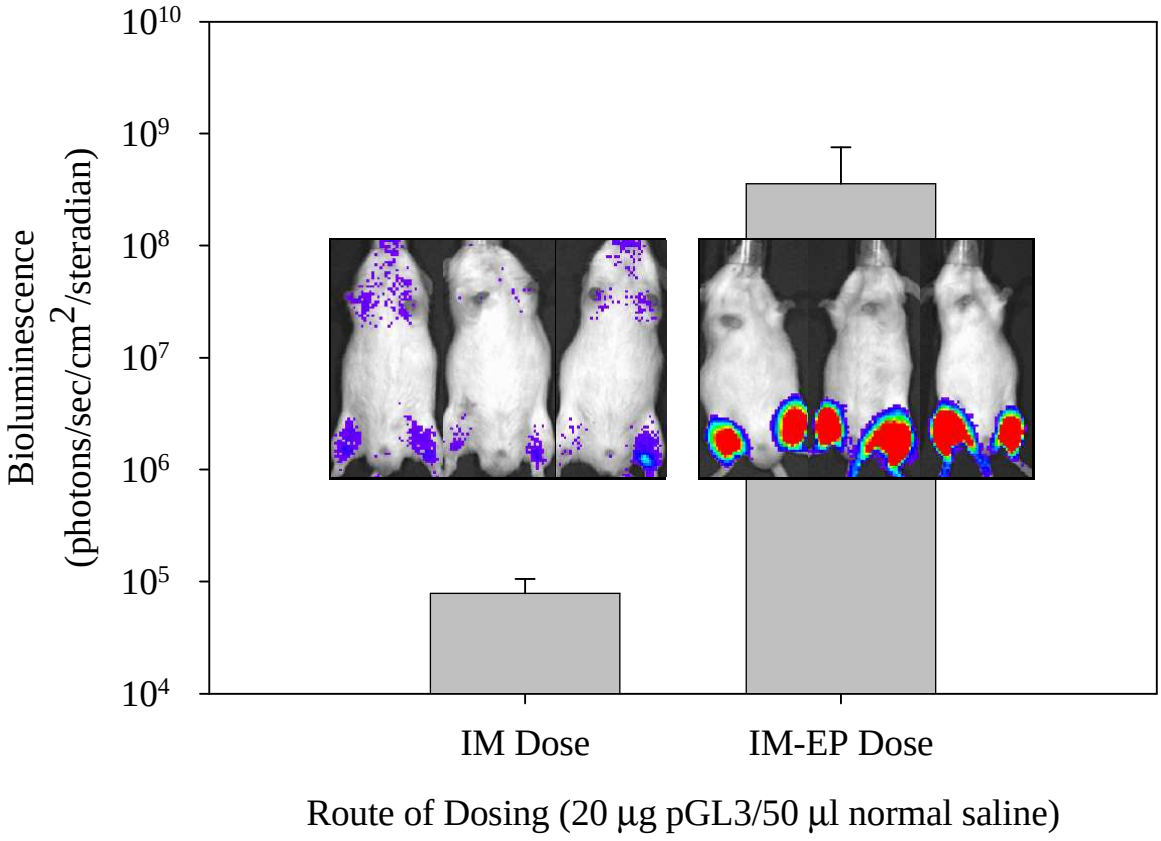

Figure 3-1. *Expression from an IM dose enhanced by EP*. Mice were dosed IM with 20 µg of pGL3. The bolus dose was followed 1 min later with EP in the second group. Mice were imaged for luciferase expression by BLI after 24 hours and an IM dose of D-luciferin (40µl, 30 mg/ml). Images were acquired 10 min following substrate dose. Error bars represent the standard deviation from the mean (n=6).

Results

EP is well-known to increase the amount of pDNA that enters a cell. A sequence of 6 successive electrical stimuli of 100 V each was applied over a 5 mm field spanning the site of pGL3 dosing. Figure 3-1 indicates that EP, applied under the above-described conditions, increased luciferase expression by more than 3 orders of magnitude when 20 µg of pGL3 was dosed in 50 µl.

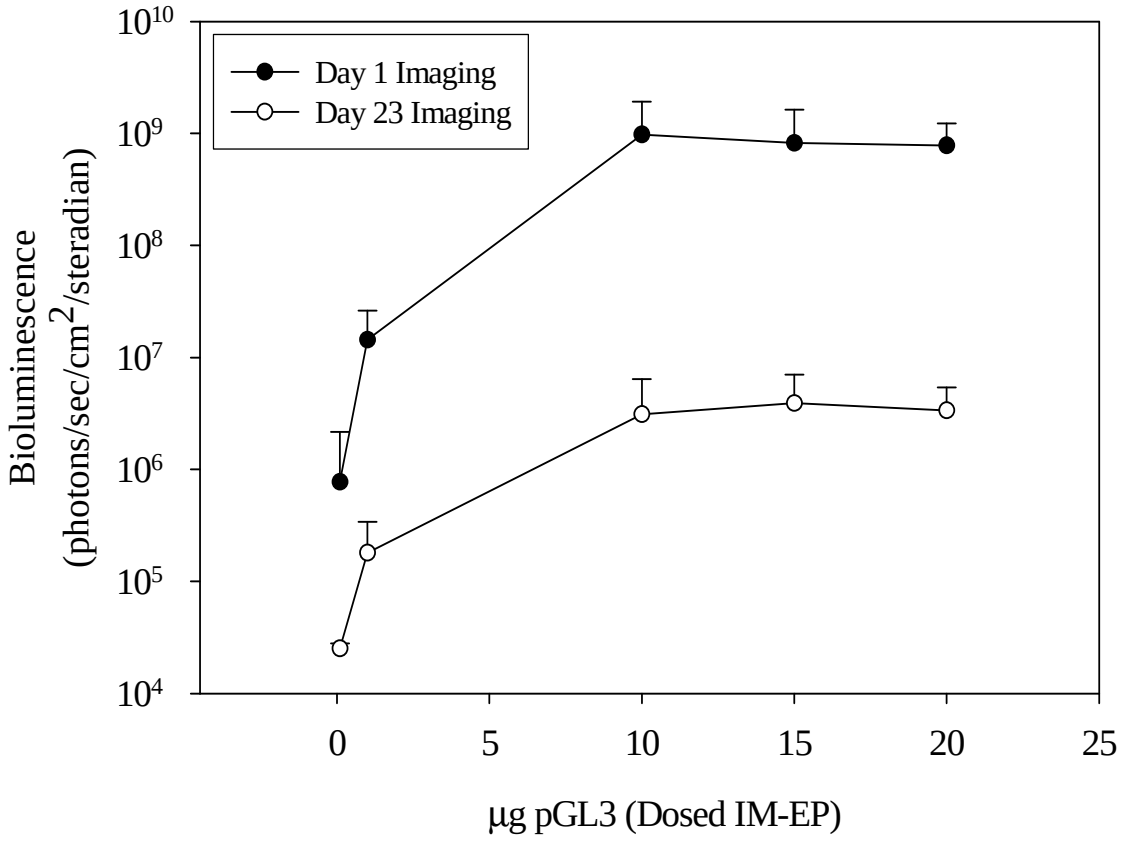

Figure 3-2. *Dose-response for pGL3 delivered by IM-EP*. Mice were dosed by IM-EP protocol with 0.1-20 µg of pGL3. Luciferase expression was measured by BLI 1 day following pGL3 dose (filled circles) and also 23 days after dosing (open circles). Imaging at both time points involved a 40 µl dose of D-luciferin (30 mg/ml) administered IM. Data represent the mean and standard deviation of n=4 doses per group.

To further investigate IM-EP dosing, a dose-response experiment was carried-out in which the dose of pGL3 showed a positive correlation with the bioluminescent response (Figure 3-2). The bioluminescent response measured 24 hrs after dosing pGL3 is represented by the filled circles on the log-linear plot. Luciferase expression levels plateaued at approximately 1 x 10^9 photons/sec/cm^2/steradian for 10, 15 and 20 µg doses of pGL3. All mice were imaged again 23 days following IM-EP dosing of pGL3. The plot of the follow-up imaging (open circles) indicated an expression profile identical to

that observed on day 1. Bioluminescence had uniformly decreased 3 orders of magnitude for 10-20 μg doses over the course of 23 days. The 1 and 5 μg doses of pGL3 showed 100-fold decreases in bioluminescence.

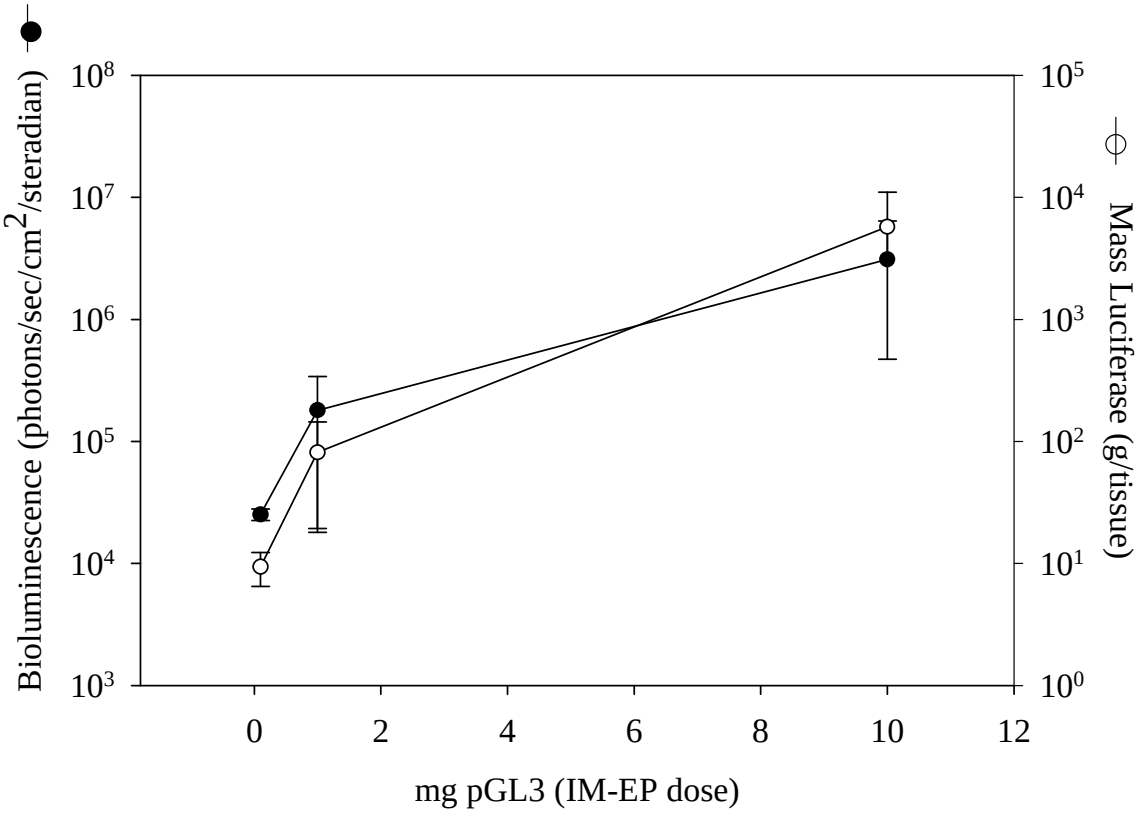

Figure 3-3. *Correlation of in vivo bioluminescence to pg of luciferase*. Mice dosed with 0.1-10 μg of pGL3 (+/+) (n=4) were imaged by BLI (solid circles) 23 days following IM-EP dose of pGL3. Subsequently, the luciferase-expressing skeletal muscle was harvested and assayed on a bench top bioluminometer to determine the absolute amount of luciferase present (open circles). Data was transformed from RLUs to pg luciferase via a standard curve generated with known amounts of enzyme in the presence of naïve skeletal muscle homogenate.

Tissue was harvested from mice dosed with 0.1 – 10 μg of pGL3 following the second image acquisition. Previously, it was shown that BLI with HD dosing of pGL3 could be correlated with the absolute levels of luciferase expressed. The same principles

were applied in this experiment to quantitatively correlate pg of luciferase and the bioluminescent response from skeletal muscle in vivo. The log-linear plot shows the direct comparison of BLI-detected expression levels with the response detected on a luminometer and converted to pg based on a known standard (Figure 3-3).

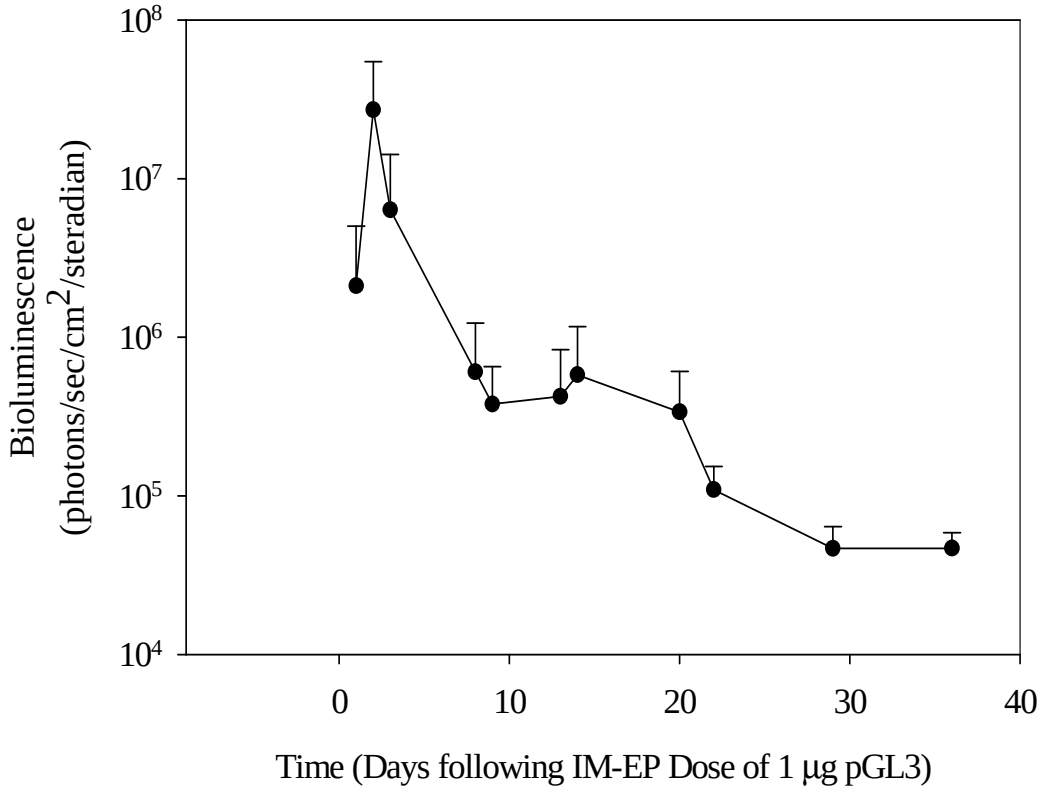

Figure 3-4. *Time course of luciferase expression following IM-EP dosing.* Mice were dosed with 1 μg of pGL3 by the IM-EP protocol (n=4). Expression was followed for 36 days following pGL3 dose. For image acquisition at each time point, D-Luciferin was delivered in an IM dose of 1.2 mg (30 mg/ml). Images were acquired 10 min following substrate administration.

One of the advantages of the IM dosing route as compared to HD is that detectable transgene expression persists for a greatly extended duration in skeletal muscle. Figure 3-4 shows that mice dosed with 1 μg of pGL3 (+/+) by the IM-EP

protocol can be serially sampled over the time course of at least 36 days. Detection of luciferase expression is maximal on day 2 (following dosing on day 0). Over the course of 36 days, the detectable photon flux decreased by nearly 3 orders of magnitude and approached the limit of detection for BLI.

Previously, D-luficerin had been delivered via an IP dose to enable distribution to the liver. In this experiment, the route of delivery was examined in order to maximize the bioluminescent response. Figure 3-5A shows, in a shortened time course, that an IM dose of D-luciferin (1.2 mg/leg) increased photon flux nearly 10-fold as compared to the same amount of substrate delivered (on a per mouse basis) by an IP dose. Figure 3-5B displays the profile of the bioluminescent response over a time course following IM dosing of D-luciferin. At 10 min following the substrate dose, bioluminescence was maximal. Over the course of 30 min, detectable photon flux decreased approximately 2-fold.

Discussion

By introducing EP as a component of the IM dosing protocol, bioluminescence was increased nearly 1,000-fold. The bioluminescent response increaseses photon flux from on the order of 10^5 units with a 1 μg dose of pGL3 up to 10^9 photons/sec/cm^2/steradina following a 10 μg dose by an IM-EP dose. By incorporating EP, much less plasmid is required to achieve skeletal muscle expression that falls in the linear range of BLI detection. The advantage of delivering less plasmid becomes clear as experiments advance towards delivering more elaborate non-viral vectors. Experimental expense can be reduced when incorporating an NLS, fusogen, PEG-peptide or other ligand into this type of dose if the amount of required reagent is reduced by 1,000-fold.

These experiments were primarily carried out as a means of investigating IM-EP as a viable method for in vivo luciferase expression. We determined which parameters could be adjusted to produce a bioluminescent output which maximized the dynamic range of detection by BLI. An interesting fiding was the dose-response (Figure 3-2)

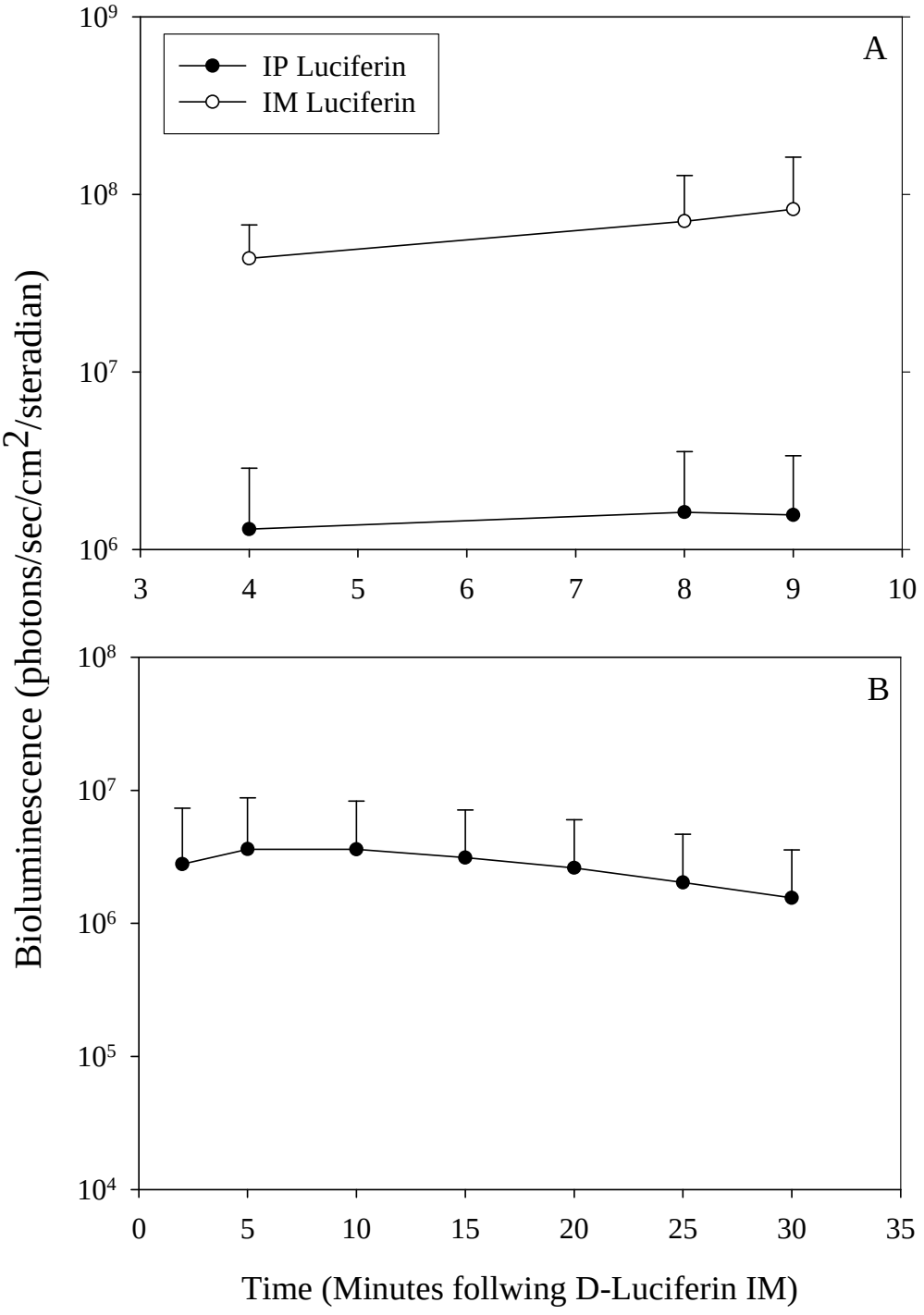

Figure 3-5. *Bioluminescent Response Dependent on Luciferin Dose*. A) Mice were IM-dosed with identical amounts of pGL3 (+/+). 24-hour BLI was preceded by either an IM dose (1.2 mg/leg, solid fill circles) or an IP dose (2.4 mg/mouse, un-filled circles) of D-luciferin (30 mg/ml). B) The bioluminescent profile was followed over an extended time course after an IM dose of D-luciferin (1.2 mg/leg; 30 mg/ml).

which indicated that a 1 μg dose of pGL3 gave expression in the dynamic range. but a 10 μg dose of the same plasmid resulted in expression that approached the limit of detection by BLI. In future experiments with IM-EP dosing, a 10 μg dose of pGL3 with varying treatments would not be useful if we expect to see an significant increase in expression from dose-matched controls.

It seemed that the plateau in expression at 10 μg doses and larger was not necessarily due to an impediment of the limit of detection. The dose-response profile remained the same when mice are imaged 23 days after dosing and the level of plateaued expression was clearly less than the limit of detection at the later date. Thus, the characteristic plateau suggests that the bioluminescent response is maximized with a 10 μg dose of pGL3 delivered to the hamstring muscle and followed by EP. This effect may be a substrate-dependent, tissue-dependent or immunogenic-related. In any case, going forward, we understand the maximal bioluminescent response to come from an IM-EP dose of 10 μg pGL3 in the hamstring muscle.

As in the case of HD dosing, we were able to quantify the relationship between the bioluminescent response detected in vivo by BLI and pg of luciferase detected on a bench top bioluminometer. Figure 3-6 displays the correlation, and the equation can be used to transform BLI signal to an absolute amount of luciferase expression from an IM dose in the hamstring muscle. In this example, we have not exhausted the full dynamic range of detection (only $2.5 \times 10^4 – 3.1 \times 10^6$ photons), and the plateau at higher doses of pGL3 indicate that this relationship may not be linear outside of our correlation plot. In the absence of data to show linearity or the inability to otherwise fit data in the linear range, we will not apply this correlation to additional plots of skeletal muscle dosing of pGL3 in the hamstring. The process completed to this point indicates that a complete correlation could be made, and suggests this is possible for other target tissues, as well.

An interesting observation comparing this correlation plot to that in Chapter 2 comes from the difference in the value of the slope. Figure 2-6 shows that 8.88×10^4

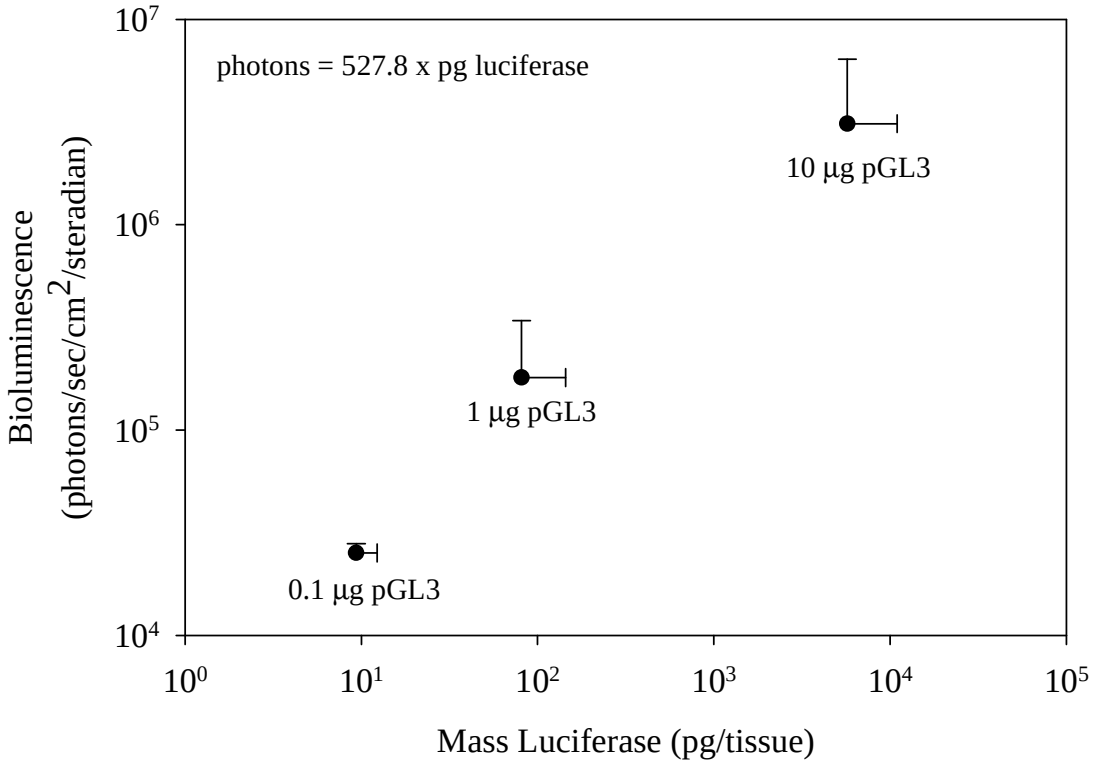

Figure 3-6. *Correlation of BLI response to pg of luciferase in the hamstring muscle tissue.* Data from Figure 3-3 is re-plotted in order to determine the equation for the linear regression line to correlate BLI response with absolute amount of luciferase expressed

photons can be attributed to 1 pg of luciferase expressed in the liver. This value is lower in skeletal muscle (527.8 photons/pg luciferase as shown in Figure 3-6) suggesting that the BLI response from the hamstring muscle is not as intense as it is from the liver. Considering the depth of the target tissue and the photon absorbance in mammalian tissue, this relationship is unexpected. Based on tissue depth, we would expect 1 pg of luciferase in the liver to manifest in the form of fewer photons than we would from 1 pg of luciferase in the hamstring muscle. Additional factors like vascularization and an increased concentration in photon-absorbing pigmentation in the liver would also lead to a decrease in the relationship of photons/pg. It is also possible that the bioluminescent

response from the hamstring appears depressed due to poor substrate availability for enzyme expressed in this tissue. Tissue specificity for the SV40 promoter and the concentration of transcriptional/translational machinery may favor expression in hepatocytes.

These experiments have proven to be useful in optimizing luciferase expression in skeletal muscle, as well as optimizing the bioluminescent detection. The protocols for IM-EP dosing and subsequent BLI will be applied to future studies of non-viral gene delivery systems tested in this target tissue. This dosing procedure is relatively simple and has the advantage of yielding observable luciferase expression for an extended time course.

CHAPTER 4

POTENCY OF SIRNA VERSUS SHRNA MEDIATED KNOCKDOWN IN VIVO

Abstract

The intracellular delivery of siRNA is a therapeutic strategy to transiently block gene expression. Two silencing RNA strategies utilize either synthetic double stranded RNA or pDNA encoding a short hairpin RNA (shRNA). In the present study, we have quantitatively compared the potency of siRNA (siLuc1) and shRNA (pShagLuc) mediated knockdown of luciferase expression in vivo using HD dosing and BLI. Following HD coadministration of siLuc1 or pShagLuc with a plasmid encoding luciferase (pGL3), mice were analyzed for transgene expression by BLI. The knockdown of luciferase expression by siLuc1 or pShagLuc was observed at 3 hrs and persisted for 3 days. The potency of siLuc1 and pShagLuc was equivalent with maximal effect at 10 µg coadministered with 1 µg of pGL3 resulting in >80% knockdown. Combined dosing of siLuc1 and pShagLuc (5 µg each) with 1 µg of pGL3 resulted in >99% knockdown. Analysis of the data established that shRNA was significantly more potent than siRNA at mediating knockdown when compared on a mol basis. The combination of HD dosing and BLI to measure siRNA or shRNA mediated knockdown of luciferase provide an attractive in vivo quantitative method to test formulations that target the liver.

Introduction

siRNA is an important method for transiently blocking protein expression achieved by loading the RNA interference silencing complex (RISC) with a short single stranded antisense RNA that is complementary to a target mRNA.[131,132] This is most commonly achieved by delivery of a synthetic double stranded RNA targeted against a specific mRNA encoding the protein of interest.[2] It is also possible to produce dsRNA by delivery of a pDNA encoding a shRNA, that upon expression, produces a substrate for the endogenous endonuclease dicer that generates the 21-mer nucleotide siRNA.

The successful delivery of siRNA or shRNA to specific cells in animals will require unique considerations and strategies.[133,134] Plasmids expressing shRNA must be delivered to the nucleus and undergo transcription to produce an RNA hairpin substrate for dicer, whereas synthetic siRNA delivered to the cytosol can directly combine with RISC. Even though plasmids expressing shRNA have the disadvantage that they must overcome delivery to the nucleus, they also have the advantage that they can be amplified by transcription, whereas siRNA is not amplified intracellularly. Furthermore, compared to plasmid DNA, siRNA is more susceptible to intracellular metabolism. Based on these considerations, it is likely that siRNA and shRNA possess different potency as well as onset and duration.

Numerous studies have demonstrated the application of siRNA and shRNA to block protein expression in vitro and in vivo resulting in a specific biological result.[135142] However, only a few studies to date have directly compared the potency of siRNA and shRNA mediated knockdown in vivo.[143,144] One of the earliest studies demonstrated the use of BLI to monitor the knockdown of coadministered siRNA or shRNA and a plasmid (pGL3) expressing luciferase.[143] The results established a significant (>80%) knockdown of luciferase expression after 72 hrs when hydrodynamic dosing 40 μg of siRNA with 2 μg of pGL3. Likewise, under the same conditions 10 μg of shRNA resulted in >95% luciferase knockdown when coadministered hydrodynamically with 2 μg of pGL3. More

recently, Davis and coworkers[144] have analyzed the kinetics of luciferase knockdown following HD dosing with siRNA, suggesting the duration of knockdown is over a 2 weeks period.

In the present study, we have quantitatively analyzed luciferase knockdown following coadministration of pGL3 and either siRNA or shRNA. To validate the BLI approach, we have measured the degree of luciferase expression knockdown in liver as a function of time and dose of pGL3 and siRNA or shRNA. The results establish HD dosing and BLI as a rapid quantitative method to investigate siRNA and shRNA mediated knockdown in the liver. This study expands on previous work[143,144] by addressing the time course of action, dose–response of both pShagLuc and siLuc1 and the use of combination dosing.

The following experiments were completed in collaboration with Dr. Marie McAnuff.

Materials and Methods

Mammalian cells (HepG2, CHO, and 3T3) were obtained from the Center for Gene Therapy of Cystic Fibrosis (University of Iowa, Iowa City, IA). Dubelco modified Eagles medium (DMEM), modified Eagles medium (MEM), Hams-F12, PBS (without Ca^{2+}/Mg^{2+}), sodium pyruvate, penicillin/streptomycin, and heat-inactivated fetal bovine serum (FBS) were purchased from Invitrogen Life Technologies, Inc. (Carlsbad, CA). pGL3 Control, a 5.3 kb luciferase plasmid containing a SV40 promoter and enhancer was obtained from Promega (Madison, WI). pShagLuc, a plasmid containing a U6 promoter which is transcribed by RNA Pol III, expressing a hairpin siRNA complimentary to luciferase was a kind gift from Dr. Mark Kay (Stanford University, CA).[143] Each plasmid was amplified in DH5α strain of *E. coli* and purified on an endotoxin-free Qiagen megaprep column (Valencia, CA) according to the manufacturer's instructions. Firefly luciferase (*Photinus pyralis*), D-luciferin and ATP were purchased from Roche

Diagnostics Corporation (Indianapolis, IN). BCA assay kit was obtained from Pierce Biotechnology, Inc. (Rockford, IL). siRNAs were obtained from Dharmacon (Lafayette, CO). Male ICR mice (20–25 g) were obtained from Harlan (Indianapolis, IN).

Table 4-1. Sequences for siRNA and shRNA

Name	Sequence	Target Sequence[a] (bp)
pShagLuc[b]	5'-GGAUUCCAAUUCAGCGGGAGCCACCUGAU A A G G 3'-UUACCUAAGGUUGAGUCGCUCUCGGUGGGCUA G C U U	1340-1368
siLuc1[c]	5'-GAUUAUGUCCGGUUAUGUAUU-3' 3'-UUCUAAUACAGGCCAAUACAU-5'	8-26
siLuc2[c]	5'-GAUUCCAAUUCAGCGGGAGUU-3' 3'-UUCUAAGGUUGAGUCGCUCUC-5'	1348-1366
siControl[c]	5'-UUCUCCGAACGUGUAUCACGUUU-3' 3'UUAAGAGGCUUGCACAUAGUGCA-5'	Nontarget

[a]Target sequence on luciferase mRNA

[b]Sequence generated by transcription of pShagLuc

[c]Sequence is 5' phosphorylated

In Vitro Transfections

CHO cells and 3T3 fibroblasts were maintained in DMEM supplemented with 10% FBS and 100 U/ml penicillin/streptomycin at 37^{o} C in a humidified incubator containing 5% CO_2. HepG2 cells were maintained in DMEM supplemented with 50% Hams F-12, 10% FBS and 250 U/ml penicillin/streptomycin. Cells were trypsinized and seeded in six-well plates ($5x10^5$ cells/well in 2 ml of transfection media) 24 hrs before transfection. Cells were co-transfected with pGL3 and synthetic siRNA or vector-

expressed shRNA using $CWK_{17}C$ as the condensing agent.[145] $CWK_{17}C$ condensates were prepared in 5 mM Hepes buffered mannitol (pH 7.4) by adding 33 μg pDNA or siRNA (330 ml) to 13.2 nmol of $CWK_{17}C$ (330 ml) followed by a 30 min incubation at room temperature. DNA condensates (200 ml/well) were added to 50–70% confluent cells followed by 2 ml transfection media.

After 24 hrs, cells were washed twice with 2 ml of ice-cold PBS (Ca^{2+}- and Mg^{2+}-free) and then treated with 0.5 ml of lysis buffer (25 mM Tris-chloride, pH 7.8, 1 mM EDTA, 8 mM magnesium chloride, 1% Triton X-100) for 10 min at 4^{o} C. The cell lysates were scraped, transferred to 1.5-ml microcentrifuge tubes, and centrifuged for 7 min at 13000 x *g* at 4^{o} C to pellet cell debris. Luciferase RLUs were measured by a Lumat LB 9501 (Berthold Systems, Bad Wildbad, Germany) with 10 sec integration after automatic injection of 100 ml of 0.5 mM D-luciferin. The RLUs were converted to pg using a standard curve generated by adding a known amount of luciferase to 35-mm wells containing 50% confluent HepG2 cells. The resulting standard curve had an average slope of 1.46×10^4 relative light units/pg enzyme . Protein concentrations were measured by BCA assay using bovine serum albumin as a standard. The amount of luciferase recovered in each sample was normalized to milligrams of protein and reported as the mean and standard deviation obtained from triplicate transfections.

Hydrodynamic Dosing and Bioluminescent Imaging

pGL3 was combined with either siLuc1, pShagLuc, or an irrelevant plasmid (pSEAP) then diluted with normal saline to volume corresponding to 9 wt/vol% of the mouse's body weight (1.8–2.25 ml). The oligonucleotide dose was administered by tail vein to triplicate mice in 5 s according to a published procedure.[59,60] At times ranging from 3 to 72 hrs, mice were dosed IP with 80 μl of D-luciferin (30 mg/ml in phosphate-buffered saline), anesthetized by 3% isofluorane, and at 4 min following the IP dose of D-luciferin were imaged for bioluminescence on an IVIS Imaging 200 Series (Xenogen,

Hopkinton, MA). BLI was performed in a light-tight chamber on a temperature-controlled, adjustable stage while isofluorane was administered by a gas manifold at a flow rate of 2%. Images were acquired at a ‘‘medium’’ binning level and a 20 cm field of view. Acquisition times were varied (1 s–1 min) depending on the intensity of the luminescence. The Xenogen system reported bioluminescence as photons/sec/cm2/steradian in a 2.86 cm diameter region of interest covering the liver. The integration area transformed to picograms of luciferase in the liver via standard curve reported previously.[66] The results were determined to be statistically significant ($p \leq 0.05$) based on analysis on a one-way ANOVA followed by a nonparametric Mann–Whitney analysis.

Results

siLuc1, siLuc2, and pShagLuc were compared for RNA silencing potency to knockdown pGL3 mediated luciferase expression in vitro and in vivo. pShagLuc contains a U6 promoter which is transcribed by RNA Pol III to produce a 29-mer nucleotide hairpin RNA complementary to 1340–1368 bp in the luciferase mRNA target sequence (Table 4-1). Likewise, siLuc2 is a synthetic dsRNA 21-mer directed against 1348–1368 bp, a sequence coincident with the target of pShagLuc. Alternatively, siLuc1 is a dsRNA 21-mer complimentary with 8–29 bp in the target sequence.

We initially screened the ability of pShagLuc, siLuc1, and siLuc2 to mediate luciferase knockdown in vitro. Despite the fact the route of delivery was different, the analysis of siLuc1, siLuc2, and pShagLuc in vitro allowed for a comparison of potency prior to a similar in vivo comparison. Peptide-DNA condensates were prepared using a polymerizable peptide ($CWK_{17}C$) that has been reported previously. Peptide DNA/RNA co-condensates (10 μg) were prepared and transfected into HepG2, CHO, and 3T3 cells and the luciferase expression was measured after 24 hrs. In each case, 5 μg of pGL3 was mixed with 5 μg of either pSEAP (irrelevant plasmid), pShagLuc, siLuc1, siLuc2, or

sicontrol RNA prior to condensation with $CWK_{17}C$. The results illustrated in Figure 4-1 indicate that each cell type is transfected to a different degree by pGL3 condensed with

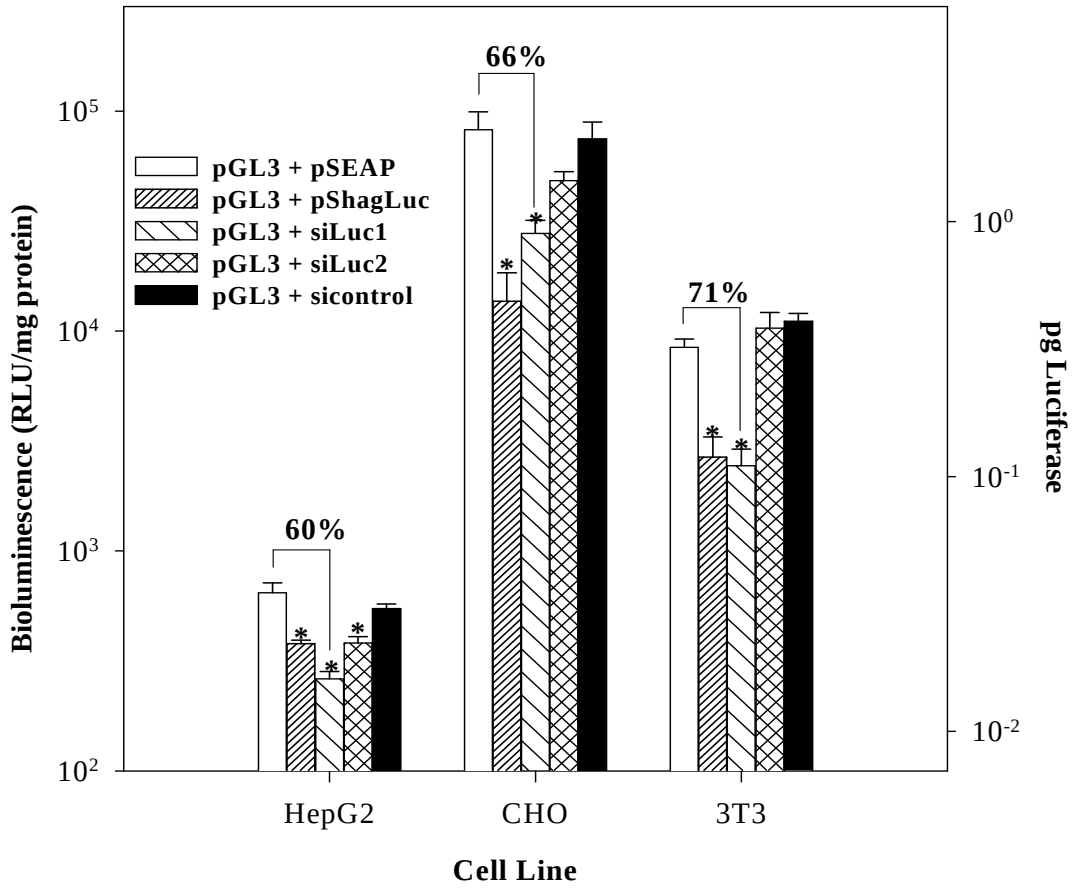

Figure 4-1. *Comparison of shRNA and siRNA mediated knockdown of luciferase in vitro.* HepG2, CHO, and 3T3 cells were transfected in triplicate with 5 µg of pGL3 combined with either 5 µg of pSEAP (control), pShagLuc, siLuc1, siLuc2, or sicontrol, condensed with 4 nmol of $CWK_{17}C$. The luciferase expression was measured after 24 h as described in the text. The results indicate, a statistically significant knockdown (p0.05) for pShagLuc and siLuc1 but not for siLuc2 or sicontrol. * $p \leq 0.05$ relative to pGL3+pSEAP.

$CWK_{17}C$. The degree of knockdown mediated by co-administration of pShagLuc was comparable to that mediated by siLuc1 and siLuc2 in HepG2 cells. However, siLuc2

failed to mediate significant knockdown in CHO and 3T3 cells. As anticipated, co-administration of pGL3 and sicontrol RNA failed to knockdown luciferase

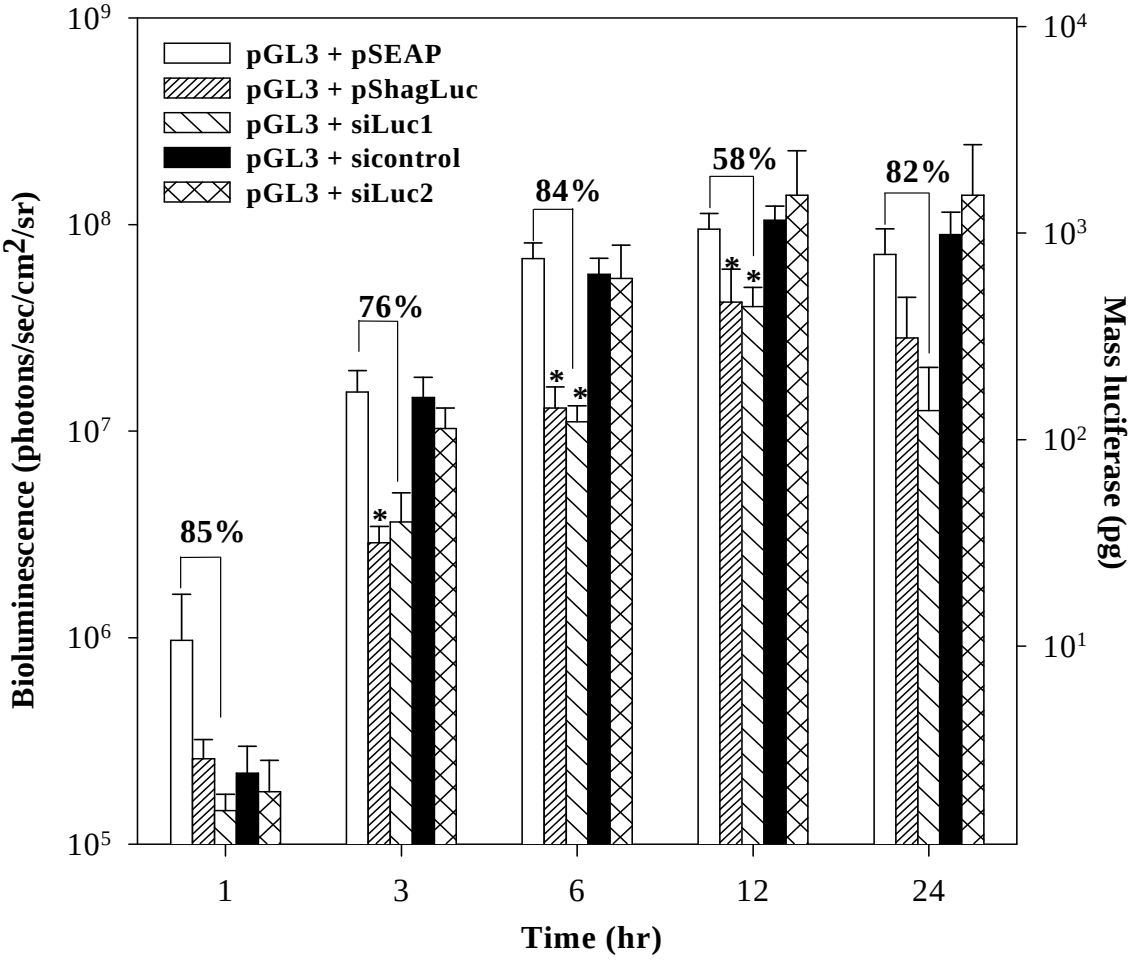

Figure 4-2. *Comparison of shRNA and siRNA mediated knockdown of luciferase in vivo*. Triplicate mice were HD dosed with 0.1 µg of pGL3 combined with either 0.1 µg of pSEAP (control), pShagLuc, siLuc1, siLuc2, or sicontrol. The luciferase expression was measured using BLI at times ranging from 1 to 24 hrs. The results indicated a statistically significant ($p \leq 0.05$) knockdown at 6–12 hrs for pShagLuc and siLuc1 relative to pGL3 combined with pSEAP, siLuc2, or sicontrol. *$p \leq 0.05$ relative to pGL3+pSEAP.

in each cell line. The degree of knockdown mediated by siLuc1 in each cell line was 60–70% and was statistically significant compared to controls. These studies established that siLuc2 was significantly less potent than pShagLuc, despite the fact that they both target overlapping regions of the luciferase mRNA, whereas siLuc1 possessed comparable potency as pShagLuc.

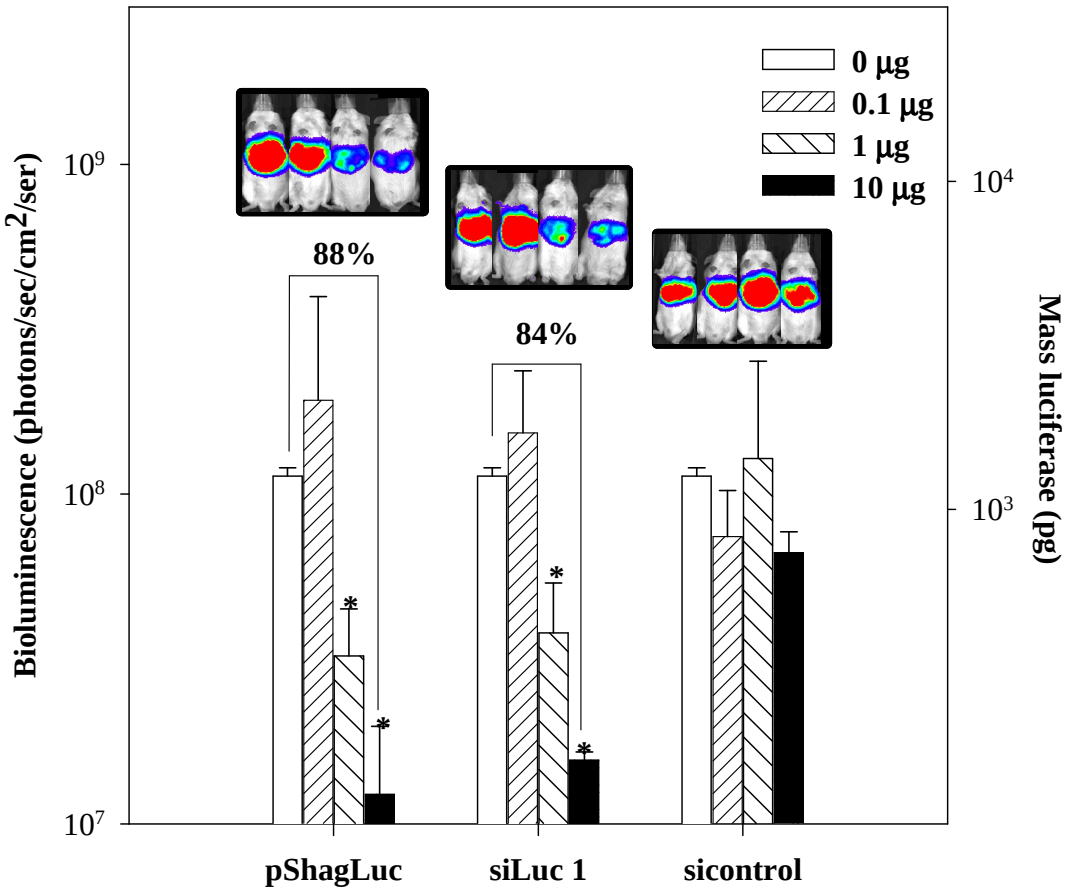

Figure 4-3. *In vivo dose–response comparison of siRNA and shRNA at a constant dose of pGL3*. Triplicate mice were HD dosed with 1 µg of pGL3 and either 0.1, 1, or 10 µg of pShagLuc, siLuc1, or sicontrol. The luciferase expression was measured by BLI at 24 hrs after injection. The results establish statistically significant knockdown for pShagLuc and siLuc1 at a dose of 1 and 10 µg . *p $\leq$ 0.05 relative to pGL3+pSEAP.

We next compared siLuc1, siLuc2, and pShagLuc mediated knockdown of pGL3 in mice. To accomplish this, mixtures of pGL3 and either siLuc1, siLuc2, or pShagLuc were prepared, then hydrodynamically dosed in triplicate mice,[146] followed by measuring luciferase by quantitative BLI as described previously.[66] Hydrodynamic dosing of 0.1 μg of pGL3, dose-normalized with either 0.1 μg of pSEAP (irrelevant plasmid) or sicontrol, resulted in luciferase expression detectable by BLI as early as 1 hr post-injection. The luciferase expression increased 100-fold resulting in 10^8 intensity units (1 ng of luciferase) expressed in the liver at 12 hrs (Figure 4-2).

Co-administration of pGL3 (0.1 μg) with either pShagLuc, or siLuc1 resulted in a knockdown of luciferase expression relative to controls at times ranging from 1 to 24 h (Figure 4-2). The decrease was not statistically significant at 1 hr but was found to be significant ($p \leq 0.05$) at 3–12 hrs. The degree of knockdown mediated by siLuc1 (58–85%) was similar to that determined during in vitro studies. Likewise, pShagLuc and siLuc1 both produced a comparable degree of knockdown as early as 3 hrs post-injection, suggesting that expression of the pShagLuc hairpin and the action of dicer was not rate limiting. Equivalent dosing studies with siLuc2 indicated that it was completely inactive at mediating knockdown in vivo (Figure 4-2). Based on these results, further in vivo studies utilized the more potent siLuc1 and pShagLuc for comparison.

The dose of siLuc1 or pShagLuc was varied over 100-fold (0.1–10 μg) against a fixed dose of pGL3 of 1 μg. When 1 μg of pGL3 was co-administered with 0.1 μg of siLuc1 or pShagLuc, the luciferase knockdown was not significant relative to control (Figure 4-3). Alternatively, when 1 μg of pGL3 was co-administered with either 10 μg of siLuc1 or pShagLuc the luciferase knockdown was >84% (Figure 4-3). The codelivery of pGL3 and either siLuc1 or pShagLuc to the same hepatocyte in the liver is a prerequisite to observing knockdown and has been noted previously as possibly limiting the utility of HD dosing as a means to deliver siRNA. The codelivery is more assured when transfecting fewer cells in vitro (10^6) with much larger doses (10 μg, 10^{12} plasmids) of

co-condensed pGL3/pShagLuc particles. However, when HD dosing, the number of hepatocytes in the liver is larger (10^8) and the pGL3 (1 µg, 10^{11} molecules) and pShagLuc doses (10 µg, 10^{12} molecules) are comparable, making it less likely that the same hepatocyte will take up both pGL3 and pShagLuc.

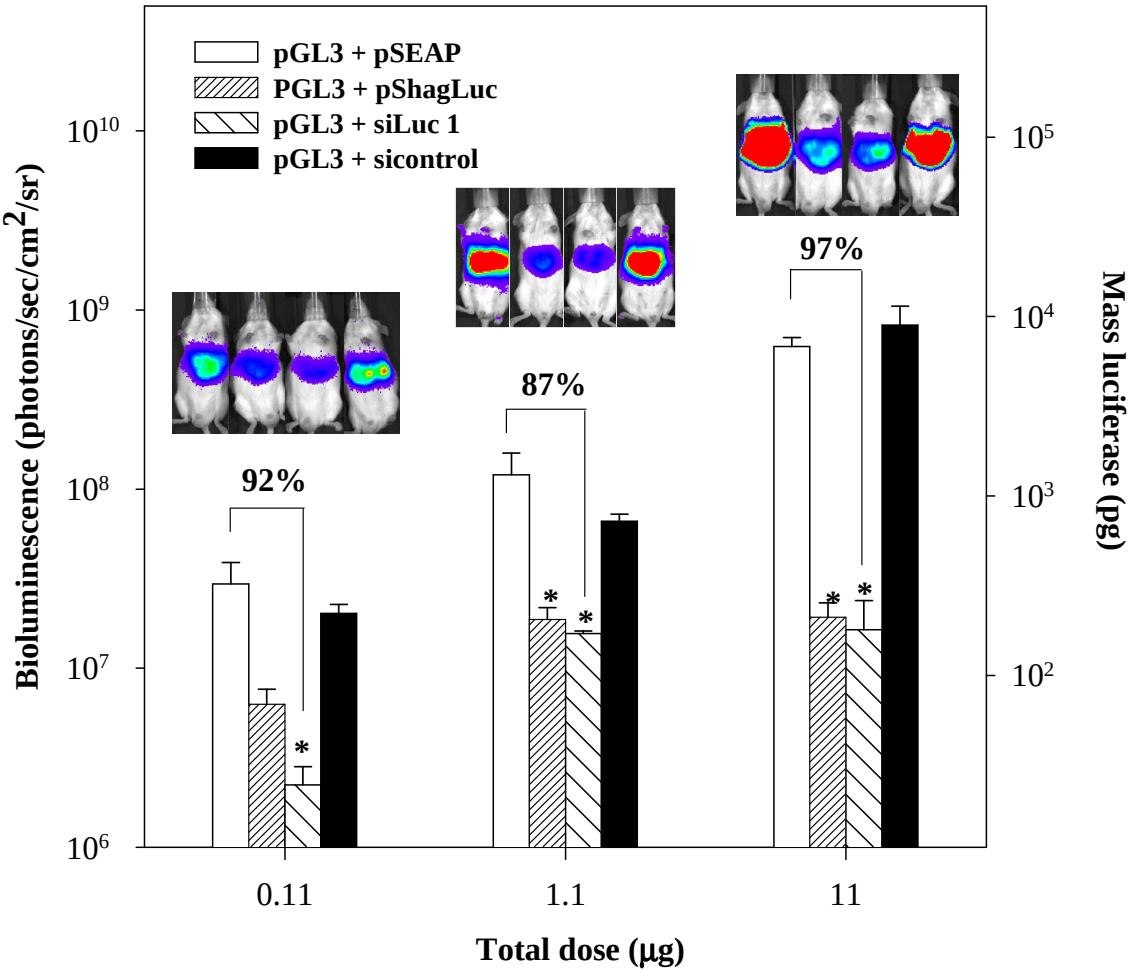

Figure 4-4. *In vivo dose–response comparison of pGL3:siRNA and pGL3:shRNA.* Triplicate mice were HD dosed with increasing amounts of pGL3 (0.01, 0.1, and 1 µg) while keeping the weight ratio of pGL3:pSEAP, pGL3:siRNA or pGL3:shRNA constant at 1:10, resulting in a total dose of 0.11, 1.1, or 11 µg of oligonucleotide. The luciferase expression was measured by BLI at 24 hrs. The results establish a statistically significant knockdown for pShagLuc and siLuc1 relative to control. *$p \leq 0.05$ relative to pGL3+pSEAP.

To examine this in more detail, the total dose of pGL3 plus siLuc1 or pShagLuc was varied from 0.11 to 11 μg while keeping the weight ratio of pGL3:siRNA or shRNA constant at 1:10 (Figure 4-4). At the lowest dose of 0.11 μg (0.01 μg of pGL3 plus 0.1 μg of siLuc1), the observed knockdown at 24 hrs was 92%. In contrast, 0.01 μg of pGL3 plus 0.1 μg of pShagLuc resulted in only 50% knockdown (Figure 4). At higher total doses of 1.1 μg and 11 μg , the knockdown was >87% for both siLuc1 and pShagLuc (Figure 4-4).

These results establish that the degree of knockdown is sensitive to total dose. When dosed in mice, pShagLuc reached a limiting knockdown potency at 0.1 μg , or 10^{11} molecules. In contrast, an equivalent dose of 0.1 μg of siLuc1, or approximately 10^{13} molecules, remained fully potent suggesting that at very low doses siLuc1 may have a potency advantage over pShagLuc.

We next determined if siLuc1 and pShagLuc could act synergistically to improve the degree of knockdown. Following HD dosing, the luciferase expression of pGL3 reached maximal expression at 12–24 hrs and then decreased by nearly 10-fold each 24 hr period for 3 days. When 5 μg of siLuc1 and pShagLuc were combined with 1 μg of pGL3, the degree of knockdown was 99% at 24 and 48 hrs, and 96% at 72 hrs (Figure 4-5). These results establish that siLuc1 and pShagLuc act synergistically and that a combination dose of 5 μg of each results in a 10-fold greater knockdown than a single 10 μg dose of either used alone.

Discussion

RNA interference is rapidly becoming an important branch of gene therapy since it allows for the selective, transient knockdown of protein expression.[131,132] The efficient delivery of siRNA in vivo is still a major bottleneck for the eventual development of therapeutics.

HD dosing of pDNA is a well established method for introduction and expression of DNA in hepatocytes in mice.[59,60] A variety of transgenes have been delivered via HD dosing resulting in a therapeutic level (mg per liver) of protein expression when delivering approximately 5 µg of plasmid DNA.[62,147,148]Hydrodynamic dosing of pGL3 in combination with BLI has resulted in a rapid and quantitative technique to benchmark liver expression.[66]

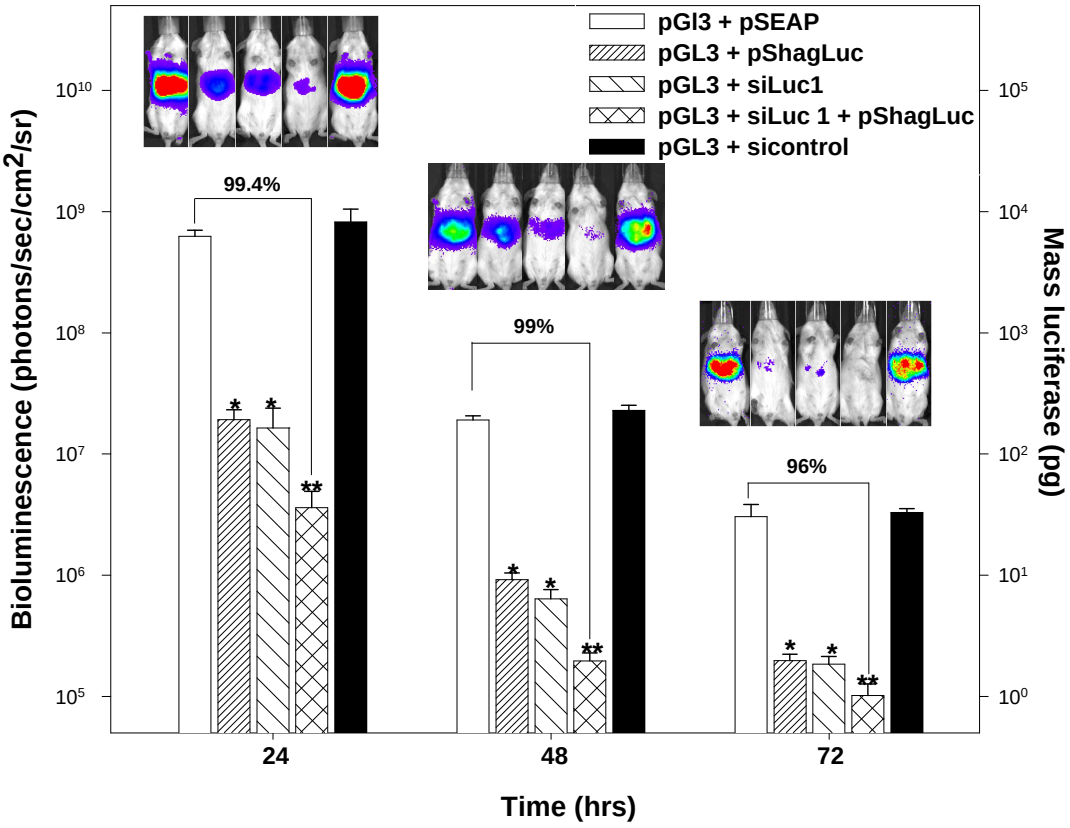

Figure 4-5. *Synergistic effect of siRNA and shRNA in vivo*. Triplicate mice HD dosed with 0.1 µg of pGL3 and either 1 µg of pSEAP, pShagLuc, siLuc1, sicontrol, or 0.5 µg of pShagLuc and siLuc1. The results demonstrate a statistically significant synergistic effect for the combined dose siLuc1 and pShagLuc in vivo. *$p \leq 0.05$ relative to pGL3+pSEAP and $p \leq 0.05$ relative to pGL3+pShagLuc.

In the present study, we have extrapolated this technique to quantitatively measure luciferase knockdown and compare the potency of siRNA and plasmid-born shRNA. A direct comparison of siLuc2 and pShagLuc, in which both were directed at the same sequence within luciferase mRNA, was not possible since both in vitro and in vivo studies revealed that siLuc2 failed to produce knockdown at doses in which pShagLuc's knockdown efficiency was 80%. Consequently, siLuc1 was used since it produced a similar degree of knockdown as pShagLuc when dosed on an equal weight basis. It should be noted however, that the dose needed to achieve knockdown of a plasmid-expressed reporter gene such as luciferase will likely be different than that needed to achieve the same affect on an endogenous gene.

An advantage of using synthetic siRNA versus plasmid-based shRNA is the ability to prepare synthetically modified siRNA possessing greater metabolic stability. Furthermore, siRNA delivery to the cytosol should be easier to achieve compared to shRNA which must enter the nucleus and undergo transcription. However, the shRNA hairpin has been established as a better substrate for dicer and displays improved RISC loading.[149,150]

Despite these potential advantages, when delivered hydrodynamically, pShagLuc appears to be much more potent than siLuc1 or siLuc2. Although, siLuc1 and pShagLuc possess similar potency when compared on a weight basis, the molecular weight of pShagLuc (5 kbp) is approximately 250 times greater than siLuc1. Thereby, 250 times fewer moles of pShagLuc results in the same degree of knockdown in vivo relative to siLuc1.

This difference in potency could result from less efficient delivery of siRNA to the cytosol compared with shRNA delivery to the nucleus. However, the delivery of shRNA to the nucleus appears to occur within the same time frame as siRNA delivery to the cytosol since the knockdown mediated by siLuc1 and pShagLuc both occur within 3 hrs of dosing (Figure 4-2). There was also no significant difference in the time course of

knockdown for siLuc1 and pShagLuc (Figure 4-5), suggesting that loading of RISC following HD dosing is sufficient to sustain knockdown for 3 days.

The magnitude of knockdown mediated by siLuc1 and pShagLuc was dose-dependent, with a 10 μg dose achieving approximately 80% knockdown. Based on the finding that siLuc1 and pShagLuc are nearly equipotent on a weight basis, but that pShagLuc is more potent on a per mole basis, we hypothesize that a significant amount of siLuc1 is lost to premature metabolism following HD dosing or that endogenously generated siRNA is more efficiently loaded into RISC.

The increased knockdown when co-administering siLuc1 and pShagLuc establishes that simultaneously targeting different sequences within the luciferase mRNA is an important strategy to increase potency and decrease dose (Figure 4-5). This finding also suggests that either siLuc1 or pShagLuc is capable of co-internalizing in the same hepatocyte with pGL3 in mice.

The results of this study establish both the magnitude and precision of knockdown at a given dose of siRNA or pShagLuc using hydrodynamic dosing. With this understanding, BLI can be adapted to provide a rapid quantitative screen for different siRNA or shRNA formulations in an attempt to achieve similar or improved knockdown without the use of HD dosing.

CHAPTER 5

TOWARD THE ENHANCEMENT OF NON-VIRAL GENE DELIVERY BY THE COVALENT INCORPORATION OF A NUCLEAR LOCALIZING SEQUENCE

Abstract

A major barrier to achieving efficient non-viral gene delivery is targeting DNA to the nucleus. Therefore, incorporating a peptide that contains a known nuclear localizing sequence (NLS) into a non-viral delivery system may boost gene expression by facilitating nuclear trafficking. The T antigen of SV40 is widely known to possess a short, lysine-rich sequence that is sufficient to mediate nuclear localization. Nuclear trafficking by this NLS is achieved via the nuclear pore complex, which is a multimeric protein that spans the nuclear membrane and allows selective uptake of particles. We have synthesized and characterized a 10 amino acid peptide containing the classic NLS sequence and an N-terminal photo-label – 4-azido-2,3,5,6-tetrafluorobenzoate. Flash-photolysis forms a highly reactive intermediate of the azide which subsequently makes a covalent adduct with DNA. The photochemical labeling of pGL3 by PL-NLS was confirmed by agarose gel electrophoresis. Labeling efficiency was quantitatively determined by using a radio-iodinated NLS. The labeling efficiency is a function of the stoichiometry of peptide and pGL3 reacted. A mol ratio of PL-NLS:pGL3 equal to 1 is achieved by reacting 2 pmol of peptide per μg of pGL3. Gene transfer studies with NLS-labeled pGL3 compared the transfection efficiency mediated by NLS-pGL3 relative to plasmid labeled with a control nuclear localizing sequence (cNLS-pGL3). In addition, several NLS analogs were incorporated into non-viral formulations and assayed as discussed. In vitro gene transfer efficiency was optimized by varying the ratio of PL-NLS to pDNA in a serum-starved culture of non-proliferative NIH 3T3 fibroblasts. The NLS-labeled pGL3 showed an increase in transgene expression compared to controls under

optimized conditions. Quantitative and qualitative analysis of the confocal microscopy images supports the conclusion that the increase in transgene expression is the result of increased nuclear localization of NLS-pGL3 when compared to the control peptide. Similar gene transfer studies were performed in vivo by dosing the formulations intramuscularly and using bioluminescence imaging to assay gene expression.

Introduction

Nuclear targeting remains a formidable barrier in optimizing the efficiency of non-viral vectors. Less than 1% of polyplexed pDNA microinjected into the cytosol actually reaches the nucleus[151]. This result highlights the great potential for an increase in transgene expression (possibly > 100-fold) by a non-viral vector that can maximize nuclear delivery. Non-viral gene transfer efficiency would be brought into a much more clinically acceptable range if nuclear targeting could be advanced by this magnitude. Unfortunately, current synthetic methods applied toward nuclear targeting of a non-viral vector have been largely unsuccessful.

An amino acid sequence within the SV40 large-T antigen (^{126}P-K-K-K-R-K-V^{132}) is well-known to be necessary and sufficient to achieve nuclear targeting[92]. This polycationic sequence is the classic NLS which is most widely used in non-viral gene delivery systems[83]. The sequence in its native form is a signal for nuclear targeting, but a ^{128}Lys→Thr mutation results in cytoplasmic localization. Along with the classic SV40 sequence, several NLS sequences have been identified and incorporated into non-viral gene delivery systems: extended SV40[101,152], M9[153] and bipartite NLS[154] among others.

An NLS-containing vector is designed to capitalize on endogenous pathways that will enable nuclear targeting. Briefly, Importin-α recognizes and binds an NLS in the cytosol. Subsequently, Importin-β binds NLS/Importin-α and shuttles the complex through the NPC. The multimeric NPC regulates nuclear targeting of macromolecules to the nucleus. Translocation is an efficient process (allowing for up to 1,000 translocations

per second), so an NLS in the architecture of a non-viral system is designed to harness this powerful capability.[85]

A variety of methods have been investigated to incorporate an NLS sequence into a non-viral delivery system. In most approaches, improved nuclear targeting of DNA is expected to be observed indirectly by way of an increase in transgene expression. Non-covalent strategies to incorporate NLS are considered advantageous because they avoid potential interruption of transcription by covalent modification of DNA. NLS has been electrostatically bound to DNA by its inherent cationic character[97] and by linking NLS to known DNA-binding peptides or polymers[105,153]. Triple-helix formation between dsDNA and an NLS-modified ssDNA oligomer[100] and an NLS coupled to a PNA clamp[102] are additional examples of non-covalent modification; however, these methods target a specific sequence of dsDNA. Covalent incorporation of NLS is potentially advantageous because an NLS-DNA complex formed by non-covalent interactions may not remain in tact while traversing the intracellular milieu. Covalent incorporation of NLS by way of base modification[108], chemical coupling[155], or photo-chemical coupling[106] has been explored.

Our approach has been focused on photo-chemical coupling because it affords a synthetically straight-forward strategy as a part of solid-phase peptide synthesis (SPPS) and is universally applicable toward labeling any nucleotide-based cargo. These PL-NLS peptides contain a photo-labile linker at the N-terminus. The para-azide of 4-azido-2,3,5,6-tetrafluorobenzoate is activated upon flash-photolysis and readily reacts with nucleophilic functional groups on DNA via a radical rearrangement mechanism[156]. The cationic nature of NLS seats the peptide on the anionic backbone of DNA, and positions it so that photoactivation of the N-terminal PL results in covalent modification of DNA.

We have synthesized and characterized a series of PL-NLS peptides (and the corresponding cNLS peptides). Following studies of photo-labeling efficiency, these peptides have been tested in non-viral gene delivery experiments ranging from cell

culture-based examination of nuclear uptake via confocal microscopy to in vivo studies monitoring bioluminescence levels upon delivery of plasmid encoding luciferase.

Materials and Methods

Synthesis of Photo-Label: 4-azido-2,3,5,6-tetrafluorobenzoate

Methyl pentafluorobenzoate, sodium azide and magnesium sulfate were purchased from Sigma-Aldrich Chemical Co. (St. Louis, MO). The synthesis of the photo-label (PL) is outlined in Scheme 5-1. Briefly, methyl pentafluorobenzoate (5 mmol) and sodium azide were combined in a 1:1 mol ratio in acetone (10 ml) and refluxed for 8 hrs. The mixture was cooled, diluted with water (15 ml) and the para-azide product was extracted into diethyl ether. The extract was dried with $MgSO_4$, and ether was removed by rotary evaporation to leave a white solid. The resultant solid was dissolved in 20% aqueous NaOH/water/methanol (1:1:10 by volume) and stirred overnight at room temperature. The solution was acidified to pH 1 with 2 N HCl and extracted into methylenechloride. The extract was again dried with $MgSO_4$ and rotary evaporation. The white solid was purified by recrystalization in hexane/ethyl acetate (10:1).

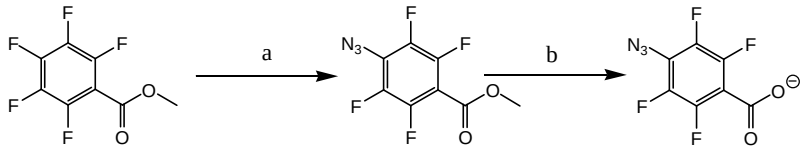

1 2 3

Scheme 5-1. *Synthesis of 4-azido-2,3,5,6-tetrafluorobenzoate*. Reagents and conditions: (a) NaN_3, acetone, reflux; (b) NaOH, methanol, water, room temperature.

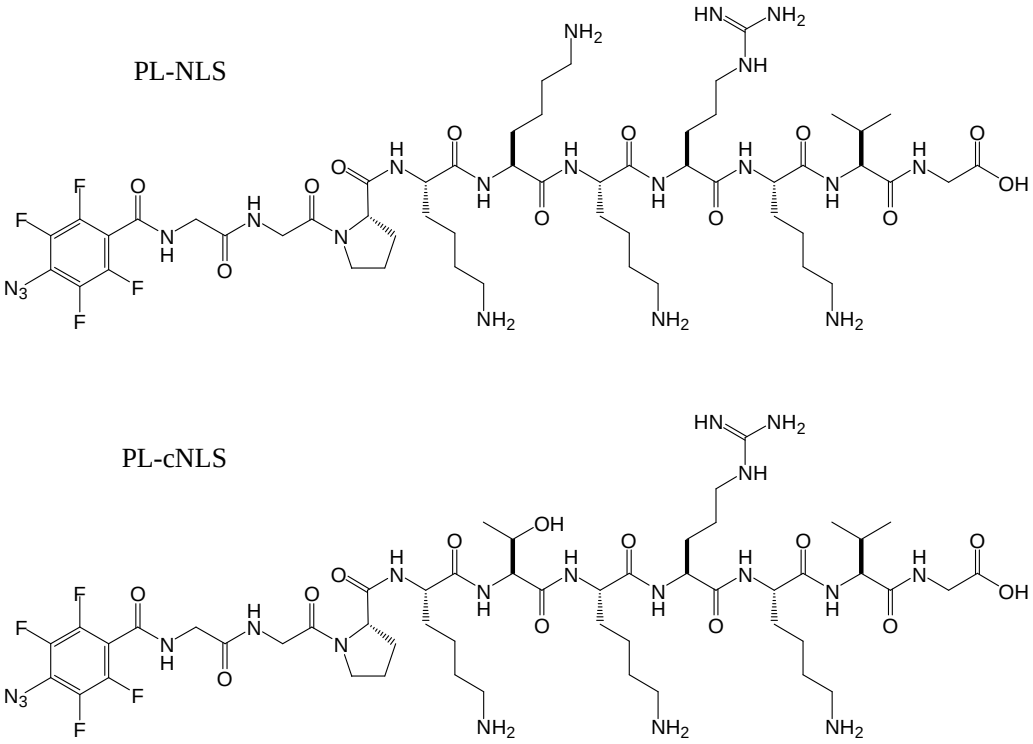

Figure 5-1. *PL-NLS and PL-cNLS*. Peptides contain the classic SV40 sequence and a 2-Gly linker between the N-terminus of the NLS and the photo-label.

Solid-Phase Peptide Synthesis of PL-NLS

N-terminal protected Fmoc amino acids, substituted Wang resin for peptide synthesis, 1-hydroxybenzotriazole (HOBt) and diisopropylcarbodiimide (DIC) were purchased from Advanced Automated Peptide Protein Technologies (formerly known as Advanced ChemTech, Louisville, KY). N-methyl pyrrolidinone, trifluoroacetic acid (TFA), acetic acid anhydride, acetonitrile, piperdine and diethylether were purchased from Fisher Scientific (Pittsburgh, PA). Diisopropylethylamine was purchased from Sigma-Aldrich Chemical Co. (St. Louis, MO).

NLS peptides with an N-terminal PL were synthesized on functionalized Wang resin for solid-phase peptide synthesis (Scheme 5-2). The resin was substituted for a 30

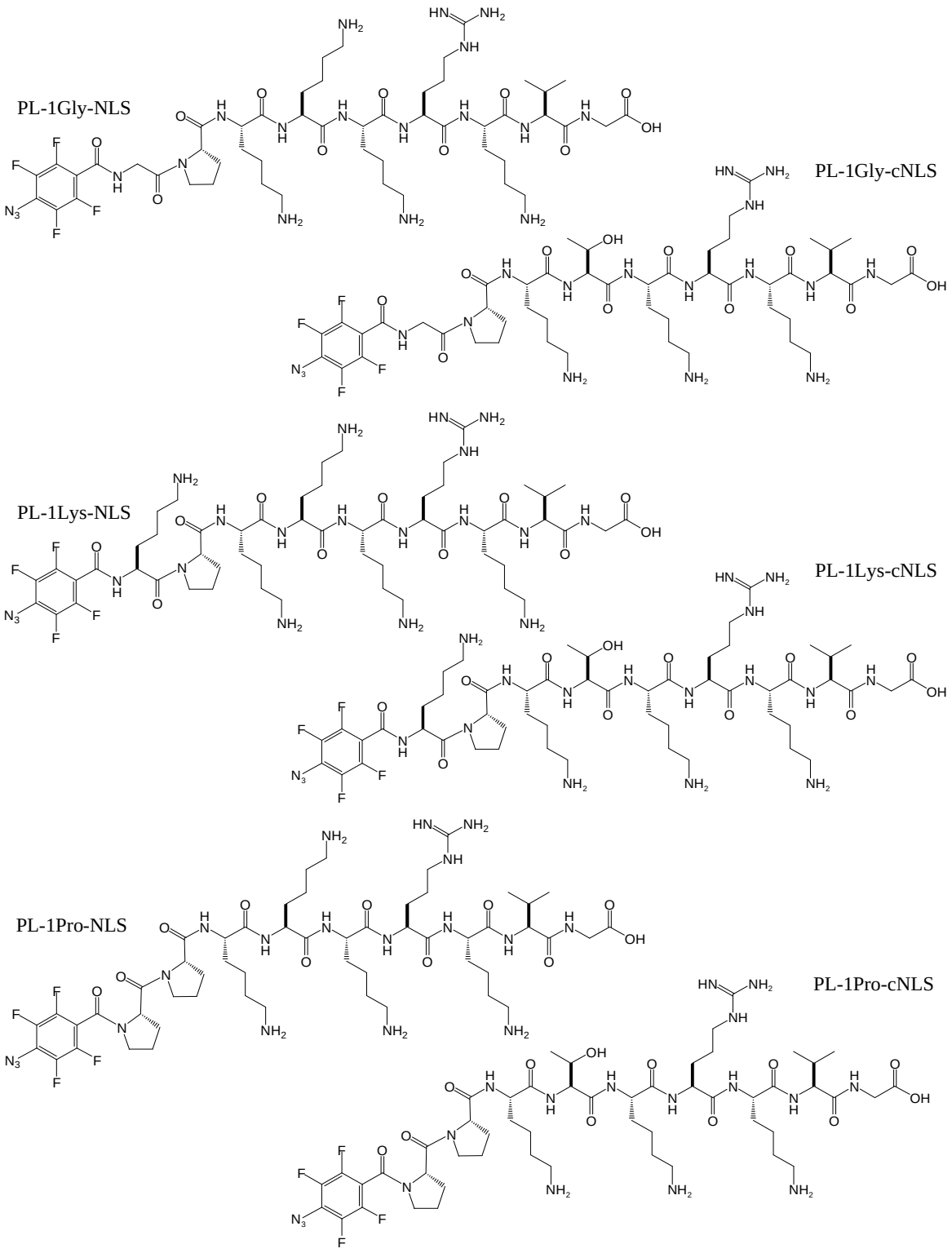

Figure 5-2. *NLS analogs: single amino acid linkers*. Peptides all contain the classic SV40 NLS sequence or the Thr-containing cNLS. Peptides are linked to the photo-label by a single amino acid (Gly, Lys or Pro).

μmol synthesis with the C-terminal amino acid in a DIC/HOBt coupling reaction. SPPS of all PL-peptides is described here in general terms. Peptide synthesis was carried out on an Apex 396 from AAPPTec using DIC/HOBt and the amino acid monomer in 5-fold mol excess with double-couplings on a 30 μmol scale. The N-terminus of a resin-linked peptide was coupled to PL over 4 hours in DMF with PL, DIC and HOBt present in 6-

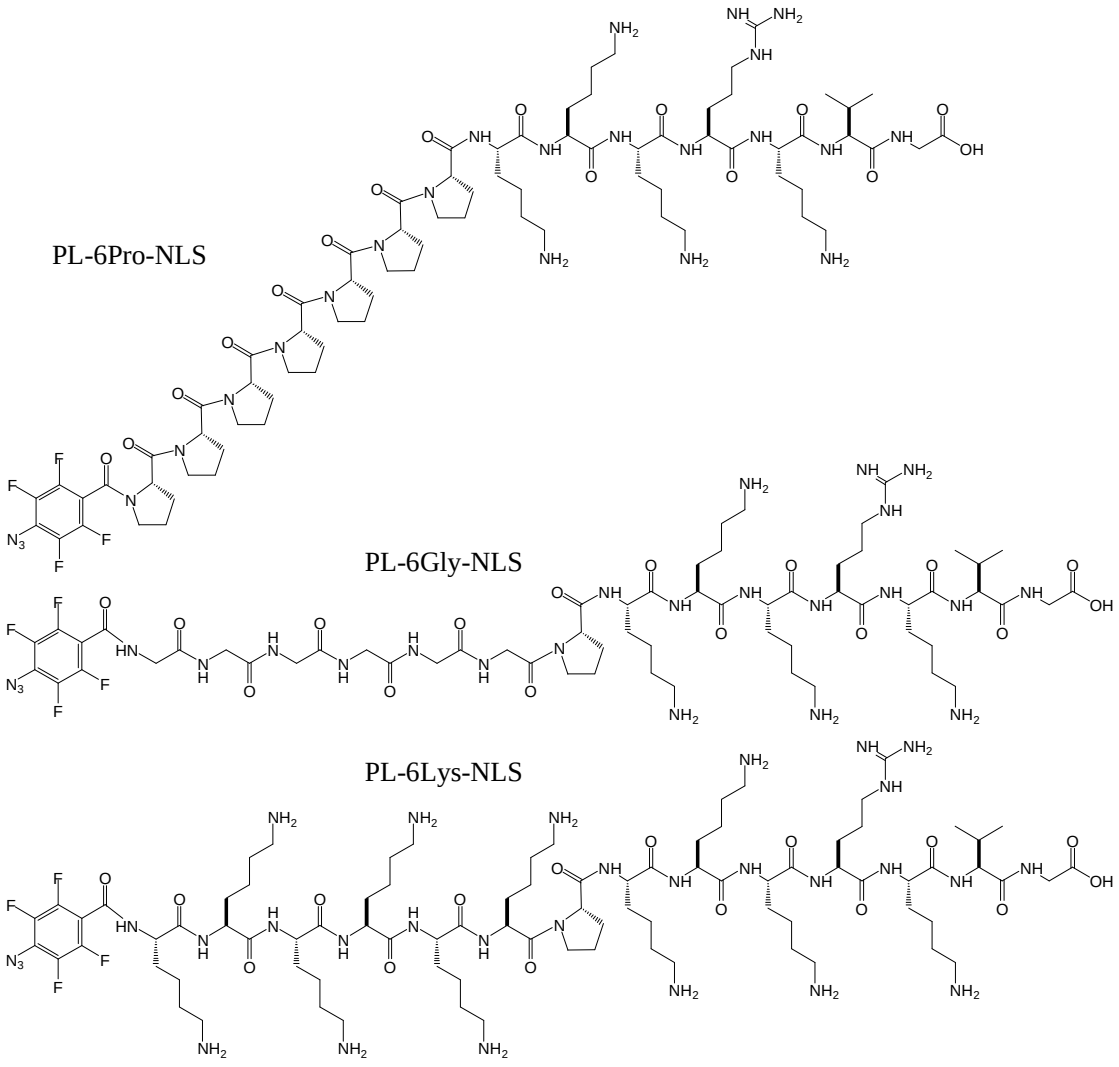

Figure 5-3. *NLS analogs: 6 amino acid linkers for NLS-containing peptides*. Peptides all contain the classic SV40 NLS sequence and are linked to the N-terminal photo-label by 6 amino acids (Gly, Lys or Pro).

fold mol excess relative to the substitution of the resin. Following synthesis, the peptide was deprotected and cleaved from the resin in the presence of 95% TFA. The above described conditions werer used to synthesize the classic PL-NLS and PL-cNLS (Figure 5-1), single amino acid linker PL-NLS and PL-cNLS (Figure 5-2), 6 amino acid linker PL-NLS (Figure 5-3) and PL-cNLS (Figure 5-4) peptides, ExtSV40 analogs (Figure 5-5) and PL-NLS-Y (Figure 5-6).

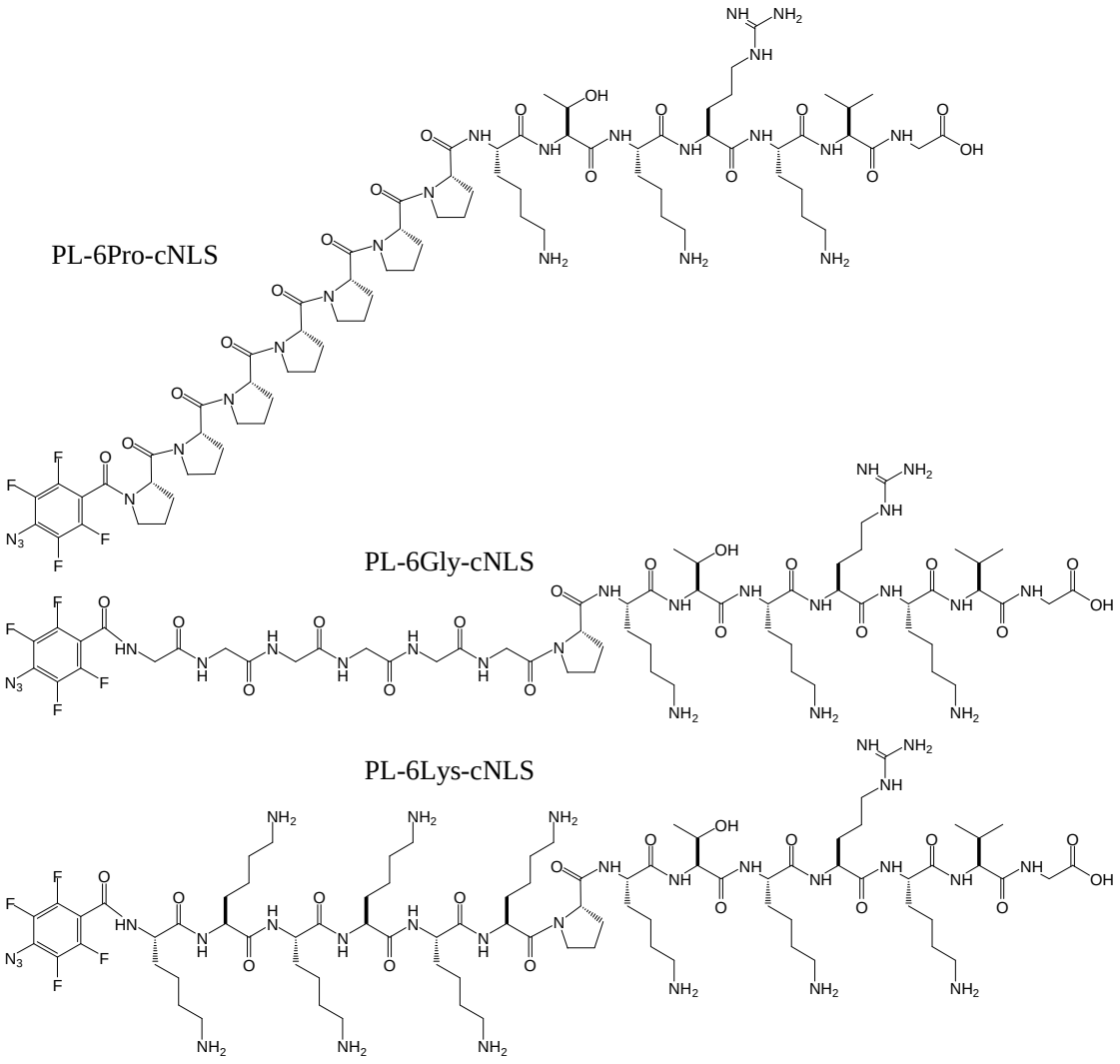

Figure 5-4. *NLS analogs: 6 amino acid linkers for cNLS peptides*. Peptides contain the control SV40 NLS sequence (cNLS) and are linked to the N-terminal photo-label by 6 amino acids (Gly, Lys or Pro).

The peptide was precipitated in ice cold diethyl ether, freeze-dried, and reconstituted in 0.1% TFA in water (v/v) as a crude mixture. The peptide was purified to homogeneity on RP-HPLC by injection onto a Vydac C_{18} semipreparative column and eluted at 10 ml/min with 0.1% TFA and a gradient of acetonitrile over 30 min while monitoring PL-absorbance at 258 nm. (See Table 5-1 for specific elution gradients for each peptide.) The peptides were collected using an automated fraction collector from ISCO (Lincoln, NE). The major peak of each peptide was collected and pooled from

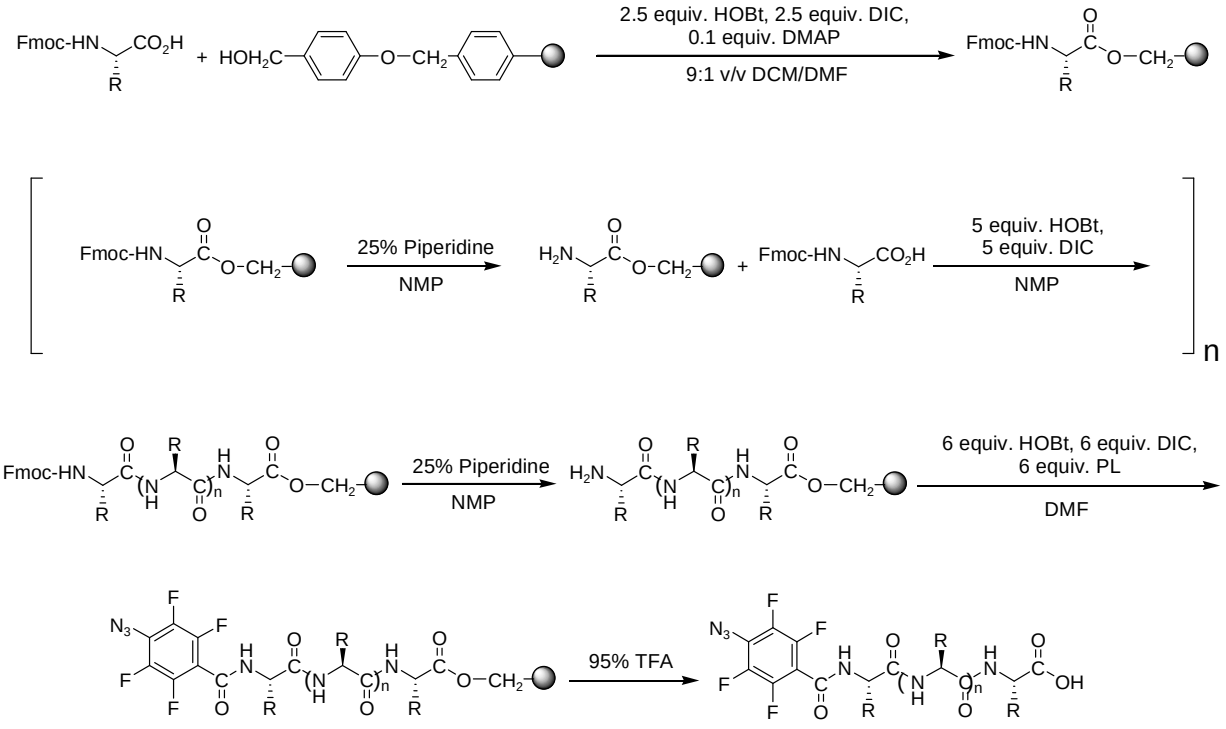

Scheme 5-2. *Solid-phase peptide synthesis of PL-peptides.* PL-NLS peptides were synthesized on Wang resin according to standard Fmoc peptide chemistry protocol. The final coupling on solid-support introduced PL at the N-terminus of the peptide chain. The peptides were cleaved and side-chain deprotected in 95% TFA (water).

several runs, concentrated by rotary evaporation, and lyophilized. The purified peptide was reconstituted in 0.1% TFA and quantified by PL absorbance (ε = 14,951 $M^{-1}cm^{-1}$ at 258 nm).

The peptide was characterized on an Agilent 1100 LC-ESI-ion trap by injecting 2 nmol onto a Vydac C_{18} analytical column and eluted at 0.7 ml/min with 0.1% TFA in water (v/v) and a gradient of acetonitrile over 30 min. The RP-HPLC eluent was directly infused into the electrospray ionization source and mass spectral data was obtained in the positive mode.

Photo-Flashing and pDNA Labeling with PL-Peptides

pGL3 Control plasmid (5.3 kbp) was purchased from Promega (Madison, WI). (pGL3 Control plasmid will henceforth be designated as "pGL3 (+/+)" as it contains both the SV40 promoter and enhancer elements). Endotoxin-free purification from *Escherichia coli* was achieved via ion-exchange chromatography on a Qiagen (Valencia, CA) giga column according to the manufacturer's instructions. PL-peptides were obtained by SPPS, as described above. Agarose was purchased from Gibco-BRL (Madison, WI). Ethidium bromide solution (10 mg/ml) was obtained from Bio-Rad (Hercules, CA).

ε Defined for PL at 258 nm

Varying amounts of PL (2.5, 10, 15 and 25 mg) were diluted into 1 ml of 0.1% TFA in triplicate. This corresponded to a concentration of PL ranging from 1.06×10^{-5} – 1.06×10^{-4} M. These dilutions were measured for UV absorbance at 258 nm (path length is 1 cm) and plotted as absorbance intensity (optical density) versus PL concentration. The slope of the linear regression line represents the molar absorptivity for the molecule ($M^{-1}cm^{-1}$).

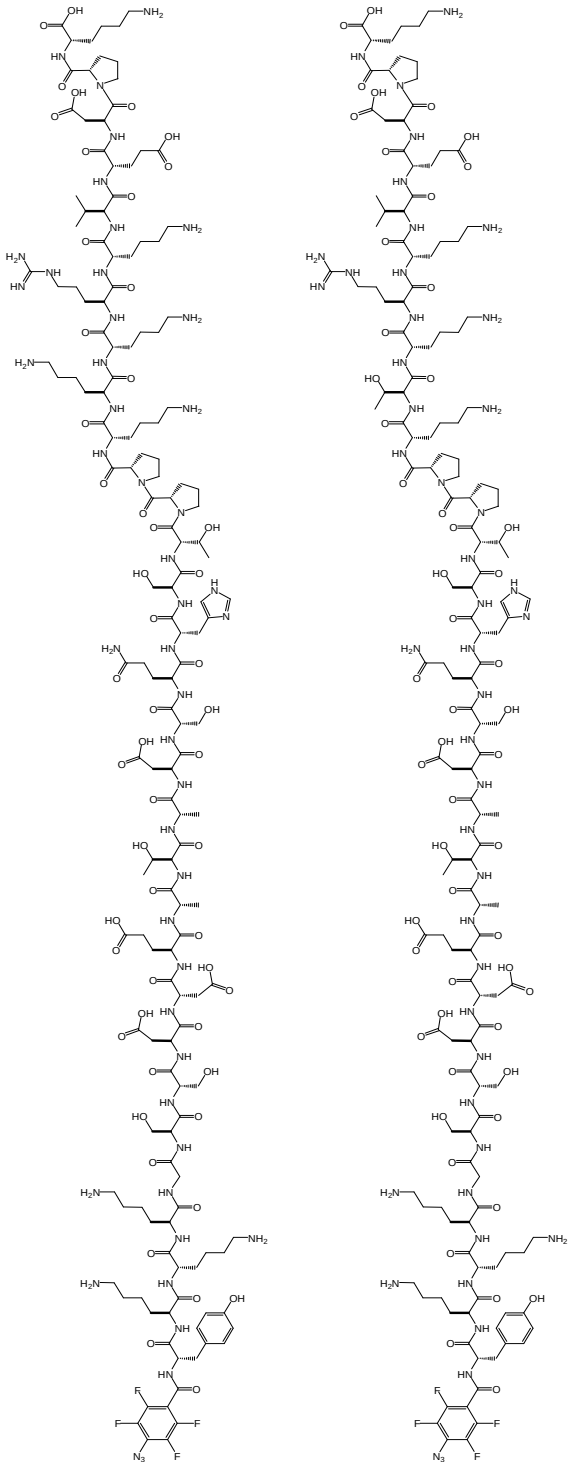

Figure 5-5. *Extended SV40 NLS analogs*. Peptides contain the classic SV40 NLS (left) or cNLS (right). The native sequence of the antigen is extended at the N-terminus to include key Ser residues that are phosphorylatable and function in nuclear localization.

Photo-Degradation of PL-NLS UV Absorbance at 258 nm

An aliqot of PL-NLS was diluted with 5 mM Hepes up to 1 ml. The final concentration of PL-NLS was 77.8 nmol/ml. The sample was held in a 1.5 ml polypropylene microfuge vial at 2 cm from a single photo-flash. The UV absorbance at 258 nm was measured prior to photo-flashing. Subsequently, absorbance measurements were made at 5-flash intervals up to 85 flashes.

Photo-Labeling

pGL3 (+/+) was diluted to 0.4 μg/μl in 5 mM Hepes buffer (pH 7.4; 0.22 μm-filtered). Stock dilutions of PL-NLS were serially diluted to 1,000, 100, 10, 1 and 0.1 pmol of peptide/μl of 5 mM Hepes. An aliquot of pGL3 (+/+) (containing the desired amount of plasmid for the photo-labeling reaction) was added dropwise to an equal volume of peptide (containing the amount required to achieve the desired photo-labeling stoichiometry) contained in a 500 μl polypropylene microcentrifuge vial. Samples were lightly vortexed and incubated at room temperature for 10 min. Covalent labeling was induced by an original photo-flashing apparatus which is comprised of a single camera flash controlled by a manually operated switch. The samples were subjected to 40 flashes when held at a distance of 2 cm from the flash source. Samples were further incubated for 30 min at room temperature prior to additional formulation methods being applied.

Agarose Gel Electrophoresis

Agarose gel electrophoresis of pGL3(+/+) covalently labeled by PL-peptides was carried out on a 1% agarose gel – 500 mg of agarose dissolved in 50 ml of TBE buffer (100 mM Trizma Base, 90 mM boric acid, 1 mM EDTA, pH 8.0). 2 μl of ethidium bromide (10 mg/ml) was added to the agarose solution and mixed briefly. The gel was cast to contain 8 x 30 μl wells and was bathed in 300 ml of TBE buffer in Mini-Sub Cell GT (Bio-Rad). The Bio-Rad PowerPac 200 induced electrophoretic movement of pDNA toward the cathode with a field of 80 V applied over 70 min.

Aliquots of NLS-pDNA that contained 500 ng of plasmid (0.2 μg/μl) were obtained from the above-described photo-labeled samples. They were combined with 5 μl of the 6x loading dye and TE buffer (10 mM Tris-HCl, 1 mM EDTA, pH 8.0) was added up to 30 μl. The total volume for each sample was loaded into a well of the 1% agarose gel.

A transilluminator (UVP, Upland, CA) was used to image the pGL3 banding pattern as represented by the fluorescence of intercalated ethidium bromide. Images of gels were acquired on Polaroid 661 Black & White Instant Pack film by a hooded photo-documentation camera (Fischer Biotech, Pittsburgh, PA).

Band-Shift Induced by PL-NLS Labeling

pGL3 (+/+) was labeled by PL-NLS at 100 and 1,000 pmol/μg. These formulations were compared to unlabeled plasmid and a non-flashed sample of pGL3 (+/+) in the presence of 100 or 1,000 pmol of PL-NLS/μg. 500 ng of pGL3 (+/+) was loaded onto a 1% agarose gel as described above. The gel was run at 80 V for 70 min which allowed for qualitative assessment of photo-labeling observed by band-shift retardation.

Agarose Gel Band-Shift Induced by Variable Linker PL-NLS Peptides

All 12 peptides included in the series of variable linker PL-NLS/cNLS peptides (Figure 5-2 to 5-4) were diluted such that the relationship to pGL3 (+/+) (0.4 μg /μl in 35 μl of 5 mM Hepes) was 1.0 nmol of peptide/μg of plasmid and the final concentration of pGL3 (+/+) in the labeling reaction was 0.2 μg/μl. A 500 ng aliquot was removed from each peptide-pDNA dilution, and the remainder was photo-flashed. For each peptide, 500 ng of non-flashed aliquot was compared to 500 ng of photo-flashed aliquot by agarose gel electrophoresis. The flashed versus non-flashed comparison for the 6-Lys (PL-6Lys-NLS

and PL-6Lys-cNLS) peptides was inconclusive, so a photo-degradation profile was generated for each, as described above.

Particle-Size Analysis

pGL3 (+/+) labeled with PL-peptides was condensed by PEI for the purpose of in vitro transfection. Prior to transfection, the size of the nanoparticles was assessed by dynamic light-scattering. An amount of 50 μg of plasmid in 1 ml was required to make reliable particle-size measurement via the Zeta-Plus (BIC, Holtsville, NY). Briefly, pGL3 was labeled with varying amounts of PL-NLS (0.1, 0.2, 0.3, 0.4, 0.8 and 1.0 nmol/μg) as described above. 50 μg of peptide-labeled pGL3 (+/+) was diluted with 5 mM Hepes to 500 μl (0.1 μg pGL3/μl). Likewise, PEI was diluted up to 500 μl. The amount of PEI in the dilution was dependent on the desired charge ratio (43 μg of PEI per 325 μg of pDNA corresponds to an $R\text{-}NH_3^+$:$PO_4R_2^-$ of 1.0). pGL3 (+/+) was added dropwise to PEI while vortexing, and samples were incubated at room temperature for 30 min. The average diameter and the distribution width (polydispersity) were measured using the Zeta-Plus (BIC, Holtsville, NY).

Iodination of PL-NLS-Y and Quantitative Photo-Labeling Efficiency

TFA and acetonitrile were purchased from Fisher Scientific (Pittsburgh, PA). Sephadex G-10, chloramine T, and sodium metabisulfite were purchased from Sigma-Aldrich Chemical Co. $Na^{125}I$ (2 mCi in 0.1 M sodium hydroxide) was obtained from MP Biomedicals, Inc. (Irvine, CA). Phosphate-buffered saline (Mg^{2+}-free and Ca^{2+}-free) was purchased from Gibco-Invitrogen (Madison, WI). MaxiClean C_{18} cartridges were purchased from Alltech (Deerfield, IL). Zeta-probe blotting membranes were obtained from Bio-Rad.

Iodination of PL-NLS-Y

The tyrosine-containing analog of PL-NLS (Figure 5-6) was synthesized as described previously on a tyrosine-functionalized Wang resin. Iodination of PL-NLS-Y was based on modifications to the chloramine T method first described by Greenwood[157]. 2 nmol of PL-NLS-Y was freeze-dried and reconstituted in 60 µl of 0.5M phosphate buffer (pH 7.0). The peptide was contained in a rubber septum-capped glass vial. 25 µl $Na^{125}I$ (0.5 mCi) was added to the peptide followed by 20 µl chloramine T (10 mM in phosphate buffer) and reacted for 3 min. The reaction was quenched by adding 80 µl of sodium metabisulfite (10 mM in above-described phosphate buffer).

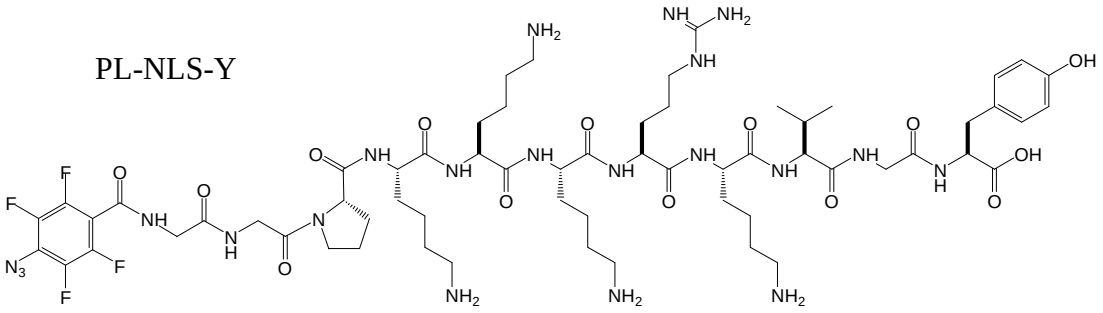

Figure 5-6. *PL-NLS-Y*. The PL-NLS peptide was synthesized with a C-terminal Tyr to allow for radio-iodination by the Greenwood method.

Gel-Filtration and Thin-Layer Chromatography of PL-NLS-$Y^{125}I$

Immediately following the iodination, the reaction mixture was transferred to a Sephadex G-10 column (0.8 x 25 cm), and eluted with phosphate-buffered saline (PBS). Column eluent was collected in 0.5 ml fractions. The presence of the iodinated peptide was detected using a survey meter (Ludlum, Sweetwater, TX) and compared to the expected peptide elution profile previously defined with the unlabeled PL-NLS-Y. Radioactivity of the collected fractions was analyzed by the Gamma Trac gamma counter

(Tm Analytic, Tampa, FL). Fractions corresponding to the iodinated peptide were pooled and transferred to a lead pig (MP Biomedical) for storage at 4^{o}C. The purity of the peptide was analyzed by spotting 5 μl (>10,000 cpm) at the origin of a TLC plate which was then developed with 90% acetic acid as the mobile phase. Quantitative densitometry was performed on a PhosphorImager (Molecular Dynamics, Sunnyvale, CA) following overnight autoradiographic exposure. Image-Quant software (Molecular Dynamics, Sunnyvale, CA) was used to integrate the densitometry trace. The specific activity of the sample was calculated to be 57.27 μCi/nmol.

Prior to iodination, the column was calibrated by eluting non-iodinated PL-NLS-Y under the same conditions as described for the iodinated sample. Elution of the peptide was monitored by UV absorbance at 258 nm. In addition, elution of NaI was monitored by UV absorbance at 240 nm.

Solid-Phase Purification of PL-NLS-Y-^{125}I

Following iodination and gel filtration of the tyrosine-containing peptide, a solid-phase purification strategy was employed to further purify and remove free $^{125}I^{-}$ from the sample. Briefly, the syringe-driven, Maxi-Clean C_{18} cartridge was equilibrated by 3 ml of 0.1% TFA in water. An aliquot of radiolabeled peptide was diluted up to 1 ml with 0.1% TFA and forced into the 300 mg resin bed. Fractions (0.5 ml) were collected in 1.5 ml microcentrifuge vials and radioactivity was measured. 3-5 ml of 0.1% TFA in water was washed through the cartridge. Subsequently, PL-NLS-Y-^{125}I was eluted with increasing amounts of acetonitrile in a step gradient up to 40% acetonitrile. Peptide-containing fractions were pooled and dried on a speed vac to remove TFA and acetonitrile. Sample purity was determined by TLC and phosphorimage analysis as described above.

Calculating Photo-Labeling Efficiency

The tyrosine-containing PL-NLS was synthesized and radiolabeled primarily to allow for specific quantification of the labeling efficiency. A small volume of the purified

stock of PL-NLS-Y-^{125}I, containing approximately 100,000 cpm, was added to a stock dilution of unlabeled peptide in 5 mM Hepes. An aliquot of the now-radioactive peptide dilution was combined with 35 µl of pGL3 (+/+) (0.4 µg of pGL3 per µl of 5 mM Hepes) in an equal volume. The pGL3 (+/+) aliquot was added to the peptide dilution and lightly vortexed. The resultant dilutions of peptide and plasmid ranged from 0.1-100 pmol of PL-NLS-Y per µg of plasmid. The samples were contained in a 1.5 ml screw-top vial and were photo-flashed (40x) to induce covalent labeling. The radioactivity of these samples was verified following photo-flashing to define the initial cpms (cpm_i). All measurements of radioactive decay were based on 1 min readings from the Gamma Trac (Tm Analytic, Tampa, FL).

pGL3 (+/+) was precipitated by the addition of 3 M sodium acetate (0.1x volume) and 100% ethanol (2x volume). Samples were centrifuged at 12,000 x *g* for 15 min at 4^{o}C. The supernatant was decanted and 150 µl of 70% ethanol in water was added to wash the remaining pellet. Samples were again centrifuged for 10 min under the same conditions. Supernatant was removed, and the final cpms (cpm_f) of the labeled plasmid were measured on the gamma counter.

Two control labeling experiments were performed using identical aliquots of radiolabeled peptide. The first involved a dilution of pGL3 (+/+) and PL-NLS-Y-^{125}I at each stoichiometry described above, but the samples were not subjected to photo-flashing ($cpm_{f\text{-No Flash}}$). This control allowed for the determination of peptide that was ionically associated with pGL3 after ethanol-precipitation but not covalently bound. The second control was PL-NLS-Y-^{125}I in the absence of pGL3. This control revealed the amount of residual peptide that remained in the microfuge vial in the absence of pGL3 ($cpm_{f\text{-No pDNA}}$). This control treatment was subjected to photo-flashing. These control values of radioactivity were subtracted from the final measurement of cpms to reflect the actual radioactivity of the covalently labeled peptide (Equation 1)

$$\% \text{ PL-NLS Bound to pGL3} = (cpm_i - [cpm_f - cpm_{f\text{-No pDNA}}])/cpm_i$$

$$\% \text{ PL-NLS Covalently Labeled to pGL3} = \% \text{ Bound} - (cpm_{f\text{-No flash}}/cpm_i)$$

Equation 1. *Calculating Photo-Labeling Efficiency.*

Stability of PL-NLS-pGL3 Covalent Linkage

Stability of the covalent interaction was investigated by incubating pGL3 (+/+) (labeled with PL-NLS-Y-^{125}I) at room temperature in either 5 mM Hepes buffer (pH 7.4) or 1 M NH_4OH (pH 11.5). Plasmid was initially labeled and ethanol-precipitated as described above. Triplicate samples were subsequently reconstituted in either buffer. Samples of peptide-pGL3 (+/+) were ethanol-precipitated and reconstituted in their respective aqueous buffers following 1, 24 and 48 hrs incubation at room temperature. The radioactive decay of reconstituted samples was observed at each time point.

Agarose Gel Electrophoresis and Autoradiography of pGL3
Labeled by PL-NLS-Y-^{125}I

Agarose gel electrophoresis of pGL3 (+/+) that was covalently labeled by PL-NLS-Y-^{125}I was used as a qualitative assessment of covalent modification. A small volume of radiolabeled peptide was added to dilutions of cold peptide ranging from 1-100 pmol of peptide/μl of 5 mM Hepes. Each peptide dilution had the same radioactivity (in terms of total cpms). pGL3 (+/+) was covalently labeled with various stoichiometries of peptide (1-100 pmol of peptide/μg pGL3) as described previously. A 10 μg aliquot of pGL3 from each labeling reaction was loaded into a well in the agarose gel with 10 μl loading dye in a total volume of 60 μl (diluted with TE buffer). Electrophoretic movement of peptide-labeled pGL3 was induced by an 80 V field applied over 70 min. Band migration was initially assessed by a transilluminator image of intercalated ethidium bromide. The gel was then dried on a slab gel drier and pGL3 was trans-blotted

onto a zeta-plus blotting membrane overnight. Radioactivity of pGL3 was determined by exposing the zeta membrane to a phosphorimager cassette overnight. The autoradiograph was assessed as described previously.

Assessing Nuclear Uptake of NLS-pDNA by Confocal Microscopy

NIH/3T3 murine fibroblasts were obtained from The University of Iowa, Gene Therapy Core (Iowa City, IA). Glass chamber slides (4 wells) were purchased from LabTek (Hatfield, PA). All tissue culture supplies were obtained from Gibco – Invitrogen Life Technologies, Inc (Carlsbad, CA). pGL3 (+/+) plasmid (5.3 kbp) and pGL3 Basic (-/-) plasmid (4.8 kbp) were purchased from Promega (Madison, WI). (pGL3 Basic plasmid will henceforth be described as "pGL3 (-/-)" as it lacks both the SV40 promoter and enhancer elements.) Purification from *Escherichia coli* was achieved via ion-exchange chromatography on a Qiagen (Valencia, CA) giga column according to the manufacturer's instructions. Cy3 *Label*IT was purchased from Mirus Bio Corporation (Madison, WI). High molecular weight polyethyleneimine (PEI) was purchased from Sigma-Aldrich (St. Louis, MO). Vectashiled mounting media (no DAPI) was purchased from Vector Laboratories (Burlingame, CA), and TO-PRO-3 was purchased from Molecular Probes (Eugene, OR). Luciferase from *Photinus pyralis* and ATP were purchased from Roche Diagnostics Corporation (Indianapolis, IN). The BCA assay kit was obtained from Pierce Biotechnology Inc. (Rockford, IL). D-luciferin was purchased from Gold Biotechnology (St. Louis, MO). Peptide-217 was previously synthesized in the laboratory on Wang resin using standard Fmoc procedures with HOBt and DIC double-couplings at a 30 μmol scale on an Apex 396 Advanced ChemTech solid phase peptide synthesizer.

Cy3- and NLS-Labeling and Transfection

A 1 ml suspension of 10^4 NIH/3T3 cells was aliquoted to each well of a 4-well chamber slide. NIH/3T3 culture media was composed of Dulbecco modified essential medium (DMEM) containing 10% heat-inactivated fetal bovine serum (FBS) and penicillin and streptomycin (100 U and 100 μg/ml). Cells were incubated in a 5% CO_2 atmosphere at 37^o C overnight.

pGL3 (+/+)was labeled with Cy3 according to the manufacturer's guidelines regarding the Label*It* method (based on DNA alkylation by cyclopropa-pyrroloindole[155]). Cy3-pGL3 was purified by ethanol precipitation and diluted to 0.4 μg pGL3/μl of 5 mM Hepes buffer (pH 7.4). Photo-labeling of Cy3-pGL3 was achieved as described previously. Briefly, Cy3-pGL3 was added dropwise to an equal volume of PL-NLS in 5 mM Hepes buffer to achieve a photo-labeling stoichiometry of 1-100 pmol of peptide per μg of pGL3. Photolysis of PL-peptides diluted with Cy3-pGL3 (+/+) was initiated using the conventional photo-flash. Samples contained in polypropylene microcentrifuge tubes were photo-flashed 40x and maintained at room temperature for 30 min incubation. Transfection of NIH/3T3 cells was carried out with PEI or an alternate DNA condensing agent, peptide-217 ($CWK_{17}C$, 2589 g/mol). Polyplex formation with either polycation was achieved at 0.05 μg pGL3/μl in 5 mM Hepes buffer for 30 min at room temperature. Prior to transfection, the culture media (10% FBS) was removed, and cells were washed with 500 μl PBS and bathed in 600 μl of 2% FBS (DMEM) transfection media. Cells in each well were transfected with 500 ng (10 μl) of polyplexed and photolabeled Cy3-pGL3 (+/+). The duration of transfection was specified for each experiment.

Confocal Microscopy Image Acquisition

At a defined time point following transfection, the culture media was removed, cells were washed with PBS and fixed with 4% paraformaldehyde (in PBS) for 10 minutes at room temperature. Cells were again washed with PBS and then permeabilized

for 10 minutes with 0.5% Triton X-100 (in PBS). Following 2 washes with PBS, nuclei were stained with TO-PRO-3 (0.5 μM) for 5 minutes. Cells were briefly washed with PBS and plastic wells were removed (along with the silicon gasket) leaving only the glass slide with fixed cells. Glass coverslips were mounted with 40 μl of Vectashield (no DAPI) mounting media. The glass slides were stored in the dark at 4^{o}C prior to confocal imaging.

Single-Plane Qualitative Analysis of NLS-Labeled pDNA Uptake over a 24 Hour Time Course

NIH 3T3 cells were seeded in glass slide chamber wells (10^4 cells/well) and incubated for 24 hours at 37^{o}C. Cy3-pGL3 (+/+) was labeled by PL-NLS or PL-cNLS prior to transfection. Transfection with the peptide-labeled plasmid was compared to two additional controls: un-labeled Cy3-pGL3 (+/+) and non-flashed PL-NLS + Cy3-pGL3 (+/+). All Cy3-pGL3 (+/+) formulations were condensed by PEI ($R\text{-}NH_3^+:PO_4R_2^- = 3$) and delivered to cells in 600 μl (500 ng of plasmid) of 2% FBS transfection media. This transfection protocol was repeated 3 times to give 4 identical slides. The transfection was carried out for 3, 6 ,12 and 24 hrs at which times 1 slide was fixed for confocal microscopy.

The prepared slides were analyzed with a Carl Zeiss LSM510 confocal laser scanning microscope using the 2 available Helium/Neon lasers (543 nm and 633 nm) to excite Cy3 (550 nm/570 nm) and TO-PRO-3 (642 nm/661 nm), respectively. Images were acquired under magnification of the 63x oil emersion lens. Images were assessed qualitatively using ImageJ. Briefly, images were acquired as ".lsm" files with the red and far-red channels in separate images. Using the "composite" function, all red and far-red fluorescence was combined into one image for that plane. Using pseudo-coloring, nuclei labeled with TO-PRO-3 appeared red and the pGL3 labeled with Cy3 appeared green.

Quantitative Nuclear Localization from Single-Plane Confocal Imaging

PL-NLS was labeled at various peptide:plasmid ratios (1, 10 and 100 pmol/μg), and all remaining peptides (except PL-NLS-Y) were labeled onto Cy3-pGL3 at 10 pmol/ μg. Plasmid was labeled, condensed by PEI and transfected for 6 hrs, as described above. Likewise, the same imaging protocol was followed. Quantitative analysis was performed using ImageJ. The "Selection Brush Tool" was used to define the perimeter of all nuclei in the field and the perimeter of all cells in the field. Images of cells were acquired in a single XY-plane, and the percentage of nuclear localization was calculated based on an assessment of all cells in one field of view. Briefly, the background-corrected value of cumulative Cy3 signal in the nuclei was divided by the background-corrected value of the cumulative Cy3 signal inside the cell membrane of all cells. The quotient indicated the percent of the internalized Cy3-pGL3 that reached the nucleus.

PEI versus Peptide-217 Polyplexes and Z-Series Image Acquisition

Cy3-pGL3 (+/+) formulation by either PEI or peptide-217 has been discussed previously. Cy3-pGL3 was delivered in the NLS-labeled form and the un-labeled form by both polycations for a 6 hr transfection. After 6 hrs, cells were fixed, nuclei were stained by TO-PRO-3, and Z-series images were acquired as follows. The prepared slides were analyzed with a Carl Zeiss LSM510 confocal laser scanning microscope using the two available Helium/Neon lasers (543 nm and 633 nm) to excite Cy3 (550 nm/570 nm) and TO-PRO-3 (642 nm/661 nm), respectively. Images were acquired under magnification of the 63x oil emersion lens. Using the coarse adjustment and Zeiss software, the vertical depth of the field was scanned and the "top" and "bottom" planes of the nuclei were set. In Z-scan mode, 6 x 1 μm slices were imaged between the two set-points.

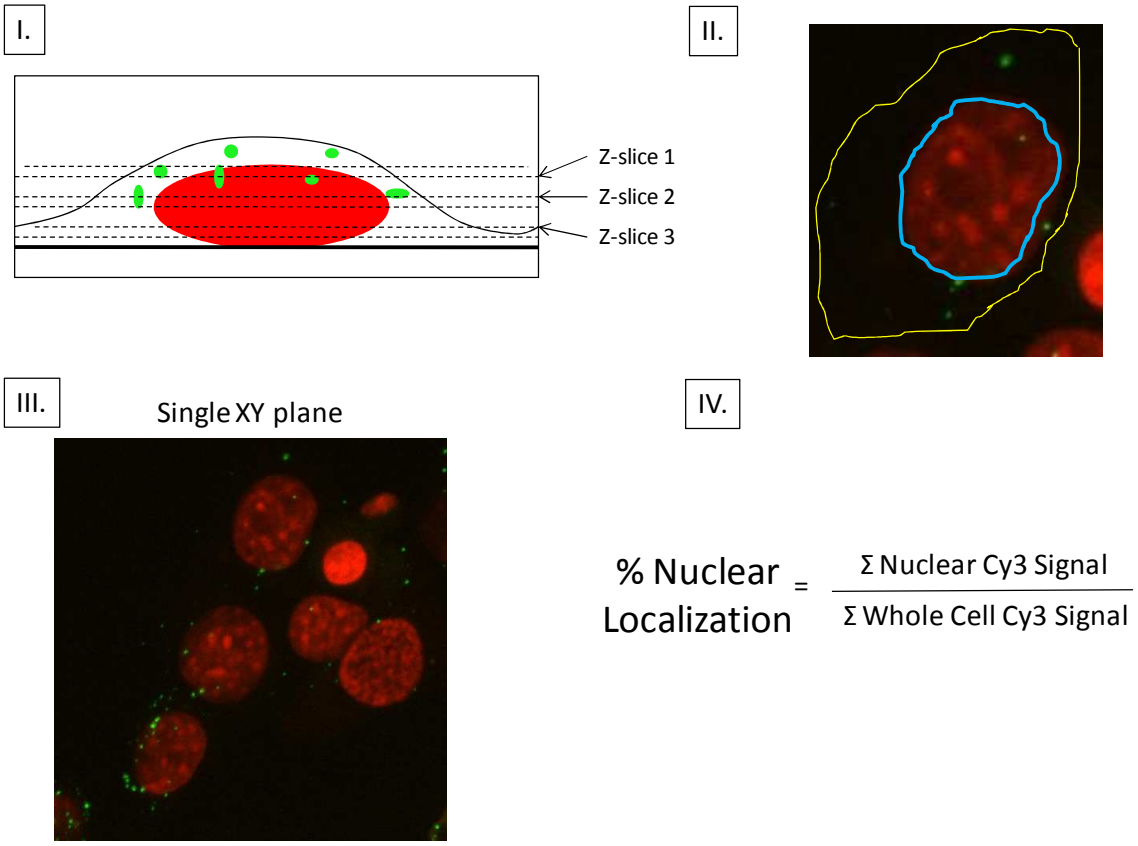

Figure 5-7. *Methodology for quantitative qssessment of nuclear localization.* I) A Z-series of images is collected for each field of view. II) Cells in the field are numbered, and Cy3 signal is measured in the nucleus and in the whole cell. III) This measurement is applied to all cells in a field and to all images in the Z-series. IV) The fraction of Cy3 localized to the nucleus in the entire volume of the cell is represented by the equation for % nuclear localization.

Data was processed using ImageJ and LSM Image Browser was used to generate and present cross-sections (Z-plane) of cells acquired as part of a Z-series. A quantitative strategy was used to calculate the percent nuclear localization from these treatments captured in Z-series. Using the "Selection Brush Tool" to define the perimeter of the nucleus in the far-red channel, total Cy3 fluorescence was measured for specified nuclei in a given Z-section. A similar measurement was also made to quantify the total Cy3 fluorescence in the whole cell. These measurements were made for several cells in each

Z-slice. After determining these measurements for all Z-slices, the sum of nuclear fluorescence for the Z-series and total fluorescence was calculated for each cell. The sum of fluorescence in each XY-plane allowed for the entire volume of the cells to be analyzed. The fraction of total fluorescence that was in the nucleus could be determined as above. This value was represented as the percent of Cy3-pGL3 localized to the nucleus (Figure 5-7).

Time course of Nuclear Uptake Determined by Z-Series Acquisition and Comparison to Luciferase Expression

Cy3-pGL3 was formulated for the following four treatments (all of which were condensed by peptide-217): no peptide labeling, PL-NLS labeled at 10 pmol/μg, PL-cNLS labeled at 10 pmol/μg and a PL-NLS non-flashed control. Transfections were done as previously described in 4 x 4-well chamber slides to allow for 4 time points (0.5, 1, 3 and 6 hrs). Z-series data were assessed both quantitatively and qualitatively.

In addition, a corollary experiment was done to compare nuclear uptake to luciferase expression in vitro. (A detailed description of the in vitro assay for luciferase expression appears in the subsequent section.) Briefly, the same 4 treatments of pGL3 were prepared for 10 μg transfections in triplicate. Peptide-217 condensates were delivered to 35 mm wells in which 10^5 NIH 3T3 cells had been seeded and incubated for 24 hrs. Luciferase expression from all treatments was assessed at 1, 3 and 6 hrs after transfection, but luciferase expression was only observed at the 6 hr time point.

6 Hour Transfection with NLS-Labeled pGL3 (-/-)

pGL3 (-/-) lacks both the SV40 promoter and enhancer elements. The notable deficiency is the absence of the SV40 enhancer which has been discussed to contain a sequence that is known to contribute to nuclear localization. In light of increased nuclear localization observed for PL-NLS labeled at 10 pmol/μg on pGL3 (+/+), this reproduction of that experiment with pGL3 (-/-) was expected to display a greater

increase in NLS-mediated nuclear localization compared to the same control treatments. The experiment with pGL3 (-/-) in a 6 hr transfection was conducted identically to the one described in the previous section but with a different luciferase-expressing plasmid.

NLS-Mediated Increase in Luciferase Expression In Vitro

Cell Passaging

All tissue culture materials and reagents were introduced in the "Confocal Microscopy" section. The same materials were utilized to complete the following experiments, as well. NIH 3T3 cells were maintained in a water jacketed incubator with an internal atmosphere of 5% CO_2 (injected) and air. The cell culture media described previously was filtered through a 0.22 μm membrane. NIH 3T3 cells were adherent in 100 mm treated polystyrene dishes and proliferated until they reached 75% confluency. The culture media was then removed, cells were washed with PBS, and the extracellular matrix of cells was trypsinized (Trypsin-EDTA, Gibco). A cell suspension of trypsin and DMEM pelleted, cells were resuspended and passaged in a 1:100 dilution.

For transfection experiments, cells were seeded in 35 mm (6-well) plates. Prior to seeding, cells in suspension were counted using a gridded hemocytometer and an inverted microscope with 10x magnification. Briefly, a 20 μl aliquot of the suspension was diluted 2-fold in trypan blue (0.4%, Gibco). Using the dissecting scope, 10 fields of cells (in a volume equal to $1mm^3$) were counted. From this count, the concentration of cells in suspension (cells/ml) was calculated. This value was used to determine the volume of an aliquot that contained the desired number of cells to be seeded in each well. Cells were seeded for transfection a total volume of 2 ml of 10% FBS culture media per well.

Transfection

Plasmid was labeled by PL-peptide as described previously. Briefly, 20 μg of pDNA (0.4 mg/ml) was added dropwise to an equal volume of PL-peptide in 5 mM

Hepes to achieve a photo-labeling stoichiometry of 0.1-100 pmol of peptide per μg of pDNA. Photolysis of PL-peptides diluted with pDNA was initiated using a conventional photo-flash. Samples contained in polypropylene microcentrifuge tubes were photo-flashed 40 x and maintained at room temperature for a 30 min incubation.

Cells were transfected 24 hrs after being seeded in 6-well plates. pDNA was delivered with PEI as the condensing agent. PEI-pGL3 ($R\text{-}NH_3^+ : PO_4R_2^- = 9$) condensates were prepared in 5 mM Hepes (pH 7.4) by adding 20 μg pGL3 (100 μl) to 119 μg of PEI (100 μl) followed by a 30 min incubation at room temperature. PEI-DNA condensates (5 μg pGL3 in 50 μl) were added to 50–70% confluent 3T3 cells in 35 mm wells. This was followed by the addition of 1 ml of 2% FBS transfection media. Cells were incubated at 37^o C. The time of transfection was specified for each experiment.

Luciferase Assay

Cells were washed twice with 2 ml of ice-cold PBS and then treated with 0.5 ml of lysis buffer for 10 min on ice. The cell lysates were scraped, transferred to 1.5-ml microcentrifuge tubes, and centrifuged for 7 min at 13,000 x *g* at 4^oC to pellet cell debris. Luciferase activity was measured in relative light units by a Lumat LB 9501 (Berthold Systems, Bad Wildbad, Germany) with 10 sec integration after automatic injection of 100 μl of 0.5 mM D-luciferin and manual injection of 4.3 μl of 165 mM ATP. The relative light units were converted to picograms of luciferase using a standard curve generated by adding a known amount of luciferase to 35-mm wells containing >50% confluent 3T3 cells. The resulting standard curve had an average slope of 1.46×10^4 relative light units/pg of enzyme. Protein concentrations were measured by BCA assay using bovine serum albumin as a standard. The amount of luciferase recovered in each sample was normalized to mg of protein and reported as the mean and standard deviation obtained from triplicate transfections.

Luciferase Expression Based on Increased PL-NLS Labeling Stoichiometry

Covalent modification could interrupt transcription of the transgene if modified in the coding region. This concern was addressed experimentally by increasing the labeling ratio of PL-NLS onto pGL3 (+/+). pGL3 (+/+) was labeled by PL-NLS at initial labeling stoichiometries ranging from 0.1 – 100 pmol of PL-NLS/μg of plasmid. PEI-pGL3 (+/+) condensates were prepared as described above. Un-labeled pGL3 (+/+) was included in the experiment as a positive control. A bench top bioluminometer was used to assay for luciferase in cell lysate following a 24 hour transfection and the BCA assay was used to normalize RLUs in terms of the total protein concentration.

Time Course of Transfection: Effects on In Vitro Expression

pGL3 was prepared in 3 treatments for this experiment: un-modified pGL3 (+/+), PL-NLS labeled at a 1 pmol/μg ratio, and PL-cNLS labeled at a 1 pmol/μg ratio. pGL3 was condensed by PEI ($R\text{-}NH_3^+:PO_4R_2^-$ = 9). Transfection of 3T3 cells followed a 24 hr incubation of 10^5 cells initially seeded in 35 mm wells. Treatments were applied in triplicate, and a luciferase assay was conducted at 12, 18, 24, 36 and 48 hrs following transfection.

Variable Seeding Number of NIH 3T3 Cells

NIH 3T3 cells were seeded at 10^4, 10^5, or 10^6 cells per well in order to introduce variation in the extent of cell confluency at the time of transfection (24 hours after cell seeding). An NLS effect of increased expression is predicted to be masked if cells are rapidly dividing because mitosis becomes the overriding factor factor contributing to nuclear localization in cell culture[158]. Cells that were more confluent at the time of transfection underwent less cell division. pGL3 (+/+) formulations were delivered in

triplicate in an identical fashion to the previous experiment. The transfection was carried out for 24 hrs and luciferase levels were measured at that time.

Serum-Starving Conditions

Based on the results of the experiment on variable seeding density, in vitro experiments looking for an NLS-mediated increase in gene expression were done in serum-starving conditions to greatly reduce mitosis and minimize nuclear restructuring as a possible mask of NLS-mediated increase in expression. Briefly, 10^5 NIH 3T3 cells were seeded in 6-well plates and incubated in 10% FBS media for 24 hours. Subsequently, cells were incubated in 0.2% FBS media for 48 hours. This was followed by transfections as described above.

Bioluminescence Imaging to Assess NLS-Mediated Increase in Luciferase Expression In Vivo

Chapter 2 and Chapter 3 offer detailed descriptions of the Materials and Methods of HD dosing, IM-EP dosing and BLI. The same protocols are applied to the following investigations of NLS-mediated increases of in vivo gene expression. A newly introduced reagent to these experiments was pGL3 Promoter (+/-) plasmid (Promega) which contains the SV40 promoter, but lacks the SV40 enhancer.

HD Dosing of NLS-Labeled pGL3

Mice were HD dosed in triplicate with 10 ng of pGL3 (+/+) that was un-labeled, labeled with 0.1 pmol of PL-NLS/μg or labeled with 0.1 pmol of PL-cNLS/μg. Plasmid was diluted in normal saline up to a volume that was equal to 9% of the body weight of the mouse to be dosed. The solution was delivered via tail vein injection in 5 sec. Mice were imaged for liver expression of luciferase after 24 hrs. Similarly, the same treatments were applied in a separate experiment in which the labeling ratio PL-NLS and PL-cNLS was increased to 10 pmol/μg and the total dose delivered was reduced to 1 ng of pGL3.

IM Dosing of NLS-Labeled pGL3

Treatment groups used in this experiment were identical to those in the previous HD experiment: un-modified pGL3 (+/+), PL-NLS labeled at 1 pmol/μg and PL-cNLS labeled at 1 pmol/μg. 20 μg of pGL3 was dosed IM in 50 μl of normal saline. In the first group of mice (n=3) the left leg (direction is based on the ventral view) was dosed with pGL3 (+/+) and the right leg was dosed with NLS-pGL3 (+/+). The second group (n=3) allowed for an intra-mouse comparison between cNLS-labeled plasmid (left leg) and NLS-pGL3 (+/+) in the right leg. Mice were imaged 24 hrs following IM dosing.

A similar experiment followed in which peptides were labeled onto pGL3 (+/+) at 0.1 pmol/μg and a 20 μg dose of pGL3 was administered to each leg. In this case, the same treatment was delivered to both legs of a given mouse and 3 mice (n=6) were in each treatment group. Again, BLI was carried out 24 hrs following IM dosing.

IM-EP Dose of pGL3 Labeled by PL-NLS or PL-cNLS

Electroporation following an IM dose of naked pGL3 (+/+), and the benefits of that approach are discussed in Chapter 3. The primary aim of incorporating EP was to increase precision and the percent of doses that showed luciferase expression by BLI. pGL3 (+/+) was labeled with PL-NLS or PL-cNLS at 1 pmol/μg. 5 μg doses of plasmid, labeled by either peptide or un-modified, were delivered (n=4) to the hamstring muscle in 50 μl of normal saline by IM methods. This administration was followed 1 min later by EP, as described previously. Mice were imaged for luciferase activity 24 hrs following IP dosing of D-luciferin.

IM-EP Dose of pGL3 Labeled by 6-AA Linker Peptides

The previous experiments have been under-whelming regarding the results generated by using PL-NLS/cNLS (containing the 2 Gly linker). Here, we introduce NLS-containing peptides that have the 6 amino acid linkers (Figure 5-3) with thoughts of

improving the structure-activity relationship for Importin-α binding to the NLS which was predicted to be projected away from the plasmid with the extended linker length.

pGL3 (+/+) was labeled with 0.1, 1.0 and 10 pmol/μg of PL-6Gly-NLS, PL-6Lys-NLS or PL-6Pro-NLS. From each labeling reaction, 1 μg doses of pGL3 in 50 μl of normal saline were administered in the hamstring muscle (n=4). These doses were followed by EP, as described previously. Luciferase expression was monitored by BLI at 24 hrs following the pGL3 dose. Values were compared to a dose of un-modified pGL3.

In the case of the 6Pro peptide, a similar experiment was conducted with control peptides included. That is, 1 μg of pGL3 (+/+) was dosed un-modified, or labeled with 1.0 pmol/μg of PL-6Pro-NLS, PL-6Pro-cNLS or PL-1Pro-NLS. The experimental protocol for these dosing groups was identical to that of the previous experiment.

IM-EP of pGL3 (+/+) with excess free PL-NLS or PL-cNLS

Previous experiments have focused on demonstrating an increase in gene expression based on covalent labeling with PL-NLS. In this alternative approach, pGL3 (+/+) with a known nuclear targeting sequence was dosed in the presence of free peptide that may compete with cytonuclear transfer of the plasmid as part of the receptor-mediated process at the NPC. All mice in each group (n=4) were dosed in the hamstring muscle with 1 μg pGL3 (+/+) in 50 μl of normal saline according to IM-EP protocol. Each 50 μl bolus dose contained 1000-fold mol excess of PL-NLS, 10,000-fold mol excess of PL-NLS, the same amounts of PL-cNLS or no free peptide. Mice were dosed with pGL3 (+/+) and imaged 24 hrs later by BLI following an IM dose of 40 μl of D-luciferin (30 mg/ml).

IM-EP Dosing of pGL3 (+/+) and (+/-)

A series of inconsistent and inconclusive experiments lead to an investigation with pGL3 Promoter plasmid (+/-). As discussed previously, pGL3 (+/+) contains an

SV40 enhancer element which has been shown to confer nuclear localizing capability on pDNA. Potentially, the presence of theSV40 enhancer is masking any nuclear-localizing effect imparted from peptide labeling. pGL3 (+/-) does not contain the SV40 enhancer element and would not have any inherent nuclear localizing capacity.

In the initial experiment, pGL3 (+/-) was labeled with 2 and 20 pmol/μg of PL-NLS. These formulations were dosed IM-EP and compared to un-modified pGL3 (+/-) and un-modified pGL3 (+/+). 1 μg of pGL3 was dosed in 50 μl of normal saline in 2 mice (n=4) and expression was monitored for 144 days. This experiment was repeated (n=6), the 20 pmol/μg was replaced by a treatment of PL-cNLS labeled at 2 pmol/μg and luciferase expression was followed for a time course of 28 days.

A subsequent experiment was conducted using ExtSV40-NLS and cNLS. pGL3 (+/-) was labeled by either peptide at 1 pmol/μg. 1 μg of pGL3 (+/-) was dosed by the IM-EP protocol.

Results

4-azido-2,3,5,6-tetrafluorobenzoate (PL) and Peptide Synthesis

The synthesis of 4-azido-2,3,5,6-tetrafluorobenzoate from the commercially available pentafluorobenzoate is completed in 2-steps. Installation of the azide in the para position under reflux conditions gives 4-azido-2,3,5,6-tetrafluoro-methylbenzoate as a white solid. It is well-known that this pentafluoro species reacts with sodium azide to give the 1,4-disubstituted tetrafluoro compound[159]. The starting material and para-azide product were analyzed by thin-layer chromatograph and developed in hexane:ethyl acetate (10:1). R_f values were 0.24 and 0.11, respectively. The subsequent basic treatment of the methyl ester left the photo-label as a white solid following re-crystallization. The product was spotted on a thin-layer plate with the para-azide methyl ester and developed in hexane:ethyl acetate (1:1). R_f values were 0.59 for compound 2

(Scheme 5-1) and 0.19 for compound 3. The final product was synthesized in 82.1% yield.

Table 5-1. *Purification and characterization of all PL-peptides*.

Peptide	**Sequence**	**% Yield[a]**	**RP-HPLC Elution Gradient**	**Elution Time**	**m/z**
	(1-letter amino acid abbreviations)	(30 µmol syntheses)	(% ACN in 0.1% TFA/min)	(min)	(calculated/observed)
PL-NLS	PL-GGPKKKRKVG	11%	10-30/30	17.2	1272.3/1272.3
PL-cNLS	PL-GGPKTKRKVG	15%	10-30/30	18.8	1245.3/1245.2
PL-NLS-Y	PL-GGPKKKRKVGY	48%	10-30/30	21.6	1435.5/1435.5
PL-ExtSV40-NLS	PL-YKKKGSSDDEATADSQHSTP-PKKKRKVEDPK	8%	10-30/30	19.5	1852.9/1852.5
PL-ExtSV40-cNLS	PL-YKKKGSSDDEATADSQHSTP-PKTKRKVEDPK	5%	10-30/30	19.7	1839.4/1839.0
PL-1Gyl-NLS	PL-GPKKKRKVG	11%	10-40/30	14.6	1215.3/1215.0
PL-1Gyl-cNLS	PL-GPKTKRKVG	8%	10-40/30	15.9	1188.3/1188.1
PL-1Lys-NLS	PL-KPKKKRKVG	28%	10-40/30	14.3	1286.4/1286.0
PL-1Lys-cNLS	PL-KPKTKRKVG	19%	10-40/30	15.2	1259.4/1259.0
PL-1Pro-NLS	PL-PPKKKRKVG	10%	10-40/30	16.9	1255.4/1255.1
PL-1Pro-cNLS	PL-PPKTKRKVG	24%	10-40/30	18.1	1228.3/1228.1
PL-6Gly-NLS	PL-GGGGGGPKKKRKVG	36%	10-40/30	14.8	1500.6/1500.1
PL-6Gly-cNLS	PL-GGGGGGPKTKRKVG	19%	10-40/30	15.3	1473.5/1473.4
PL-6Lys-NLS	PL-KKKKKKPKKKRKVG	12%	10-40/30	13.8	1926.3/1926.4
PL-6Lys-cNLS	PL-KKKKKKPKTKRKVG	22%	5-35/30	19.2	1900.2/1900.2
PL-6Pro-NLS	PL-PPPPPPPKKKRKVG	13%	20-40/30	13.8	1741.0/1740.1
PL-6Pro-cNLS	PL-PPPPPPPKTKRKVG	17%	10-40/30	23.2	1713.9/1714.0

[a]Based on UV $Abs_{258\ nm}$; $\varepsilon = 14.951\ M^{-1}cm^{-1}$

Synthesis of all peptides was carried out according to standard methods for SPPS using Fmoc-protected amino acids. These peptides contained either the classic SV40 NLS sequence (PKKKRKV) or the control, non-nuclear localizing control (cNLS) sequence (PKRTKRKV). For each peptide, PL was coupled to the N-terminus in the final step of SPPS. The first pair of NLS/cNLS peptides synthesized contained a 2-Gly linker region between PL and NLS. Figure 5-1 displays the chemical structures and Figure 5-8 shows the RP-HPLC chromatograms and mass spectra of PL-NLS and PL-cNLS, respectively. Table 5-1 summarizes relevant synthetic, purification and characterization results for these and all peptides synthesized.

For purposes of precisely quantifying the amount of peptide present, a Tyr-containing analog of PL-NLS was synthesized. The presence of Tyr at the C-terminus enables iodination, using $Na^{125}I$, by the Greenwood method. A Tyr-functionalized Wang resin provided the solid support for SPPS of PL-NLS-Y. Results associated with PL-NLS-Y synthesis are displayed in Figure 5-15 and Table 5-1.

A series of NLS/cNLS peptides with variation in the linker region was synthesized on a Gly-functionalized Wang resin. Within this series, the linker was varied by incorporating either 1 or 6 amino acids and was comprised of Gly, Lys or Pro residues. The 6 different linkers were devised to test the effect of NLS presentation as it is projected away from pDNA. Relevant information for this series of NLS and cNLS peptides is displayed in Figures 5-9 to 5-14 and Table 5-1.

The final peptides that were synthesized were termed “PL-ExtSV40”. Each peptide (NLS and cNLS) was synthesized to contain an extension of the native amino acid sequence toward the N-terminus. Jans and co-workers have shown that this region contains 2 phosphorylatable Ser residues – ^{112}Ser and ^{120}Ser. These peptides were

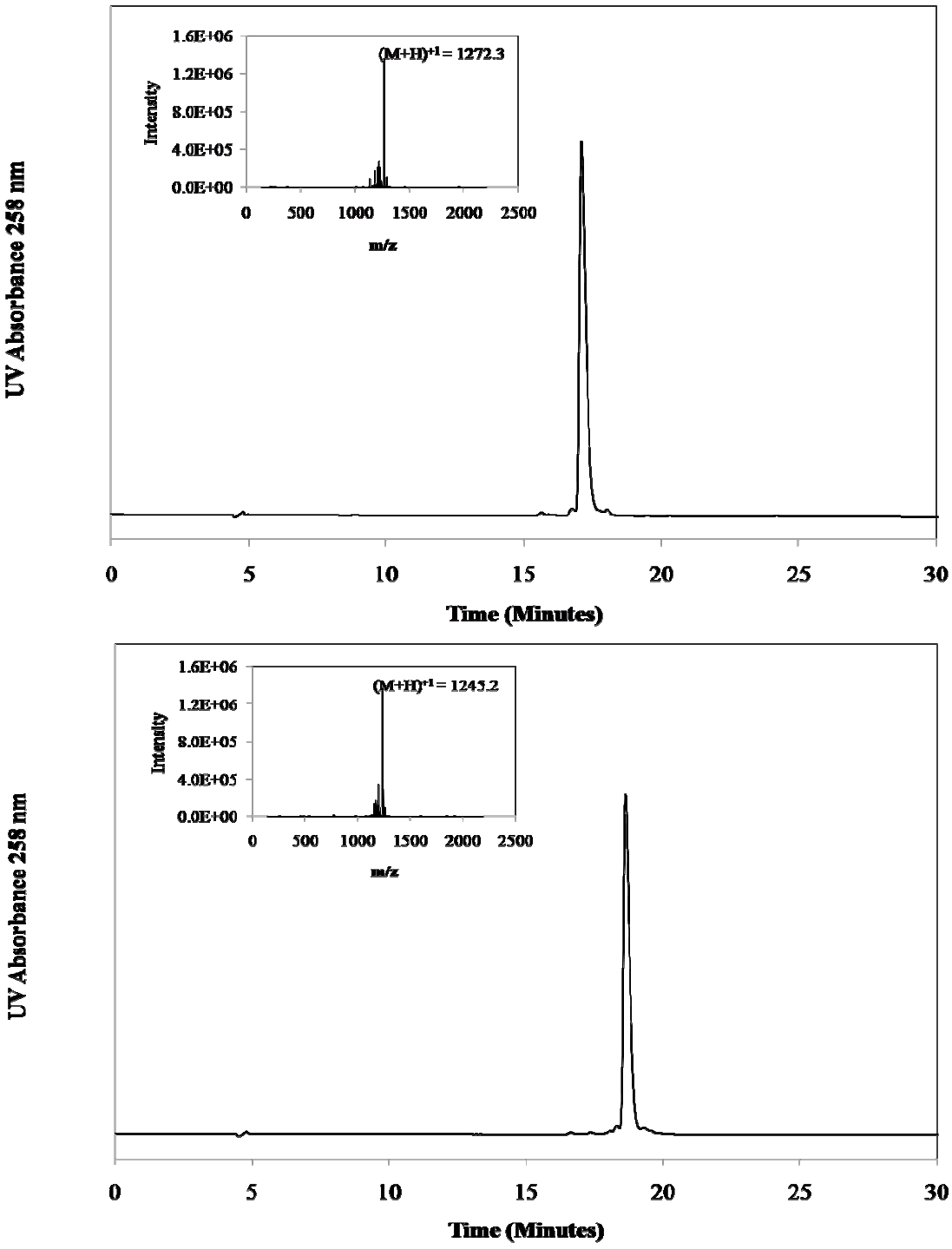

Figure 5-8. *LC-MS chromatograph of PL-NLS/cNLS (2-Gly linker).* PL-NLS (top) and PL-cNLS (bottom) with a 2 Gly linker between the N-terminal PL and the SV40 sequence. Specific data of chromatography/ spectroscopy can be found in Table 5-1

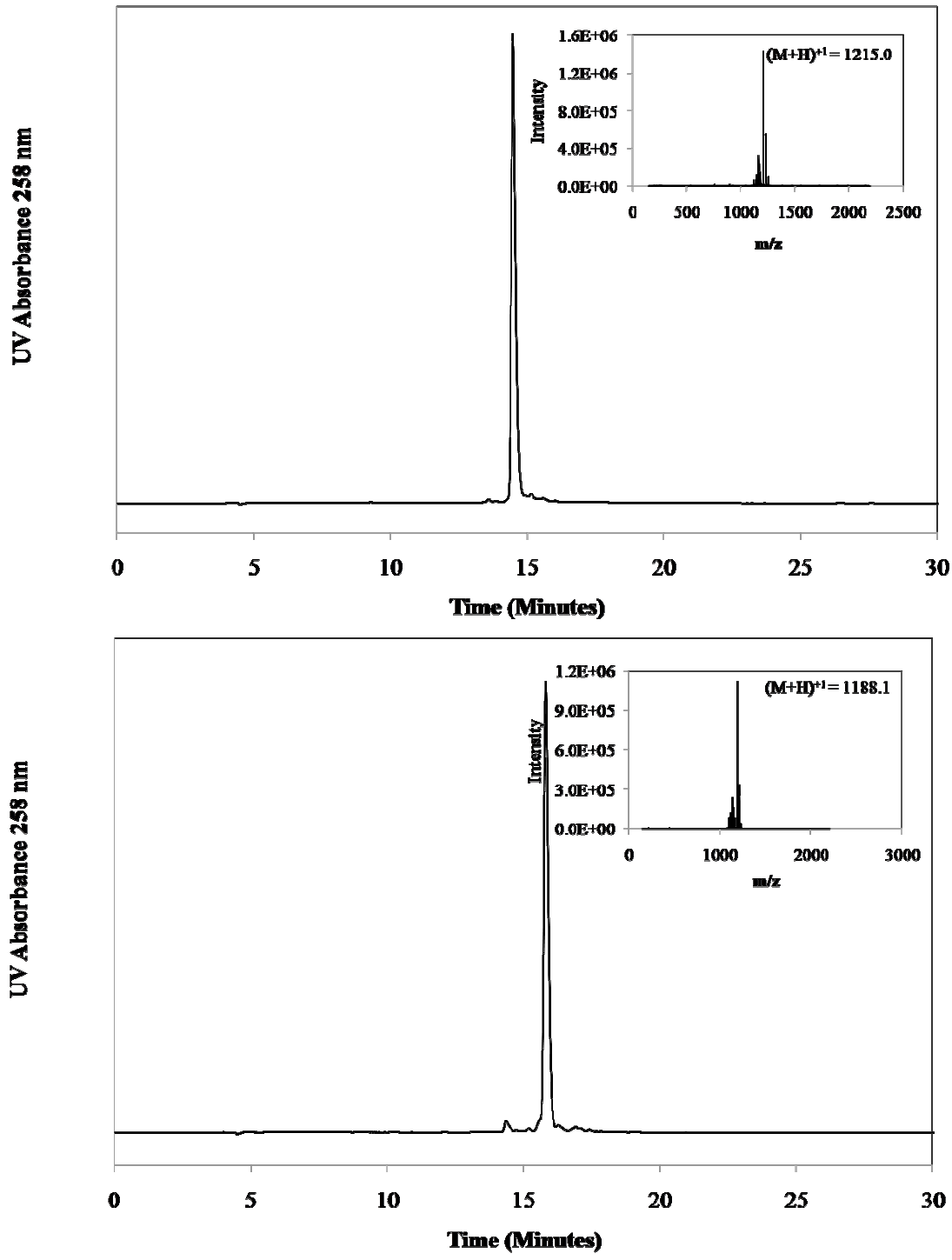

Figure 5-9. *LC-MS chromatograph of PL-NLS/cNLS 1-Gly linker*. PL-NLS (top) and PL-cNLS (bottom) with a 1 Gly linker between the N-terminal PL and the SV40 sequence. Specific data of chromatography/ spectroscopy can be found in Table 5-1.

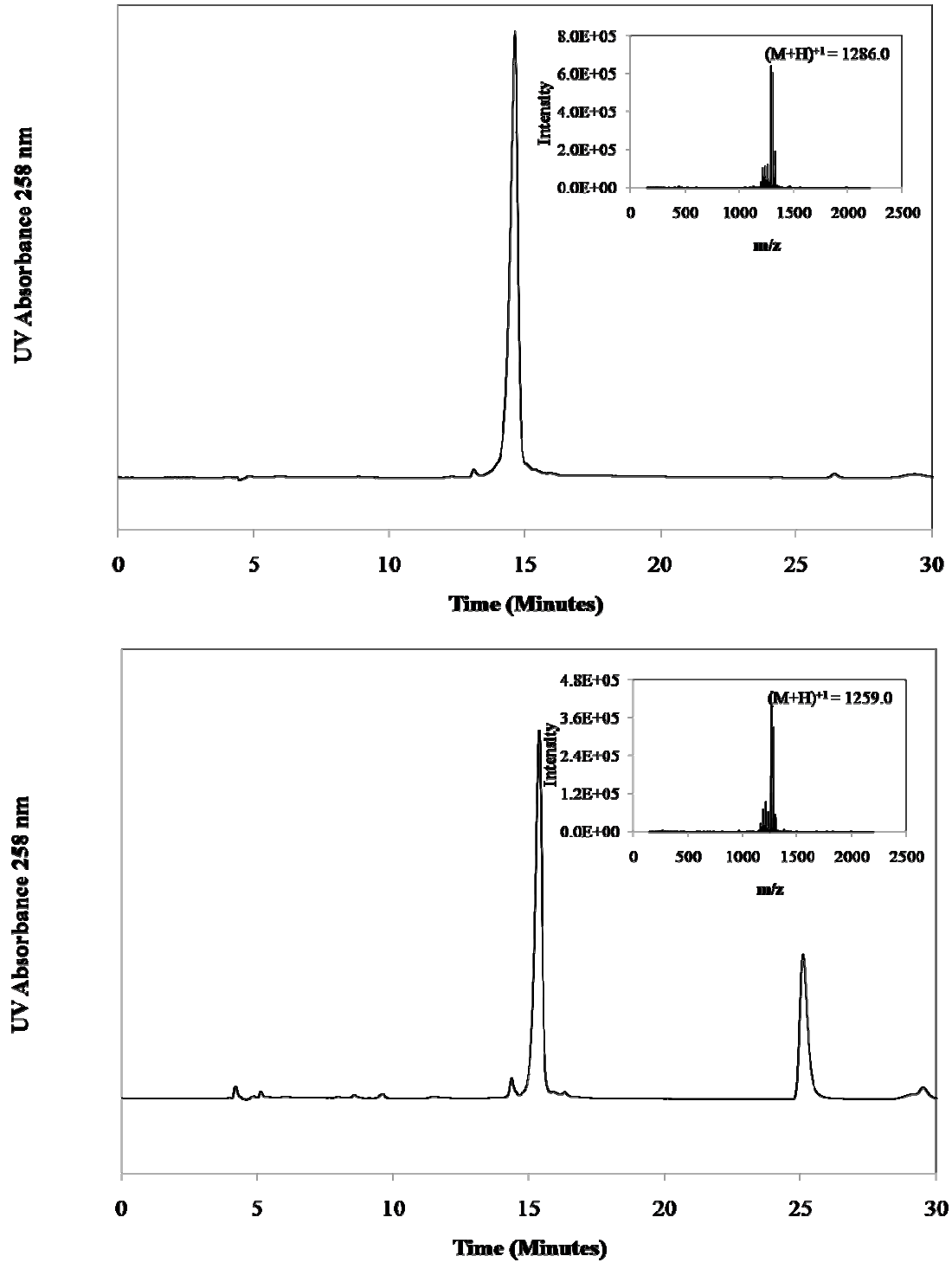

Figure 5-10. *LC-MS chromatograph of PL-NLS/cNLS 1-Lys linker*. PL-NLS (top) and PL-cNLS (bottom) with a 1 Lys linker between the N-terminal PL and the SV40 sequence. Specific data of chromatography/ spectroscopy can be found in Table 5-1.

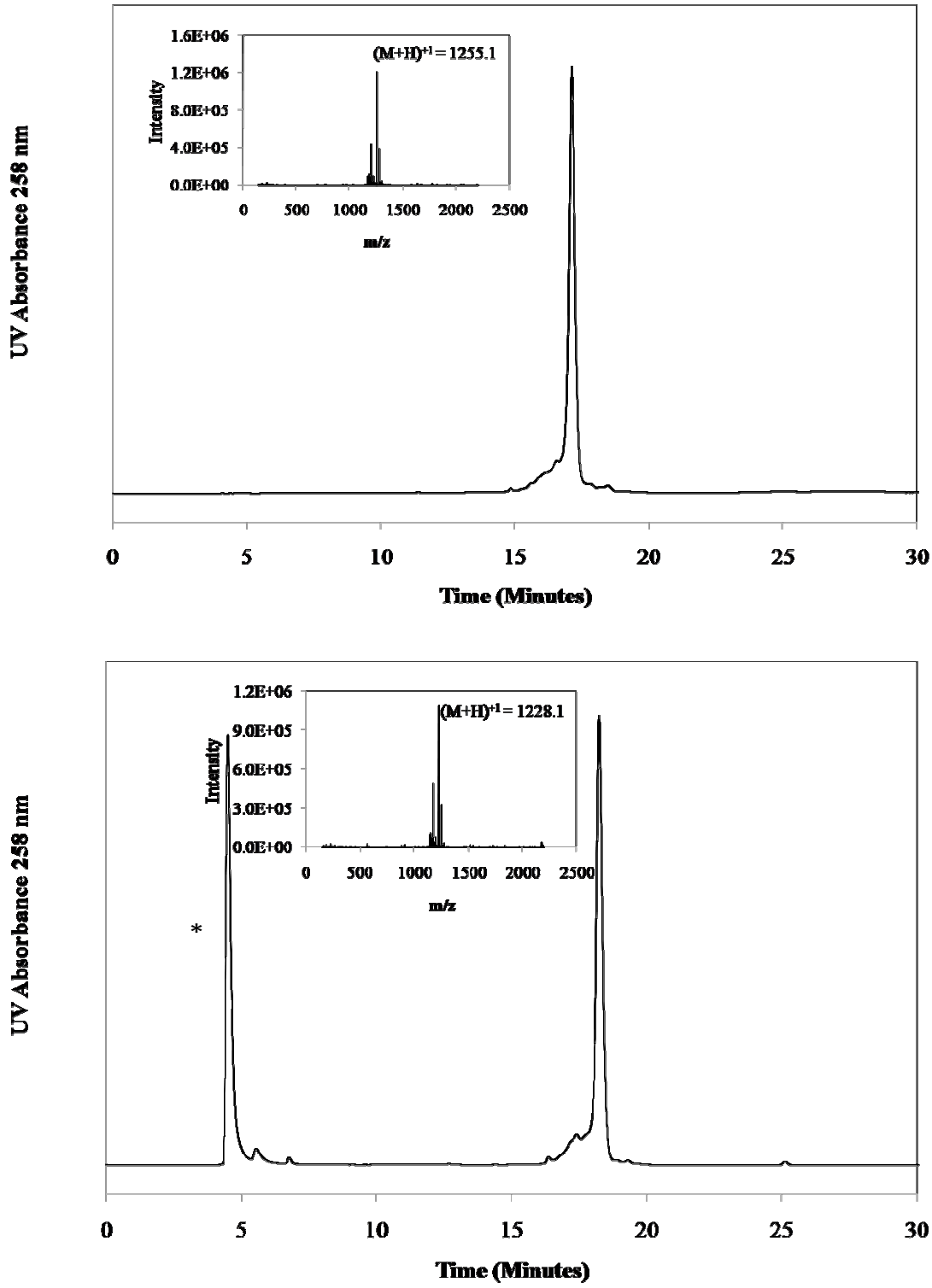

Figure 5-11. *LC-MS chromatograph of PL-NLS/cNLS 1-Lys linker.* PL-NLS (top) and PL-cNLS (bottom) with a 1 Pro linker between the N-terminal PL and the SV40 sequence. Specific data of chromatography/ spectroscopy can be found in Table 5-1. * Indicates non-peptide void peak

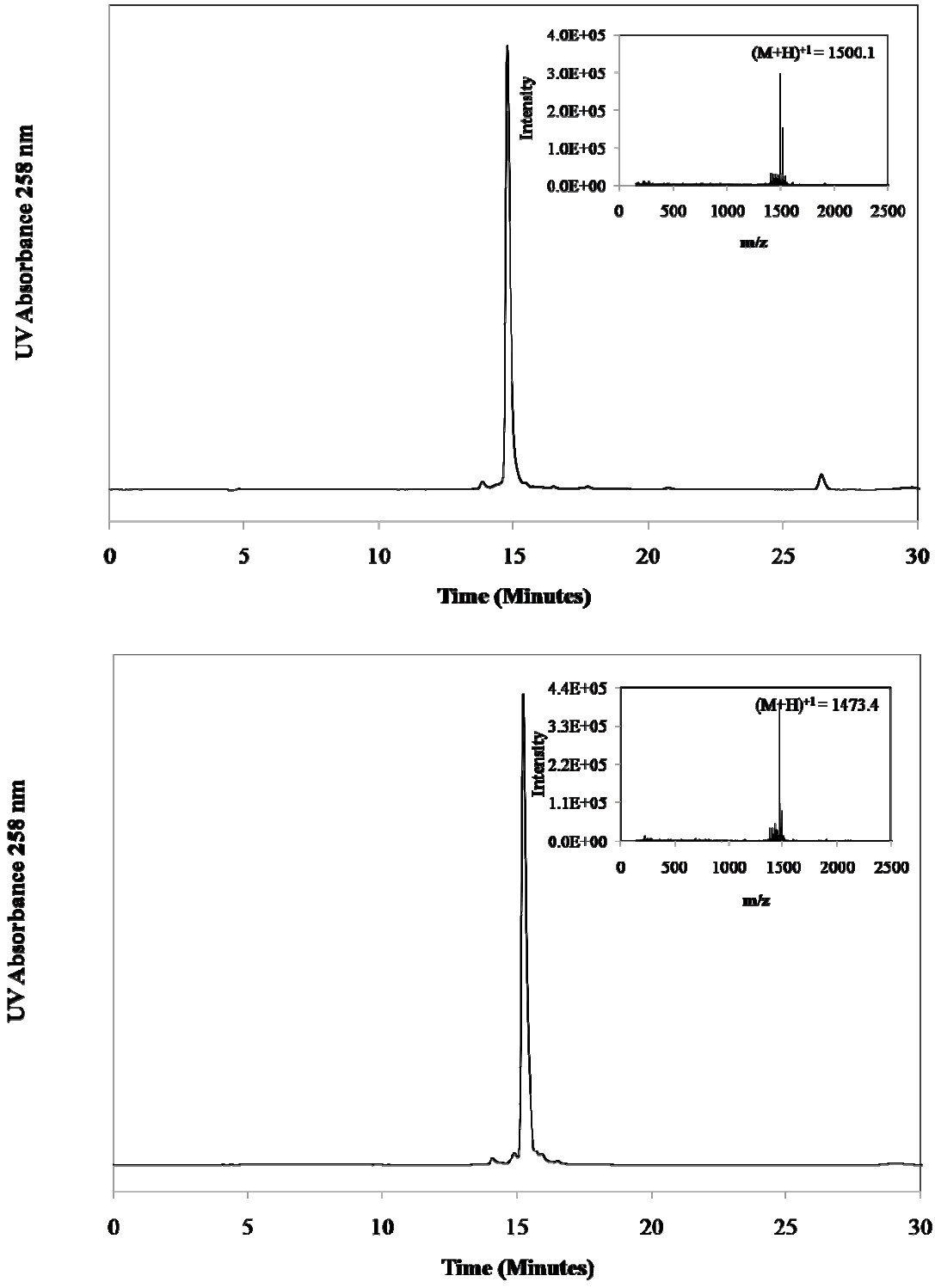

Figure 5-12. *LC-MS chromatograph of PL-NLS/cNLS 6-Gly linker*. PL-NLS (top) and PL-cNLS (bottom) with a 6 Gly linker between the N-terminal PL and the SV40 sequence. Specific data of chromatography/ spectroscopy can be found in Table 5-1.

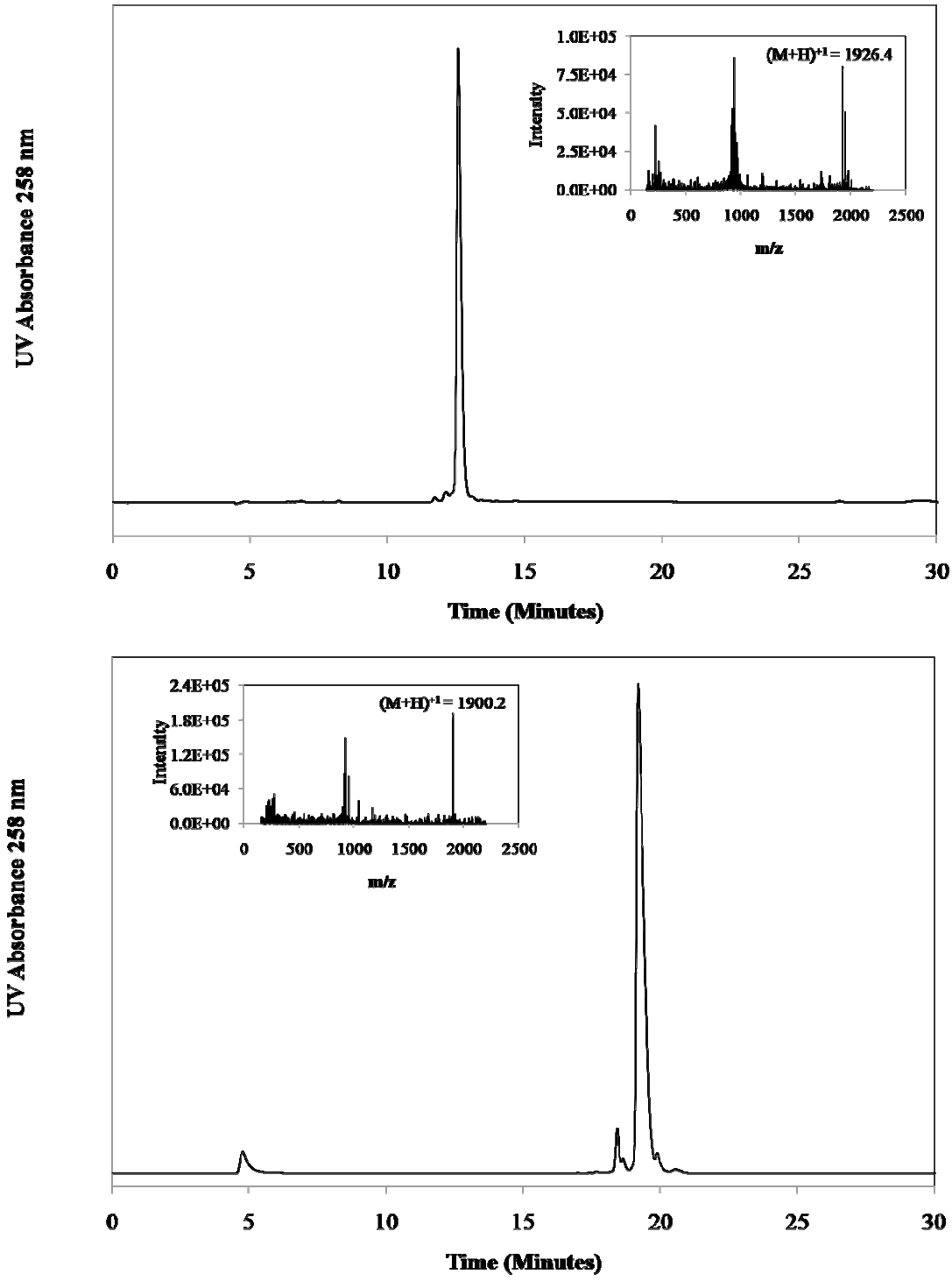

Figure 5-13. *LC-MS chromatograph of PL-NLS/cNLS 6-Lys linker*. PL-NLS (top) and PL-cNLS (bottom) with a 6 Lys linker between the N-terminal PL and the SV40 sequence. Specific data of chromatography/ spectroscopy can be found in Table 5-1.

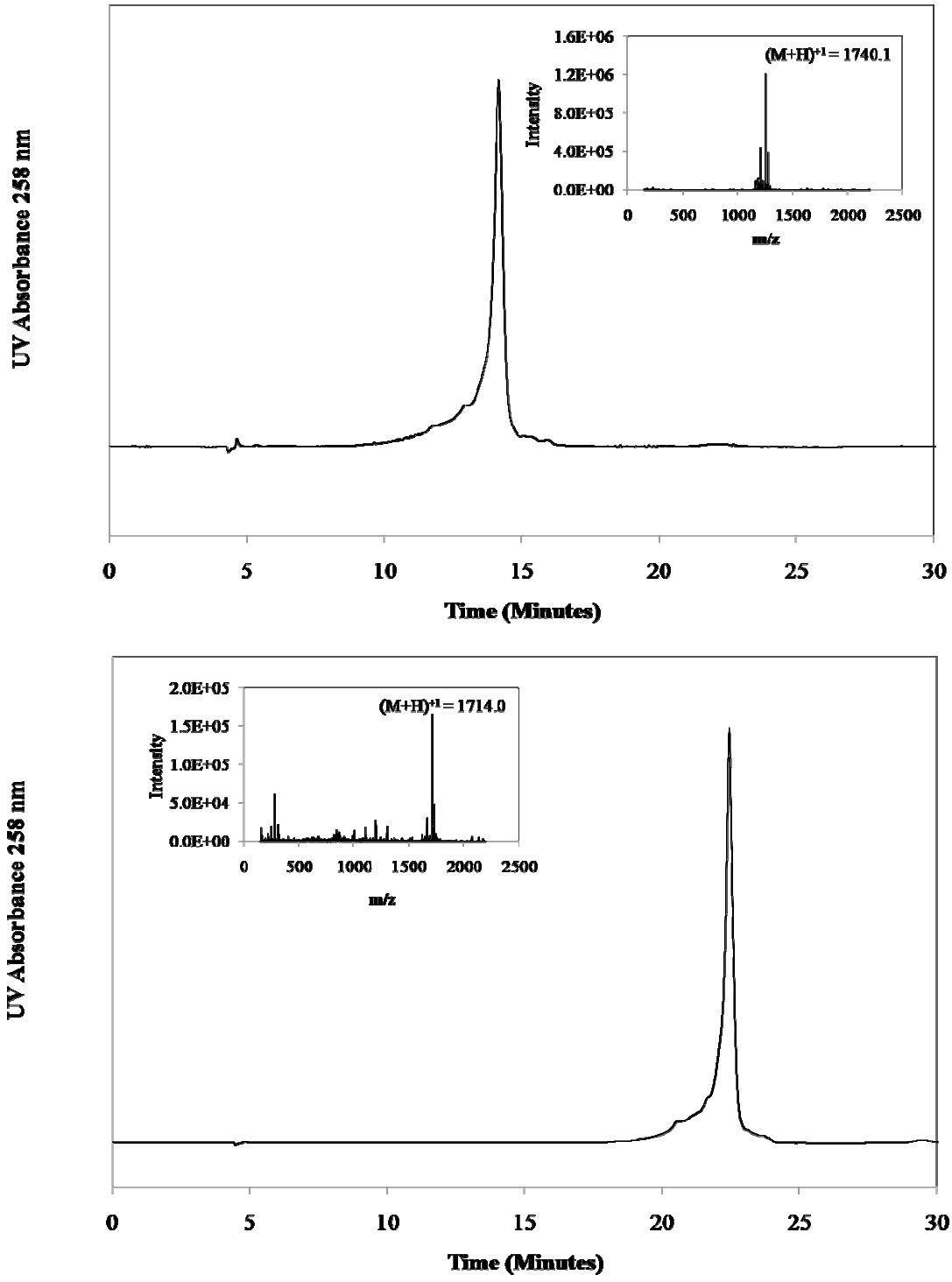

Figure 5-14. *LC-MS chromatograph of PL-NLS/cNLS 6-Pro linker*. PL-NLS (top) and PL-cNLS (bottom) with a 6 Pro linker between the N-terminal PL and the SV40 sequence. Specific data of chromatography/ spectroscopy can be found in Table 5-1.

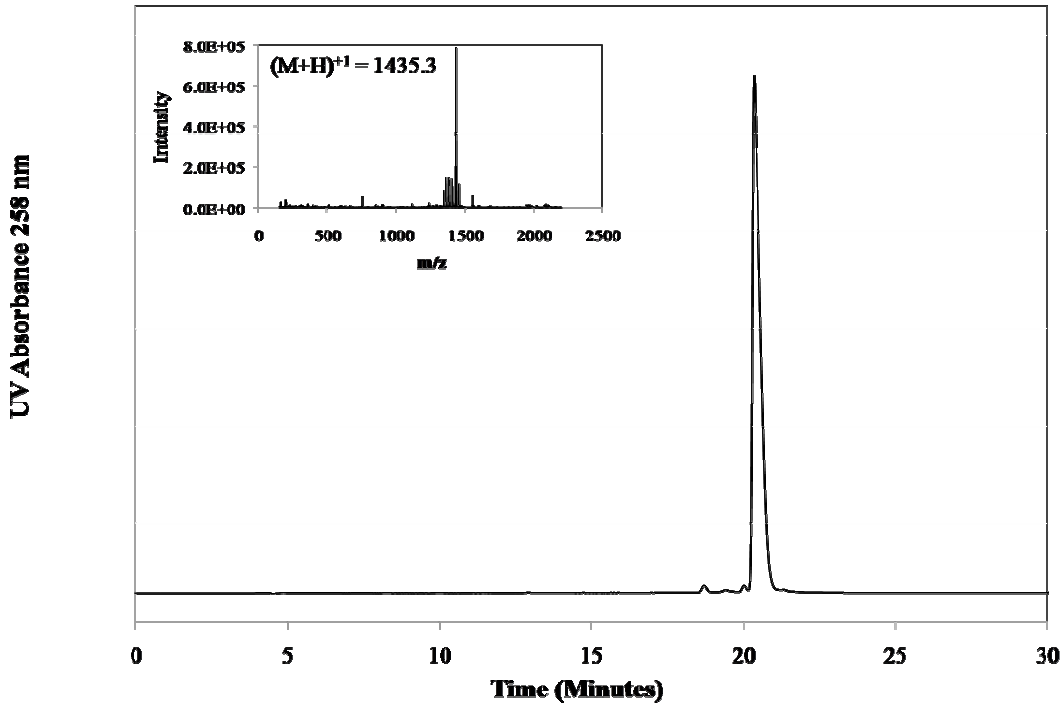

Figure 5-15. *LC-MS chromatograph of PL-NLS-Y.* PL-NLS-Y contains a Tyr residue at the C-terminus of the SV40 sequence. Specific data of chromatography/ spectroscopy can be found in Table 5-1.

synthesized on Lys-functionalized Wang resin. RP-HPLC and ESI-MS data are shown in Figure 5-15. Again, Table 5-1 displays additional information regarding these peptides.

Photo-Flashing and pDNA Formulation

PL-NLS peptides were not synthesized containing any UV-active amino acids. Hence, quantitation of these peptides was by the UV absorbance of PL at 258 nm. The molar absorptivity (ε) of PL was determined from the UV absorbance of dilutions that contained 10-120 nmol of PL (Figure 5-17). The slope of UV absorbance at 258 nm versus the concentration of PL represents the molar absorptivity (ε_{PL} = 14,951 $M^{-1}cm^{-1}$).

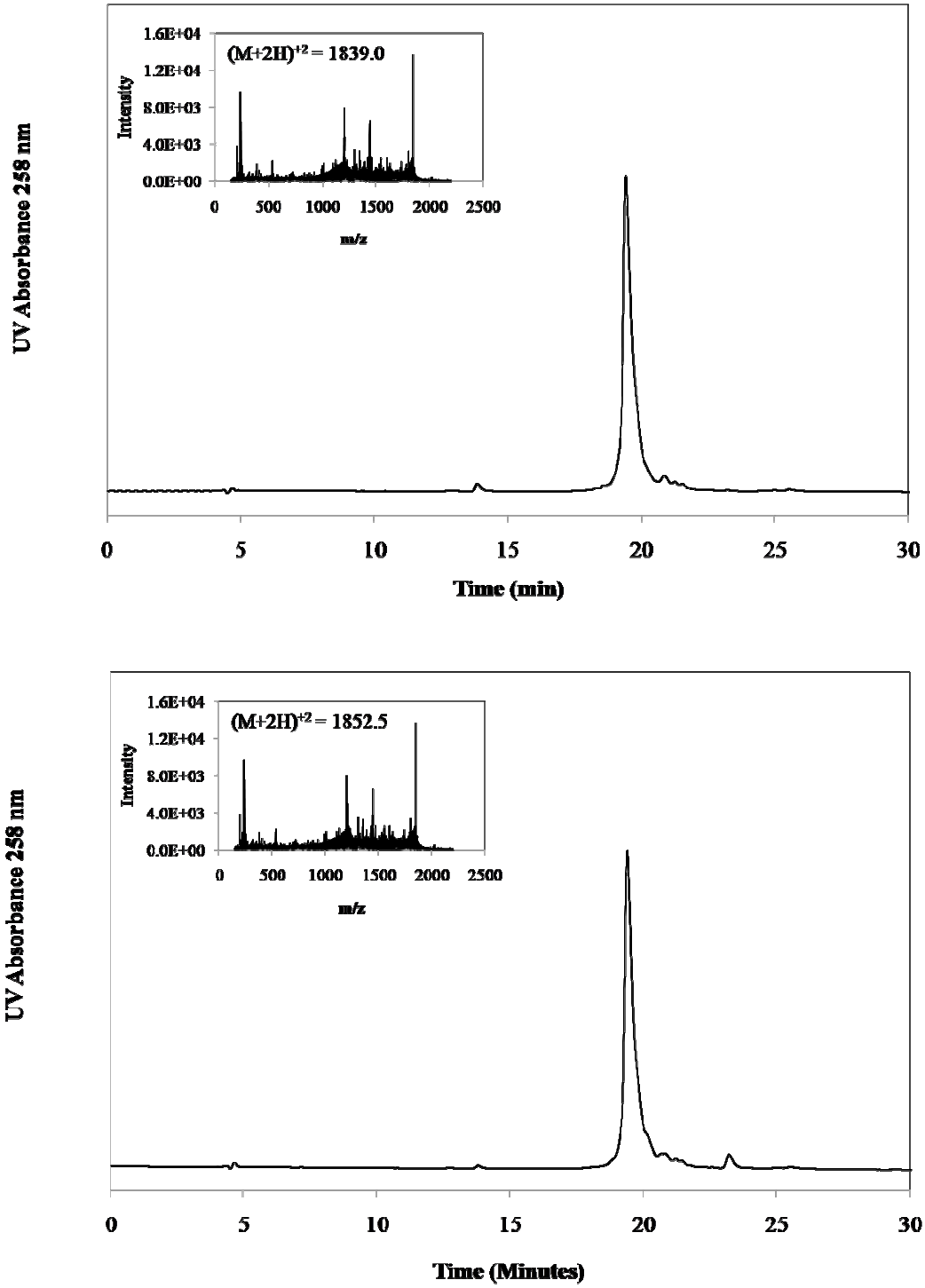

Figure 5-16. *LC-MS chromatograph of PL-ExtSV40-NLS/cNLS*. ExtSV40 peptides NLS (top) and cNLS (bottom) contain an extension of the native sequence at the C-terminus of the classic SV40 NLS sequence. Specific data of chromatography/ spectroscopy can be found in Table 5-1.

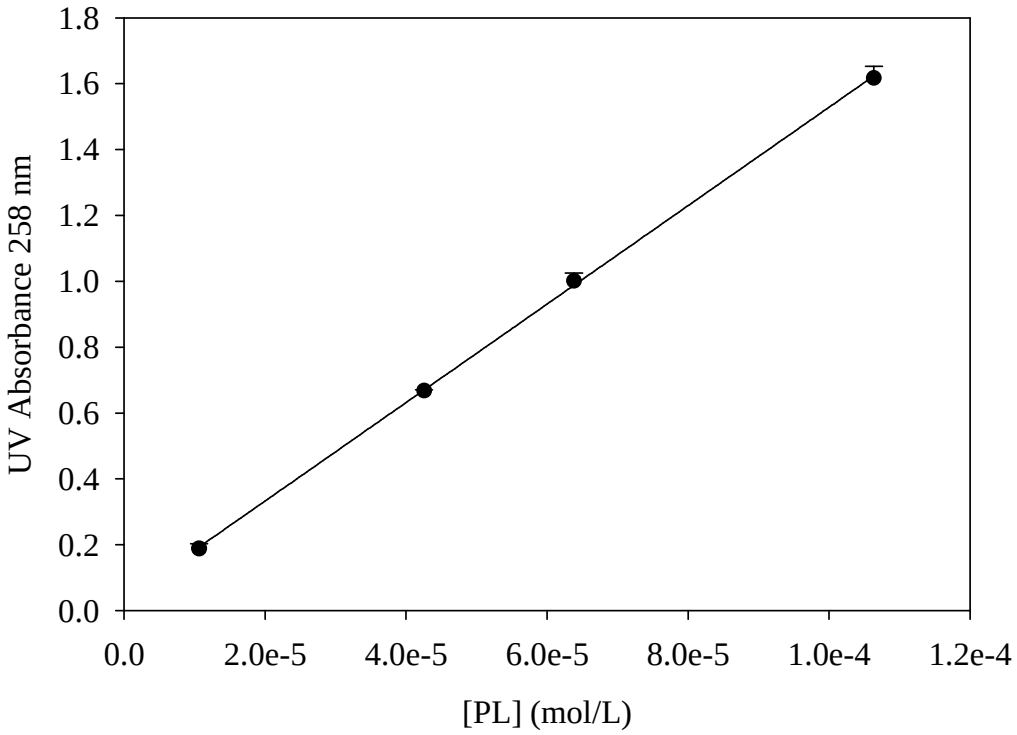

Figure 5-17. *Defining the molar absorptivity for PL.* 1 ml dilutions of the PL monomer in varying concentrations were assessed for UV Absorbance at 258 nm. The slope of the plot of Abs vs. M represents the molar absorptivity.

To indirectly show the photoactivation of PL-peptide alone, a dilution of PL-NLS (77.8 nmol/ml) was extensively photo-flashed. The UV absorbance at 258 nm was monitored after every 5 flashes. Figure 5-18 indicates that the chromogenic character of PL-NLS was diminished with successive flashes. The plot of absorbance versus the number photo-flashes indicates an inflection point at approximately 40 flashes. The absorbance of this dilution of PL-NLS showed a decrease of 0.8 O.D. units. The minimum absorbance is taken to represent complete photo-activation of the photo-labile, para-azide.

Agarose gel electrophoresis was used in a qualitative representation of PL-NLS photo-labeling of pGL3 (+/+). Figure 5-19 represents band-shifting toward the origin as the initial labeling stoichiometry of peptide to plasmid increased from 100 pmol (lane 2)

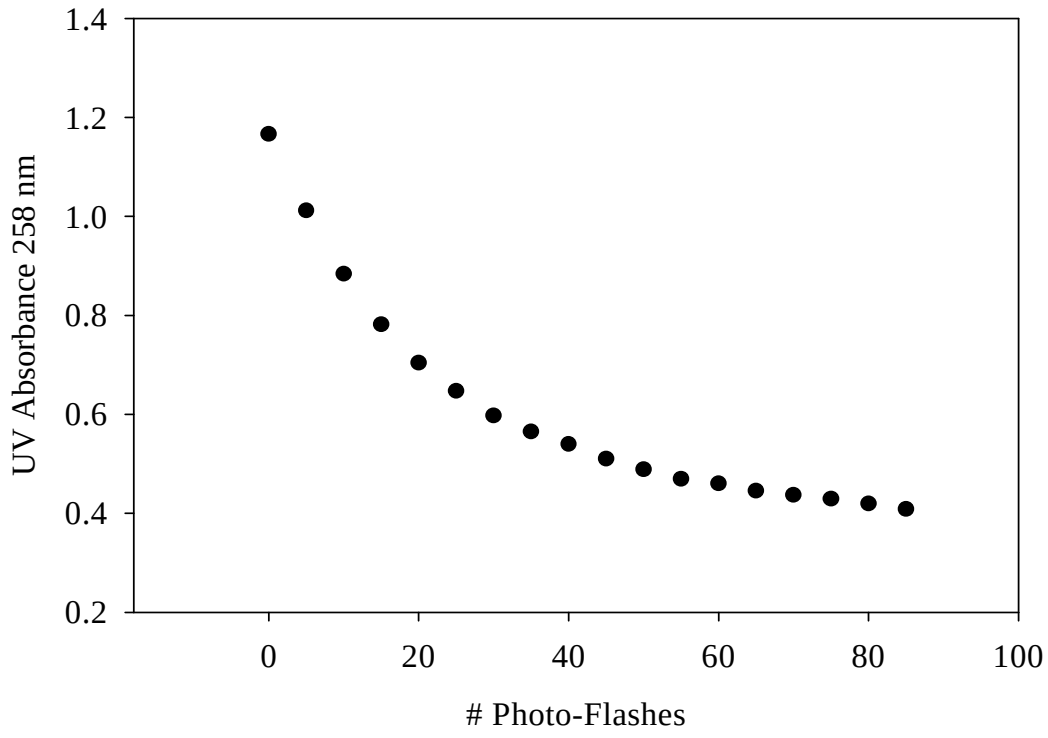

Figure 5-18. *Photo-degradation of PL-NLS absorbance*. A known amount of PL-NLS was subjected to successive photo-flashing and UV absorbance at 258 nm was continually monitored after every 5 flashes.

to 1 nmol (lane 4) as compared to unmodified plasmid (lane 1). Lanes 3 and 5 are denoted by an "*" which indicates that samples were not subjected to a photo-flash, and no band-shift retardation was observed in either case. In addition, a 250 nmol, stepwise increase in labeling stoichiometry from lane 100 pmol to 1 nmol showed a successive retardation of band migration (data not shown).

Qualitative photo-labeling assessment was carried out for the entire spectrum of PL-NLS analogs that have been synthesized. In each case, we observed near-complete retardation of band migration by labeling at 1 nmol of peptide per μg of pGL3 (+/+). Figure 5-20A demonstrates flashed versus non-flashed samples of each peptide at this

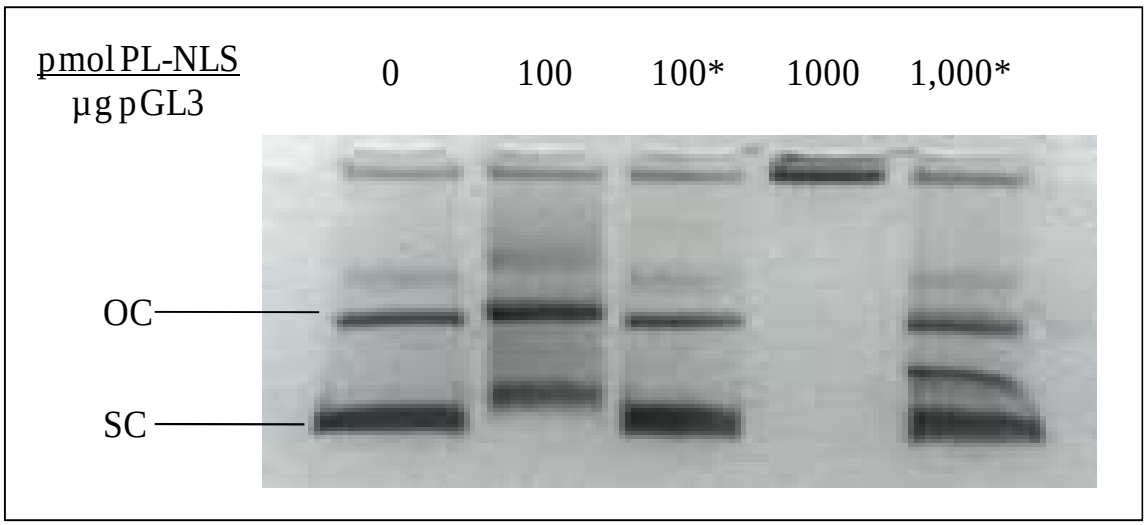

Figure 5-19. *Agarose gel electrophoresis of pGL3 labeled by increasing amounts of PL-NLS.* Stoichiometry of labeling reaction: Lane 1, 0 pmol/µg; Lane 2, 100 pmol/µg; Lane 3, 100 pmol/µg, non-flashed control; Lane 4, 1,000 pmol/µg; Lane 5, 1,000 pmol/µg, non-flashed control. The photo above represents a negative image of that acquired by imaging ethidium bromide fluorescence on the transilluminator after samples were run for 70 min at 80 V. "SC" indicates super-coiled band of pGL3 and "OC" indicates pGL3 in its open-circular form

stoichiometry. Note that both peptides containing the 6-Lys linker did not demonstrate any band migration for the non-flashed control. This was a result of the 6 additional cationic residues on the peptide which allowed for condensation of pGL3 (+/+). Thus, in the absence of covalent labeling, PL-6Lys-NLS/cNLS did not allow plasmid to freely migrate on agarose gel. For these 2 peptides, we demonstrated their photo-activation (which simply suggests photo-labeling ability) via the photo-degradation experiment. Figure 5-20B demonstrates that both peptides were photo-activatable.

Several factors can influence the transfection efficiency of a non-viral particle. A potentially influential factor is the particle size of the polyplex. The data in Figure 5-21 shows the effect that PL-NLS labeling of pGL3 (+/+) has on the particle size of peptide-labeled plasmid as it is condensed by PEI ($R\text{-}NH_3^+ : PO_4R_2^- = 9$). With a stoichiometry of labeling $\leq$ 300 pmol of PL-NLS per µg of plasmid, the particle size was maintained at an

A

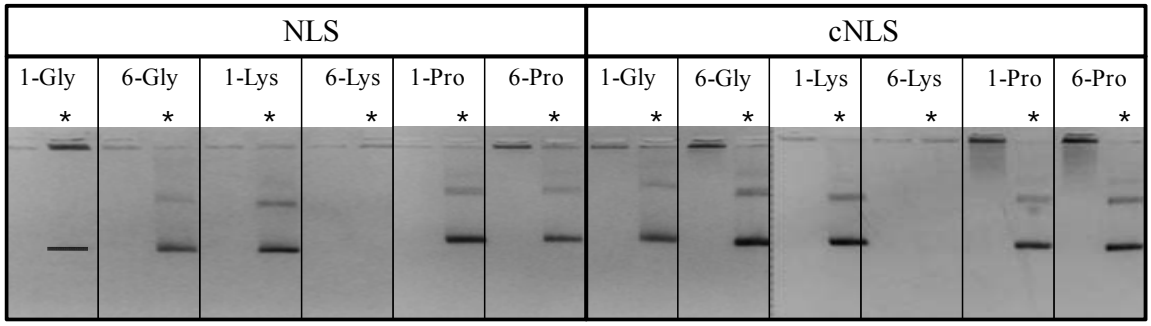

B

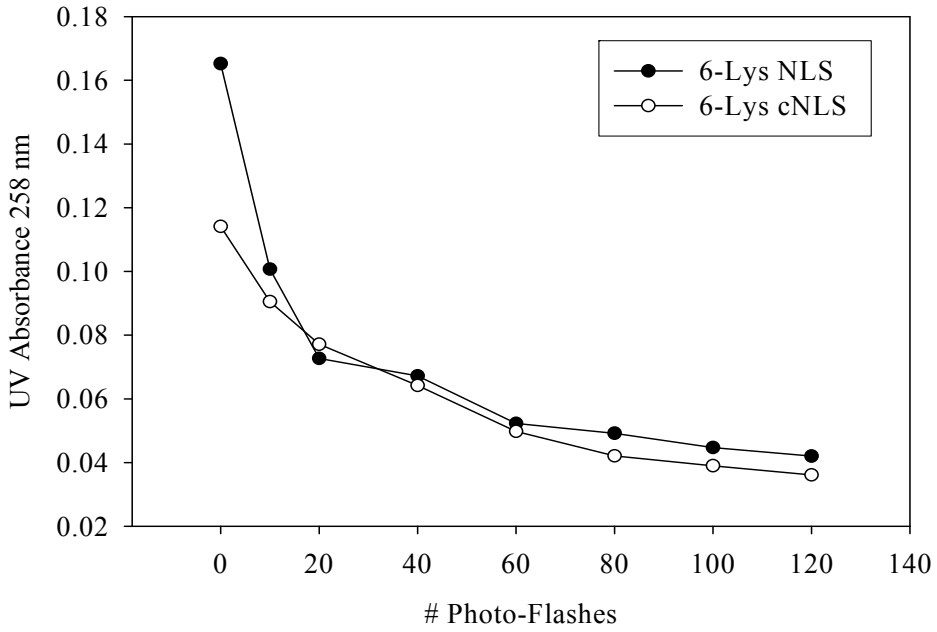

Figure 5-20. *Photo-Labeling of pGL3 by the series of variable-linker PL-NLS/cNLS peptides*. A) PL-containing peptides were introduced at a labeling ratio of 1 nmol/µl and photo-flashed 40x. In each case, "*" indicates the non-flashed control. Samples of 500 ng of pGL3 (+/+) were run for 70 min at 80 V on a 1% agarose gel. B) The poly-Lys linker region of PL-6Lys-NLS/cNLS condensed the plasmid at 1 nmol/µg and did not allow the pGL3 to run out of the well for the non-flashed controls. Here, these peptides were subjected to photo-flashing to show photo-degradation as an alternate indicator of photo-activation and photo-labeling ability

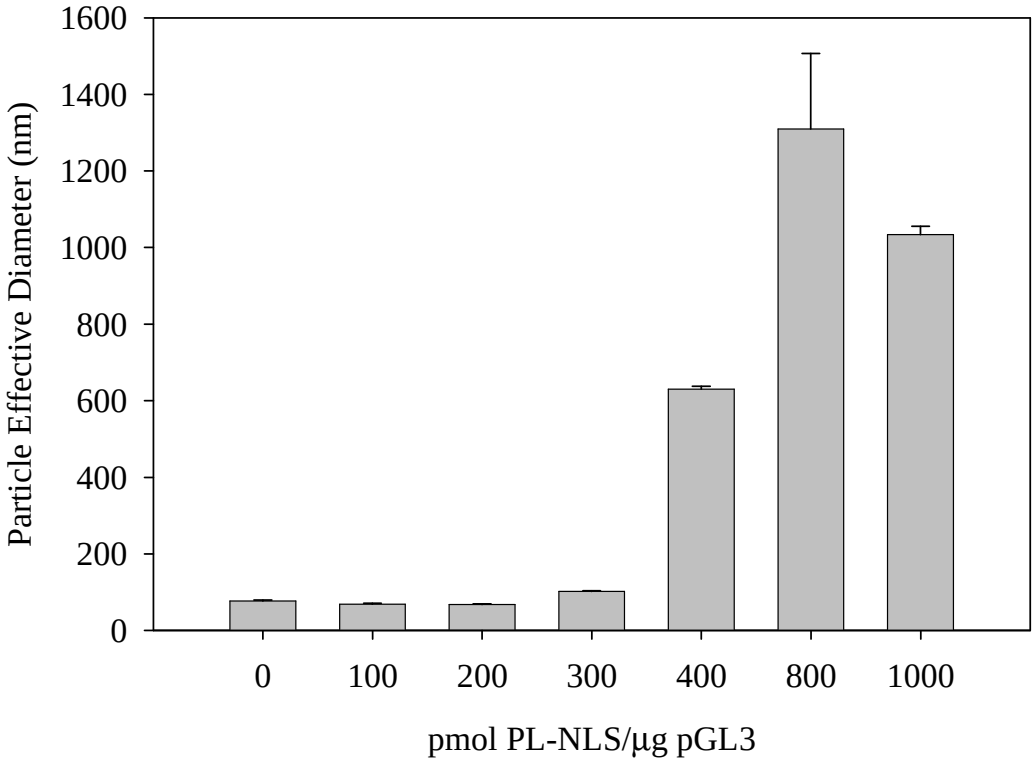

Figure 5-21. *Relationship between particle size of PEI-pGL3 condensates and stoichiometry of the photo-labeling reactions.* pGL3 (+/+) was labeled with the indicated stoichiometry of PL-NLS. NLS-pGL3 was condensed by PEI at a 9:1 charge ratio ($R\text{-}NH_3^+$:$PO_4R_2^-$). Particle size was determined by dynamic light-scattering analysis

effective diameter <100 nm. An increase is the stoichiometry, up to 1 nmol per μg, resulted in particle sizes exceeding 1 μm. Thus, the effective diameter of particles increased 200-fold from labeling with 200 pmol/μg up to 1 nmol/μg.

Iodination of PL-NLS-Y and Quantitative Photo-Labeling Efficiency

Synthesis of the tyrosine-containing PL-NLS was confirmed by LC-MS (Figure 5-15). The predicted mass of the peptide was 1434.5 amu as compared to the actual mass of 1434.3 amu. Figure 5-22 compares the elution of PL-NLS-Y from the G-10 column detected by UV absorbance at 258 nm to the elution of the iodinated peptide detected by a gamma counter. The simultaneous elution of peaks indicated by both detection methods

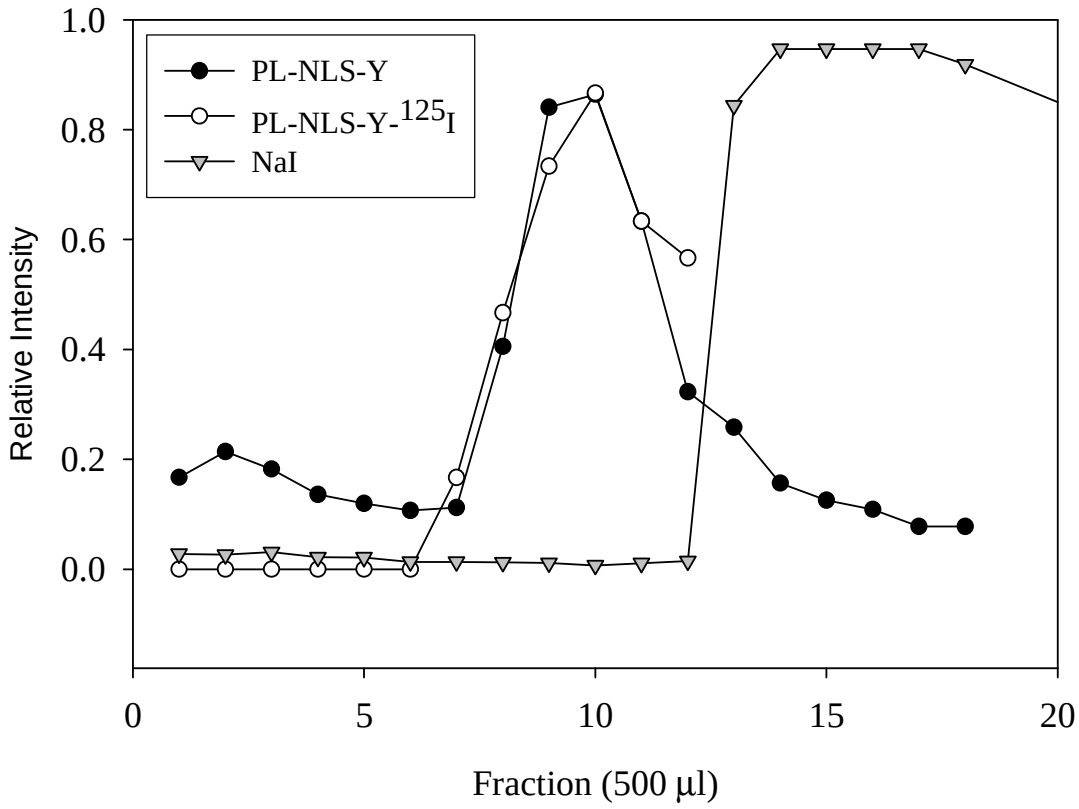

Figure 5-22. *Elution of PL-NLS-Y, NaI and Iodinated PL-NLS-Y-^{125}I by Sephadex G-10 Column.* PL-NLS-Y elution (black circles) was detected by UV absorbance at 258 nm. The cpms associated with iodinated peptide elution were detected by gamma counter (oben circles). NaI elution is detected by UV absorbance at 240 nm (gray triangles).

confirmed the identity of the iodinated peptide. The specific activity (57.27 µCi/nmol) of the peptide was calculated based on the amount of cold peptide collected (58%) and the total cpm of the fractions pooled (9, 10 and 11) from PL-NLS-Y-^{125}I. The identity of the radiolabeled product was further confirmed by thin-layer chromatography based on a positive ninhydrin test and the autoradiograph of PL-NLS-Y-^{125}I (Figure 5-23).

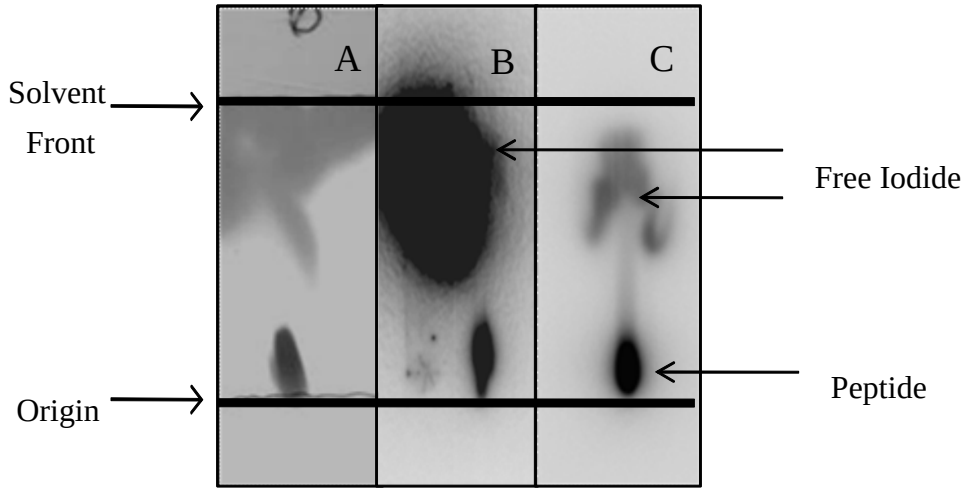

Figure 5-23. *Thin Layer Chromatography of PL-NLS-Y*. Panel A represents non-iodinated peptide developed with 90% acetic acid and stained for the presence of peptide by ninhydrin spray. Panel B is an autoradiographic image that shows the migration of $Na^{125}I$ (left spot) and radio-iodinated PL-NLS-Y (right). Panel C shows an aliquot of the iodinated peptide with a "halo" of free $^{125}I^-$ moving with the solvent front.

PL-NLS-Y-^{125}I was further purified from free $^{125}I^-$ by solid-phase C_{18} cartridges. Integration of thin-layer chromatography slides indicated that purification via the G-10 column resulted in samples that had approximately 40% of the observed radioactivity attributable to free iodide (Figure 5-23C). Following one solid-phase separation (Figure 5-24), the amount of free iodide was reduced to 19% of the total radioactivity of the sample. Fraction 16 from the elution in Figure 5-24 was taken through a second separation and the peak fraction (10) gave a sample of peptide that contained 96% of the measured radioactivity (Figure 5-25)

Figure 5-27 shows that photolabeling efficiency is dependent on the stoichiometry of the peptide/plasmid in the initial labeling reaction (A) and on the total amount of pGL3 used in the labeling reaction (B). The data shows a logarithmic relationship between

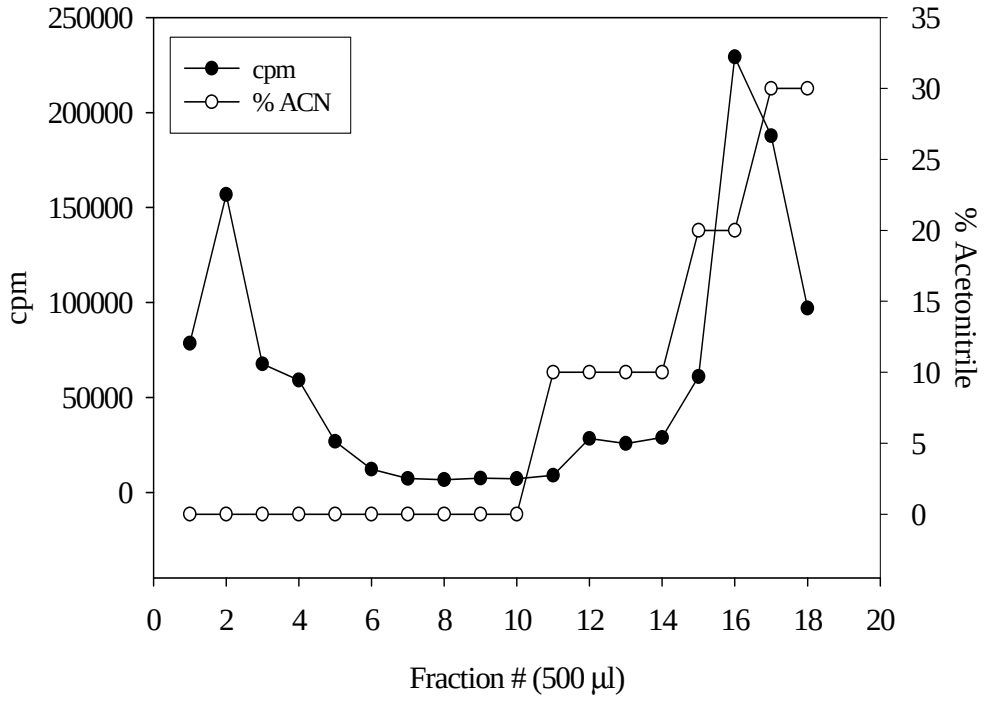

Figure 5-24. *Solid-phase separation of PL-NLS-Y-^{125}I.* Free ^{125}I is eluted initially from the C_{18} cartridge. With a step gradient of acetonitrile, the iodinated peptide is eluted in later fractions. Fraction #16 was collected, freeze-dried and reconstituted in 0.1% TFA.

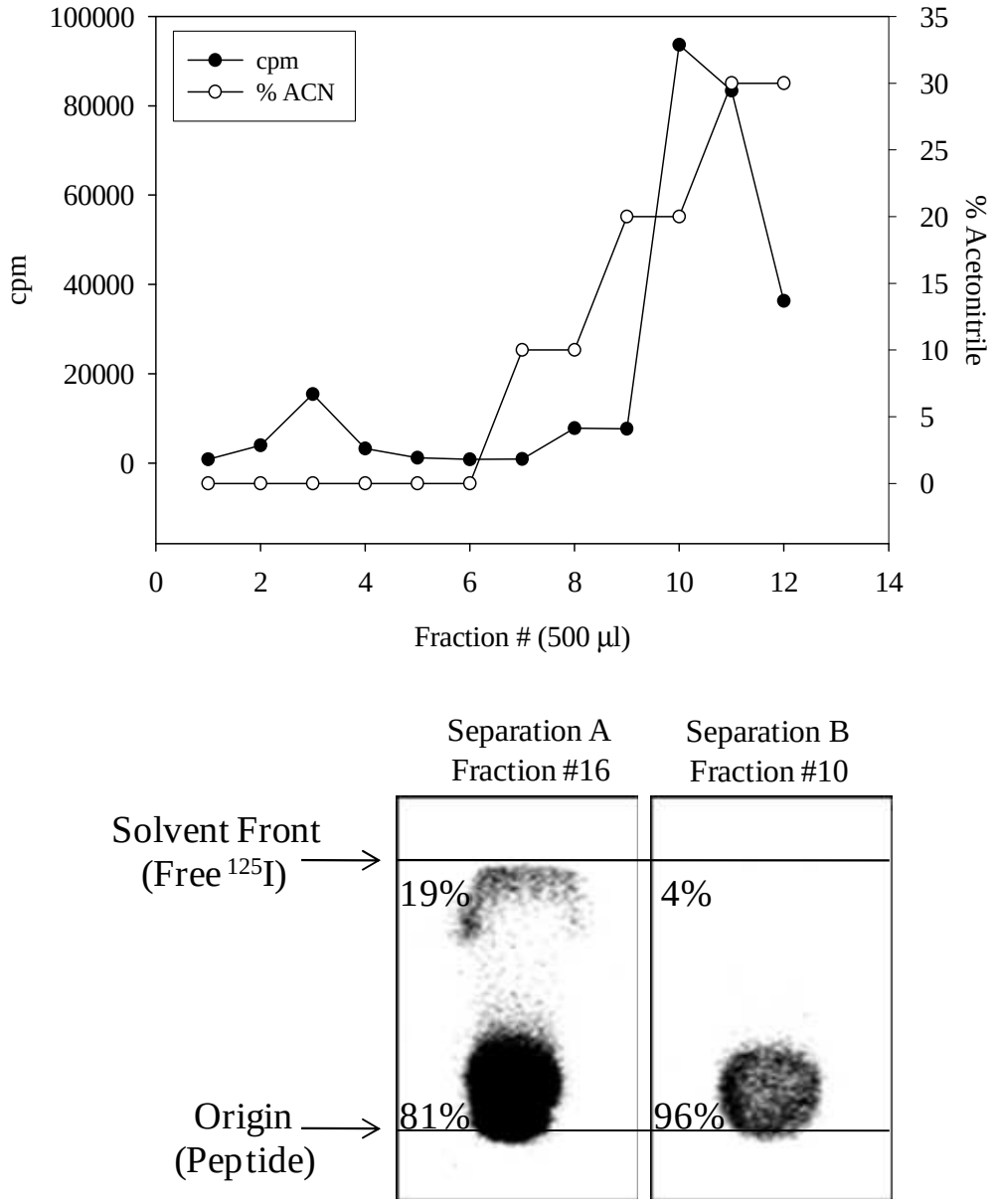

Figure 5-25. *2nd Solid-phase separation of PL-NLS-Y-125I.* The top graph shows the elution of iodinated peptide that was reconstituted from the fraction identified in Figure 5-24. As in the previous case, the peak fraction (10) was collected, freeze-dried and reconstituted in 0.1% TFA. The bottom figure represents an autoradiograph and density integration of purified fractions on TLC.

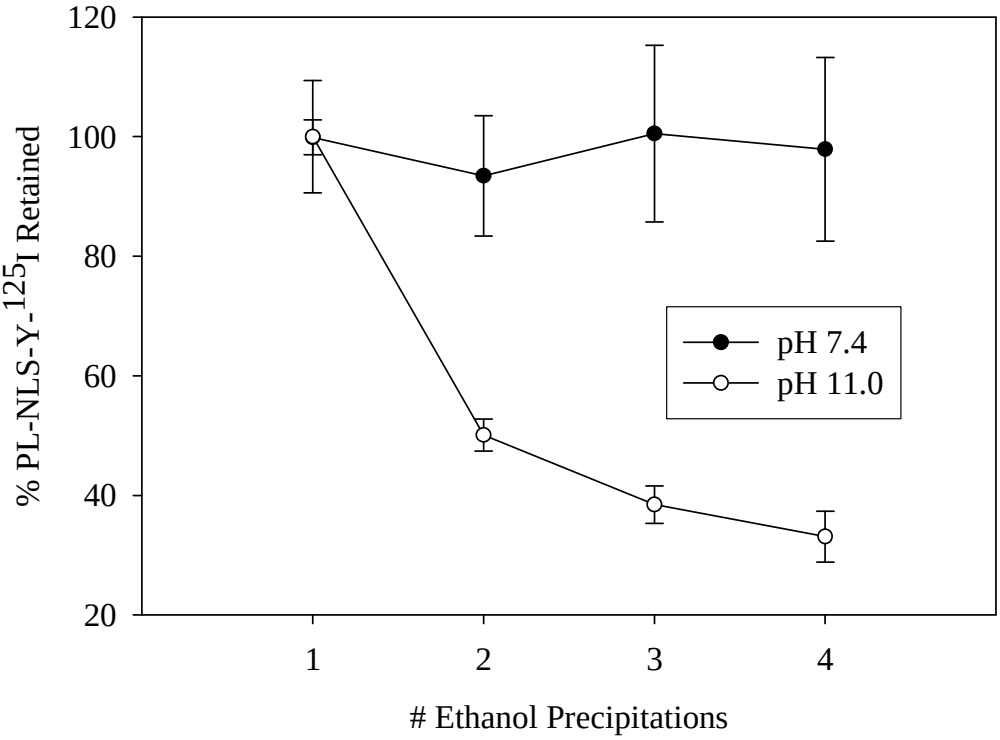

Figure 5-26. *Stability of the Covalent Interaction between PL-NLS and pGL3*. pGL3 (+/+) was photolabeled with PL-NLS-Y-^{125}I. Triplicate samples were maintained at room temperature in either 5 mM Hepes (pH 7.4) or 1 M NH_4OH (pH 11.5). Radioactivity (as a measure of covalently-labeled peptide) was monitored after successive ethanol-precipitations over the course of 48 hours.

peptide stoichiometry and photo-labeling efficiency, given a constant amount of pGL3. From this fit line, we can calculate the absolute number of peptides labeled onto pGL3 (+/+), given an initial labeling stoichiometry (Table 5-3).

The stability study highlighted in Figure 5-26 shows that the covalent adduction of pGL3 (+/+) by iodinated PL-NLS-Y is stable at physiological pH as compared to a positive control for depurination in which 70% of the peptide is lost over 48 hrs.

Previous agarose gel electrophoresis experiments have demonstrated that peptide labeling at an initial stoichiometry of 100 pmol of peptide per μg of pGL3 (+/+) could induce band retardation. Qualitatively, this suggests covalent adduction at relatively high

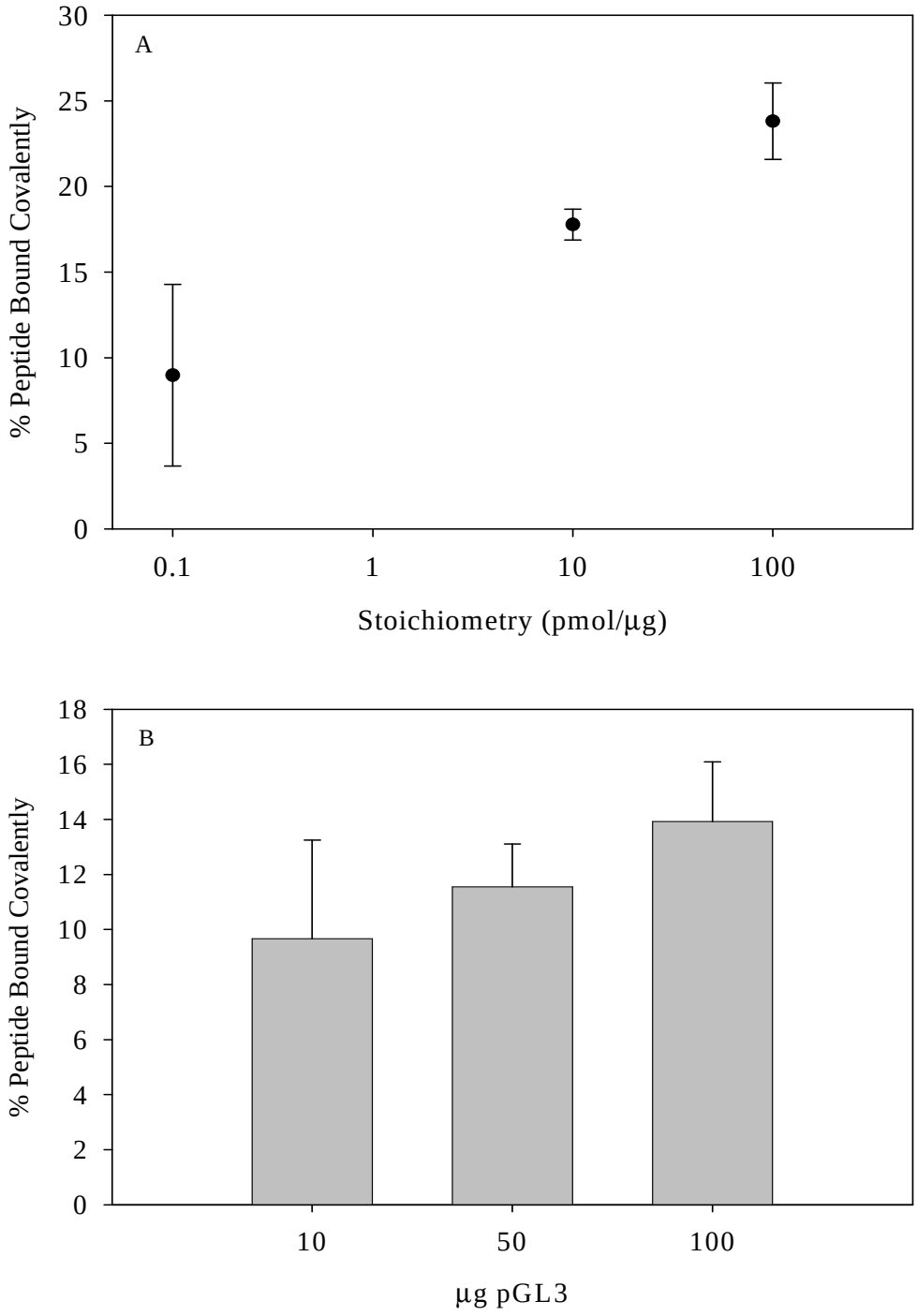

Figure 5-27. *Quantitative determination of photo-labeling efficiency*. A) The variable stoichiometry of PL-NLS-Y-^{125}I is plotted on the above log-linear plot versus its relationship to the percent of peptide that was calculated as bound covalently to pGL3 (+/+). The relationship is represented by the equation: y = 0.021ln(x) + 0.136. B) The amount of pGL3 (+/+) in the labeling reaction was increased, but the concentration of plasmid and peptide was kept constant (0.2 µg/µl and 0.1 pmol PL-NLS-Y/µg, respectively).

stoichiometries. Figure 5-28 qualitatively confirms that pGL3 is covalently labeled by a reaction with an initial stoichiometry of 1 pmol of peptide per μg of pGL3.

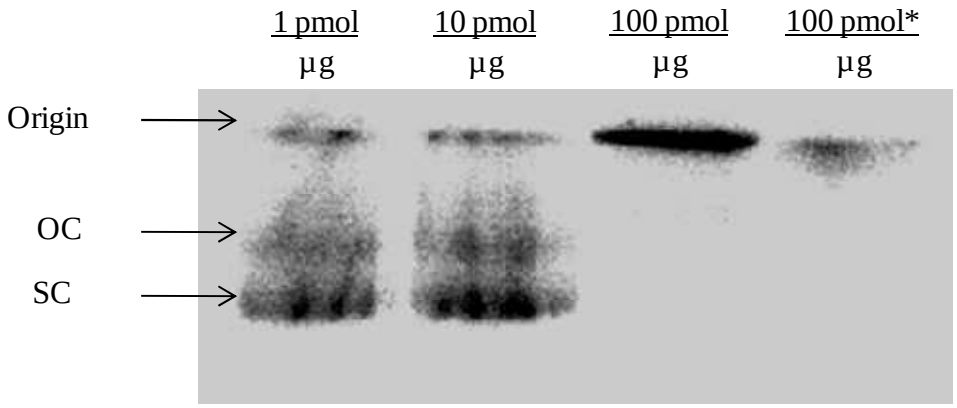

Figure 5-28. *Agarose gel electrophoresis of pGL3 labeled by PL-NLS-Y-^{125}I.* The autoradiographic image shows 10 μg of pGL3 labeled by 1, 10, and 100 pmol of PL-NLS-Y-^{125}I per μg (left to right in the first 3 lanes). The final lane includes 100 pmol/ μg, but represents the non-flashed (*) control. Bands indicate the presence of the iodinated peptide.

Assessing Nuclear Uptake of NLS-pDNA by Confocal Microscopy

The initial confocal experiments involved image acquisition of a single XY-plane. Images were assessed qualitatively using the ImageJ software for merging the red and far-red signals. Figure 5-29 shows the results of a PEI-mediated transfection of Cy3-pGL3 (+/+) labeled with 10 pmol of peptide per μg of plasmid. The time course of the experiment was 24 hrs and uptake was assessed at 3, 6, 12 and 24 hrs. The cytosol of all cells carried a strong and punctate Cy3 signal that represented intracellular pGL3 (+/+). The amount of Cy3 signal internalized appeared to increase for each treatment over the course of 24 hrs.

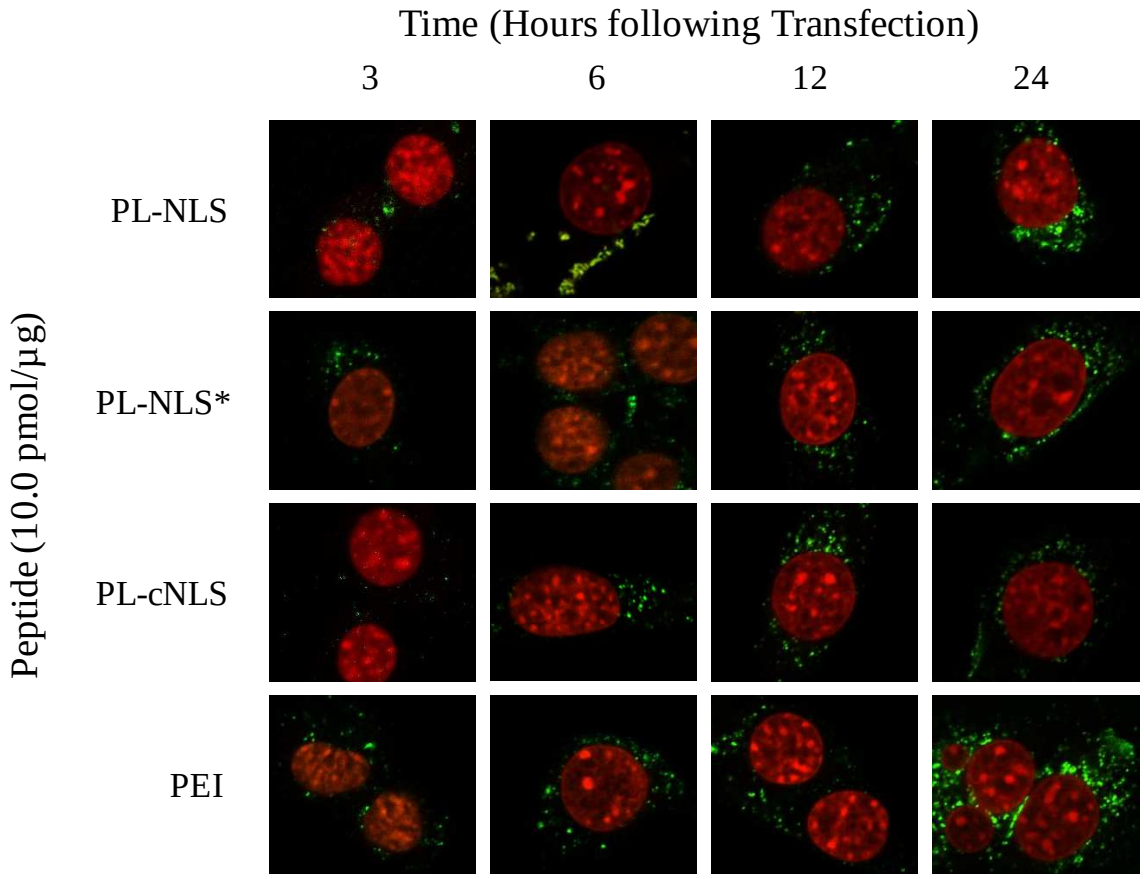

Figure 5-29. *3-24 hr transfection with 500 ng of Cy3-pGL3*. Cy3-pGL3 was labeled by 10 pmol of NLS per µg,10 pmol of cNLS per µg, unmodified, but formulated in the presence of 10 pmol per µg (NLS*=No flash control) or simply condensed by PEI prior to transfection. All treatments are condensed by PEI ($R\text{-}NH_3^+:PO_4R_2^-$ =3). Nuclei labeled with TO-PRO-3 are shown in the red pseudocolor and Cy3-pGL3 is shown in the green pseudocolor.

Transfection experiments were extended to 24 hrs to observe whether or not nuclear uptake was time-dependent. We observed no qualitative or quantitative (Figure 5-30) increase in nuclear uptake from 3 hrs out to 24 hrs. The percent nuclear uptake for all treatments ranged from 2-14% at the 3 hr time point, and became more consistent (2-7% nuclear uptake) for 6 hr to 24 hr transfections. The qualitative observation of increasing internalization over time is shown quantitatively in Figure 5-31. Between formulations at a given time point, there was no significant difference (a favorable result given that this

assumption is built-in to the experiment). However, the mean cellular uptake of all formulations increased from 3 hrs (6.6 x 10^4 relative fluorescent units) to 24 hrs (1.5 x 10^5 relative fluorescent units).

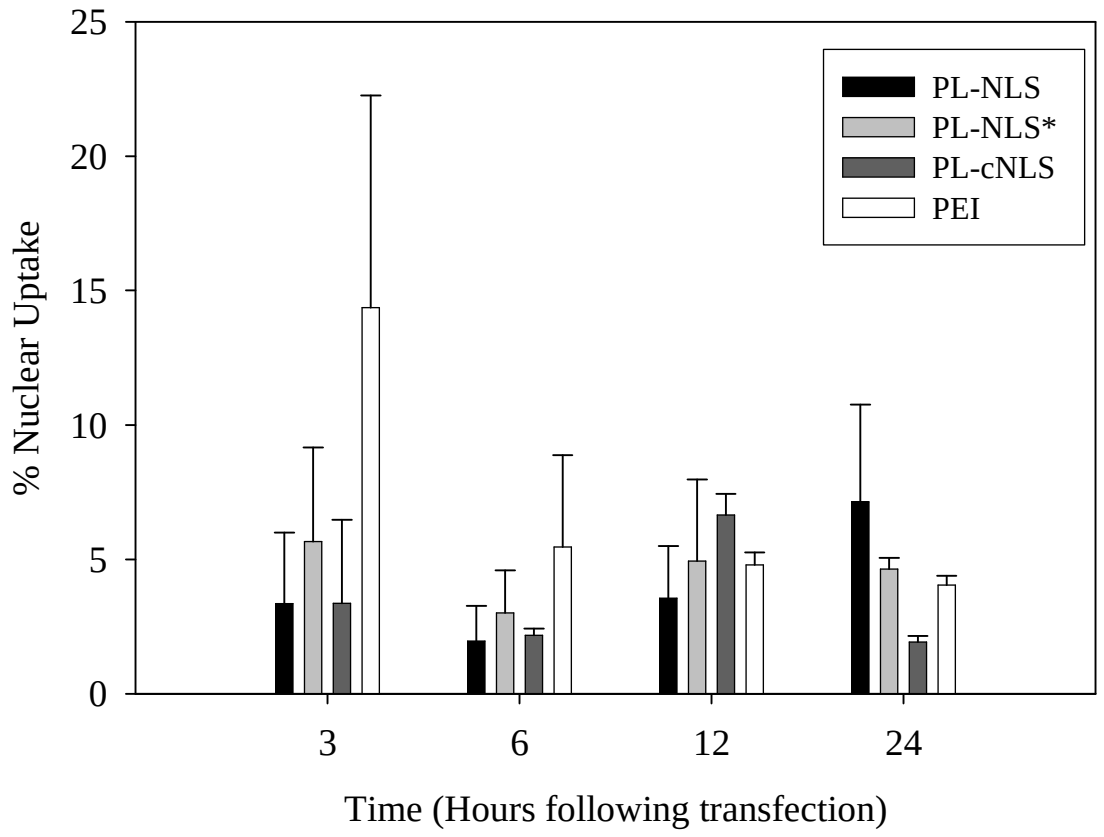

Figure 5-30. *Time course of nuclear uptake assessed quantitatively*. NIH/3T3 cells were transfected with 500 ng of Cy3-pGL3 (PEI; R-NH_3^+:$PO_4R_2^-$ =3). pGL3 was labeled with PL-NLS or PL-cNLS at 10 pmol/μg prior to transfection. Also included was a non-flashed control with PL-NLS and an unmodified control. Nuclear localization was monitored from 3-24 hrs. The measure of % nuclear uptake is based on the Cy3 fluorescence in the nucleus as compared to the total Cy3 fluorescence in the whole cell.

Additional treatments were applied to this experimental protocol with a 6 hr transfection. The ratio of NLS was varied from 1 pmol/μg pGL3 (+/+) up to 100 pmol/μg

plasmid. NLS and cNLS analogs (PL-6Pro, PL-6Lys, PL-6Gly, PL-1Pro, PL-1 Lys and PL-ExtSV40) were also examined (Table 5-2). The quantitative analysis suggests that PL-NLS containing a 6-lysine linker is the most potent nuclear localizing analog.

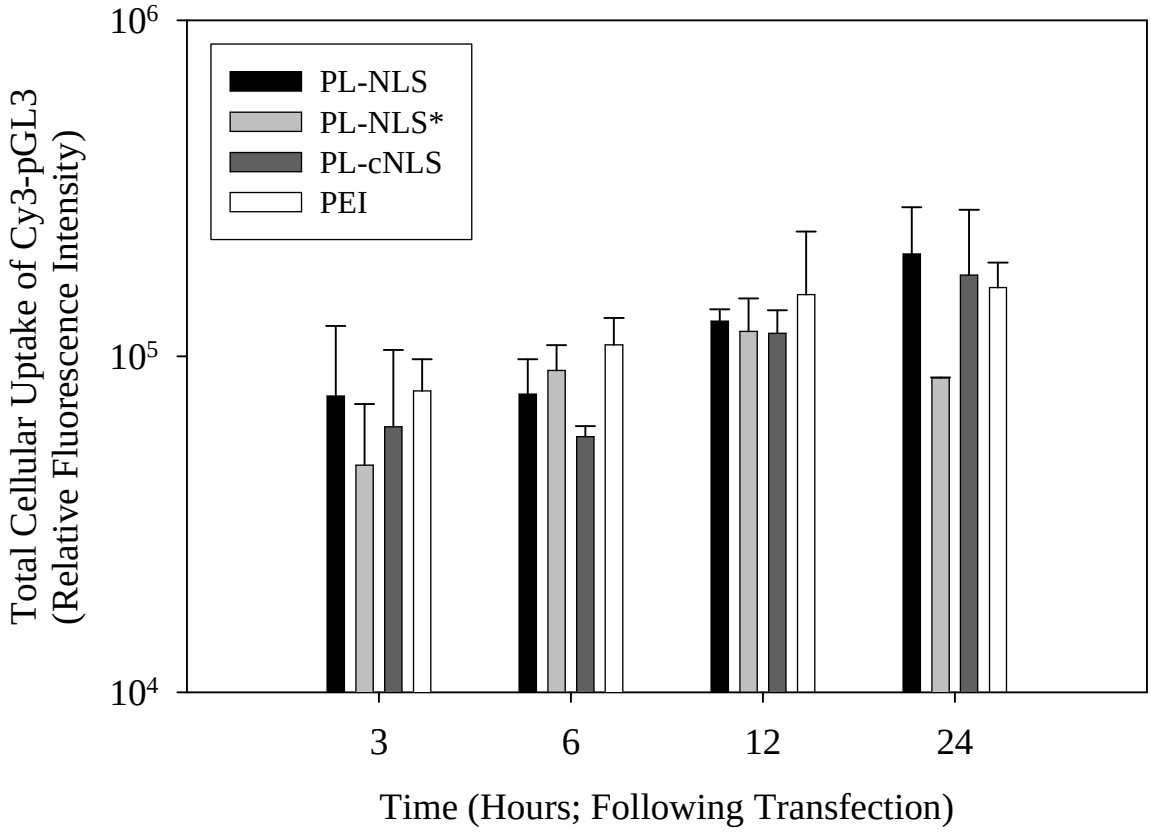

Figure 5-31. *Time course of cellular uptake assessed quantitatively*. NIH 3T3 cells were transfected with 500 ng of Cy3-pGL3 (PEI; $R\text{-}NH_3^+ : PO_4R_2^- = 3$). pGL3 was labeled with PL-NLS or PL-cNLS at 10 pmol/μg prior to transfection. Also included was a non-flashed control with PL-NLS and an unmodified control. Cellular uptake of the Cy3 signal was monitored from 3-24 hrs

Table 5-2. *Quantitative image analysis - single XY plane*. In a series of transfection experiments, various NLS controls were compared. PEI, at a charge ratio of $R\text{-}NH_3^+:PO_4R_2^-$ =3, was used as the transfecting agent in each case. The duration of transfection was 6 hrs.

	Peptide	Labeling	Nuclear Localization	Std Dev
PL-NLS Controls (2-Gly Linker)	PL-NLS	10 pmol/μg	9.8%	5.3%
	PL-cNLS	10 pmol/μg	6.9%	1.4%
	PL-NLS*	10 pmol/μg	12.8%	7.6%
	PL-NLS	1 pmol/μg	12.8%	7.6%
	PL-NLS	100 pmol/μg	10.3%	3.7%
	--	--	6.9%	8.7%
PL-NLS Analogs Variable Linker	PL-ExtSV40-NLS	10 pmol/μg	4.4%	3.1%
	PL-ExtSV40-cNLS	10 pmol/μg	4.7%	5.7%
	PL-1Lys-NLS	10 pmol/μg	9.2%	3.9%
	PL-1Lys-cNLS	10 pmol/μg	9.3%	9.5%
	PL-6Lys-NLS	10 pmol/μg	17.3%	7.6%
	PL-6Lys-cNLS	10 pmol/μg	1.3%	0.1%
	PL-1Pro-NLS	10 pmol/μg	1.2%	1.4%
	PL-1Pro-cNLS	10 pmol/μg	7.4%	4.2%
	PL-6Pro-NLS	10 pmol/μg	7.4%	3.0%
	PL-6Pro-cNLS	10 pmol/μg	2.7%	2.8%
	PL-6Gly-NLS	10 pmol/μg	13.8%	7.7%
	PL-6Gly-cNLS	10 pmol/μg	4.4%	6.2%

"PL-NLS*" represents non-flashed control

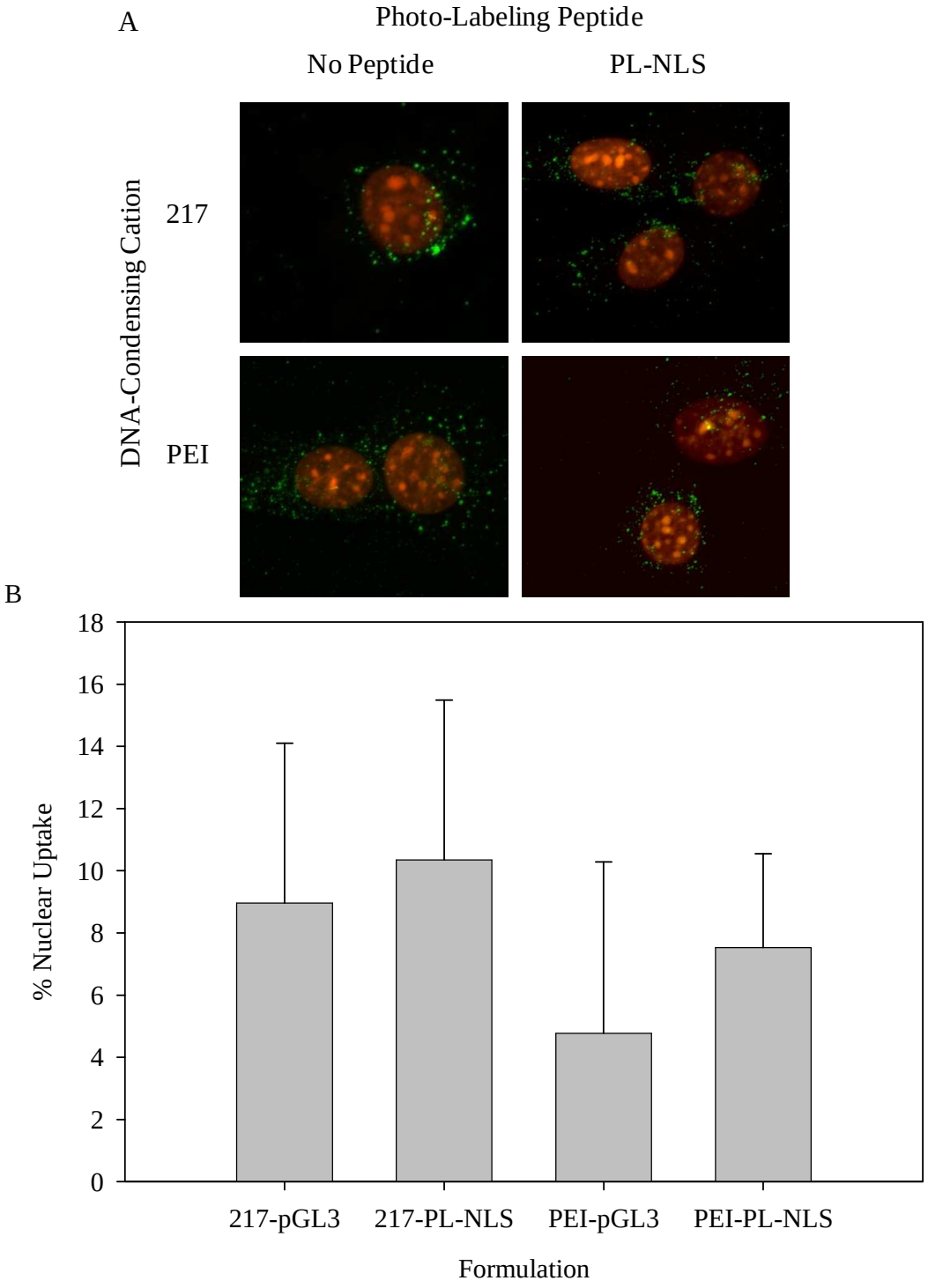

Figure 5-32. *PEI vs peptide 217 delivery*. Unmodified Cy3-pGL3 delivery by PEI was compared to that with peptide 217. Likewise, Cy3-pGL3 labeled by PL-NLS (10 pmol/μg) was compared. The 3 hr transfection was analyzed by Z-series acquisition. Panel A shows representative composite images for the entire Z-projection. Panel B represents the quantitative data.

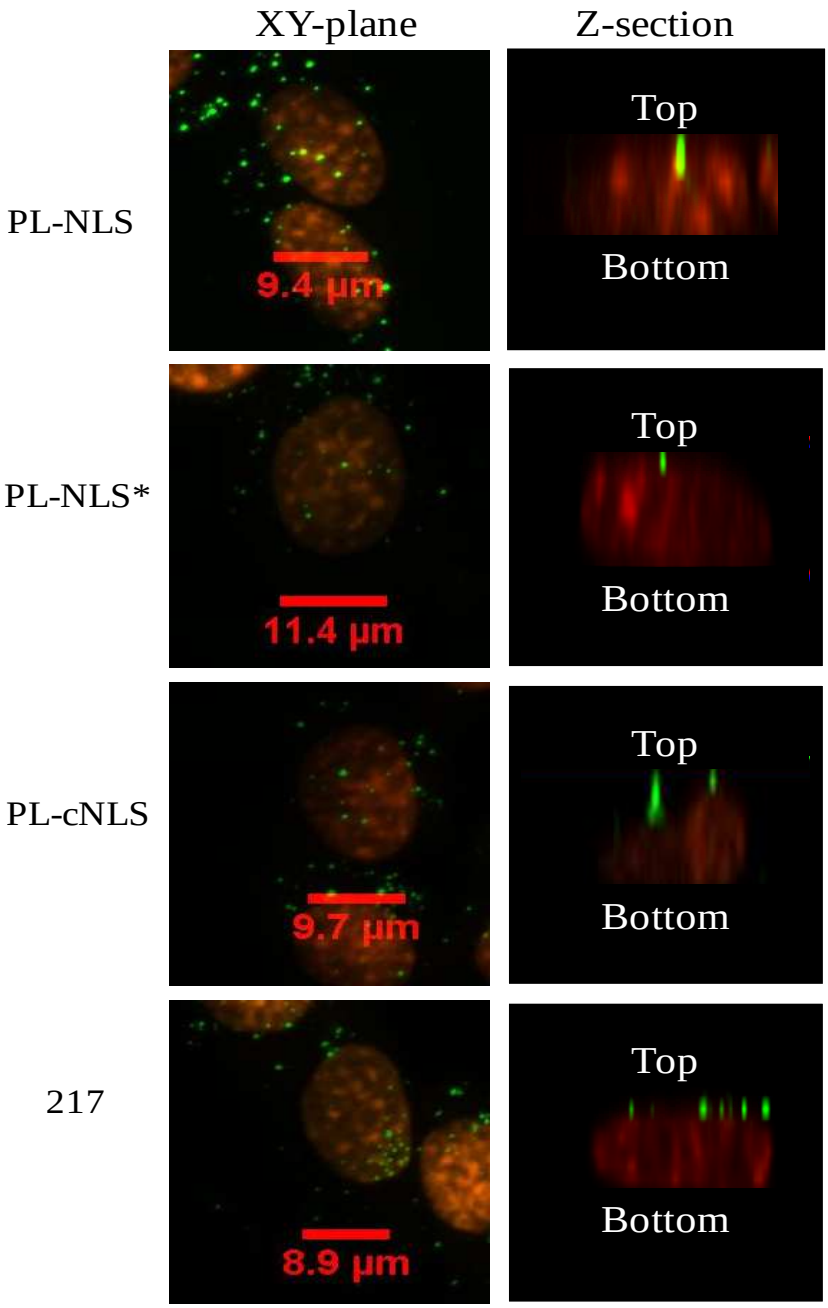

Figure 5-33. *6 hour tme point of Cy3-pGL3 delivered by 217: qualitative Z-series assessment*. Cy3-labeled pGL3 (+/+) was transfected into NIH/3T3 cells. They were fixed, permeabilized and stained with TO-PRO-3 at various time points post-transfection . The 6 hr transfection is shown here with images of the XY-plane and Z-series reconstruction images.

Qualitative analysis of images via ImageJ occasionally produced merged images that showed diffuse pixels of Cy3 fluorescence in the nuclei. It was determined that this

was an artifact of the laser during image acquisition. Specifically, an increase in the intensity of the Helium/Neon laser (ex: 543 nm) produced emission from the nuclear TO-PRO-3 that was detected in the red spectrum. This phenomenon resulted in artifactual, diffuse red signal in the nuclei that appeared in the absence of Cy3-pGL3 transfection. In early experiments, this emission in the red channel was incorrectly observed as colocalizing with the far-red emission and confounded interpretation of the colocalization mask image. This diminished the reliability of the quantitative analysis of nuclear uptake.

In an effort to more fully quantify nuclear uptake in the entire volume of the cell (rather than in a single XY-plane), the acquisition protocol was amended to collect Z-series data. In the first experiment implementing the Z-series acquisition protocol, plasmid delivery by PEI was compared to delivery by peptide 217. Peptide 217 ($CWK_{17}C$), is a gene transfer peptide that undergoes DNA template polymerization by sulfhydryl crosslinking to form condensates. The endosomal environment is suspected to trigger intracellular release of DNA by reducing the sulfhydryl linkages[9]. Cy3-pGL3 (+/+) formulations were either labeled by PL-NLS (10 pmol/μg) or unmodified. Plasmid was condensed by each polycation at an $R\text{-}NH_3^+:PO_4R_2^- = 3$ by both PEI and peptide 217. The transfection was carried out for 3 hrs (Figure 5-32). Both qualitative (panel A) and quantitative (panel B) data are displayed in the figure. There was no significant difference between the delivery systems when compared by quantitative methods, although 217 delivery showed an increase in nuclear localization for both NLS-pGL3 and pGL3 (10.3 and 8.9 %, respectively) as compared to PEI-mediated delivery of the same formulations (7.5 and 4.8%, respectively).

A 6 hr time course of Cy3-pGL3 (+/+) delivery by peptide-217 was carried out for NLS-pGL3 (10 pmol/μg), cNLS-pGL3 (10 pmol/μg), NLS*pGL3 (10 pmol/μg) and unmodified pGL3. As before, the total cellular uptake of polyplex increased over 6 hrs. The Z-section reconstruction of the 6 hr time point (Figure 5-33) showed that the polyplexes were in the perinuclear region and appeared spatially on top of the cells.

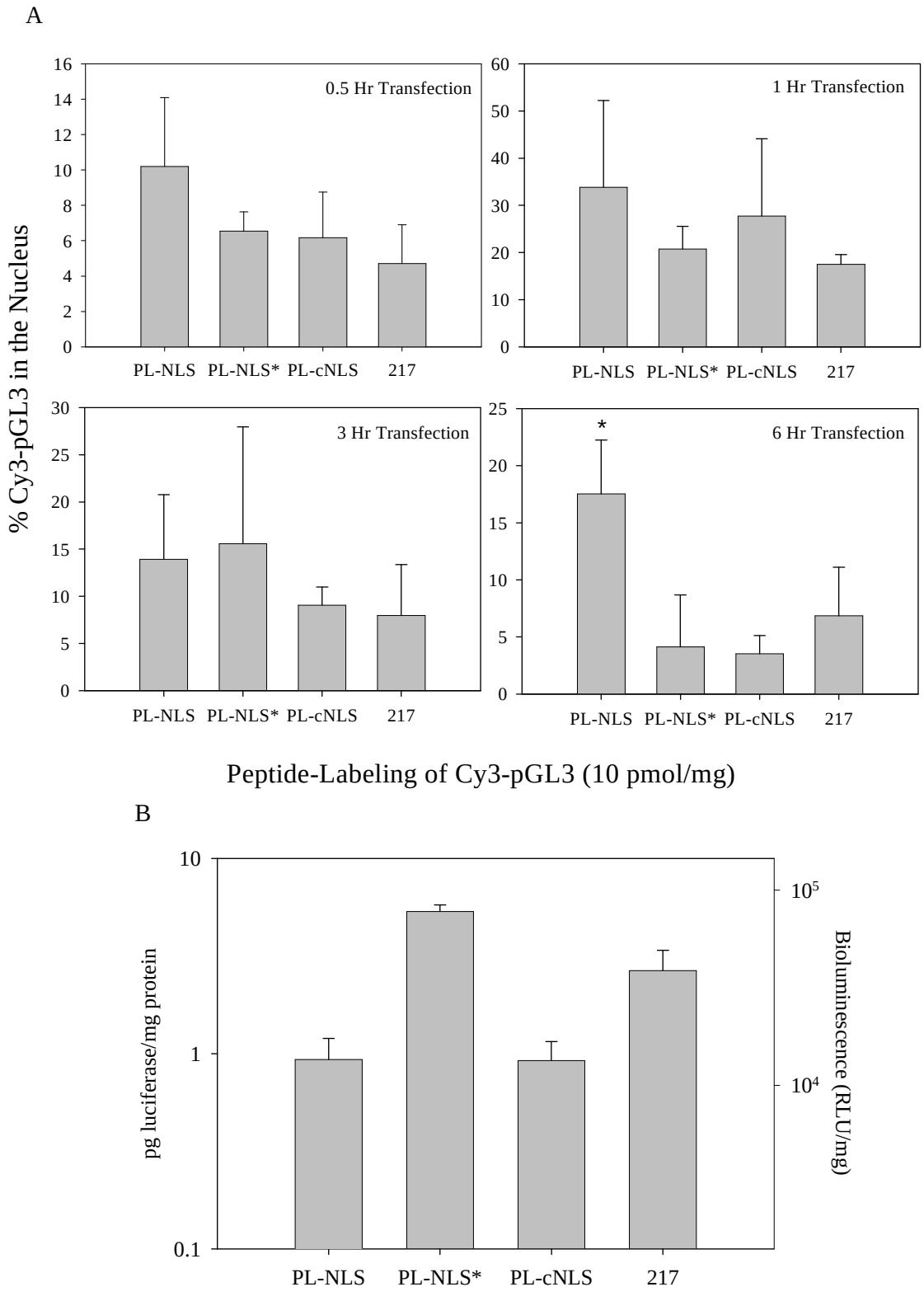

Figure 5-34. *Quantitative assessment of Z-series data: 6 hr time course.* NIH/3T3 cells

were transfected with 500 ng of Cy3-pGL3 (+/+) for 0.5, 1, 3 and 6 hrs. Peptide-217 served as the delivery agent ($R\text{-}NH_3^+:PO_4R_2^- = 3$). NLS is compared to controls at each time point (panel A). In a separate experiment including the same controls, luciferase expression was quantified for a 6 hr transfection for the purposes of comparing % nuclear uptake to luciferase expression (Panel B).* = statistically significant ($p \leq 0.05$) compared to controls.

There is at least one Cy3 label localized to the nucleus in the case of the NLS-labeled pGL3 (+/+).

The time course data from the Z-series collection is represented graphically in Figure 5-34A. There is not any distinct gain in nuclear uptake mediated by Cy3-pGL3-NLS compared to controls until the 6 hr time point. At 6 hrs, 17.5% of the Cy3 signal was in the nuclei of cells transfected with NLS-pGL3. The other treatments gave nuclear localization ranging from 3.5-6.8%. NLS-pGL3 gave nearly a 3-fold increase in % nuclear uptake over controls, and this increase was found to be statistically significant ($p \leq 0.05$) in each case. The corollary in vitro gene expression experiment was completed to complement the 6 hr transfection (Figure 5-34B). (Earlier time points are not displayed here because luciferase expression levels for the 0.5, 1 and 3 hr transfections were below the limit of detection for the assay). The expression data did not correlate with the uptake data derived from confocal imaging. Rather, luciferase expression was shown to be decreased by 3-6 fold due to labeling plasmid with either NLS or cNLS at 10 pmol of peptide per μg of pGL3.

The luciferase-expressing plasmid, pGL3 (-/-) was incorporated in a similar experiment. pGL3 (-/-) lacks both the SV40 promoter and enhancer elements that are present in pGL3 (+/+). Of particular importance is the absence of the SV40 enhancer element which contains a 72-bp repeat that has been shown to be a nuclear localizing DNA sequence. pGL3 (-/-) was labeled with Cy3 and the experimental protocol was identical to that described for pGL3 (+/+). Transfection was carried out for 6 hrs, and the nuclear localization profile (Figure 5-35) appears similar to that observed when pGL3

(+/+) was delivered and assessed after 6 hrs. NLS-pGL3 (-/-) showed that 14.8% of the Cy3 signal was nuclear localized compared to a range of 2.9-4.6% for the control formulations. Again, NLS-pGL3 showed a 3-fold increase in % nuclear uptake compared to controls.

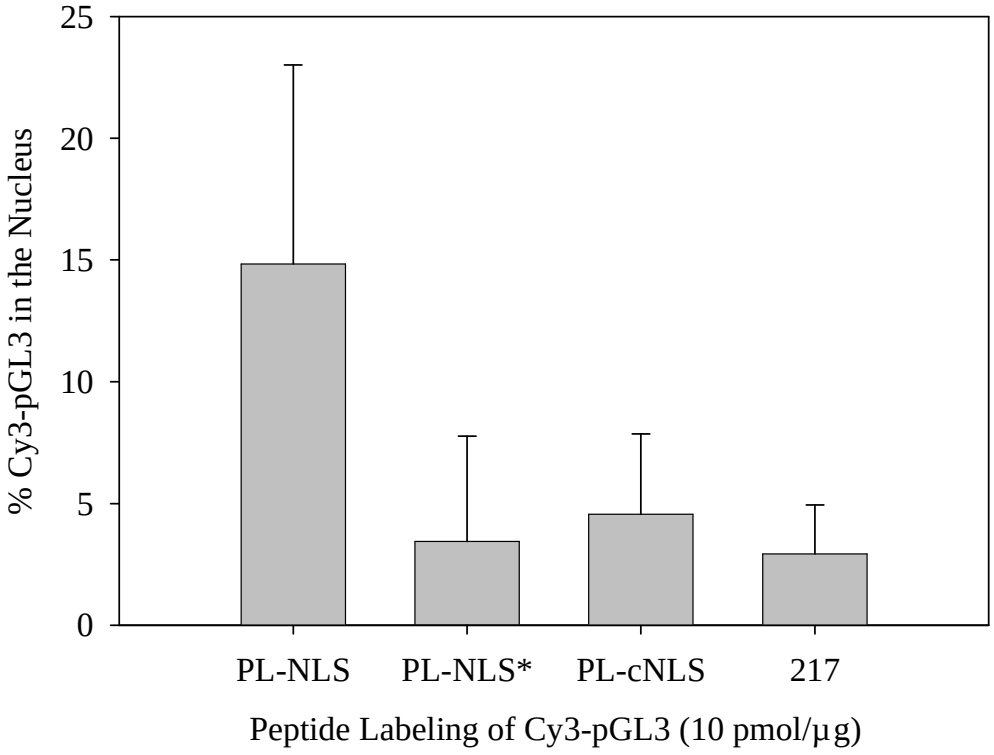

Figure 5-35. *Quantitative nuclear localization of pGL3 (-/-).*NIH/3T3 cells were transfected with 500 ng of Cy3-pGL3 (-/-) for 6 hrs. Peptide-217 served as the delivery agent ($R\text{-}NH_3^+:PO_4R_2^-$ = 3).

NLS-Mediated Increase in Luciferase Expression In Vitro

Initial experiments were conducted along the lines of varying the amount of PL-NLS incorporated into the formulation to observe the effects of increased covalent labeling on luciferase expression in a dose-response fashion (Figure 5-36). Expression was maximal when pGL3 (+/+) was labeled with 0.1 pmol of PL-peptide per µg. At this

lowest labeling ratio, expression was greater than plasmid labeled with PL-cNLS or unlabeled in a standard PEI transfection ($R\text{-}NH_3^+:PO_4R_2^-$ = 9). As the labeling ratio increased to 1 pmol/μg, the data actually showed a 2-fold decrease in transgene expression. Further increasing to 10 and 100 pmol of PL-NLS/μg, expression decreased by 10-fold and >1,000-fold, respectively, compared to the PEI-pGL3 (+/+) control.

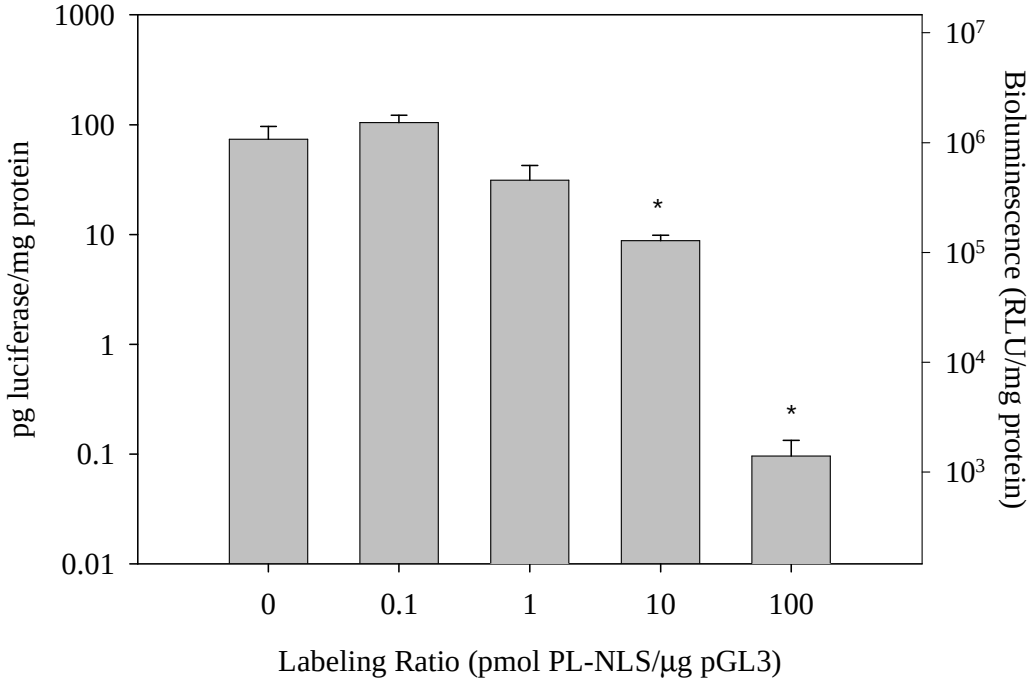

Figure 5-36. *In vitro luciferase expression from variable labeling with PL-NLS*. NIH/3T3 cells were transfected with 5 μg of pGL3 condensed by PEI (N:P=9). Prior to PEI condensation, formulations were photo-labeled with PL-NLS at an initial stoichiometry of reaction designated above. * Represents statistically significant difference relative to unlabeled pGL3 (+/+) ($p \leq 0.05$).

The time course experiment indicates the optimal duration of transfection which yields the maximal increase in NLS-mediated luciferase expression as compared to the relevant controls (Figure 5-37). Under conditions of 24 hr cell seeding in 10% FBS culture media and subsequent transfection in 2% FBS media, NLS-mediated expression (by 0.1 pmol/μg labeling) was maximized at 18 hrs as it was increase by 4-fold over both

the cNLS and un-labeled control. This increase was statistically significant ($p \leq 0.05$). Under these conditions, initial expression levels are detectable at the 3 hr time point, but no difference in expression levels was observable. Expression levels become normalized at the 24 and 48 hour time points for NLS relative to controls.

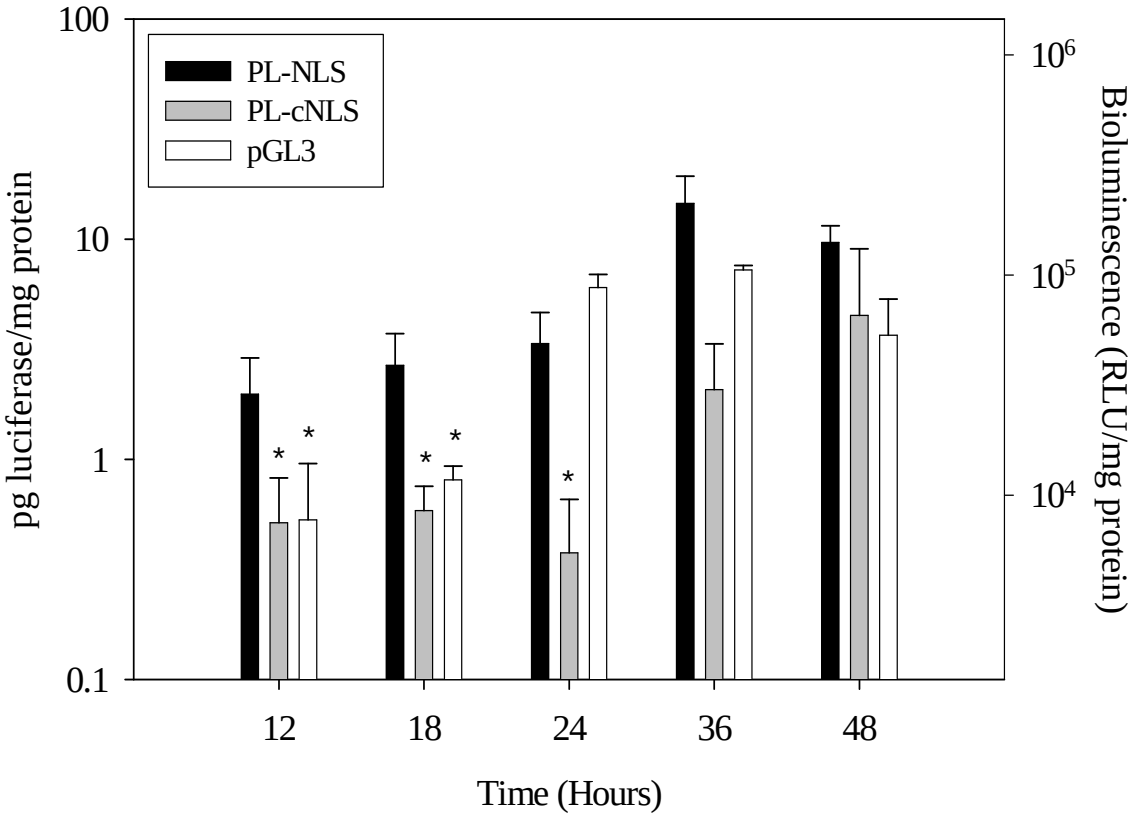

Figure 5-37. *In vitro time course of luciferase expression*. NIH/3T3 cells were transfected with 5 μg of pGL3 (+/+) labeled by 1 pmol of PL-NLS per μg . Formulations were condensed by PEI ($R\text{-}NH_3^+ : PO_4R_2^-$ =9). Lysate was harvested and measured for luciferase content in triplicate at each time point. * Represents statistically significant difference relative to PL-NLS ($p \leq 0.05$).

The variable cell seeding number allowed for the observation of cells at different growth rates for a 24 hr transfection. Cells were seeded and incubated for 24 hrs prior to transfection. We observed an increase in normalized luciferase expression of about 1 log

unit with each log increase in cell seeding number. Only the treatments that had seeded 1 million cells per 35 mm well displayed an NLS-mediated increase in nuclear uptake when pGL3 (+/+) was labeled at 0.1 pmol of PL-NLS per μg. The increase was 3-fold over cNLS and 5-fold compared to un-labeled pGL3 (+/+). In the case of 10^4 and 10^5 cells seeded per well, there was no observed statistical increase relative to controls (Figure 5-38).

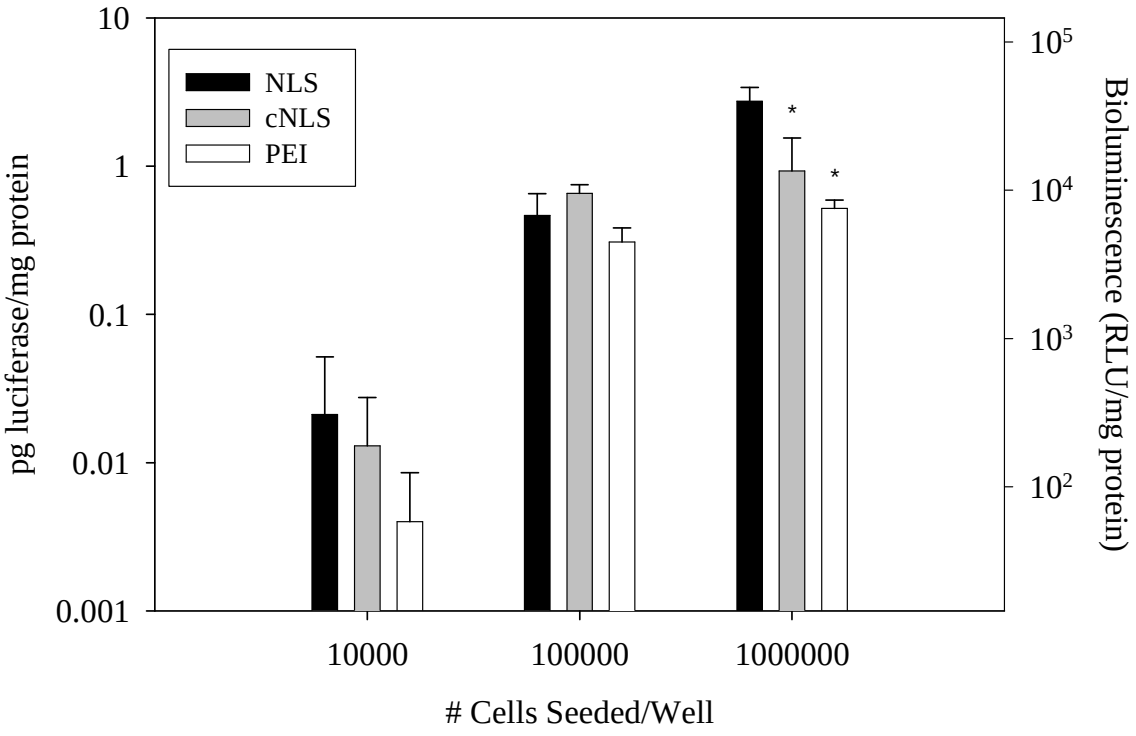

Figure 5-38. *Cell proliferation conditions effect NLS-mediated increase in luciferase expression.* NIH/3T3 cells were seeded at increasing concentrations (10,000 - 1,000,000 cells/well). Each well is transfected with 5 μg of pGL3 (+/+). Plasmid is labeled by 1 pmol PL-NLS per μg. * Represents statistically significant difference relative to PL-NLS ($p \leq 0.05$).

Figure 5-39 displays the results of an in vitro transfection that was carried out in growth-retardant condition (i.e., 0.2% FBS media). Cells were transfected with 5 μg of pGL3 (+/+) per well and transfected for 18 hrs. The results indicate that, under these

conditions, NLS-labeled pGL3 (+/+) (1 pmol/μg) had an increase in gene expression of 3-8-fold as compared to cNLS-labeled pGL3 and un-modified pGL3. The increased expression, in each case was determined to significant. All treatments of pGL3 (+/+) were delivered by PEI at a charge ratio = 9.

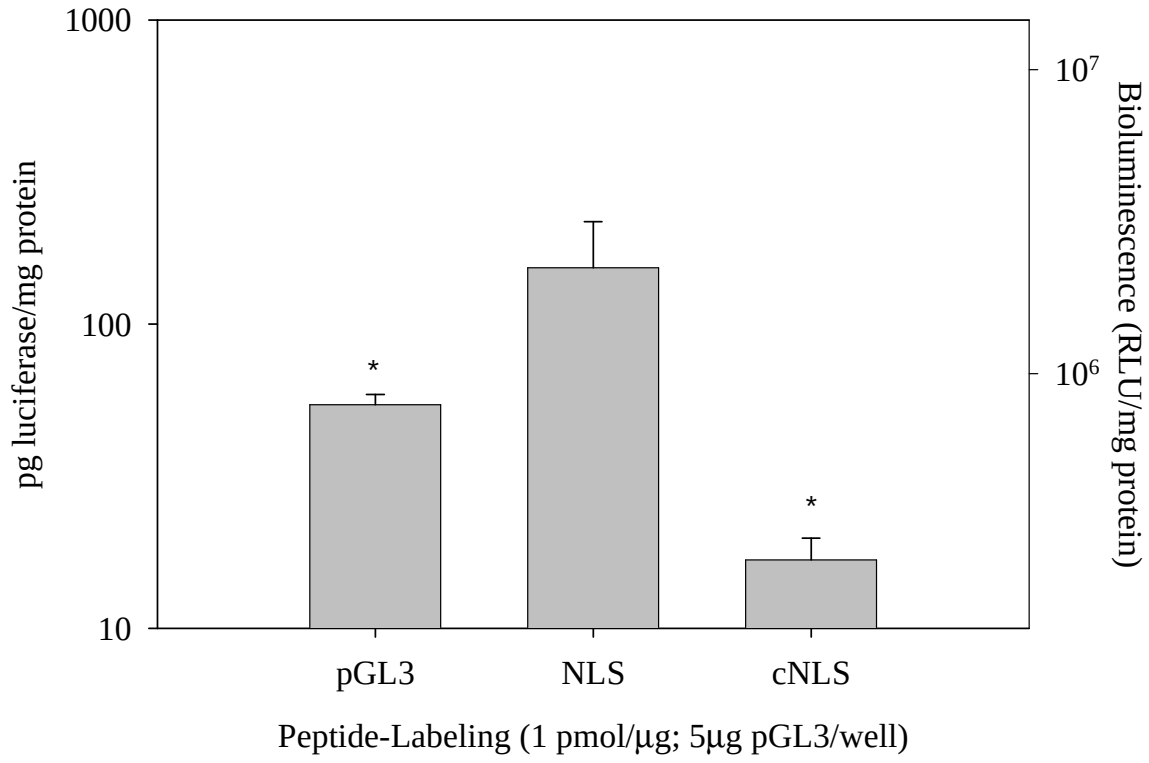

Figure 5-39. *In vitro transfection under serum-starved conditions*. NIH/3T3 cells were incubated for 48 hrs in 0.2% FBS media to induce a non-mitotic environment. Cells were transfected with 5 μg pGL3. Plasmid was labeled 1 pmol/μg with PL-NLS/cNLS or un-modified. * Represents statistically significant difference relative to PL-NLS ($p \leq 0.05$).

In Vivo NLS Effect as Detected by Bioluminescence Imaging

HD dosing was believed to be a reasonable dosing route to observe nuclear localization by way of increased expression levels. Mice were HD dosed with 1 ng of

pGL3 (+/+) and luciferase expression was monitored 24 hrs later by BLI. Mice that were

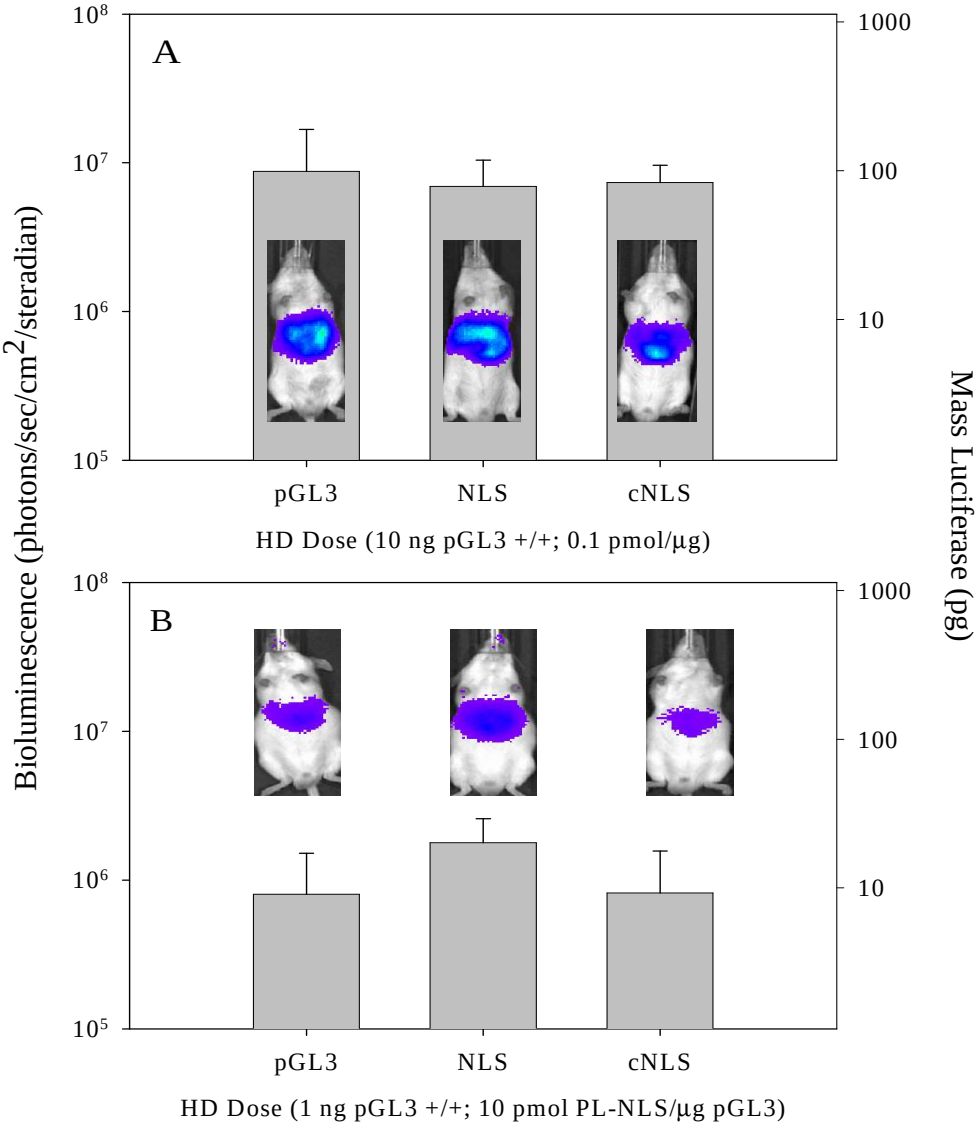

Figure 5-40. *Hydrodynamic dosing of pGL3 labeled by PL-NLS and PL-cNLS.* A) Mice were HD dosed with 10 ng of pGL3 (+/+) alone, pGL3 labeled by 0.1 pmol PL-NLS/µg, or pGL3 labeled by 0.1 pmol PL-cNLS/µg. B) Mice were dosed with 1 ng of pGL3 (+/+) or pGL3 labeled by 10 pmol PL-NLS/µg. All mice were imaged 24 hrs later by BLI to measure luciferase expression. Images were acquired 4 min after IP dose of D-luciferin (2.4 mg/mouse). Inset images are representative of each group (scale max = 10^6 photons normalized). Error bars represent standard deviation of the mean for n=4 (A) and n=3 (B).

dosed with pGL3 (+/+) labeled with 10 pmol of PL-NLS or PL-cNLS per μg showed no significant change in luciferase as compared to a control dose of unmodified pGL3 (+/+). This is an interesting result because we expect 10 pmol/μg photo-labeling to give 10-fold knockdown in expression based on in vitro data. The mean value of NLS-pGL3 expression is increased by >2-fold compared to each control, but the data lacks the precision to make it statistically significant (5-40 A). In an experiment with the same treatment groups, mice were dosed with 10 ng of pGL3 that was labeled with 0.1 pmol of peptide per μg of pGL3. There was no difference in expression levels for this particular experiment among the dosing (Figure 5-40 B). The measured photon flux from all groups gave a mean value of ~10^7.

IM dosing was concurrently explored for usage as a method to deliver NLS-labeled pGL3 in vivo. Mice were dosed with NLS-labeled pGL3 and compared to mice dosed with cNLS-labeled pGL3 and unmodified pGL3. Figure 5-41 A represents mice that were dosed with unmodified pGL3 (left leg of each mouse) as compared to pGL3 labeled with 10 pmol of PL-NLS/μg (right leg of each mouse). Figure 5-41 B is similar but compares NLS-pGL3 (right let) to plasmid labeled by PL-cNLS (left leg) (Figure 5-36). Clearly, the mean values for NLS-pGL3 expression are greater than the respective controls in both A and B. Internally, there are inconsistencies in this experiment with some mice not reporting expression. Also, the comparison of expression from NLS-pGL3 from 5-41 A to 5-41 B shows a 3-fold difference in expression (which is approximately the fold increase NLS-pGL3 shows over the control in each figure). The data from these 20 μg doses of pGL3 are not statistically significant.

Attempts to establish increased confidence in these data fell short in a repeated experiment. The data displayed in Figure 5-42 are less consistent than that represented in

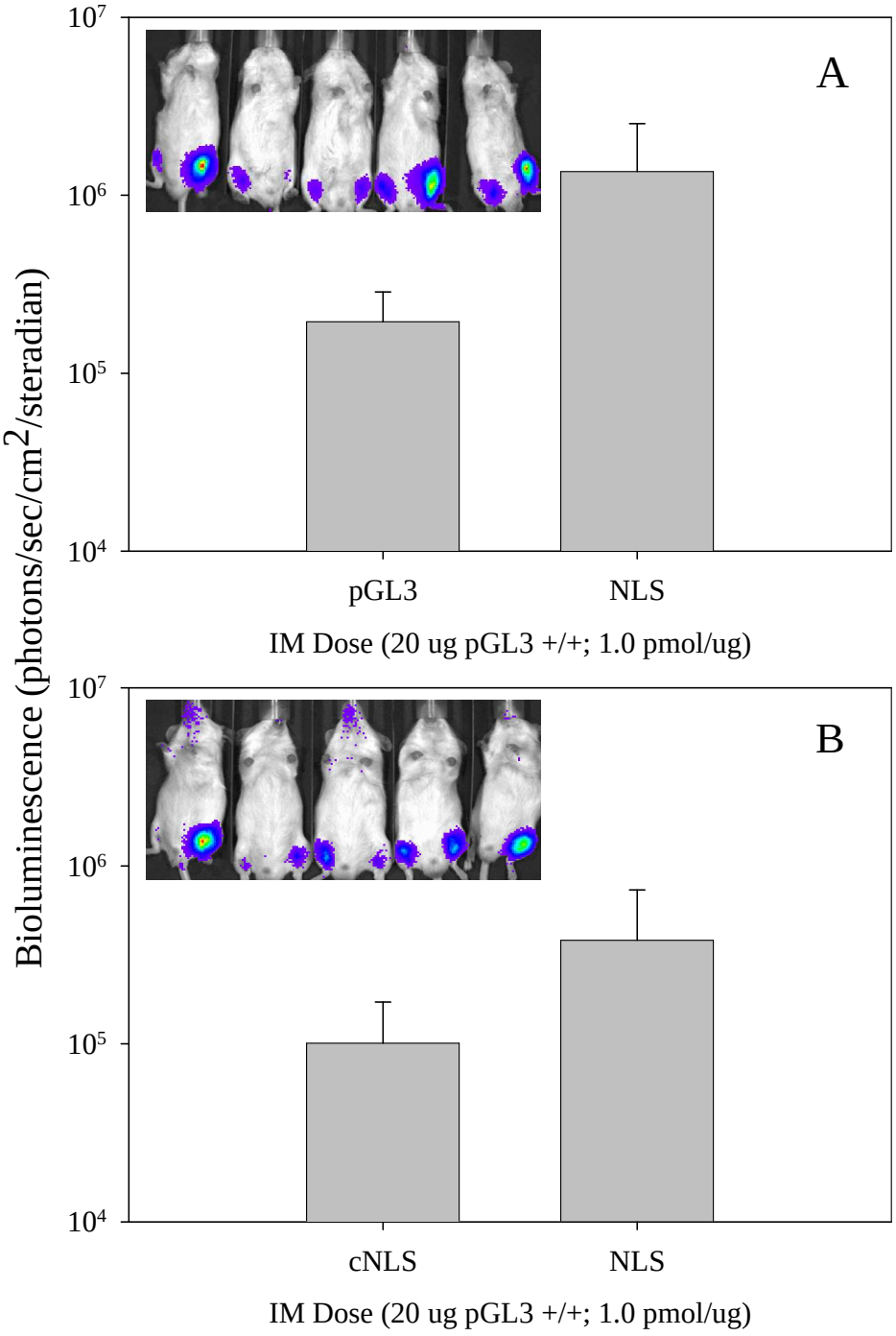

Figure 5-41. *Intramuscular dosing of pGL3 (+/+) labeled by PL-NLS and PL-cNLS.* 20 µg of pGL3 (in 50 µl PBS) was IM dosed to the left and right hamstring muscles of each mouse. In A, the left legs are dosed with unmodified pGL3 and the right is dosed with NLS-pGL3. Panel B compares cNLS-pGL3 (left leg) to NLS-pGL3 (right leg). All labeling is done at the 1 pmol/ µg stoichiometry and directional references are based on the viewer's

perspective. Inset images of the raw data were acquired 24 hours after dosing pGL3 and a subsequent IM dose of 1.2 mg D-luciferin (scale max = 10^5 photons normalized).

the previous figure. pGL3 (+/+) shows equivalent mean expression levels to NLS-pGL3 (+/+), and both are increased 4-fold over cNLS-pGL3 (+/+). Qualitative assessment (see figure inset) reveals that several dosing sites that are non-reporting and fall below the limit of detection for the instrument.

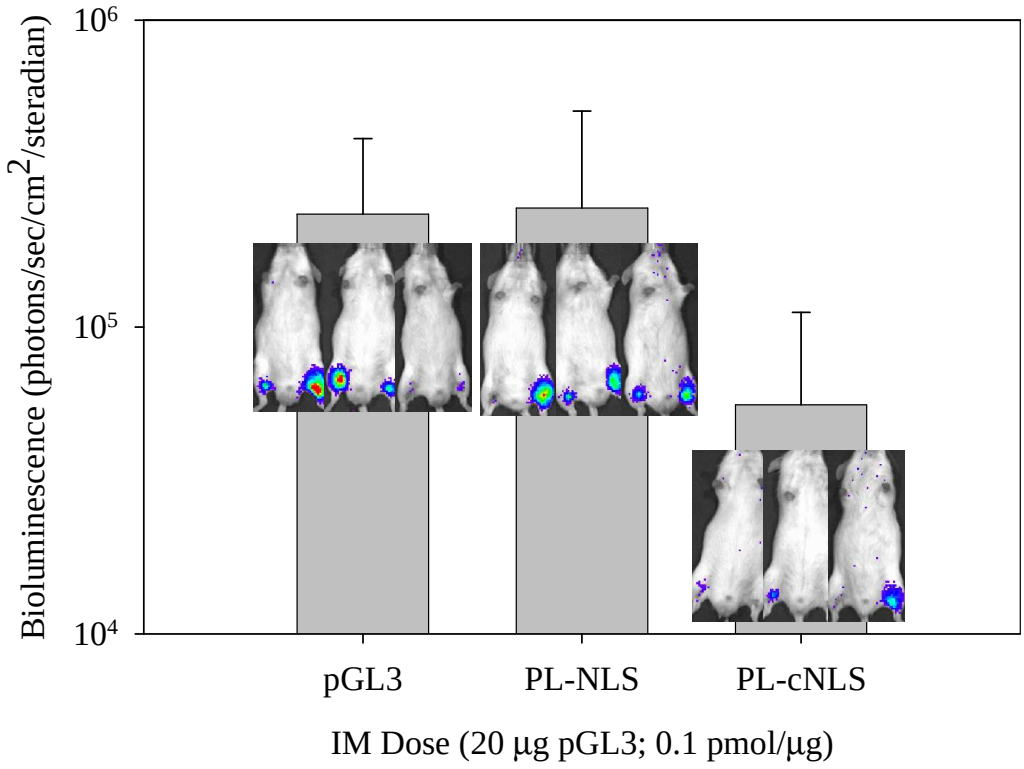

Figure 5-42. *Intramuscular dose of pGL3 (+/+) labeled by PL-NLS or PL-cNLS – 0.1 pmol/µg* . Mice were IM dosed with 20 µg of pGL3 unmodified, labeled with 0.1 pmol PL-NLS/µg , or labeled with 0.1 pmol PL-cNLS/µg . Inset images of the raw data were acquired 24 hours after dosing pGL3 and a subsequent IM dose of 1.2 mg D-luciferin (scale max = 10^5 photons normalized).

As discussed in Chapter 3, expression from an IM dose can show a dramatic increase in expression by introducing EP to skeletal muscle tissue at the site of dosing. Figure 5-43 indicates an overall increase in expression levels (though they are not in alignment with expected levels compared to Chapter 3 work because D-luciferin was administered IP), but did not produce a result that showed an NLS-specific increase compared to controls.

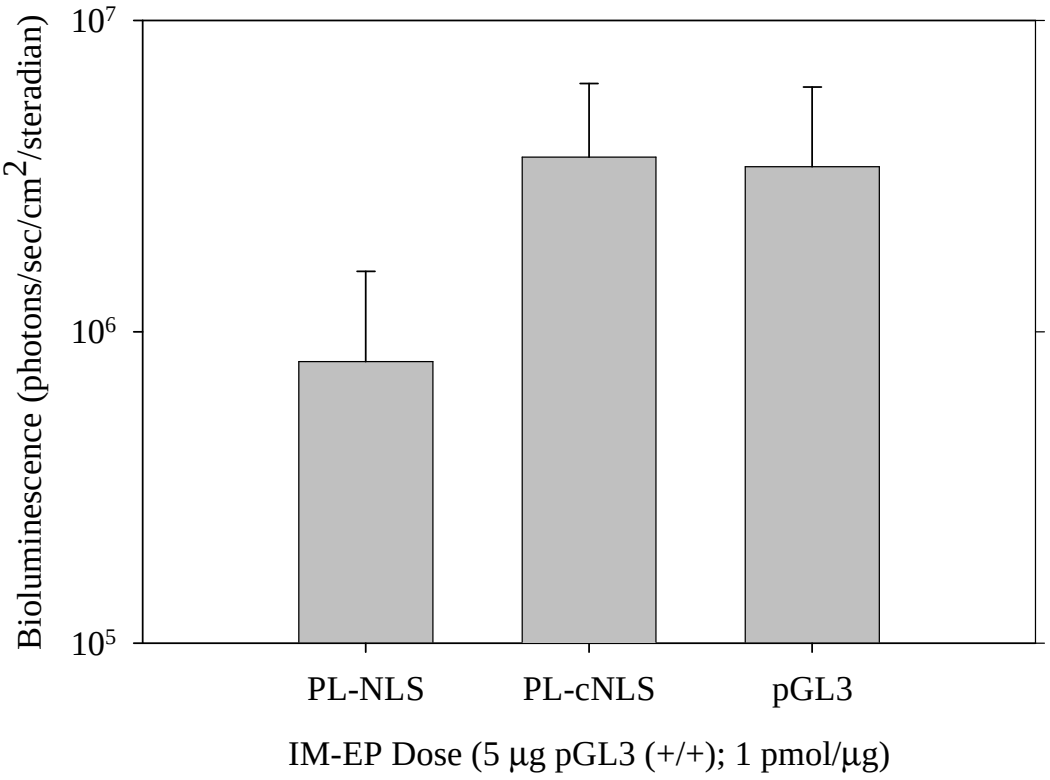

Figure 5-43. *Intramuscular Dose of pGL3 (+/+) followed by electroporation*. pGL3 (+/+) was labeled by PL-NLS or PL-cNLS at 1 pmol/μg. Labeled plasmid or unmodified plasmid was dosed IM to the hamstring muscle – 5 μg in 50 μl of normal saline (n=4). After 24 hrs, mice were dosed IP with 80 μl (30 mg/ml) of D-luciferin and imaged 12 min following substrate dose. Vertical bars and error bars represent the mean and standard deviation, respectively.

PL-NLS peptides with 6 amino acid linker regions were tested in the IM-EP assay to determine if an increase in the linker length would allow for increased expression. For each peptide (PL-6Gly-NLS, PL-6Lys-NLS and PL-6Pro-NLS) the stoichiometry of the labeling reaction was increased from 0.1-10 pmol of peptide/μg of pGL3 (+/+). The corollary experiment was carried out for the controls for pGL3 labeled by PL-6Pro-NLS (i.e., PL-6-Lys-cNLS, PL-1Pro-NLS peptides, as well (Figure 5-44 A and B). The end result gave no conclusive data as to notable increase in gene expression levels.

Experiments which were centered on an NLS-mediated increase in gene expression to demonstrate nuclear localization did not demonstrate any advances in providing statistically significant data from which to draw conclusions. This included explorations in HD dosing, IM dosing and incorporating EP. With this in mind competition experiments were planned in an attempt to take advantage of the receptor-mediated cytonuclear transport that is regulated by the NPC. In data not shown, mice were IM-EP dosed with NLS and cNLS labeled pGL3 (+/+) and unmodified pGL3 (+/+) in the presence of wheat-germ agglutinin (WGA). WGA is a lectin that is widely known to bind cytoplasmic nucleoporins of the NPC and occlude cytonuclear transport. With increasing concentration of WGA, the lectin knocked down expression of all treatments to an equal degree. Following that approach, we turned to using a large mol excess of free PL-NLS or PL-cNLS to act as a competing ligand at the NPC. A 1 μg dose of pGL3 (+/+) in the presence of 1000-fold mol excess of free peptide (PL-NLS or PL-cNLS) resulted in no-change in expression (Figure 5-45). However, we see knockdown when adding 10,000-fold mol excess, but both NLS and cNLS knockdown expression (by 11-fold and 3-fold relative to the pGL3-only control, respectively).

Studies conducted in the area of DNA-based nuclear targeting sequences indicated that the often-used pGL3 (+/+) plasmid may be problematic when searching for an NLS-related effect. As a result, pGL3 Promoter (+/-) plasmid was used, as it does not contain the SV40 enhancer element – known to have nuclear localizing properties.

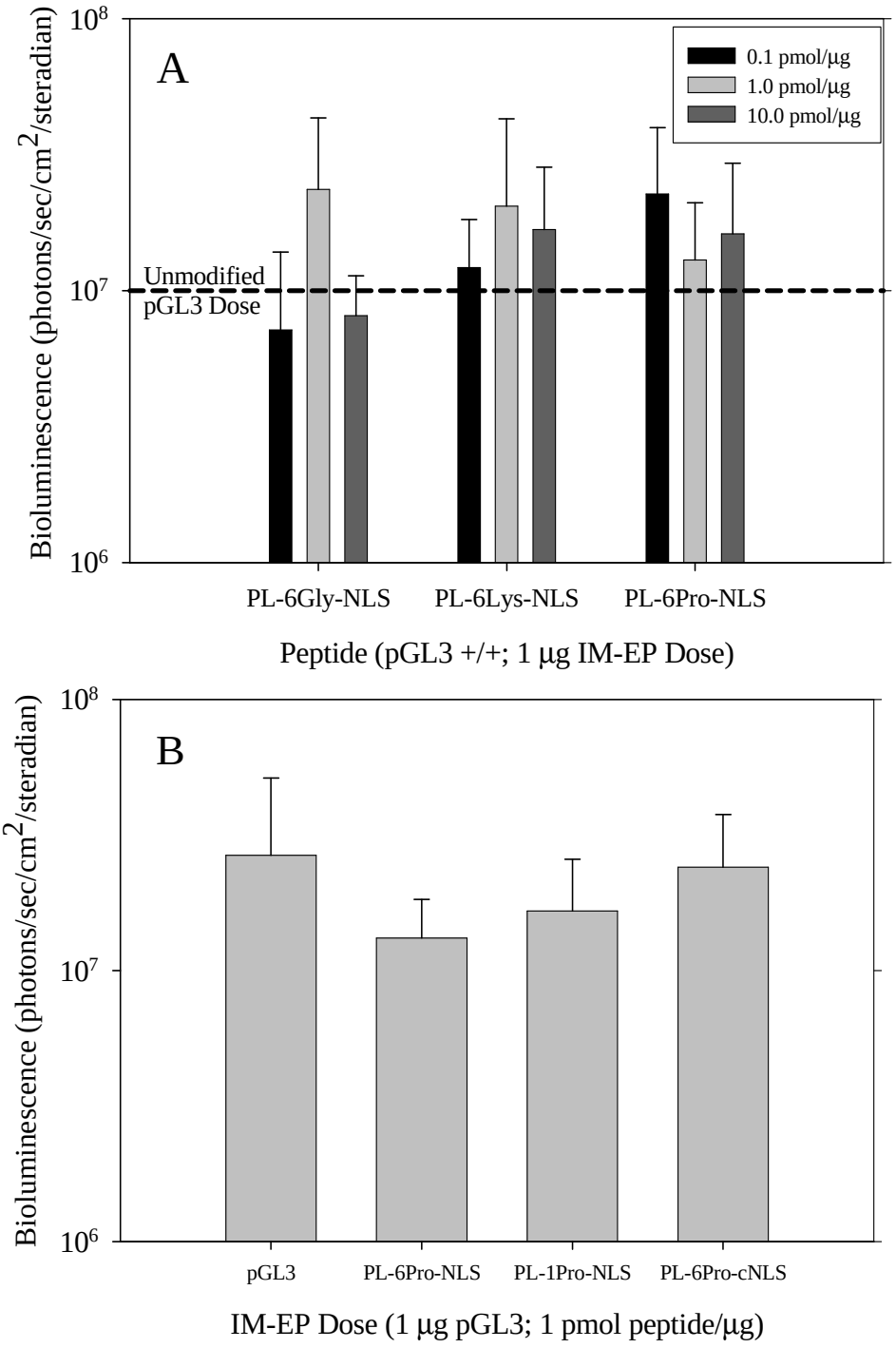

Figure 5-44. *IM-EP dose of pGL3 (+/+) labeled by 6 amino acid linker analogs*. A) Mice were IM-EP dosed with 1 μg pGL3 unmodified (bioluminescence represented by the dashed line), and pGL3 labeled with 0.1, 1.0 and 10 pmol of PL-6Gly-NLS, PL-6Lys-NLS or PL-6Pro-NLS – all on a per μg basis. Images were acquired 24 hrs following IM-EP dosing of pGL3 and a subsequent IM dose of 1.2 mg D-luciferin. Vertical bars represent the mean, and error bars

indicate the standard deviation (n=4). B) Mice were IM-EP dosed with 1 μg of unmodified pGL3, or pGL3 labeled with 1.0 pmol of PL-6Pro-NLS, PL-1Pro-NLS or PL-6Pro-cNLS – all on a per μg basis. Images were acquired 24 hrs following IM-EP dosing of pGL3 and a subsequent IM dose of 1.2 mg D-luciferin. Vertical bars represent the mean, and error bars indicate the standard deviation (n=4).

The expectation remained that NLS-labeling of pGL3 (+/-) would improve nuclear localization and increase gene expression. However, the specific focus was modified to target pGL3 that lacked the aforementioned SV40 enhancer element. We hypothesized that the increase in expression from pGL3 (+/-) labeled by NLS would be greater than the differences we have been observing between pGL3 (+/+) labeled by PL-NLS and the respective controls. Specific results from the David Dean group showed a 3 to 4-fold increase in expression from the SV40 enhancer-containing plasmid compared to a control plasmid when dosed by IM-EP methods in skeletal muscle[160]. Furthermore, they demonstrated a 10-fold increase after 1 day and a 40-fold increase 3 days after dosing in mesenteric vasculature by EP methods[46]. pGL3 (+/-) is not predicted to have an inherent ability to nuclear localize, so we set-out to label this plasmid with PL-NLS and exploit this characteristic.

This line of experiments involved labeling pGL3 (+/-) with PL-NLS and observing expression over an extended time course (Figure 5-45). On day 1, pGL3 (+/+) showed >10-fold increase in expression levels over all other dosing groups. Also on day 1, 2 pmol and 20 pmol labeling with PL-NLS showed 6-fold and 1.5 fold increases, respectively, over unmodified pGL3 (+/-). All pGL3 (+/-) treatments showed uniformed decrease in luciferase levels through day 27 at which point expression plateaued. pGL3 (+/+) expression levels dropped up much more quickly in the early stages and actually decreased below that of the labeled pGL3 (+/-) at 27 days. It is noteworthy, here, to recognize that we see observable expression by BLI for >140 days in all treatment groups

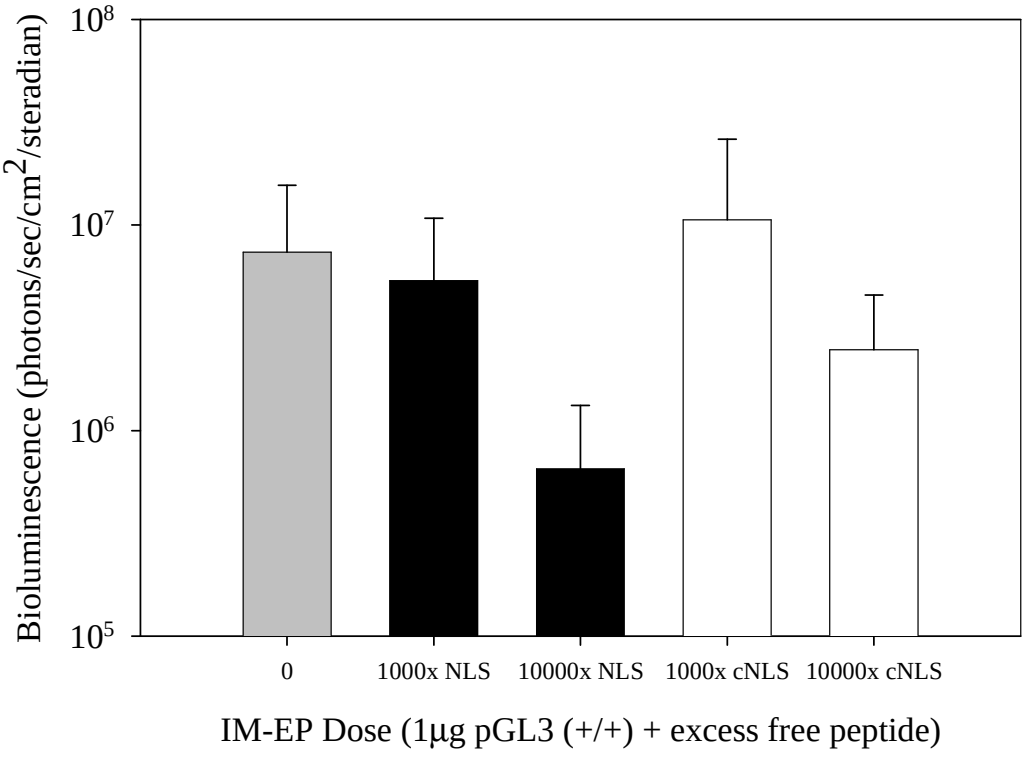

Figure 5-45. *Influence of free peptide on bioluminescence from an IM-EP dose of pGL3 (+/+).* Mice were IM-EP dosed with 1 µg pGL3 in 50 µl of normal saline. The dose contained no free peptide (gray bar), 1,000- or 10,000-fold mol excess of PL-NLS (black bars) or PL-cNLS (white bars). After 24 hrs and an IM dose of D-luciferin (1.2 mg in 40 µl PBS), and bioluminescence was quantified 10 min following substrate dose. Vertical bars represent the mean (n=4), and error bars for both data sets represent the standard deviation.

Experimental validation was pursued by recreating the study to include cNLS-modified pGL3, as well as increasing the power of the experiment by adjusting the sample size to n=6 in anticipation of finding statistically significant results. The data are quite similar to that observed in the previous experiment, with the crucial difference being that pGL3(+/-) is now shown to display increased expression levels over other treatments through the extended time course (Figure 5-46).

The ExtSV40 peptides were tested for activity by the standard IM-EP protocol. Expression levels were measured on day 1 and day 30 following bolus dose of pGL3 (+/-

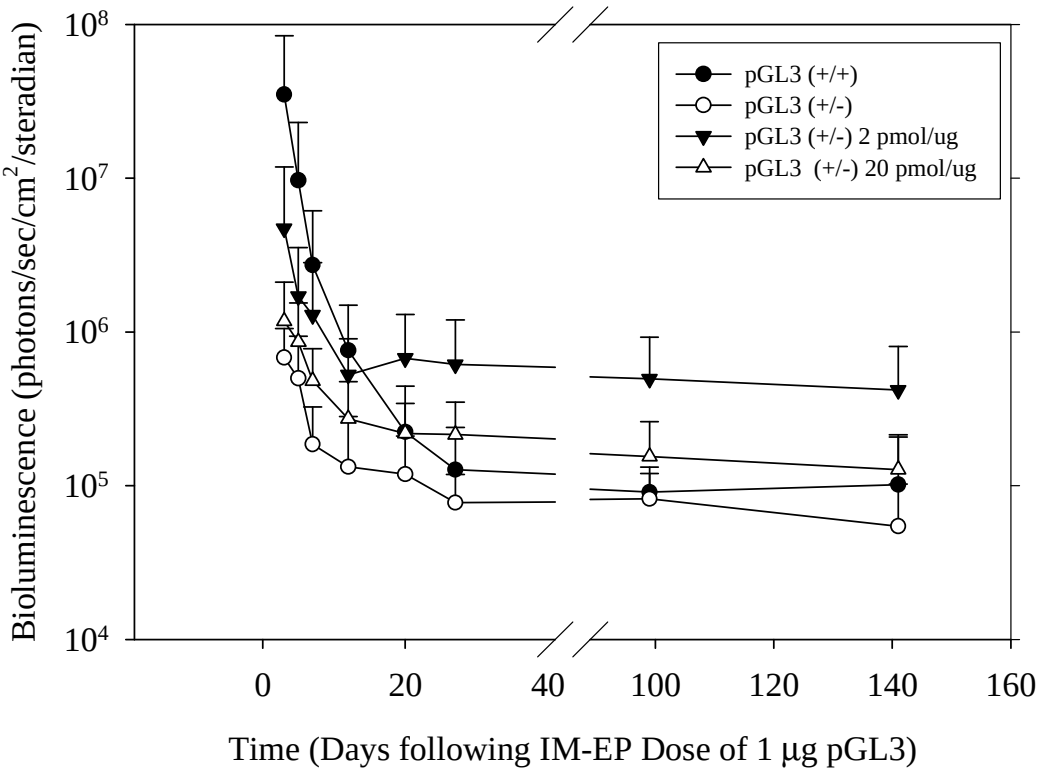

Figure 5-46. *Time course of luciferase expression – Incorporating DNA- and peptide-based NLS sequences.* Mice were IM-EP dosed with 1 μg of unmodified pGL3 (+/+) (solid circle) and (+/-) (open circle), or pGL3 (+/-) labeled with 2.0 (filled triangle) or 20 pmol (open triangle) of PL-NLS – on a per μg basis. Images were acquired periodically out to 141 days following plasmid dosing. On each day, BLI was carried out 10 min following IM dose of 1.2 mg D-luciferin. Vertical bars represent the mean, and error bars indicated the standard deviation (n=4).

). We did not observe any NLS-mediated increase in luciferase expression when plasmid was labeled by the PL-ExtSV40 sequence (Figure 5-47).

Discussion

Biological studies with PL-NLS/cNLS peptides were dependent on our ability to first synthesize PL and the PL-peptides. We confirmed the identity of PL and the fact that it was incorporated at the N-terminus of NLS-containing peptides by several methods. Characterization of the peptide by ESI-MS and comparison of the observed mass to the

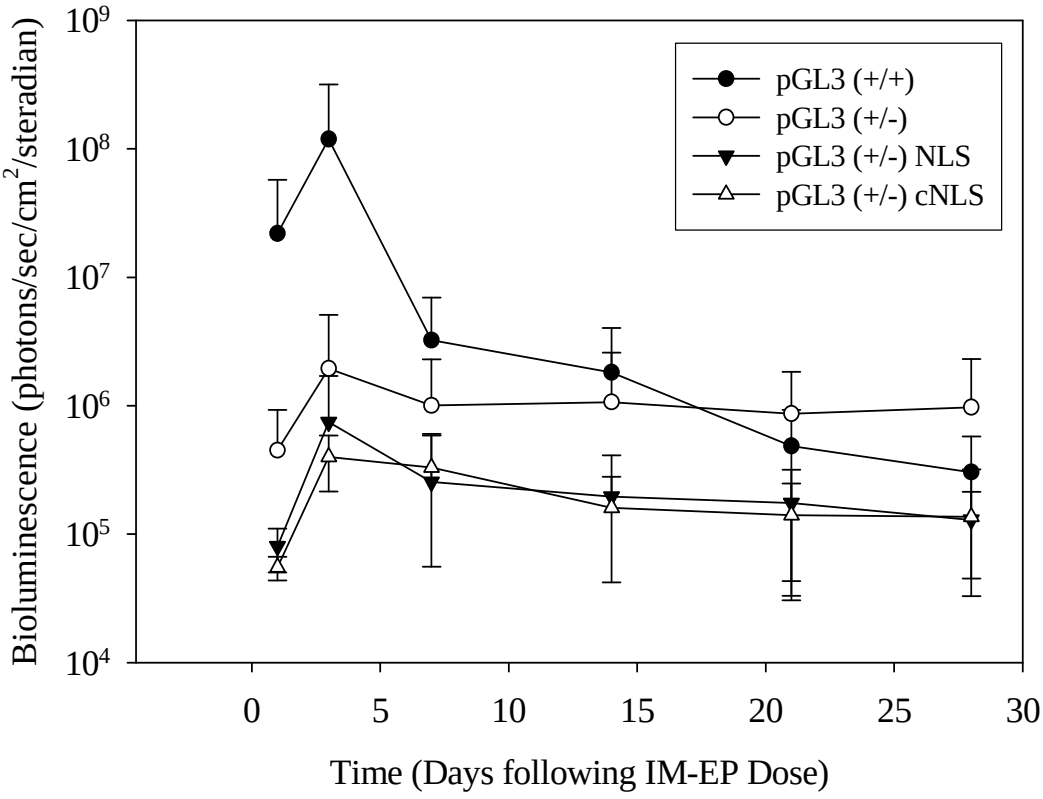

Figure 5-47. *Follow-up Time course of luciferase expression – Incorporating DNA- and peptide-based NLS sequences.* Mice were IM-EP dosed with 1 μg of unmodified pGL3 (+/+) (solid circle) and (+/-) (open circle), or pGL3 (+/-) labeled with 2.0 (filled triangle) or 2 pmol (open triangle) of PL-cNLS – on a per μg basis. Images were acquired periodically out to 27 days following plasmid dosing. On each day, BLI was carried out 10 min following IM dose of 1.2 mg D-luciferin. Vertical bars represent the mean, and error bars indicated the standard deviation (n=6).

calculated mass was the most significant confirmation of PL identity and its incorporation into the peptide (Table 5-1). In addition, there were no other chromophores in the classic NLS sequence or any of the variable linker amino acids that have been used. The observation that all PL-peptides had a maximum absorbance value at 258 nm confirms the presence of PL (and the observation of a single peak when assessing the crude peptide was an indication that PL is at the N-terminus). The photo-degradation characteristics were easily identifiable by successive photo-flashing and absorbance measurements.

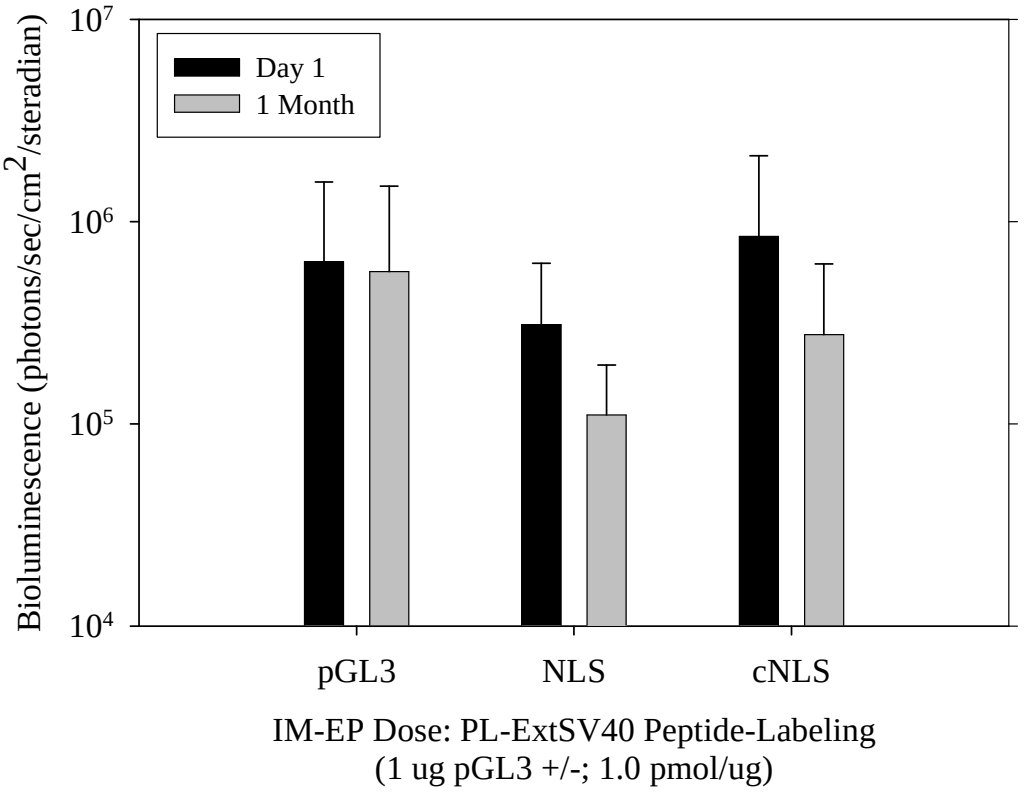

Figure 5-48. *IM-EP dose of pGL3 (+/-) labeled by ExtSV40 peptides.* Mice were IM-EP dosed with 1 μg of unmodified pGL3, or pGL3 labeled with 1.0 pmol of PL-ExtSV40-NLS or PL-ExtSV40-cNLS– all on a per μg basis. Images were acquired 24 hours following IM-EP dosing of pGL3 and again one month later. BLI was carried out 10 min following IM dose of 1.2 mg D-luciferin. Vertical bars represent the mean, and error bars indicated the standard deviation (n=4).

Further, photo-flashing PL-peptides in the presence of pGL3 induced an observable band-shift as the samples were covalently labeled. Previously, it has been shown that photo-labeled pDNA remains in the supercoiled form[161] – a significant finding since linear dsDNA is much more susceptible to nucleases.

Studies in the formulation of peptide-DNA conjugates allowed for an understanding of the protocol for photo-flashing samples for covalent labeling. Defining the molar absorptivity for PL (ε=14,951 $M^{-1}cm^{-1}$) allowed us to confirm the concentration

of peptide and precisely control the initial stoichiometry of the photo-labeling reaction. The photo-degradation experiment demonstrated that 40 photo-flashes were required to fully "photo-activate" PL-peptide. This type of photo-label decomposition has been previously used to determine the requisite levels of irradiation[162]. Biological studies in vitro (both confocal and luciferase expression experiments) required NLS-pGL3 to be delivered as a condensate. The information derived from the particle-sizing experiment was valuable as it gave us confidence that observable variability between treatments was not related to any differences in particle size.

The experiments with the iodinated PL-NLS-Y allowed us to make confident, quantitative measurements as to the extent of photo-labeling. The identity of PL-NLS-Y-^{125}I was confirmed by Sephadex G-10 elution and thin-layer chromatography coupled with phosphorimage analysis. The C_{18} cartridges used in solid-phase separation were important to the process of optimally purifying PL-NLS-Y-^{125}I from free radioactive iodide. The log-linear plot of photo-labeling efficiency is valuable in predicting the mol relationship regarding peptides labeled onto a given plasmid. As discussed previously, there are contrasting viewpoints represented in the literature by notable figures in the field regarding the number of peptides that would ideally be labeled onto a plasmid to maximize nuclear uptake[101,108]. Though we utilize a random labeling method, the table below (Table 5-3) shows the utility with which we can calculate an expected mol:mol labeling ratio. Notably, we see that it is an initial photo-labeling stoichiometry of ~2 pmol of peptide per μg of pGL3 that is predicated to yield a 1:1 ratio of peptide labeled onto pGL3 (+/+).

The experiment investigating the stability of the covalent bond between peptide and pGL3 demonstrated that the bond can be regarded as stable at near-physiological conditions. The experiment is significant in light of the positive control which triggers dissociation between the peptide and pGL3 via base-catalyzed depurination. The pH 11.5 conditions show loss of the peptide-pGL3 covalent relationship via a decrease in

radioactivity following successive ethanol-precipitations and incubation over a time course of 48 hrs.

Table 5-3. Mol ratio of photo-labeling (peptide:plasmid)

	10 pmol/µg reaction	1 pmol/µg reaction	1.95 pmol/µg reaction
plasmid size (kbp)	5.3	5.3	5.3
total bases	10,600	10,600	10,600
plasmid mol wt (µg/pmol)	3.45	3.45	3.45
plasmid wt/rxn (µg)	14	14	14
plasmid/rxn (pmol)	4.06	4.06	4.06
peptide/rxn (pmol)	140	14	27.3
initial reaction stoichiometry (pmol/µg)	10	1	1.95
%bound = 0.21 x ln(initial pmol/µg) + 0.136	18%	14%	15%
peptide amount bound (pmol)	25.81	1.90	4.10
mol ratio (peptide:plasmid)	6.35	0.47	1.01

The confocal microscopy experiments specifically addressed the goal of incorporating PL-NLS into a non-viral gene delivery vector. That is, we predicted that an NLS would improve the nuclear localizing ability of a labeled plasmid; however, the more general goal of achieving an increase in gene transfer efficiency was based on an assumption that there is a direct and measurable correlation between nuclear uptake efficiency and the efficiency of transgene expression. In the experiments of Z-series acquisition, we saw qualitative evidence of uptake via NLS-labeled Cy3-pDNA. Quantitatively, we have utilized a method by which to measure this effect. It was shown to be present when 10 pmol of PL-NLS/µg of Cy3 pGL3 was used in transfecting pGL3 (+/+ and pGL3 (-/-) in independent experiments. The correlative experiment for expression verified that we may be making the aforementioned assumption in error as there is no increase in gene expression by the formulation that was shown to more efficiently target the nucleus.

In vitro and in vivo experiments were focused on producing an NLS-specific effect in the form of an increase in transgene expression. As seen in the figures above, there was some success in achieving that goal, but these expression experiments were met with challenges. Perhaps the experiment most indicative of these challenges was the in vitro comparison of expression from pGL3 (+/+) labeled with increasing amounts of PL-NLS. Even at 10 pmol/μg, we observed a significant decrease in transgene expression. This labeling ratio produced the greatest amount of nuclear uptake, but happens to be one which knocks down expression. This makes the successful execution of these experiments precarious. Another conclusion that can be made from the in vitro data is that there is a time course and cell growth-rate dependent factor – both of which could be encompassed in the hypothesis that cells are required to be non-dividing in order to observe an NLS-related increase in gene expression. Otherwise, polyplexes are randomly and efficiently targeted to the nuclei restructuting in cells that are undergoing mitosis[158].

Based on our extensive work with in vivo dosing methods – HD delivery to the liver and IM-EP dosing of skeletal muscle – we chose to focus on observing an NLS-mediated increase in gene expression in vivo. This remains to be an effect that has yet to be reliably demonstrated in vivo by a non-viral delivery system. In addition, we recognized in vitro to in vivo disconnect in experimental results:

The perceived necessity of non-dividing or post-mitotic cells lead us to pursue IM dosing as the most promising in vivo route of delivery. Our early experiments with HD dosing did not yield any notable results, the mechanism of HD delivery is unknown at the intracellular level, and there is speculation within the literature that HD dosing induces mitosis in hepatocytes. On the other hand, there is literature precedent for IM dosing coupled with EP in observing an NLS-effect in vivo. Also, skeletal muscle cells are post-mitotic and multinucleate – properties that could potentially increase an NLS effect.

Results from work described in Chapter 3 indicated that we could consistently achieve measurable luciferase expression following a 1μg dose of pGL3 by IM-EP

protocol. This was valuable information that was applied to searching for an increase in expression based on variable stoichiometry of labeling with NLS-containing peptides that contained 6 amino acids in the linker region. We felt that ligand presentation (i.e., NLS relationship to pGL3) was an important factor in enabling binding by Importin-α. For this reason, the NLS peptides that contained the longer linker region were thought to be promising due to their ability project the binging sequence from the plasmid and reduce inhibitory steric effects. Although, the results indicated some increase in expression over a pGL3 un-modified control, the follow-up experiment introduced additional controls that showed NLS to have no effect.

Success in gain-of-expression experiments was elusive, so we turned to in vivo experiments that were hypothesized to predict nuclear localizing function based on competition at the NPC. The IM-EP experiment involved pGL3 (+/+) which is known to have inherent nuclear localizing character. We expected that an excess of PL-NLS would preferentially occupy endogenous machinery at some level of nuclear translocation and out-compete the plasmid, which is targeted to the NPC by the same mechanism. Likewise, excess PL-cNLS was co-delivered with pGL3 (+/+) and not expected to knockdown expression to the same degree. The difference in the degree of knockdown was not significant, but may hold promise as a method to assay for potent NLS analogs.

In the final attempts to demonstrate an in vivo NLS effect, we turned to using a plasmid, pGL3 (+/-), which lacked the SV40 enhancer element and presumably, the ability to inherently target the nucleus. As in previous biological experiments, the initial study turned out to be positive, but further experimentation with increased levels of control treatments were not able to produce the convincing data we desired.

The methods and results for in vivo experiments represent a sampling of approaches that were followed in pursuit of our aim of demonstrating an NLS-dependent increase in gene expression in vivo. The following experiments, described briefly, offer further detail of our thoughts throughout this process. In line with the experiment

incorporating excess free peptide, we also attempted to out compete pGL3 (+/+) and NLS-labeled pGL3 with wheat germ agglutinin (WGA). WGA is a lectin known to bind with strong affinity to the NPC, so we hypothesized that co-delivery of WGA and nuclear targeted plasmid would result in decreased expression of those plasmids versus control-treatments. We pursued the hypothesis that heightened NLS labeling (>100 per plasmid) would lead to increased nuclear uptake. It was obvious that this excess labeling would lead to greatly diminished expression levels, so we used restriction endonucleases to remove a non-coding segment of the plasmid, heavily labeled it with PL-NLS or PL-cNLS, and attempted to ligate the fragment back into the plasmid. However, expression remained greatly diminished and to the same extent for each peptide. Also, ligation was challenging due to ligase not recognizing the altered substrate. As a final example, we incorporated a widely used approach for normalizing luciferase expression. We attempted to reduce dose-to-dose variability by co-delivering plasmids encoding both *Photinus pyralis* and *Renilla* luciferase. By this method, we would normalize firefly luciferase expression for each dose to sea sponge luciferase expression to increase precision of measurement. Unfortunately, the substrate for *Renilla*, ceoleterazene, has a great amount of autoluminescence, and though the substrates are not cross-reactive between species, an equal dose of ceoleterazene gives identical bioluminescence in the presence or in the absence of *Renilla* luciferase.

CHAPTER 6

STRATEGIES IN NUCLEAR LOCALIZATION: A REVIEW OF THE RESULTS AND EXPANDED DISCUSSION

HD Dosing as a Potential Route to Observe an NLS Effect In Vivo

Our plan to develop peptides for nuclear localization began with defining in vivo assays which would give us robust methods to measure transgene expression in vivo. The first of these involved the hydrodynamic dosing route – a method which is widely recognized as very efficient at achieving liver-selective transgene expression. In these studies, we systematically varied dosing and imaging parameters to optimize the BLI readout. BLI is rapidly becoming the most widely used form of in vivo analysis of gene transfer efficiency. HD dosing is the most efficient form of non-viral gene delivery to the liver, and we used it in conjunction with BLI to define the benchmark for attainable in vivo expression from a non-viral system. We were not the first to use either method, but we can make a conclusion about this idealized system. HD dosing produces significant expression levels from pDNA which could possibly be attained if a non-viral vector, dosed systemically, was strategically designed and synthesized to circumvent barriers associated with primary, secondary and tertiary targeting. This amount of gene product produced has been shown to be therapeutically relevant in mouse models of some disease states. A dose-response effect of this magnitude should be recognized as "setting the bar" for expression that could be attained by non-viral delivery methods.

In addition to highlighting the expression potential from DNA, HD dosing was considered a reasonable delivery route for demonstrating an NLS-mediated increase in gene expression based on rationalizations and findings in the literature. First, the rapid, high volume dose meant that the duration of plasmid in the systemic circulation would be short. Thus, the exposure to damaging DNases and other systemic factors that could

inhibit circulation of a polyanionic macromolecule were minimized. Evidence of this is the high levels of expression that were observed following HD dosing – clearly, DNase digestion was minimized if expression of that magnitude was achieved from a relatively small dose of pGL3. Second, work from the laboratory of John Wolff indicated that there was an observable size-exclusion cut-off of DNA that reached the nucleus when HD dosing DNA of varying lengths[163]. The observed relationship between DNA size and nuclear uptake suggested that cytonuclear transport was still controlled by the NPC in this dosing route. Wolff suspected that the nuclear envelope was still in place as a barrier for intracellular trafficking since nuclear uptake decreased when DNA was larger than 200 bp. Given that other literature references suggested that we could optimally load hepatocytes by HD dosing, and assuming that tertiary targeting remained the only significant barrier to intracellular trafficking, we concluded that pGL3 labeled with an NLS would then be preferentially trafficked to the nucleus, and an NLS-related increase in transgene expression would be observed.

IM-EP Dosing as a Potential Route to Observe an NLS Effect In Vivo

We also investigated intramuscular dosing in association with electroporation as an additional route by which to observe an NLS-related effect in vivo. The literature in this area allows us to more confidently conclude that IM-EP dosing is a reasonable route to observe nuclear localization. The work of David Dean played a significant role in shaping this idea. Work in his lab produced results which demonstrated that nuclear-targeting transcription factors had high affinity for specific DNA sequences. They demonstrated that DNA containing these known sequences was selectively targeted to the nucleus based on nucleotides alone. Quite significant was the contribution that showed in vivo evidence that DNA containing this nuclear localizing sequence was selectively taken-up by nuclei in these cells and displayed increased expression in a NLS-specific

manner. It is significant to note that the intracellular machinery harnessed by the Dean approach (i.e., DNA-based NLS) has been shown to be the same (importin-α, importin-β via the NPC) as that which we expect to take advantage of with our peptide-mediated method. In short, there is a literature precedent for IM-EP being used to show the type of NLS effect that we were attempting to capture.

Another factor that made us confident in the IM-EP route was that more was known about the specific intracellular mechanism by which EP allows for enhanced transgene expression. The membrane permeabilization is created as an effect of the membrane potential across the cell membrane. In the presence of an electric field, instability and morphological changes are induced and the membrane becomes permeable. However, a similar membrane potential does not exist across the nuclear membrane. As a result, introduction of an electric field would not be expected to trigger that same type of DNA electrophoresis from the cytoplasm to the nucleus. This was reiterated by Dr. Richard Heller at the 10th annual meeting of the American Society of Gene Therapy, Seattle, Washington. Heller is one of the leaders in clinically applying this type physical delivery of naked DNA. Heller expected that this type of approach would prove advantageous for observing an NLS effect.

HD Delivery and RNAi: an Aside from Nuclear Targeting

The experiments and results from Chapter 4 deviate from the overall focus of nuclear targeting effects. In fact, a component of this strategy for knockdown is attractive because it contains *no* nuclear targeting requirements. That is, siRNA is functional in the cytoplasm where it couples with RISC and mediates strand cleavage of its corresponding mRNA. Nonetheless, RNAi is quite significant in light of the breadth it contributes to the field of gene therapy. Since the time of its discovery, RNAi has been rapidly advanced toward becoming a therapeutic platform. This pathway can be induced to knockdown

aberrant protein over expression. The ability to test these dsRNAs in vivo is a significant contribution as an in vivo assay for quantifying knockdown of expression by RNAi.

Testing Nuclear-Targeted Non-Viral Gene Delivery Vectors In Vivo

Nuclear targeting of non-viral vectors is a key to improving transfection efficiency of these systems. We have discussed this point extensively and have also discussed the reasoning for incorporating the peptides covalently by the random photo-labeling method. In experiments closely related to ours, Scherman and co-workers had previously reported a similar method of covalently labeling DNA and, like us, showed results that indicated functional assays of gene expression were largely unsuccessful. We felt that a major complicating factor with their approach was the incorporation of a sterically bulky fluorophore in the linker region (between 4-azido, 2,3,5,6-tetrafluorobenzoate and the N-terminus of the NLS). The strong fluorescence emission allowed them to quantify covalent adduction of DNA, but also may have diminished NLS ligand recognition by Importin-α due to the presence of the large fluorophore. Based on the modification we made in removing the fluorophore, this labeling method allowed us the most conceivably facile methods to synthesize and test several different PL-NLS analogs in vivo.[106]

In translating our findings of optimal nuclear uptake in confocal experiments to in vitro experiments for gene expression, we observed loose and inconsistent evidence that NLS could mediate an increase in transgene expression in NIH/3T3 cells. Our experience and observations of in vitro assays indicated that this may not be a reliable method by which to show expression levels that would translate to a reasonable conclusion on an NLS effect. This notion of an in vitro to in vivo disconnect is well established in the field and was recently highlighted in a review article on polymeric non-viral vectors written by

Earnst Wagner. Wagner states, “Regrettably, in vitro cell culture has only very limited predictive value for in vivo gene transfer.”[164]

The in vitro transfection efficiency of mammalian cells is still widely used as an initial predictor of in vivo gene transfer efficiency for experimental non-viral vectors. Peptides, dendrimers, lipids, and other polymers have been engineered to be efficient in vitro gene transfer agents. Non-viral vectors are preferred for routine in vitro gene delivery because, compared to viral vectors, they are inexpensive, easy to use, safe to handle, and produce acceptable levels of transient gene expression in a variety of cell lines.

The protocol for in vitro transfection involves formation of pDNA polyplexes or lipoplexes, to yield cationic colloidal particles with sizes typically ranging from 50-250 nm in diameter. When added to cultured mammalian cells, these particles sediment to form intimate contact with the cell surface. The primary mechanism by which cationic DNA nanoparticles are internalized is pinocytosis. The net positive surface charge on particles initiates this action once in contact with the net negative charge of proteoglycans or glycoproteins on the cell surface[165]. The proliferative state of cells greatly influences the transfection efficiency through control over the uptake pathway[166,167]. The gene transfer efficiency is known to be significantly augmented by active cell proliferation due to a depleted nuclear membrane resulting from nuclear restructuring.

Investigations into the active nuclear targeting of DNA have also been primarily conducted in vitro with the hope that this concept will boost in vivo gene delivery[108]. However, the rapid cell division of almost all cell lines used, relative to the quiescence of most cells in vivo, confounds most attempts to study transport of DNA through the nuclear pore complex in a controlled in vitro environment. The DNA gains access to the nucleus in mitotic cells during the cell division when the nuclear membrane is leaky or poorly formed due to restructuring events in M-phase.

Many investigators have assumed that optimized transfection in vitro will correlate with the same in vivo; whereas, more than a decade of experience has taught the field that this is rarely true of a non-viral gene delivery system. The reason for this lack of in vitro-in vivo correlation is obviously related to barriers that exist in vivo that can not be simulated in a tissue-culture environment.

It is important to note that in vitro transfection experiments are valuable and necessary to draw initial conclusions regarding how carrier modifications improve gene transfer efficiency. There are many examples in which in vitro transfections have been used to demonstrate the specificity of ligands in an attempt to improve selectivity relative to non-specific transfection[168,169]. Likewise, investigations into endosomal escape have yielded much valuable information regarding the mechanisms by which proton-sponging or fusogenic activity can be functional in achieving secondary targeting. However, PEI, fusogenic peptide, and cationic lipids dramatically influence the properties of DNA polyplexes and lipoplexes. The physical properties affect their interaction with blood components and alter biodistribution. PEI and cationic lipids are also poorly metabolized and cause inflammation, all of which contribute to a lack of in vitro-in vivo correlation for these relatively simple gene transfer agents. Finally, it is seldom recognized that free PEI is largely responsible for the endosomal buffering effect in cell culture and that this concentration of free PEI is unattainable in a target cell via systemically delivered non-vectors.

In light of the noted lack of in vitro/in vivo correlation, and considering that we optimized two in vivo delivery routes with BLI detection of luciferase expression, we placed an emphasis on in vivo work rather than in vitro experiments. This focus was influenced by our experience level, understanding of diminished in vitro/in vivo correlation and the fact that demonstrating an NLS-mediated effect in vivo would be quite novel for peptide-mediated transfection. Unfortunately, reliable evidence of an NLS-related increase of in vivo expression was elusive. We could not confidently

conclude that NLS-modification had any effect on transfection efficiency. In vivo assays are inherently less precise though we optimized methods and standardized protocols for dosing and imaging mice. Several factors may have been in play to decrease the reliability of our results.

When the data do not support the hypothesis, and there is no clear reason as to why, several possible reasons can be entertained. First and foremost (because it is based on our experimental observations), we observed less than a 5-fold increase in nuclear uptake in vitro from confocal experiments. Considering the above discussion and the value of in vitro experiments, it should perhaps not be surprising that an in vivo experiment designed to give a more disconnected result (i.e., gene expression rather than just nuclear uptake) did not produce reliable results. Also following from our own experiments, we observed that a labeling ratio of 10 pmol/μg (corresponding to ~10 peptides covalently labeled onto each plasmid) was optimal for mediating nuclear uptake. We also observe that this level of labeling knocked down gene expression by greater than an order of magnitude. The modification that enhances uptake also hampers our cause by contributing to a decrease in expression. The expression knockdown data can be reliably observed in vitro and in vivo, and was confirmed in the literature by a similar strategy for introducing an NLS. This factor has been identified as the most probable reason for not achieving the in vivo aim. The discussion continues with additional factors that could have played a role in confounding the results.

Second, luciferase has been shown to be immunogenic, so in ICR mice it is possible that there is an expression maxima that is set by the immune response[170]. Third, data collected via both IM and IP dosing routes of D-luciferin display no relative difference in expression levels between doses. The absolute levels changed based on the route of substrate administration, but relative expression remained consistent (data not shown). As a result, we can conclude that the variation must be introduced at the moment of pGL3 dosing. We have strived to improve and *have* improved on consistency in this

regard, but the inherent lack of precision may contribute to the absence of statistically significant results.

Going a step further, perhaps neither of the idealized in vivo delivery systems allows for the observation of a detectable NLS effect from non-viral vectors. As discussed previously, there is literature precedent or at least relevant data in the literature that has lead us to believe that either IM-EP dosing or HD dosing would be a reasonable method by which to test these non-viral vectors. However, it has also been discussed and noted that there remains a 'black box' surrounding some of the steps involved in intracellular trafficking and nuclear targeting for each delivery method. Parameters within these "black boxes" may be hampering our ability to see the desired effect.

Regardless of the results, we have implemented what we determined to be the requisite of controls in reasonable experiments throughout this project. Properly controlled experiments proved valuable in avoiding misleading conclusions of a positive NLS effect, and lead us to explore several distinct strategies to demonstrate an NLS-mediated increase in gene expression from our non-viral vectosr.

Conclusions

After reviewing experiments, results and drawing conclusions, it is clear that introducing an NLS via covalent adduction of pGL3 by photo-chemical methods did not produce a non-viral vector that was superior in terms of its ability to mediate transgene expression in vivo. However, there are a multitude of endogenous examples in every cell where this pathway works to target proteins to the nucleus. It seems reasonable that a peptide-labeled plasmid could utilize the signaling pathways and to traffic a non-viral vector with an NLS to the nucleus (once appropriately recognized by endogenous shuttling proteins) in the same way as a nuclear localizing protein.

In our estimation, the required experiments are in play for nuclear localizing of a non-viral vector to be sufficiently tested. That is, we have worked through the proper

experiments of increasing complexity, included the proper controls, but have not observed reliable, consistent, or statistically significant data. One experiment at the most basic level that we did not pursue was demonstrating binding affinity of Importin-α to the NLS. This type of experiment was not given a high-priority early in the planning stages because it had been widely demonstrated in the literature that all peptides containing the classic SV40 sequence reliably showed strong affinity for Importin-α.

Regarding the literature in this area, there is a long trail of very limited success. It is relevant to note that there has not been a recent surge in publications related to this aspect of the gene therapy field. A heightened focus on siRNA (functional in the cytosol) and its potential as a therapeutic platform may be responsible for the departure. In addition, there is a focus on the finding more developed and functional, physical methods to deliver DNA. These physical methods of delivery are often more clinically acceptable, and a clinical trial with a molecular conjugate that is dosed systemically requires significantly development to reach the same level of efficiency. Also, approaches like electroporation or a modified HD dose remove all concerns of venous injection/delivery of the biomolecule, and it is delivered directly to the site of action. Physical methods may be less-tolerated *pharmaceutically*, but they allow for proof-of-principle experiments that continue to advance the therapeutic relevance of a non-viral approach to gene delivery. For all of the ability to understand the aberrant protein expression responsible for a disease state, identify the associated DNA/mRNA sequences, and define the required nucleotides to increase or decrease gene expression, the ability to successfully *deliver* functional nucleotides remains the most significant challenge associated with gene therapy.

REFERENCES

1 Mancheno-Corvo P, Martin-Duque P (2006). Viral gene therapy. *Clinical & Translational Oncology*; **8** (12): 858-867.

2 Fire A *et al.* (1998). Potent and specific genetic interference by double-stranded RNA in Caenorhabditis elegans. *Nature*; **391** (6669): 806-11.

3 Konopka K *et al.* (2005). Serum-resistant gene transfer to oral cancer cells by Metafectene and GeneJammer: application to HSV-tk/ganciclovir-mediated cytotoxicity. *Cellular and Molecular Biology Letters*; **10** (3): 455-470.

4 Pietersz GA, Tang C-K, Apostolopoulos V (2006). Structure and Design of Polycationic Carriers For Gene Delivery. *Mini Reviews in Medicinal Chemistry*; **6** (12): 1285-1298.

5 Pietersz G, Tang C, Apostolopoulos V (2006). Strucutre and design of polycationic carriers for gene delivery. *Mini Rev Med Chem*; **6** (12): 1285-1298.

6 Hwang S, Davis M (2001). Cationic polymers for gene delivery: designs for overcoming barriers to systemic administration. *Curr Opin Mol Ther*; **3** (2): 183-191.

7 Godbey WT, Wu KK, Mikos AG (1999). Tracking the intracellular path of poly(ethylenimine)/DNA complexes for gene delivery. *Proceedings of the National Academy of Sciences of the United States of America*; **96** (9): 5177-81.

8 Heidel J, Mishra S, Davis ME (2005). Gene Therapy and Gene Delivery Systems: Molecular Conjugates. Heidelberg, Springer Berlin / Heidelberg.

9 McKenzie D *et al.* (2000). Low molecular weight disulfide cross-linking peptides as nonviral gene delivery carriers. *Bioconj. Chem*; **11** 901-909.

10 Dash PR *et al.* (1999). Factors affecting blood clearance and in vivo distribution of polyelectrolyte complexes for gene delivery. *Gene Therapy*; **6** 643-650.

11 Nomura T *et al.* (1998). Effect of particle size and charge on the disposition of lipid carriers after intratumoral injection into tissue-isolated tumors. *Pharmaceutical Research*; **15** (1): 128-32.

12 Brannon-Peppas L, Blanchette JO (2004). Nanoparticle and targeted systems for cancer therapy. *Advanced Drug Delivery Reviews*; **56** (11): 1649-1659.

13 Read ML *et al.* (2005). A versatile reducible polycation-based system for efficient delivery of a broad range of nucleic acids. *Nucleic Acids Research*; **33** (9): e86.

14 Kwok KY, Yang Y, Rice KG (2001). Evolution of cross-linked non-viral gene delivery systems. *Current Opinion in Molecular Therapeutics*; **3** (2): 142-146.

15 Yang Y *et al.* (2001). Cross-linked Low Molecular Weight Glycopeptide Mediated Gene Delivery: Relationship Between DNA Metabolic Stability and the Level of Transient Gene Expression In Vivo. *J. Pharm. Sci.*; **90** 2010-2022.

16 Takakura Y *et al.* (1999). Characterization of Plasmid DNA Binding and Uptake by Peritoneal Macrophages from Class A Scavenger Receptor Knockout Mice. *Pharmaceutical Research*; **V16** (4): 503-508.

17 Hisazumi J *et al.* (2004). Significant role of liver sinusoidal endothelial cells in hepatic uptake and degradation of naked plasmid DNA after intravenous injection. *Pharm. Res.*; **21** (7): 1223-1227.

18 Li S *et al.* (1999). Dynamic changes in the characteristics of cationic lipidic vectors after exposure to mouse serum: implications for intravenous lipofection. *Gene Ther.*; **6** (4): 585-594.

19 Read ML, Logan A, Seymour LW (2005). Barriers to Gene Delivery Using Synthetic Vectors. Advances in Genetics. J. C. Hall, J. C. Dunlap, T. Friedmann and V. van Heyningen, Academic Press. **53:** 19-46.

20 Ishida T *et al.* (2006). Injection of PEGylated liposomes in rats elicits PEG-specific IgM, which is responsible for rapid elimination of a second dose of PEGylated liposomes. *J. Control Release*; **112** (1): 115-125.

21 Blessing T *et al.* (2001). Different Strategies for Formation of PEGylated EGF-Conjugated PEI/DNA Complexes for Targeted Gene Delivery. *Bioconj. Chem*; **12** 529-537.

22 Sudimack J, Lee RJ (2000). Targeted drug delivery via the folate receptor. *Adv. Drug. Deliv. Rev.*; **41** (2): 147-162.

23 Martin ME, Rice KG (2007). Peptide-Guided Gene Delivery. *The AAPS Journal*; **9** (1): E18-E29.

24 Wu GY, Wu CH (1988). Evidence for Targeted Gene Delivery to Hep G2 Hepatoma Cells in Vitro. *Biochemistry*; **27** (3): 887-892.

25 Wu GY, Wu CH (1988). Receptor-mediated Gene Delivery and Expression In Vivo. *J. Biol. Chem.*; **263** (29 (15 October)): 14621-14624.

26 Frisch B *et al.* (2004). A New Triantennary Galactose-Targeted PEGylated Gene Carrier, Characterization of Its Complex with DNA, and Transfection of Hepatoma Cells. . *Bioconjugate Chemistry*; **75** (4): 754-764.

27 Kwok KY, Park, Y., Yongsheng, Y., McKenzie, D.L., Rice, K.G. (2003). In Vivo Gene Transfer using Sulfhydryl Crosslinked PEG-peptide/Glycopeptide DNA Co-Condensates. *J Pharm Sci*; **92** (6): 1174-1185.

28 Morimoto K *et al.* (2003). Molecular weight-dependent gene transfection activity of unmodified and galactosylated polyethyleneimine on hepatoma cells and mouse liver. *Mol. Ther.*; **7** (2): 254-261.

29 Hildebrandt IJ *et al.* (2003). Optical imaging of transferrin targeted PEI/DNA complexes in living subjects. *Gene Therapy*; **10** (9): 758-764.

30 Collard WT *et al.* (2000). Biodistribution, metabolism, and *in vivo* gene expression of low molecular weight glycopeptide polyethylene glycol peptide DNA co-condensates. *Journal of Pharmaceutical Sciences*; **89** (4): 499-512.

31 Yasuda H (2008). Solid tumor physiology and hypoxia-induced chemo/radio-resistance: novel strategy for cancer therapy: nitric oxide donor as a therapeutic enhancer. *Nitric Oxide*; **19** (2): 205-216.

32 Fenske D, Chonn A, Cullis P (2008). Liposomal nanomedicines: an emerging field. *Toxicol Pathol*; **36** (1): 21-29.

33 Belur L *et al.* (2007). Lung-directed gene therapy in mice using the nonviral Sleeping Beauty transposon system. *Nat Protoc*; **2** (12): 3146-3152.

34 Lungwitz U *et al.* (2005). Polyethylenimine-based non-viral gene delivery systems. *European Journal of Pharmaceutics and Biopharmaceutics*; **60** (2): 247-266.

35 Intra J, Salem A (2008). Characterization of the transgene expression generated by branched and linear polyethylenimine-plasmid DNA nanoparticles in vitro and after intraperitoneal injection in vivo. *J Control Release*; **[Epub ahead of print]**

36 Plank C *et al.* (1994). The Influence of Endosome-disruptive Peptides on Gene Transfer Using Synthetic. *J. Biol. Chem.*; **269** (17 (29 Apr)): 12918-12924.

37 Parente RA, Nir S, Szoka FC, Jr. (1990). Mechanism of leakage of phospholipid vesicle contents induced by the peptide GALA. *Biochemistry*; **29** (37): 8720-8.

38 Ogris M *et al.* (2001). Melittin Enables Efficient Vesicular Escape and Enhanced Nuclear Access of Nonviral Gene Delivery Vectors. *Journal of Biological Chemistry*; **276** (50): 47550-47555.

39 Boeckle S *et al.* (2006). Melittin analogs with high lytic activity at endosomal pH enhance transfection with purified targeted PEI polyplexes. *J Control Release*; **112** (2): 240-8.

40 Hama S *et al.* (2007). Quantitative and mechanism-based investigation of post-nuclear delivery events between adenovirus and lipoplex. *Nucleic Acids Res*; **35** (5): 1533-1543.

41 Riu E *et al.* (2007). Histone modifications are associated with the persistence or silencing of vector-mediated transgene expression in vivo. *Mol Ther*; **15** (7): 1348-1355.

42 Hatakeyama H *et al.* (2007). Development of a novel systemic gene delivery system for cancer therapy with a tumor-specific cleavable PEG-lipid. *Gene Therapy*; **14** (1): 68-77.

43 Chen C-P *et al.* (2006). Gene transfer with poly-melittin peptides. *Bioconjugate Chemistry*; **17** (4): 1057-62.

44 Vaughan EE, Dean DA (2006). Intracellular Trafficking of Plasmids during Transfection Is Mediated by Microtubules. *Mol Ther*; **13** (2): 422-428.

45 Bremner KH *et al.* (2004). Factors influencing the ability of nuclear localization sequence peptides to enhance nonviral gene delivery. *Bioconjugate Chemistry*; **15** (1): 152-61.

46 Young JL, Benoit JN, Dean DA (2003). Effect of a DNA nuclear targeting sequence on gene transfer and expression of plasmids in the intact vasculature. *Gene Ther.*; **10** (17): 1465-1470.

47 Wannenes F *et al.* (2005). Vector-based RNA interference against vascular endothelial growth factor-A significantly limits vascularization and growth of prostate cancer in vivo. *Cancer Gene Ther.*; **12** 926-934.

48 Alton EW *et al.* (1999). Cationic lipid-mediated CFTR gene transfer to the lungs and nose of patients with cystic fibrosis: a double-blind placebo-controlled trial. *Lancet*; **353** (9157): 947-954.

49 Madhusudan S *et al.* (2001). A Multicenter Phase I Gene Therapy Clinical Trial Involving Intraperitoneal Administration of E1A-Lipid Complex in Patients with Recurrent Epithelial Ovarian Cancer Overexpressing HER-2/neu Oncogene. *Clin. Cancer Res.*; **10** (9): 2968-2996.

50 Contag CH, Bachmann MH (2002). Advances in in vivo bioluminescence imaging of gene expression. *Annu Rev Biomed Eng*; **4** 235-60.

51 Contag C *et al.* (1995). Photonic detection of bacterial pathogens in living hosts. *Mol Microbiol*; **18** (593):

52 Sweeny T *et al.* (1999). Visualizing the kinetics of tumor-cell clearance in living animals. *Proc Natl Acad Sci USA*; **96** 12044-12049.

53 Luker K, Luker G (2008). Applications of bioluminescence imaging to antiviral research and therapy: Multiple luciferase enzymes and quantitation. *Antiviral Research*; **78** 179-187.

54 Drake J, Gabriel C, Henry M (2005). Assessing tumor growth and distribution in a model of prostate cancer metastasis using bioluminescence imaging. *Clin Exp Metastasis*; **22** (8): 674-684.

55 McCaffrey A, Kay MA, Contag CH (2003). Advancing molecular therapies through in vivo bioluminescent imaging. *Mol Imaging*; **2** (2): 75-86.

56 Pathak A, Vyas S, Gupta K (2008). Nano-vectors for efficient liver specific gene transfer. *Int J Nanomedicine*; **3** (1): 31-49.

57 Zhang G *et al.* (2004). Intraarterial delivery of naked plasmid DNA expressing full-length mouse dystrophin in the mdx mouse model of duchenne muscular dystrophy. *Hum Gene Ther*; **15** (8): 770-782.

58 Yuan T (2008). Vaccination by muscle electroporation: The injury helps. *Vaccine*; **26** (33): 4105-4106.

59 Zhang G, Budker V, Wolff JA (1999). High levels of foreign gene expression in hepatocytes after tail vein injections of naked plasmid DNA. *Human Gene Therapy*; **10** (10): 1735-1737.

60 Liu F, Song Y, Liu D (1999). Hydrodynamics-based transfection in animals by systemic administration of plasmid DNA. *Gene Ther*; **6** (7): 1258-66.

61 Suda T *et al.* (2007). Structural impact of hydrodynamic injection on mouse liver. *Gene Ther*; **14** 129-137.

62 Zhang G *et al.* (2004). Hydroporation as the mechanism of hydrodynamic delivery. *Gene Ther.*; **11** 675-682.

63 Crespo A *et al.* (2005). Hydrodynamic liver gene transfer mechanism involves transient sinusoidal blood stasis and massive hepatocyte endocytic vesicles. *Gene Ther*; **12** (11): 927-935.

64 Herweijer H, Wolff J (2007). Gene therapy progress and prospects: hydrodynamic gene delivery. *Gene Ther*; **14** (2): 99-107.

65 Suda T, Suda K, Liu D (2008). Computer-assisted hydrodynamic gene delivery. *Mol Ther*; **16** (6): 1098-1104.

66 Rettig G *et al.* (2006). Qantitative Bioluminscence Imaging of Transgene Expression In Vivo. *Analytical Biochemistry*; **335** 90-94.

67 Pergolizzi RG *et al.* (2006). Correction of a murine model of von Willebrand disease by gene transfer. *Blood*; **108** (3): 862-869.

68 Rols M (2008). Mechanism by which electroporation mediates DNA migration and entry into cells and targeted tissues. *Methods Mol Biol*; **423** 19-33.

69 Ivorra A, Rubinsky B (2007). In vivo electrical impedance measurements during and after electroporation of rat liver. *Bioelectrochemistry*; **70** (2): 287-295.

70 Zhou R, Norton J, Dean D (2008). Electroporation-mediated gene delivery to the lungs. *Methods Mol Biol*; **423** (233-247):

71 Sadadcharam M, Soden D, O'sullivan G (2008). Electrochemotherapy: an emerging cancer treatment. *Int J Hyperthermia*; **24** (3): 263-273.

72 Ugen K *et al.* (2006). Regression of subcutaneous B16 melanoma tumors after intratumoral delivery of an IL-15-expressing plasmid followed by in vivo electroporation. *Cancer Gene Ther*; **13** (10): 969-974.

73 Liu F, Huang L (2002). Electric gene transfer to the liver following systemic administration of plasmid DNA. *Gene Ther*; **9** (16): 1116-1119.

74 Elbashir SM *et al.* (2002). Analysis of gene function in somatic mammalian cells using small interfering RNAs. *Methods*; **26** (2): 199-213.

75 Kim D, Rossi J (2008). RNAi mechanisms and applications. *Biotechniques*; **44** (5): 613-6.

76 Soutschek J *et al.* (2004). Therapeutic silencing of an endogenous gene by systemic administration of modified siRNAs.[see comment][comment]. *Nature*; **432** (7014): 173-8.

77 Kumar P *et al.* (2007). Transvascular delivery of small interfering RNA to the central nervous system. *Nature*; **448** (7149): 39-43.

78 McAnuff MA, Rettig GR, Rice KG (2007). Potency of siRNA versus shRNA mediated knockdown in vivo. *J Pharm Sci*; **96** (11): 2922-30.

79 Boulo S *et al.* (2007). Nuclear traffic of influenza virus proteins and ribonucleoprotein complexes. *Virus Res*; **124** (1-2): 12-21.

80 Suzuki Y, Craigie R (2007). The road to chromatin - nuclear entry of retroviruses. *Nat Rev Microbiol*; **5** (3): 187-196.

81 Dowty ME *et al.* (1995). Plasmid DNA Entry Into Postmitotic Nuclei of Primary Rat Myotubes. *Proc Natl Acad Sci USA*; **92** (10): 4572-4576.

82 Wolff J (2002). The "grand" problem of synthetic delivery. *Nat Biotechnol*; **20** (8): 768-769.

83 Wagstaff K, Jans D (2007). Nucleocytoplasmic transport of DNA: enhancing non-viral gene transfer. *Biochem J*; **406** (2): 185-202.

84 Beck M *et al.* (2007). Snapshots of nucler pore complexes in action captured by cryo-electron tomography. *Nature*; **449** 611-615.

85 Beck M, Medalia O (2008). Structural and functional insights into nucleocytoplasmic transprot. *Histol Histopathol*; **23** 1025-1033.

86 Lusk C, Blobel G, King M (2007). Highway to the inner nuclear membrane: rules for the road. *Nat Rev Mol Cell Biol*; **8** (5): 414-420.

87 Pouton C *et al.* (2007). Targeted delivery to the nucleus. *Adv Drug Deliv Rev*; **59** (8): 698-717.

88 Pante N, Aebi U (1996). Sequential binding of import ligands to distinct nucleopore regions during their nuclear import. *Science*; **273** (5282): 1729-1732.

89 Rout M *et al.* (2003). Virtual gating and nuclear transport: the hole picture. *Trends Cell Biol*; **13** (12): 622-628.

90 Frey S, Richter R, Gorlich D (2006). FG-rich repeats of nuclear pore proteins form a three-dimensional meshwork with hydrogel-like properties. *Science*; **314** (5800): 815-817.

91 Miller M, Park MK, Hanover JA (1991). Nuclear pore complex: structure, function, and regulation. *Physiological Reviews*; **71** (3): 909-49.

92 Kalderon D *et al.* (1984). Sequence requirements for nuclear location of simian virus 40 large-T antigen. *Nature*; **311** (5981): 33-8.

93 Dean DA *et al.* (1999). Sequence Requirements for Plasmid Nuclear Import. *Experimental Cell Research*; **253** (2): 713-722.

94 Murray K *et al.* (2001). Enhanced cationic liposome-mediated transfection using the DNA-binding peptide mu (mu) from the adenovirus core. *Gene Ther*; **8** (6): 453-460.

95 Benimetskaya L *et al.* (2002). Protamine-fragment peptides fused to an SV40 nuclear localization signal deliver oligonucleotides that produce antisense effects in prostate and bladder carcinoma cells. *Bioconjug Chem*; **13** (2): 177-187.

96 Chan CK, Jans DA (1999). Enhancement of polylysine-mediated transferrinfection by nuclear localization sequences: polylysine does not function as a nuclear localization sequence. *Hum Gene Ther*; **10** (10): 1695-702.

97 Ritter W *et al.* (2003). A novel transfecting peptide comprising a tetrameric nuclear localization sequence. *Journal of Molecular Medicine*; **81** (11): 708-17.

98 Corradni R *et al.* (2007). Peptide nucleic acids with a structurally biased backbone: effects of conformational constraints and stereochemistry. *Curr Top Med Chem*; **7** (7): 681-694.

99 Zelphati O *et al.* (2000). PNA-dependent gene chemistry: stable coupling of peptides and oligonucleotides to plasmid DNA. *Biotechniques*; **28** (2): 304-10, 312-4, 316.

100 Branden LJ, Mohamed AJ, Smith CI (1999). A peptide nucleic acid-nuclear localization signal fusion that mediates nuclear transport of DNA. *Nat Biotechnol*; **17** (8): 784-7.

101 Ludtke JJ *et al.* (1999). A nuclear localization signal can enhance both the nuclear transport and expression of 1 kb DNA. *Journal of Cell Science*; **112** (Pt 12): 2033-41.

102 Roulon T, Helene C, Escude C (2002). Coupling of a targeting peptide to plasmid DNA using a new type of padlock oligonucleotide. *Bioconjug Chem*; **13** (5): 1134-9.

103 Shiraishi T, Hamzavi R, Nielsen PE (2005). Targeted Delivery of Plasmid DNA into the Nucleus of Cells via Nuclear Localization Signal Peptide Conjugated to DNA Intercalating Bis- and Trisacridines *Bioconjugate Chemistry*; **16** (5): 1112-1116.

104 Boulanger C, Di Giorgio C, Vierling P (2005). Synthesis of acridine-nuclear localization signal (NLS) conjugates and evaluation of their impact on lipoplex and polyplex-based transfection. *Eur J Med Chem*; **40** (12): 1295-306.

105 Carlisle R *et al.* (2001). Adenovirus hexon protein enhances nuclear delivery and increases transgene expression of polyethylenimine/plasmid DNA vectors. *Mol Ther*; **4** 473-483.

106 Ciolina C *et al.* (1999). Coupling of Nuclear Localization Signals to Plasmid DNA and Specific Interaction of the Conjugates with Imortin α. *Bioconjugate Chemistry*; **10** (1): 49-55.

107 Nagasaki T *et al.* (2003). Can nuclear localization signals enhance nuclear localization of plasmid DNA? *Bioconjug Chem*; **14** (2): 282-6.

108 Zanta MA, Belguise-Valladier P, Behr JP (1999). Gene delivery: A single nuclear localization signal peptide is sufficient to carry DNA to the cell nucleus. *Proc. Natl. Acad. Sci.*; **96** (1): 91-96.

109 van der Aa MA *et al.* (2005). An NLS peptide covalently linked to linear DNA does not enhance transfection efficiency of cationic polymer based gene delivery systems. *The Journal of Gene Medicine*; **7** (2): 208-217.

110 Tanimoto M *et al.* (2003). No enhancement of nuclear entry by direct conjugation of a nuclear localization signal peptide to linearized DNA. *Bioconjug Chem*; **14** (6): 1197-202.

111 Craft N *et al.* (2005). Bioluminescent imaging of melanoma in live mice. *J. Invest. Dermatol.*; **125** (1): 159-65.

112 Jenkins D *et al.* (2003). Bioluminescent imaging (BLI) to improve and refine traditional murine models of tumor growth and metastasis. *Clin Exp Metastasis*; **20** (8): 733-744.

113 van der Pluijm G *et al.* (2005). Interference with the microenvironmental support impairs the *de novo* formation of bone metastases *in vivo*. *Cancer Res.*; **65** (17): 7682-90.

114 Hoffman R (2005). *In vivo* cell biology of cancer cells visualized with fluorescent proteins. *Curr. Top. Dev. Biol.*; **70** 121-144.

115 Jawhara S, Mordon S (2004). In vivo imaging of bioluminescent Escherichia coli in a cutaneous wound infection model for evaluation of an antibiotic therapy. *Antimicrobial Agents & Chemotherapy*; **48** (9): 3436-41.

116 Doyle T *et al.* (2006). Visualizing fungal infections in living mice using bioluminescnet pathogenic *Candida albicans* strains transfromed with the firefly luciferase gene. *Microb. Pathog.*; **Epub ahead of print**

117 Opas E *et al.* (2000). Parathyroid hormone and prostaglandin E2 preferentially increase luciferase levels in bone of mice harboring a luciferase transgene controlled by elements of the pro-alpha1(I) collagen promoter. *Bone*; **26** (1): 27-32.

118 Iris B *et al.* (2003). Molecular imaging of the skeleton: quantitative real-time bioluminescence monitoring gene expression in bone repair and development. *J. Bone Miner. Res.*; **18** (2): 570-578.

119 De A, Gambhir S (2005). Noninvasive imaging of protein-protein interactions from live cells and living subjects using bioluminescence resonance energy transfer. *FASEB J*; **19** (14): 2017-2019.

120 Sato A, Klaunberg B, Tolwani R (2004). In vivo bioluminescence imaging. *Comparative Medicine*; **54** (6): 631-4.

121 Banerjee P *et al.* (2004). Novel hyperbranched dendron for gene transfer *in vitro* and *in vivo*. *Bioconjug. Chem.*; **15** 960-968.

122 Iyer M *et al.* (2002). Noninvasive imaging of cationic lipid-mediated delivery of optical and PET reporter genes in living mice. *Mol. Ther.*; **6** (4): 555-562.

123 Yoshimitsu M *et al.* (2004). Bioluminescent imaging of a marking transgene and correction of Fabry mice by neonatal injection of recombinant lentiviral vectors. *Proc. Natl. Acad. Sci. USA*; **101** (48): 16909-16914.

124 Bartlett D, Davis M (2006). Insights into the kinetics of siRNA-mediated gene silencing from live-cell and live-animal bioluminescent imaging. *Nucleic Acids Res.*; **34** (1): 322-33.

125 Liu F, Song Y, Liu D (1999). Hydrodynamics-based transfection in animals by systemic administration of plasmid DNA. *Gene Ther.*; **6** 1258-1266.

126 Zhang G, Budker V, Wolff J (1999). High levels of foreign gene expression in hepatocytes after tail vein injections of naked plasmid DNA. *Hum. Gene Ther.*; **10** 1735-1737.

127 Jenkins D *et al.* (2003). In vivo monitoring of tumor relapse and metastasis using bioluminescent PC-3M-luc-C6 cells in murine models of human prostate cancer. *Clin Exp Metastasis*; **20** (8): 745-756.

128 Lee K *et al.* (2003). Cell uptake and tissue distribution of radioiodine labelled D-luciferin: implications for luciferase based gene imaging. *Nucl. Med. Commun.*; **24** (9): 1003-1009.

129 Zhang G, Song YK, Liu D (2000). Long-term expression of human alpha1-antitrypsin gene in mouse liver achieved by intravenous administration of plasmid DNA using a hydrodynamics-based procedure. *Gene Ther.*; **7** 1344-9.

130 Kobayashi N *et al.* (2001). Hepatic uptake and gene expression mechanisms following intravenous administration of plasmid DNA by conventional and hydrodynamics-based procedures. *J. Pharmacol. Exp. Ther.*; **297** (3): 853-60.

131 Shankar P, Manjunath N, Lieberman J (2005). The prospect of silencing disease using RNA interference. *Jama*; **293** (11): 1367-73.

132 Xie FY, Woodle MC, Lu PY (2006). Harnessing in vivo siRNA delivery for drug discovery and therapeutic development. *Drug Discov Today*; **11** (1-2): 67-73.

133 Golzio M *et al.* (2005). Inhibition of gene expression in mice muscle by in vivo electrically mediated siRNA delivery. *Gene Ther*; **12** (3): 246-51.

134 Urban-Klein B *et al.* (2005). RNAi-mediated gene-targeting through systemic application of polyethylenimine (PEI)-complexed siRNA in vivo. *Gene Therapy*; **12** (5): 461-6.

135 Zhang Y *et al.* (2004). Intravenous RNA interference gene therapy targeting the human epidermal growth factor receptor prolongs survival in intracranial brain cancer. *Clin Cancer Res*; **10** (11): 3667-77.

136 Zender L *et al.* (2003). Caspase 8 small interfering RNA prevents acute liver failure in mice. *Proc Natl Acad Sci U S A*; **100** (13): 7797-802.

137 Xu J *et al.* (2005). Reduction of PTP1B by RNAi upregulates the activity of insulin controlled fatty acid synthase promoter. *Biochem Biophys Res Commun*; **329** (2): 538-43.

138 Hassani Z *et al.* (2005). Lipid-mediated siRNA delivery down-regulates exogenous gene expression in the mouse brain at picomolar levels. *Journal of Gene Medicine*; **7** (2): 198-207.

139 Hamar P *et al.* (2004). Small interfering RNA targeting Fas protects mice against renal ischemia-reperfusion injury. *Proc Natl Acad Sci U S A*; **101** (41): 14883-8.

140 Ge Q *et al.* (2004). Inhibition of influenza virus production in virus-infected mice by RNA interference. *Proc Natl Acad Sci U S A*; **101** (23): 8676-81.

141 Pichler A *et al.* (2005). In vivo RNA interference-mediated ablation of MDR1 P-glycoprotein. *Clin Cancer Res*; **11** (12): 4487-94.

142 McCaffrey AP *et al.* (2003). Inhibition of hepatitis B virus in mice by RNA interference. *Nat Biotechnol*; **21** (6): 639-44.

143 McCaffrey AP *et al.* (2002). RNA interference in adult mice. *Nature*; **418** (6893): 38-9.

144 Bartlett DW, Davis ME (2006). Insights into the kinetics of siRNA-mediated gene silencing from live-cell and live-animal bioluminescent imaging. *Nucleic Acids Research*; **34** (1): 322-333.

145 McKenzie DL, Kwok KY, Rice KG (2000). A potent new class of reductively activated peptide gene delivery agents. *Journal of Biological Chemistry*; **275** (14): 9970-9977.

146 Lewis DL, Wolff JA (2005). Delivery of siRNA and siRNA expression constructs to adult mammals by hydrodynamic intravascular injection. *Methods Enzymol*; **392** 336-50.

147 Zhang G, Song Y, Liu D (2000). Long-term expression of human alpha 1-antitrypsin gene in mouse liver achieved by intravenous administration of plasmid DNA using a hydrodynamics -based procedure. *Gene Therapy*; **7** 1344-1349.

148 Liu D, Knapp JE (2001). Hydrodynamics-based gene delivery. *Curr Opin Mol Ther*; **3** (2): 192-7.

149 Kim DH *et al.* (2005). Synthetic dsRNA Dicer substrates enhance RNAi potency and efficacy.[see comment]. *Nature Biotechnology*; **23** (2): 222-6.

150 Siolas D *et al.* (2005). Synthetic shRNAs as potent RNAi triggers. *Nature Biotechnology*; **23** 222-226.

151 Pollard H *et al.* (1998). Polyethylenimine but not cationic lipids promotes transgene delivery to the nucleus in mammalian cells. *Journal of Biological Chemistry*; **273** (13): 7507-11.

152 Chan CK, Jans DA (2001). Enhancement of MSH receptor- and GAL4-mediated gene transfer by switching the nuclear import pathway. *Gene Ther*; **8** (2): 166-71.

153 Subramanian A, Ranganathan P, Diamond SL (1999). Nuclear targeting peptide scaffolds for lipofection of nondividing mammalian cells. *Nat Biotechnol*; **17** (9): 873-7.

154 Robbins J *et al.* (1991). Two interdependent basic domains in nucleoplasmin nuclear targeting sequence: identification of a class of bipartite nuclear targeting sequence. *Cell*; **64** (3): 615-23.

155 Sebestyen MG *et al.* (1998). DNA vector chemistry: the covalent attachment of signal peptides to plasmid DNA. *Nat Biotechnol*; **16** (1): 80-5.

156 Cline M, Mandel S, Platz M (2007). Identification of the reactive intermediates produced upon photolysis of p-azidoacetophenone and its tetrafluoro analogue in aqueous and organic solvents: implications for photoaffinity labeling. *Biochemistry*; **46** (7): 1981-1987.

157 Greenwood FC, Hunter WM, Glover JS (1963). The Preparation of 131I-Labelled Human Growth Hormone of High Specific Radioactivity. *J. Biochem.*; **89** 114-123.

158 Escriou V *et al.* (2001). Critical assessment of the nuclear import of plasmid during cationic lipid-mediated gene transfer. *J Gene Med*; **3** (2): 179-187.

159 Keana J, Cai S (1990). New Reagents for Photoaffinity Labeling: Synthesis and Photolysis of Functionalized Perfluorophenyl Azides. *J Org Chem*; **55** 3640-3647.

160 Li S *et al.* (2001). Muscle-specific enhancement of gene expression by incorporation of SV40 enhancer in the expression plasmid. *Gene Ther*; **8** (6): 494-7.

161 Neves C *et al.* (2000). Novel method for covalent fluorescent labeling of plasmid DNA that maintains structural integrity of the plasmid. *Bioconjugate Chemistry*; **11** 51-55.

162 Radeke H, Snapper M (1998). Photoaffinity study of the cellular interactions of ilimaquinone. *Bioorg Med Chem*; **6** (8): 1227-1232.

163 Sebestyen MG *et al.* (2006). Mechanism of plasmid delivery by hydrodynamic tail vein injection. I. Hepatocyte uptake of various molecules. *J Gene Med*; **8** 852-873.

164 Schaffert D, Wagner E (2008). Gene therapy progress and prospects: synthetic polymer-based systems. *Gene Ther*; **15** 1131-1138.

165 Rejman J *et al.* (2004). Size-dependent internalization of particles via the pathways of clathrin- and caveolae-mediated endocytosis. *Biochemical Journal*; **377** (1): 159-169.

166 Wadhwa MS *et al.* (1995). Targeted gene delivery with a low molecular weight glycopeptide carrier. *Bioconjug. Chem.*; **6** (3): 283-291.

167 Bellocq NC *et al.* (2003). Transferrin-Containing, Cyclodextrin Polymer-Based Particles for Tumor-Targeted Gene Delivery. *Bioconjugate Chemistry*; **14** (6): 1122-1132.

168 Plank C *et al.* (1992). Gene Transfer into Hepatocytes Using Asialoglycoprotein Receptor Mediated Endocytosis of DNA Complexed with an Artificial Tetra-Antennary Galactose Ligand. *Bioconjug. Chem.*; **3** 533-539.

169 Gottschalk S *et al.* (1994). Folate receptor mediated DNA delivery into tumor cells: potosomal disruption results in enhanced gene expression. *Gene Therapy*; **1** (3): 185-91.

170 Vandermeulen G *et al.* (2007). Optimisation of intradermal DNA electrotransfer for immunisation. *J Control Release*; **124** (1-2): 81-87.